Vol. 281, No. 2, September 10, 1993 ISSN 0003-2670

ANALYTICA CHIMICA ACTA

An international journal devoted to all branches of analytical chemistry

ELSEVIER

ANALYTICA CHIMICA ACTA

Scope. *Analytica Chimica Acta* publishes original papers, preliminary communications and reviews dealing with every aspect of modern analytical chemistry. Reviews are normally written by invitation of the editors, who welcome suggestions for subjects. Preliminary communications of important urgent work can be printed within four months of submission, if the authors are prepared to forego proofs.

Submission of Papers

Americas

Prof. Harry L. Pardue
Department of Chemistry
1393 BRWN Bldg, Purdue University
West Lafayette, IN 47907-1393
USA

Tel:(+1-317) 494 5320
Fax:(+1-317) 496 1200

Computer Techniques

Prof. J.T. Clerc
Universität Bern
Pharmazeutisches Institut
Baltzerstrasse 5, CH-3012 Bern
Switzerland

Tel:(+41-31) 654171
Fax:(+41-31) 654198

Prof. Sarah C. Rutan
Department of Chemistry
Virginia Commonwealth University
P.O. Box 2006
Richmond, VA 23284-2006
USA
Tel:(+1-804) 367 1298
Fax:(+1-804) 367 8599

Other Papers

Prof. Alan Townshend
Department of Chemistry
The University
Hull HU6 7RX
Great Britain

Tel:(+44-482) 465027
Fax:(+44-482) 466410

Prof. Willem E. van der Linden
Laboratory for Chemical Analysis
Department of Chemical Technology
Twente University of Technology
P.O. Box 217, 7500 AE Enschede
The Netherlands
Tel:(+31-53) 892629
Fax:(+31-53) 356024

Prof. Paul Worsfold
Dept. of Environmental Sciences
University of Plymouth
Plymouth PL4 8AA
Great Britain

Tel:(+44-752) 233006
Fax:(+44-752) 233009

Submission of an article is understood to imply that the article is original and unpublished and is not being considered for publication elsewhere. *Anal. Chim. Acta* accepts papers in English only. There are no page charges. Manuscripts should conform in layout and style to the papers published in this issue. See inside back cover for "Information for Authors".

Publication. *Analytica Chimica Acta* appears in 16 volumes in 1994 (Vols. 281–296). *Vibrational Spectroscopy* appears in 2 volumes in 1994 (Vols. 6 and 7). Subscriptions are accepted on a prepaid basis only, unless different terms have been previously agreed upon. It is possible to order a combined subscription (*Anal. Chim. Acta* **and** *Vib. Spectrosc.*).
Our p.p.h. (postage, packing and handling) charge includes surface delivery of all issues, except to subscribers in the U.S.A., Canada, Australia, New Zealand, China, India, Israel, South Africa, Malaysia, Thailand, Singapore, South Korea, Taiwan, Pakistan, Hong Kong, Brazil, Argentina and Mexico, who receive all issues by air delivery (S.A.L.–Surface Air Lifted) at no extra cost. For Japan, air delivery requires 25% additional charge of the normal postage and handling charge; for all other countries airmail and S.A.L. charges are available upon request.

Subscription orders. Subscription prices are available upon request from the publisher. Subscription orders can be entered only by calendar year and should be sent to: Elsevier Science Publishers B.V., Journals Department, P.O. Box 211, 1000 AE Amsterdam, The Netherlands. Tel: (+31-20) 5803 642, Telex: 18582, Telefax: (+31-20) 5803598, to which requests for sample copies can also be sent. Claims for issues not received should be made within six months of publication of the issues. If not they cannot be honoured free of charge. Readers in the U.S.A. and Canada can contact the following address: Elsevier Science Publishing Co. Inc., Journal Information Center, 655 Avenue of the Americas, New York, NY 10010, U.S.A. Tel: (+1-212) 6333750, Telefax: (+1-212) 6333990, for further information, or a free sample copy of this or any other Elsevier Science Publishers journal.
Advertisements. Advertisement rates are available from the publisher on request.

US mailing notice – Analytica Chimica Acta (ISSN 0003-2670) is published biweekly by Elsevier Science Publishers (Molenwerf 1, Postbus 211, 1000 AE Amsterdam). Annual subscription price in the USA US$ 3035.75 (subject to change), including air speed delivery. Second class postage paid at Jamaica, NY 11431. *USA Postmasters*: Send address changes to Anal. Chim. Acta, Publications Expediting, Inc., 200 Meacham Av., Elmont, NY 11003. Airfreight and mailing in the USA by Publication Expediting.

ANALYTICA CHIMICA ACTA

An international journal devoted to all branches of analytical chemistry

(Full texts are incorporated in CJELSEVIER, a file in the Chemical Journals Online database available on STN International; Abstracted, indexed in: Aluminum Abstracts; Anal. Abstr.; Biol. Abstr.; BIOSIS; Chem. Abstr.; Curr. Contents Phys. Chem. Earth Sci.; Engineered Materials Abstracts; Excerpta Medica; Index Med.; Life Sci.; Mass Spectrom. Bull.; Material Business Alerts; Metals Abstracts; Sci. Citation Index)

VOL. 281 NO. 2 CONTENTS SEPTEMBER 10, 1993

(Continued overleaf)

Contents (continued)

Analytica Chimica Acta, 281 (1993) 229–242
Elsevier Science Publishers B.V., Amsterdam

The use of a pH gradient in flow-injection analysis in differentiating zinc and cadmium in a binary mixture

N. Porter, B.T. Hart and R. Morrison

Water Studies Centre and Department of Chemistry, Monash University, Clayton, Victoria 3145 (Australia)

I.C. Hamilton

B.H.P. Research Laboratories, Newcastle, N.S.W. (Australia)

(Received 4th January 1993; revised manuscript received 5th April 1993)

Abstract

A flow-injection system, designed to provide highly reproducible pH gradients, was used to discriminate between fluorescent metal chelates of zinc and cadmium. The chelating agent used, 8-hydroxyquinoline-5-sulphonic acid (HQS), has only minimal background fluorescence and its reaction with metals is pH dependent. A pH gradient was generated within the flow-injection system and the fluorescence intensity of zinc, cadmium and mixtures of the two metal species in the presence of HQS, was measured as a function of time. With a pH gradient ranging from 4 to 12 and back to 4 over a period of 90 s, a doublet fluorescence response was produced for both cadmium and zinc. The distance between the two peaks of each doublet differed sufficiently to allow the resolution of binary mixtures of the two metal species. Detection levels of 0.05 μM for both zinc and cadmium were obtained. The method of steepest descent was the mathematical procedure used to resolve the individual components of the binary mixture.

Keywords: Flow injection; Cadmium; pH gradient in FIA; Zinc

There are many methods available for the analysis of heavy metals including atomic absorption spectrophotometry (AAS), inductively coupled plasma atomic emission spectrophotometry (ICP-AES) [1], anodic stripping voltammetry [2] and chemical complexation followed by UV–visible spectrophotometry [3].

The increasingly stringent environmental controls on industry have increased the need for analytical systems which are sensitive, moderately priced, portable and capable of measuring a number of variables at one time. AAS and ICP-AES are expensive and do not lend themselves readily to portability. Batch chemical methods are time consuming and are generally aimed at single component analysis.

In the 1970s, flow-injection analysis (FIA) was developed as a relatively inexpensive technique to automate tedious batch chemical methods [4]. Since then, many chemical analyses previously carried out by batch methods have been replaced by FIA methods. The advantages of FIA are that analysis times are much shorter, smaller quantities of reagents are required and the results are highly reproducible. FIA also lends itself to on-line monitoring and the development of portable field instrumentation. While the possible methods of detection used are many, UV–visible spectrophotometry is most frequently used.

Initially FIA was applied to single component analysis but it is sufficiently versatile to be uti-

Correspondence to: B.T. Hart, Water Studies Centre and Department of Chemistry, Monash University, Clayton, Victoria 3145 (Australia).

lized for multicomponent analysis. A review by Valcarcel et al. [5] provides a comprehensive survey of the applications of FIA to multicomponent analysis. While most of the methods surveyed concern the resolution of binary mixtures, a few methods for the analysis of mixtures containing more than two components were also discussed. The methods include the use of anodic and potentiometric stripping voltammetry, differential rates of reaction, sample splitting, on-line preconcentration on ion exchange resins followed by ICP-AES and pH gradients.

The use of pH gradients has the advantage that a multiple stream system is not required. Furthermore, there is the added potential for a large amount of information to be gained about the pH dependence of a particular chemical system from a single injection. While this information can be obtained from batch methods, it would require a large number of experiments repeated at different pH to obtain the same information. A pH gradient can be produced within a flow system very simply by injecting acid into base or base into acid. The gradient of the pH depends upon the buffering capacity of the reagents, the flow-rate and the distance travelled in the flow system. The sample and reagents can then be merged with the pH variable carrier stream. If the formation of a detectable complex is pH dependent, then the maximum signal intensity will occur at the optimum pH for that reaction. This method has been applied to mixtures containing cobalt and manganese [6] and vanadium and lead [7], with 4-(2-pyridylazo)resorcinol (PAR) as the complexing agent and UV–visible absorption spectrophotometry as the detection method. Co(II) reacts with PAR at low pH, while Mn(II) reacts at high pH. Similarly, V(V) reacts at low pH and Pb(II) reacts at high pH. The pH dependent absorption–time scans for the components of these two sets of binary mixtures are well resolved and simple multiple regression can be used to solve for the initial concentrations. A literature search revealed only one paper in which an attempt had been made to resolve overlapping time scans using the pH gradient technique [8]. In this case binary and ternary mixtures with ppm levels of Cu(II), Ni(II) and Co(II) were combined with 3,5-diBr-PADAT as the chromogenic agent. The subsequent absorption spectra were analyzed using partial least squares.

The generation of pH gradients using variable flow-rates has also been investigated [9] and used in the simultaneous determination of calcium and magnesium [10] and in the simultaneous determination of vanadium and lead [11].

All the above examples utilized UV–visible absorption spectrophotometry to detect the reaction products, but its use in the detection of metals is limited by poor detection limits and by the number of known reactions producing viable chromophores. Fluorescence spectrophotometry offers an alternative to absorption spectrophotometry for those metals which can form fluorescent chelates. The advantage of fluorescence over absorption is that detection limits are improved, often by a factor of 1000 or more. Of the chelating agents known to form fluorescent metal complexes, 8-hydroxyquinoline (HQ) is the most universally used [12]. Since HQ is insoluble in water, the sulphonic acid derivative [HQS] is used for aqueous samples. Like its parent compound, HQS also reacts with many metals to form fluorescent chelates [13]. The emission spectra of these complexes are of little use in distinguishing between metal species since they tend to overlap, having broad fluorescence bands with even less structural detail than their corresponding absorption spectra. On the other hand, HQS reacts with different metals at different optimum pH values and, by creating a time-dependent pH gradient within a flow-injection system and monitoring the fluorescence signal at set emission and excitation wavelengths, a "spectrum" can be obtained which differs for each metal. By using the pH dependent fluorescence–time scan obtained for the individual metal species at known concentrations, it is possible to determine the concentration of each component in a mixture containing those species, using similar mathematical algorithms to those used in the analysis of absorption data of mixtures.

Multicomponent analysis, without the need for separation, has the advantage that losses due to pre-treatment are kept to a minimum and the time spent in collecting and analyzing data is

generally reduced. The integration of multicomponent analysis with portable field instrumentation, should result in more powerful methods of monitoring environmental pollutants.

This paper reports the first use of the pH gradient method with FIA and fluorescence detection in the analysis of zinc and cadmium in synthetic binary mixtures. Given the success of the relatively simple mathematical procedure used in this experiment with components having severely overlapping fluorescence time scans, it is anticipated that the more powerful mathematical methods available [14] will be able to deal with 'real' solutions containing various interfering species and variable matrices. This will be the subject of a following paper.

EXPERIMENTAL

Instrumentation

The flow-injection system used for this experiment is shown in Fig. 1. An Ismatec CAE840 peristaltic pump (40 rpm) was used to deliver the reagents to a mixing manifold. Tygon pump tubes were used for all reagent and sample lines. The internal diameter of the pump tubes used for all solutions was 0.889 mm providing a total flow-rate of 4.6 ml/min. An electrically activated 4-way 5020 Rheodyne injection valve with a 500-μl Teflon loop was used for injections.

Fluorescence measurements were obtained using an Hitachi F2000 fluorescence spectrophotometer fitted with a 90-μl flow cell. The signal-to-noise ratio of 231 was measured according to the manufacturers instructions, by monitoring the Raman signal of Milli-Q water over a period of 10 min at an excitation wavelength of 350 nm and an emission wavelength of 400 nm. Excitation and emission wavelengths at which the metal chelates were monitored were set at 367 nm and 520 nm respectively. The timing of the start of the data collection, control of the rotary valve and pump were handled by a 386SX PC connected via an RS232 serial port. The fluorescence signal was sampled every 0.1 s.

The pH of the solution after passing through the fluorescence cell was measured using a Sensorex combination electrode with a 50-μl flow through chamber attached to a Radiometer PHM82 pH meter, connected to a Radiometer REC 80 servograph.

Chemicals

Analytical grade 8-hydroxyquinoline-5-sulphonic acid (HQS), zinc nitrate and cadmium nitrate were obtained from Aldrich and used without further treatment. Analytical grade borax, potassium hydroxide and potassium dihydrogen orthophosphate obtained from Ajax were used to prepare the buffers. Analytical grade 1,10-phenanthroline was used to obtain the dispersion curve of the system.

Method

A pH gradient was formed by injecting a borax solution (0.025 M borax and 0.1 M KOH, pH 12.2) into a buffered acidic carrier (0.04 M potassium dihydrogenorthophosphate, pH 4.8). The pH variable carrier stream was then merged with 0.1 mM HQS followed by a sample stream containing the metal ions of interest (Fig. 1). The pH was measured using the flow through pH cell placed directly after the fluorescence cell. The output was recorded on a chart recorder. The pH was also calculated utilizing the dispersion character-

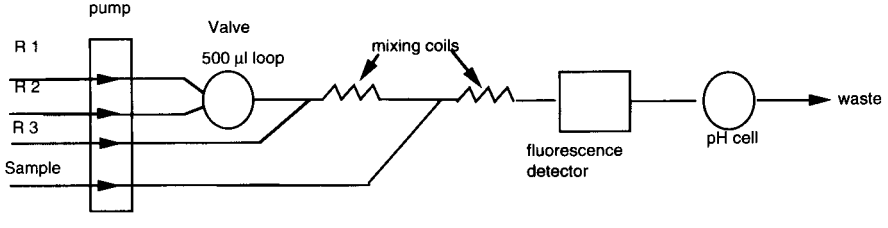

Fig. 1. FIA Setup: R1 = 0.1 M potassium dihydrogenorthophosphate carrier, R2 = 0.025 M borax + 0.1 M KOH (pH 12.2), R3 = HQS. Sample = metal ion solution.

istics of the system and MINEQL, a commercially available chemical equilibrium program [15]. The dispersion characteristics were determined using a 6 μM solution of 1,10-phenanthroline buffered with 5 mM borax. The maximum fluorescence signal from the buffered solution of 1,10-phenanthroline was determined by flowing the solution through all lines of the FIA system shown in Fig. 1. The dispersion and subsequent dilution of the 500 μl injection plug was determined by injecting the 1,10-phenanthroline into the FIA system with all other lines containing Milli-Q water buffered with the same concentration of borax as the 1,10-phenanthroline. The total dispersion and dilution of the carrier was determined similarly by reversing the carrier and injection lines.

For the analysis of binary mixtures, working solutions of 0.1 mM zinc nitrate and cadmium nitrate were prepared from 0.01 M stock solutions and the concentrations of these working solutions were checked by AAS against USEPA standards. The concentration of the HQS used was 0.1 mM. Two test sets of solutions were prepared from various combinations of the two working solutions delivered to 100-ml volumetric flasks using a variable volume 5-ml pipette and made up to the mark. In each test set the total metal ion concentration was kept constant, set A being 1 μM and set B being 10 μM.

A blank solution containing only Milli-Q water was introduced into the sample line and monitored at the beginning of the experiment, after each standard, between samples and at the end of the experiment. Standard solutions of zinc and cadmium were monitored in triplicate at both the beginning and end of the series of binary mixtures. These measurements showed that there was no significant change in the signals for the blank or the standards during the measurement period. An average of three time scans was used for each analysis, each scan taking 60 s. The valve was timed to inject the borax solution simultaneously with the fluorescence measurement start time. At the end of each complete time scan, the data were transferred through an RS232 serial port to the PC. This added an extra 60 s to the time between analyses since the maximum baud rate for the F2000 fluorescence spectrometer is 4800. At the end of each set of three scans, the data were read into the data analysis program to calculate the concentrations.

Data analysis

There are a number of ways for processing spectral data and there are some excellent reviews of current multivariate analyses by Martens and Naes [16,17]. MacClaurin et al. [18] compared a variety of methods to resolve the absorption spectra of 3 and 4 component systems. The methods compared were direct multicomponent analysis (DMA) using weighted least squares, principal component regression (PCR) and partial least squares regression (PLSR). They found that for well behaved systems with no significant interferences, as in the case of the present research, there was little difference between DMA, PCR and PLSR. Hence a DMA type algorithm, written in Microsoft C and based on the method of steepest descent [19], was used to process the data obtained in this work.

The above authors compared the various methods of analyses using the relative estimate of prediction (REP) defined by Eqn. 1. It is essentially an average of the percentage error between real and predicted concentrations for a series of mixtures in a test set. It was used in the current work to provide a measure of the percentage error between known and calculated concentrations in the two sets of binary mixtures under investigation.

$$\mathrm{REP} = \left(100/\bar{x}_{ij}\right)\left[\left(1/N\right)\sum\sum\left(x_{ij}-\hat{x}_{ij}\right)2\right]1/2 \quad (1)$$

where $\bar{x}_{ij}$ = mean of the true concentrations in the prediction set; $\hat{x}_{ij}$ = predicted concentration of analyte j in the i^{th} sample; x_{ij} = true concentration of analyte j in the i^{th} sample; and N = total number of measurements (number of components × number of samples).

Since the method of steepest descent is an iterative numerical technique it requires a set of initial guesses for the concentration of each component. These guesses were obtained by solving a set of simultaneous equations derived from data at positions along the fluorescence–time scan

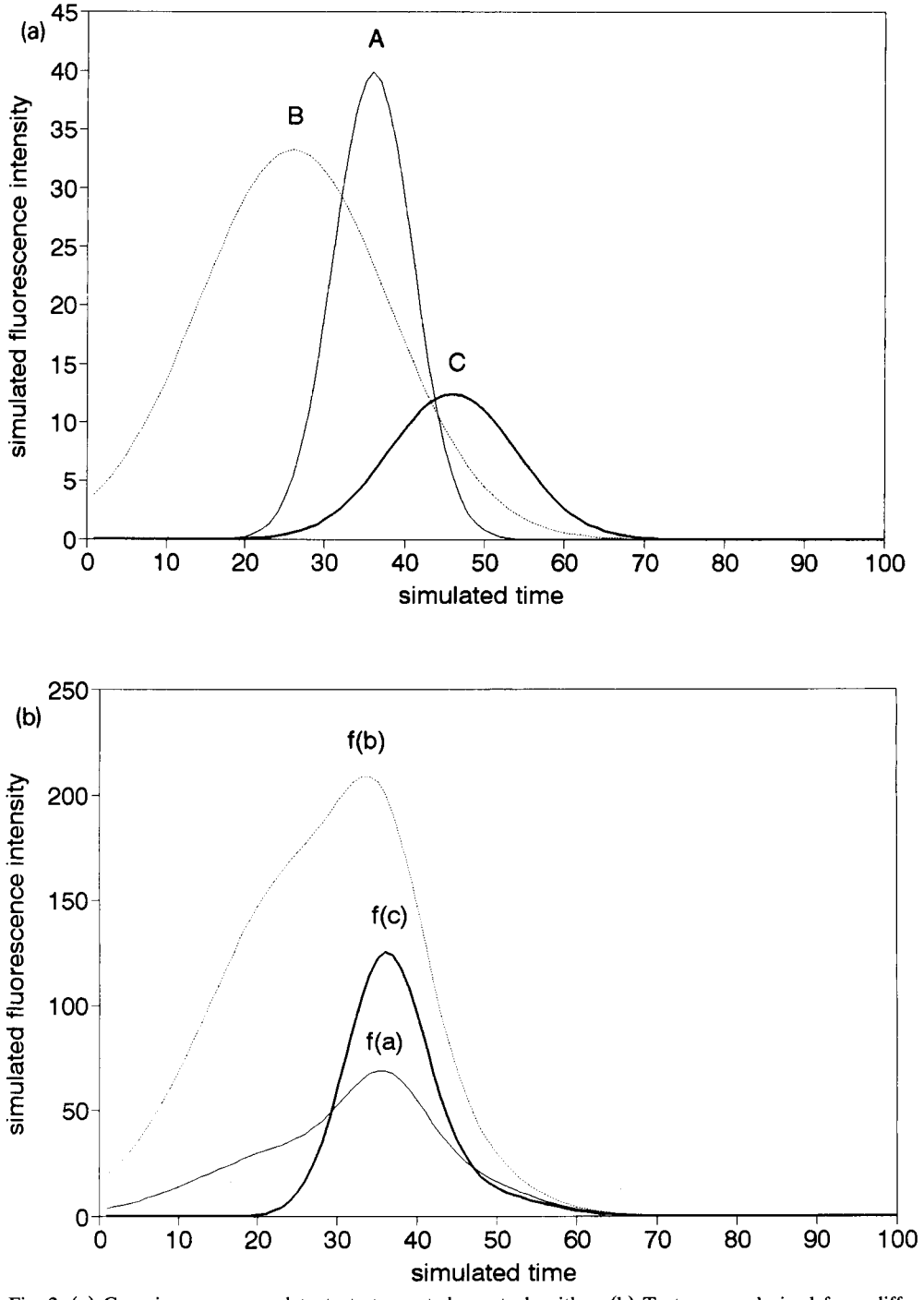

Fig. 2. (a) Gaussian curves used to test steepest descent algorithm. (b) Test curves derived from different combinations of the "standard curves" in (a). f(a) = A + B + C; f(b) = 2A + 5B + 0.5C; f(c) = 3A + C.

where the individual spectra differed most. However, it became apparent that the choice of points was not critical as the steepest descent algorithm converged on the same result regardless of the initial starting values.

The simultaneous equations were generated from the fluorescence intensity data and calculated time concentration coefficients (α_{ij}). These coefficients were determined by subtracting the blank signal from the fluorescence intensity for each standard and dividing by its concentration at each point along the time scan (Eqn. 2).

$$\alpha_{ij} = (I_{ij} - B_j)/C_i \quad (2)$$

α_{ij} is the time concentration coefficient of component i at time j, I_{ij} is the fluorescence intensity of component i at time j, B_j is the blank signal at time j, and C_i is the concentration of component i.

The intensity of the mixture at any point along the fluorescence–time scan should be equal to the sum of the concentrations of each component multiplied by its time concentration coefficient (Eqn. 3), providing the intensity of each component is linear with concentration within the concentration range of interest, and there are no interactive effects between the components.

$$I_j = C_1^*\alpha_{1j} + C_2^*\alpha_{2j} + C_3^*\alpha_{3j} + ...C_n^*\alpha_{nj} \quad (3)$$

where I_j is the intensity of fluorescence of the mixture at time j.

For a binary mixture, the two simultaneous equations required to obtain an approximation to the two unknowns C_1 and C_2 are:

$$I_1 = C_1^*\alpha_{11} + C_2^*\alpha_{21}$$

$$I_2 = C_1^*\alpha_{12} + C_2^*\alpha_{22}$$

These values C_1 and C_2 are then used as initial values for the method of steepest descent algorithm which minimizes the sum of the difference squared between the calculated and experimentally obtained time scan.

Verification of mathematical treatment

The steepest descent algorithm was tested on a simulated set of ternary mixtures. A series of three gaussian curves A, B and C shown in Fig. 2a were used to generate the three artificial "mixtures" shown in Fig. 2b.

The generated "mixtures" were resolved using both the method of simultaneous equations described above and the method of steepest descent. The results are given in Table 1.

Since the data were ideal, it was to be expected that resolving the "mixtures" by solving a set of simultaneous equations would give perfect answers. Therefore, to provide a more valid test of the steepest descent algorithm, values quite different from the true values were fed into the steepest descent part of the program. The steepest descent algorithm quickly converged on a close approximation to the real values taking

TABLE 1

Comparison of results obtained from using simultaneous equations with those obtained using the steepest descent method to solve a simulated set of data

(The starting guesses for the steepest descent routine were arbitrarily set at 3.0, 0.5 and 10.0 respectively in order to test the routine if given values values widely different from the true values)

	Method of solution	Components		
		A	B	C
f(a)	Real values	1.00000	1.00000	1.00000
	Simultaneous Eqns.	1.00000	1.00000	1.00000
	Steepest descent	0.99999	1.00000	1.00001
f(b)	Real values	2.00000	5.00000	0.50000
	Simultaneous Eqns.	2.00000	5.00000	0.50000
	Steepest descent	2.00000	5.00000	0.50001
f(c)	Real values	3.00000	0.00000	1.00000
	Simultaneous Eqns.	3.00000	0.00000	1.00000
	Steepest descent	3.00000	$-1.0 \cdot 10^{-7}$	1.00010

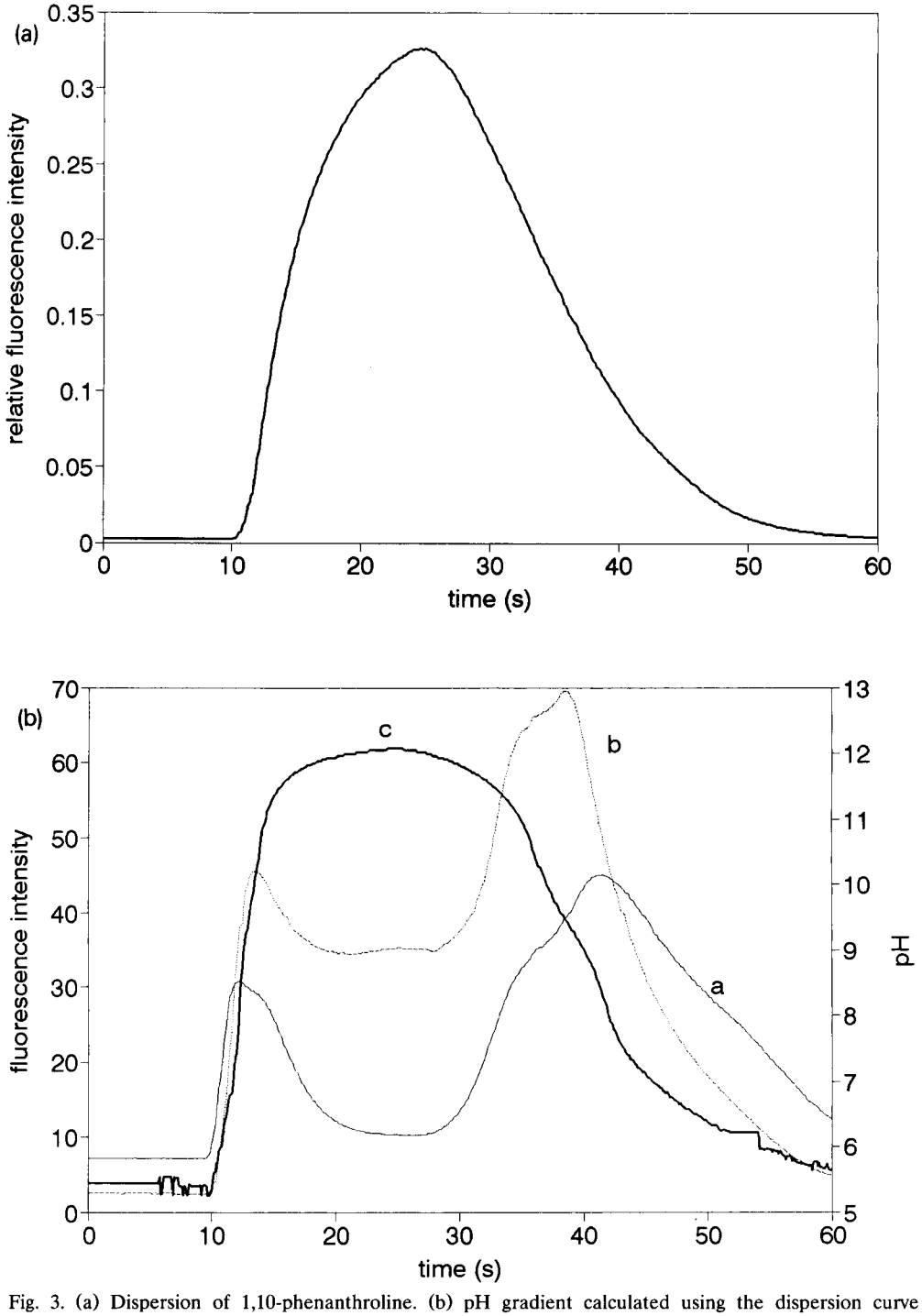

Fig. 3. (a) Dispersion of 1,10-phenanthroline. (b) pH gradient calculated using the dispersion curve in (a) and MINEQL, superimposed over fluorescence time scans for 2.5 μM zinc and 2.5 μM cadmium solutions. a is the fluorescence time scan for zinc; b is the fluorescence time scan for cadmium; c is the calculated pH gradient.

about 100 iterations to converge on values for which successive approximations differed by less than 0.00001. The fact that the mathematical solution converged on the correct answer to within 4 significant figures illustrates the viability of this routine for the type of "spectra" generated in this experiment.

RESULTS AND DISCUSSION

Dispersion of the injected plug

The dispersion curve obtained from the injection of buffered 1,10-phenanthroline (Fig. 3a) shows that the injected plug reached a maximum of about 0.35 of its initial concentration. The linear correlation coefficient of the 1,10-phenanthroline fluorescence signal versus concentration over the range from 1% of its original concentration to twice its original concentration was 0.999998 making it a reliable tracer for the determination of dispersion over the required range, that is from 1% of the original concentration to 100% of its original concentration.

Determination of a suitable pH gradient

Since the optimum pH for the formation of the zinc and cadmium HQS complexes has been reported to be in the range from 7 to 8 [20], a pH gradient was required which would range from below 7 to above 8. A number of different combinations of acid and bases were tried, including ammonia with acetic acid and tris(hydroxymethyl)aminomethane (Tris) with acetic acid. The ammonia/acetate system did not have the buffering capacity required over the pH range of 7–9 in order to distinguish between zinc and cadmium and the Tris/acetic acid system did not produce a high enough pH (pH 9). On the other hand, the borax/phosphate system, which was eventually chosen, gave a pH range from below 5 to above 12.

The dispersion curve obtained from 1,10-phenanthroline was used to predict the optimal concentrations of the borax and phosphate buffers. This was achieved by using the dispersion data to create a data file containing the fraction of the injected plug and the fraction of carrier at every 0.1 s interval over the time scan and hence the amount of borax, KOH, and phosphate at each time interval, for a particular set of starting concentrations of the buffers. This information was then input to MINEQL which had been modified to produce another data file containing the calculated pH value at each point. A 0.025 M borax solution containing 0.1 M KOH injected into a 0.04 M potassium dihydrogen orthophosphate carrier was predicted to give an appropriate pH gradient. This calculated gradient is shown superimposed over the fluorescence–time scans of zinc and cadmium in Fig. 3b.

The pH was also measured using a flow-through pH cell located immediately after the fluorescence cell. However the particular pH cell used was not ideal since the sample plug could undergo additional dispersion between the fluorescence cell and the pH cell as well as in the pH cell itself. Furthermore there was also a problem with liquid flowing up the sides of the pH probe and contaminating the incoming flow. Nevertheless the shape of the pH curve recorded on a chart recorder, was very similar to that calculated, and the top and bottom of the calculated pH range were within 0.1 of a pH unit of those recorded.

While a pH gradient can be obtained by injecting either acid into base or base into acid, the injection of base into acid prevents the build up of metal hydroxides or the metal chelates on the inside of tubing and flow cell as the acid carrier removes any adsorbed species between injections. This makes a separate wash cycle between samples unnecessary. However, sufficient time has to be allowed for the sample line to be cleared of the old sample and flushed with the new sample. This occurred during the time taken for the data to be transferred from the fluorescence detector to the computer.

Optimum HQS concentration

The correlation between fluorescence intensity and concentration at the two maxima for zinc was tested using HQS ranging from 0.5 μM to 100 μM with zinc ranging from 0.1 μM to 10 μM. For the first maximum a linear relationship was apparent over the whole range when HQS was 50

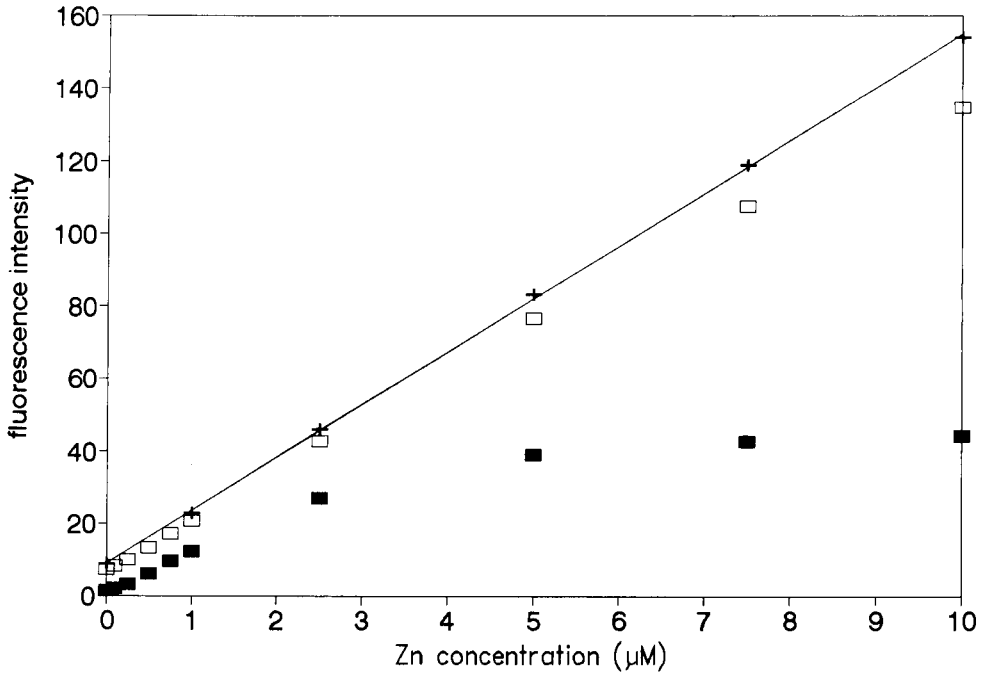

Fig. 4. Correlation between fluorescence intensity and concentration with varying concentrations of HQS for zinc at the second maximum. Plus sign = 100 μM HQS; open square = 50 μM HQS; filled square = 10 μM HQS.

μM but 100 μM was required to achieve the same degree of linearity for the second maximum, as shown in Fig. 4. The increase in peak height of the second maximum (see Fig. 3b) is believed to be due to the adsorption of either zinc hydroxide or zinc HQS onto the walls of the flow cell as the highly alkaline part of the plug passes through the system. Then, as the pH starts to drop, the adsorbed species are released, adding to the total amount of chelated zinc detected by the fluorescence detector at the time of the second peak maximum. If the zinc was adsorbed in the hydroxide form or some other non-chelated form, the total amount of HQS required would

TABLE 2

Detection limits and linear correlation coefficients for zinc and cadmium over the range 0 to 1 μM with varying HQS concentrations

Metal	Conc of HQS (μM)	Average blank (μM)	S.D. blank (μM)	r [a]	Det. limit (μM)	
					[21]	[22]
Zinc	0.50	0.11	0.01	0.9960	0.05	0.10
	1.0	0.18	0.02	0.9968	0.07	0.09
	5.0	0.60	0.10	0.9885	0.11	0.16
	10	0.94	0.14	0.9954	0.10	0.10
	50	2.93	0.13	0.9962	0.08	0.09
	100	4.54	0.15	0.99999	0.09	0.16
Cadmium	10	0.85	0.01	0.9987	0.03	0.05
	50	3.13	0.02	0.9985	0.03	0.06
	100	5.13	0.04	0.9978	0.03	0.07

[a] Linear correlation coefficient.

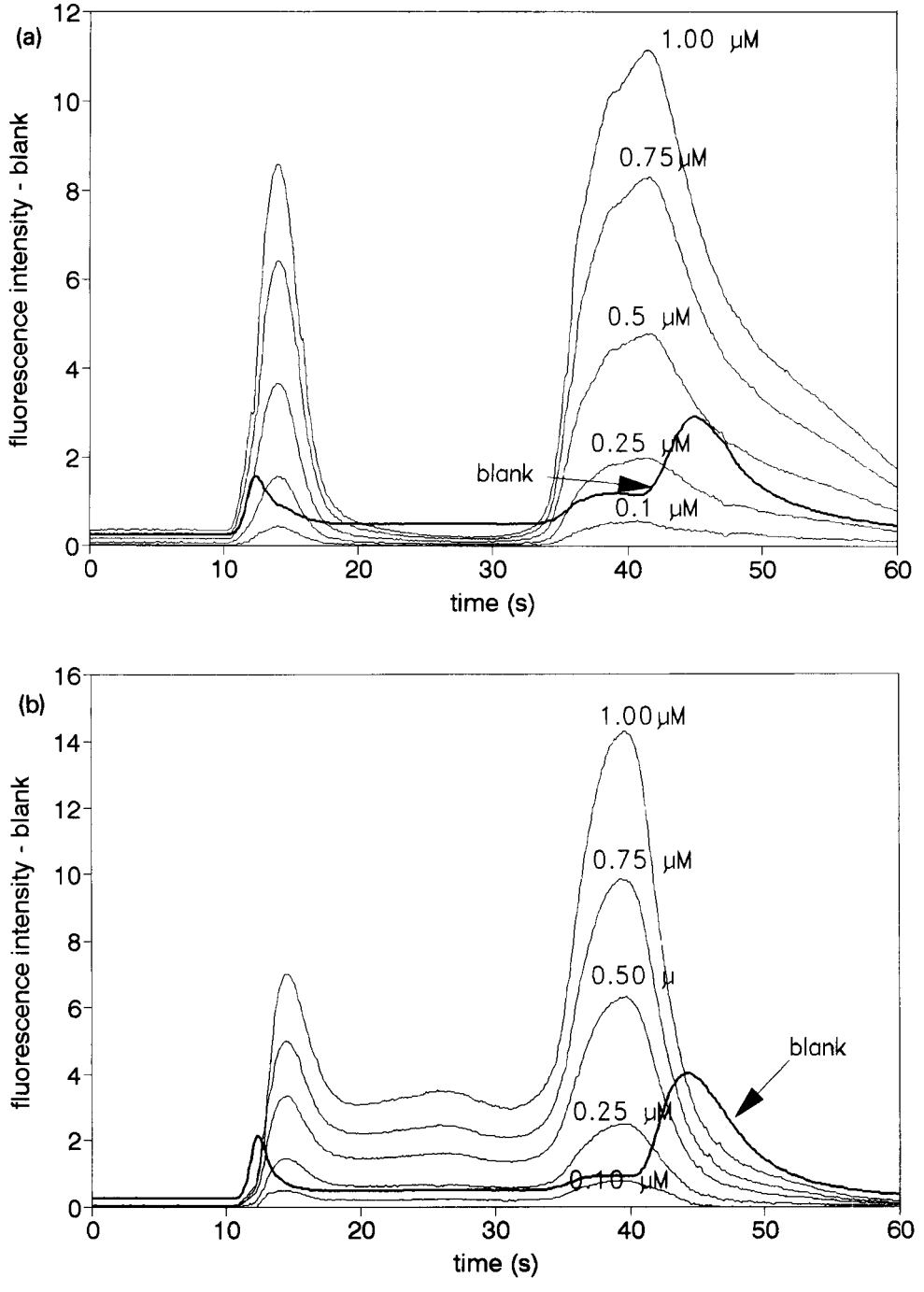

Fig. 5. (a) Comparison of the fluorescence–time scan for the blank with the fluorescence–time scans for zinc at varying concentrations. The blank has been subtracted from the scans for zinc. [HQS] = 10 μM. (b) Comparison of the fluorescence–time scan for the blank with the fluorescence–time scans for cadmium at varying concentrations. The blank has been subtracted from the scans for cadmium. [HQS] = 10 μM.

be greater at the second maximum than at the first. This could explain the loss of linearity at the second maximum at the higher zinc concentrations. From these results it is evident that HQS needs to be in at least 10-fold excess for linearity to be maintained.

A similar set of experiments was carried out with cadmium ranging from 0.1 μM to 10 μM and HQS ranging from 10 μM to 100 μM. As before, the second maximum was higher and the required HQS concentration is 100 μM for a set of cadmium solutions ranging from 0.1 μM to 10 μM.

Linearity of standards

The correlation coefficients between fluorescence intensity and concentration for zinc and cadmium with 100 μM HQS are shown in Table 2. Correlation coefficients were also calculated at each point along the time scans for zinc and cadmium and showed excellent linearity between fluorescence and concentration for both zinc and cadmium over the whole time scan.

Detection limits

The detection limits shown in Table 2, were calculated using a range of HQS concentrations and two different methods. The first method uses 3 times the standard deviation of the blank [21], while the second is essentially 3 times the standard deviation of the residuals between the calculated intensities from the regression equation and the experimental values [22]. The use of the standard deviation of the blank at the lower HQS concentrations poses a problem since the blank is higher than the intercept on the regression curve. This could mean that at low HQS concentrations, a contaminant in the reagents competes with the metal being sampled for the HQS, making the use of a linear regression curve unreliable at low metal concentrations (< 0.1 μM). It might also mean the ratio of the metal to ligand in the resulting complex differs at lower HQS concentrations, i.e. 1:1 rather than 1:2 or 1:3. The use of the residuals provides an average of the detectable concentration over the linear range. From these calculations, the minimum concentration for both zinc and cadmium which could be detected was 0.05 μM (3.2 μg/l) for zinc with HQS at 0.5 μM and 0.03 μM (3.3 μg/l) for cadmium with HQS ranging from 10 μM to 100 μM.

Blank signal

As can be seen in Fig. 5a and b the blank signal is greater than the signal for either 0.25 μM zinc or cadmium after subtracting the blank. It was thought likely that this signal was due to a combination of trace contamination of the high concentrations of borax and phosphate buffers used and fluorescence of the ligand itself at high pH. It was subsequently shown by the use of graphite furnace atomic absorption spectrophotometry, that the borax buffer had trace levels of both zinc and aluminium.

Increasing the concentration of the HQS increased the signal in the centre of the time scan but not the height of the doublet. This is consistent with the basic form of the HQS ligand having a small but observable fluorescence signal.

Obviously the blank signal can be reduced by reducing the concentrations of buffers. However, while the pH gradient obtained from using buffers of weaker concentrations is maintained for samples of moderate pH, it is not maintained for samples of very high or low pH. Hence there is a trade off between reducing the blank signal and having a buffering capacity large enough to maintain the pH gradient regardless of the nature of the sample.

Clearly, there is scope for additional work in optimizing the reagents to achieve a reduction in the blank signal whilst maintaining a constant pH gradient. It should also be possible to choose other buffer systems and flow-rates (variable or fixed) which will spread out the pH gradient and enhance the differences between the metals.

Additivity of spectra

While it was not expected that there would be any interactions between zinc and cadmium or their HQS complexes, the assumption that the fluorescence–time scans for zinc and cadmium are additive was tested by comparing the result of adding the individual fluorescence–time scans of zinc and cadmium with the fluorescence–time scan obtained experimentally from a mixture of

the two metal species. The blank signal was subtracted prior to the addition and compared with experimental data from which the blank had been subtracted. Figure 6 shows the result of adding the individual spectra of 5 μM zinc and 5 μM cadmium solutions and the fluorescence–time scan of a solution containing these concentrations of zinc and cadmium.

It can be seen from Fig. 6 that the fluorescence–time scan of the test solution and the calculated fluorescence–time scan are virtually indistinguishable. A number of tests were performed with similar results, justifying the assumption that the spectra are additive and therefore not subject to any significant interactions.

Resolution of binary mixtures

Having verified that the spectra are additive and non-interactive within the concentration range of interest, a series of binary mixtures were prepared. Files containing the fluorescence intensity data (collected at 0.1 s intervals) of an average of the blank, standards and mixtures were read into the data processing algorithm. The algorithm subtracts the blank from the spectra, calculates the time–concentration coefficients, solves a set of simultaneous equations to obtain initial guesses for the concentrations of the components and then uses these initial guesses to start the steepest descent minimisation procedure, using the whole "spectrum" of the mixture. The results from two series of binary mixtures are shown in Table 3. In set A, the total metal ion concentration was kept at 1 μM while in set B the total metal ion concentration was kept at 10 μM.

Predictability

Using Eqn. 1 for the relative estimate of predictability, the REP was calculated to be 18.4% for set A and 4.6% for set B. The results in set B are particularly good for cadmium and generally good for zinc except where cadmium is 9 times in excess. The results for set A were expected to be poorer since the lowest concentrations of both zinc and cadmium were close to the estimated detection limits.

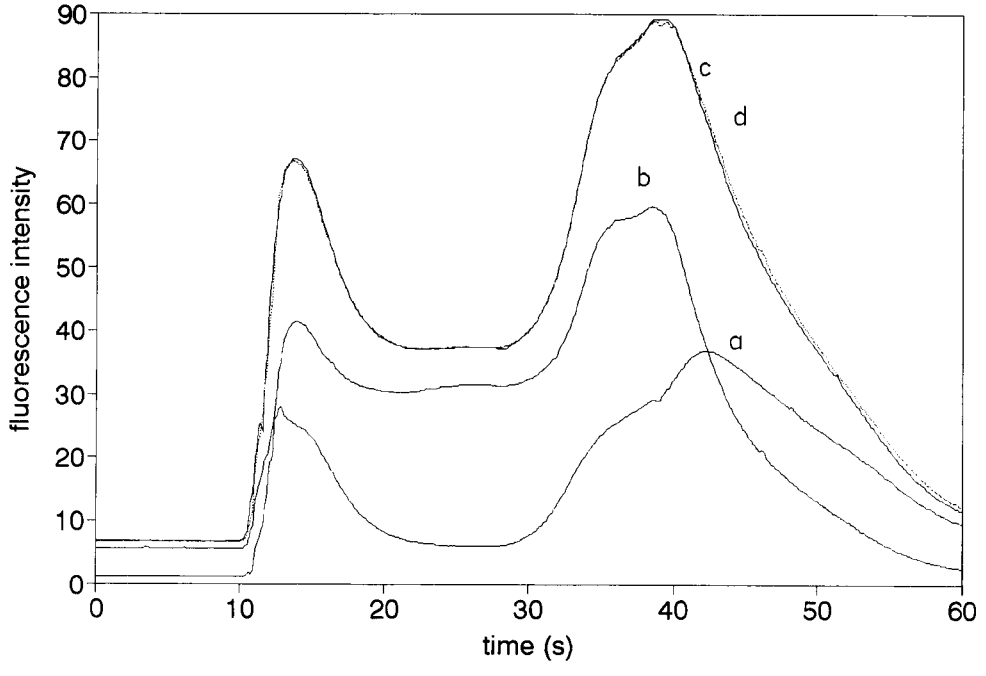

Fig. 6. Comparison of added spectra (2.5 μM Zn + 2.5 μM Cd) with experimental data for a mixture 2.5 μM in Zn and 2.5 μM in Cd. The blank was subtracted from all time scans. (a) 2.5 μM Zn–blank; (b) 2.5 μM cadmium–blank; (c) mixture (2.5 μM in Zn and 2.5 μM in Cd)–blank (solid line); (d) a + b (dotted line).

TABLE 3

Analysis of binary mixtures with total metal ion concentrations of 1 and 10 μM
(HQS = 100 μM. Buffer = borax + KOH and phosphate. 500 μl loop; all 0.889 mm i.d. tubing. Standards are 0.5 μM in set A and 5 μM in set B)

Zn/Cd ratio	Concentration (μM)		Predicted values		% Error	
	Zn	Cd	Zn	Cd	Zn	Cd
Set A						
9:1	0.90	0.10	1.02	0.07	14	−35
9:1	0.90	0.10	1.06	0.03	17	−68
9:1	0.90	0.10	1.06	0.03	18	−72
8:2	0.80	0.20	0.86	0.22	7	9
8:2	0.80	0.20	0.86	0.20	8	0
8:2	0.80	0.20	0.87	0.19	9	−4
7:3	0.70	0.30	0.76	0.30	8	1
7:3	0.70	0.30	0.87	0.24	24	−19
7:3	0.70	0.30	0.88	0.24	26	−20
6:4	0.60	0.40	0.66	0.47	10	18
6:4	0.60	0.40	0.61	0.47	1	18
6:4	0.60	0.40	0.62	0.47	3	17
5:5	0.50	0.50	0.57	0.56	15	12
5:5	0.50	0.50	0.66	0.50	32	0
5:5	0.50	0.50	0.65	0.51	29	1
4:6	0.40	0.60	0.42	0.60	6	1
4:6	0.40	0.60	0.49	0.57	23	−5
4:6	0.40	0.60	0.44	0.60	10	0
3:7	0.30	0.70	0.24	0.79	−20	12
3:7	0.30	0.70	0.18	0.80	−40	14
3:7	0.30	0.70	0.22	0.78	−25	12
2:8	0.20	0.80	0.09	0.97	−56	21
2:8	0.20	0.80	0.16	0.93	−21	16
2:8	0.20	0.80	0.10	0.96	−49	19
1:9	0.10	0.90	−0.03	1.02	−125	13
1:9	0.10	0.90	0.01	0.99	−88	10
1:9	0.10	0.90	0.00	1.00	–	11
REP [a]	18.4%					
Set B						
9:1	9.00	1.00	8.70	1.01	−3	1
9:1	9.00	1.00	8.80	0.95	−2	−5
9:1	9.00	1.00	8.85	0.92	−2	−8
8:2	8.00	2.00	7.68	1.94	−4	−3
8:2	8.00	2.00	7.66	1.94	−4	−3
8:2	8.00	2.00	7.81	1.87	−2	−7
7:3	7.00	3.00	6.60	2.98	−6	−1
7:3	7.00	3.00	6.75	2.92	−4	−3
7:3	7.00	3.00	6.74	2.92	−4	−3
6:4	6.00	4.00	5.76	3.89	−4	−3
6:4	6.00	4.00	5.69	3.93	−5	−2
6:4	6.00	4.00	5.91	3.84	−2	−4
5:5	5.00	5.00	4.56	5.00	−9	0
5:5	5.00	5.00	4.48	4.86	−10	−3
5:5	5.00	5.00	4.37	4.75	−13	−5
4:6	4.00	6.00	3.82	5.92	−5	−1
4:6	4.00	6.00	3.82	5.91	−5	−1
4:6	4.00	6.00	3.81	5.91	−5	−1
3:7	3.00	7.00	2.53	7.09	−16	1
3:7	3.00	7.00	2.74	7.00	−9	0
3:7	3.00	7.00	2.66	7.01	−11	0
2:8	2.00	8.00	1.70	7.97	−15	0
2:8	2.00	8.00	1.93	7.88	−4	−1
2:8	2.00	8.00	2.03	7.87	1	−2
1:9	1.00	9.00	0.77	9.02	−23	0
1:9	1.00	9.00	0.69	9.03	−31	0
1:9	1.00	9.00	0.68	9.03	−32	0
REP	4.6%					

[a] REP = relative estimate of prediction (see Eqn. 1).

Conclusions

It has been shown that when a pH gradient is introduced into a flow-injection system, the fluorescence intensity data from the generation of pH-dependent fluorescent metal complexes can be used to resolve binary mixtures of metal cations even when the optimum pH for the formation of their complexes are similar. The best detection limits given here are in the vicinity of 0.05 μM for both zinc and cadmium. The upper limit to the use of this method with HQS as the chelating ligand, is governed by the solubility of the ligand and self-absorption which reduces the fluorescence signal at high concentrations. The method has been shown to be applicable to solutions containing a total metal ion concentration of zinc and cadmium ranging from 0.1 μM to 10 μM.

The detection limits reported here for cadmium and zinc are similar to those obtained by AAS but the advantage of the FIA system is that it is cheaper and has the potential to be made portable and measure a number of variables simultaneously.

It has already been demonstrated within our laboratory that ternary mixtures can be resolved successfully using the experimental setup described here combined with the steepest descent algorithm [23].

We would like to thank Dr. Alan Stuart of B.H.P and Dr. Ian McKelvie of the Water Studies Centre, Monash University for their useful advice on the various aspects of the project. Nichola Porter also gratefully acknowledges the financial support given by D.E.E.T. and B.H.P. Research in funding an APRA (industry) scholarship, and the additional financial support given by the Water Studies Centre, Monash University.

REFERENCES

1 W. Fresenius, K.E. Quentin and W. Schneider (Eds.), Water Analysis: A practical guide to physico-chemical, chemical and microbiological water examination and quality assurance, Springer-Verlag, Berlin, Heidelberg, 1988.
2 M.S. Shuman and M. Martin-Goldberg, in R.A. Minear and L.H. Keith (Eds.), Water Analysis, Vol. II, Inorganic Species, Part 2, Academic Press, Orlando, FL, 1984.
3 Standard Methods for the Examination of Water and Waste Water, 15th edn, American Public Health Association, Washington, DC, 1981.
4 J. Ruzicka and E. Hansen, Flow Injection Analysis, Wiley-Interscience, New York, 1981.
5 M. Valcarcel, M.D. Luque De Castro, F. Lazaro and A. Rios, Anal. Chim. Acta, 216 (1989) 275.
6 D. Betteridge and B. Fields, Anal. Chim. Acta, 132 (1981) 139.
7 A. Rios, M.D. Luque De Castro and M. Valcarcel, Anal. Chim. Acta, 187 (1986) 139.
8 H. Li, R. Man and X. Zhao, Zhongnan Kuangye Xueyuan Xuebao, 23 (1992) 105.
9 M. Aguado, J. Marcos, A. Rios and M. Valcarcel, Anal. Chim. Acta, 239 (1990) 211.
10 J. Marcos, A. Rios and M. Valcarcel, Analyst, 117 (1992) 1629.
11 J. Marcos, G. Del Campo, A. Rios and M. Valcarcel, Fresenius' J. Anal. Chem., 342 (1992) 76.
12 K. Burger, Organic Reagents in Metal Analysis, Pergamon Press, Oxford, 1973.
13 K. Soroka, R.S. Vithanage, D.A. Phillips, B. Walker and P.K. Dasgupta, Anal. Chem., 59 (1987) 629.
14 H. Martens and T. Naes, Multivariate Calibration, Wiley, New York, 1989.
15 J.C. Westall, J.L. Zachary and F.M.M. Morel, MINEQL A computer program for the calculation of chemical equilibrium composition of aqueous systems, Tech. Note 18, Dept. Civil Eng., Massachusettes Institute of Technology, Cambridge, MA, 1976.
16 H. Martens and T. Naes, Trends Anal. Chem., 3 (1984) 204.
17 T. Naes and H. Martens, Trends Anal. Chem., 3 (1984) 266.
18 P. MacLaurin, P.J. Worsfold, M. Crane and P. Norman, Anal. Proc., 29 (1992) 65.
19 E. Kreysig, Advanced Engineering Mathematics, Wiley, New York, 6th edn., 1988, p. 1114.
20 Y. Nishikawa, K. Hiraki, K. Morishige and T. Katagi, Bunseki Kagaku, 26 (1977) 365.
21 D.A. Skoog, Principles of Instrumental Analysis, Saunders College Publishing, New York, 1985.
22 J.C. Miller and J.N. Miller, Statistics for Analytical Chemistry, Ellis Horwood, Chichester, 2nd edn., 1988, p. 227.
23 N. Porter, B.T. Hart, R. Morrison and I.C. Hamilton, in preparation.

Analytica Chimica Acta, 281 (1993) 243–247
Elsevier Science Publishers B.V., Amsterdam

Flow-injection determination of tylosin in fermentation broth

Frank L. Neely

Lilly Research Laboratories, Indianapolis, IN 46285 (USA)

(Received 15th January 1993; revised manuscript received 22nd March 1993)

Abstract

A flow-injection analysis method has been developed for the rapid determination of tylosin in fermentation broth. The method is based on the reaction of the tertiary amine moiety with *cis*-aconitic anhydride in non-aqueous media to form a red internal salt. The applicability of the method for other antibiotics possessing a tertiary amine moiety is also investigated.

Keywords: Flow injection; Fermentation broth; Tylosin

The tertiary amine functional group is present in the structure of numerous biologically active compounds, including the antibiotics clindamycin, erythromycin, penicillin, tetracycline, and tylosin. A flow-injection analysis (FIA) procedure was developed for the determination of tylosin in fermentation broth based upon the reactivity of the tertiary amine functional group. Several methods have been published for the derivatization of tertiary amines in a complex matrix [1–8]. Rubinstein et al. [9], Leland and Powell [10] and Noffsinger and co-workers [11–15] have utilized chemiluminescence detection based upon the reaction of tertiary amines with Ru(III). This reaction was coupled to a reversed-phase chromatographic separation and used successfully with clindamycin and erythromycin. Preparation of the reagent required bulk electrolysis of the Ru(II) precursor to generate the Ru(III) reagent and was not practical for our application. Kudoh et al. [16] have described the derivatization of simple tertiary amines using a citric acid/acetic anhydride reagent in a post-column reaction detector for normal phase chromatography. In their work, optimal sensitivity was found after 24 h of storage of the reagent. Although the mechanism of the reaction remains unclear, the acetic anhydride is postulated to dehydrate citric acid to produce *cis*-aconitic anhydride, which then reacts with tertiary amine to form a red internal salt as shown in Fig. 1 [17]. In this work, a flow-injection analysis method was developed based upon the reaction of *cis*-aconitic anhydride with the tertiary amine functional group. The rapid determination of tylosin in fermentation broth is presented and application to other tertiary amine-bearing antibiotics investigated.

EXPERIMENTAL

All solvents were of HPLC grade and were obtained from Fisher. *cis*-Aconitic anhydride was obtained from Aldrich (Milwaukee, WI). Ery-

Correspondence to: F.L. Neely, Lilly Research Laboratories, Indianapolis, IN 46285 (USA).

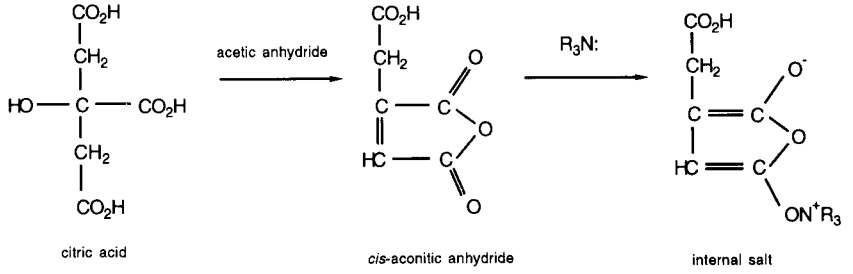

Fig. 1. Proposed reaction sequence for the reaction of tertiary amine with citric acid in the presence of acetic anhydride.

thromycin and clindamycin were purchased from Sigma (St. Louis, MO). Tylosin and penicillin V were obtained from Lilly (Indianapolis, IN).

The flow-injection manifold consisted of a Perkin Elmer LC600 autosampler, a Beckman Model 1108 pump, a Waters Model 481 UV–visible absorbance detector, and a FIAtron FH40 heater and TC50 controller. The reactor consisted of 13′ of 0.010″ stainless-steel tubing wrapped tightly around the heater core. The temperature of the reactor was maintained at 45°C. The injection volume was 5 μl and reagent flow-rate was 3 ml/min. Absorbance data at 525 nm were collected at a frequency of 10 Hz using a PE-Nelson 900 interfaced to an HP1000 data aquisition system developed in house. Biological assays were conducted using the method of Coleman [18,19] using similar equipment.

The reagent solution was prepared by dissolving *cis*-aconitic anhydride in a 1:1 mixture of acetic anhydride–isopropyl acetate to a final concentration of 16 mM (2.5 mg/ml) unless othwise mentioned. Upon standing, the reagent slowly changed color form a pale yellow to violet. Despite the color change of the reagent, minimal effect was observed on the assay. The reagent was stored at 0°C and was stable for at least a month. Samples were prepared by extracting fermentation broth with sufficient isopropyl acetate to obtain a final concentration of about 1 mM. A known volume of the organic extract was evaporated to dryness in vacuo and reconstituted in isopropyl acetate, mixed by vortex, and injected directly. Standards were prepared in isopropyl acetate.

RESULTS AND DISCUSSION

The response of the system was optimized for tylosin analysis by systematically varying the concentration of reagent. The reagent flow-rate was held constant to facilitate a sampling period of 3 × the duty cycle of the autosampler to give a throughput of about 3.5 samples per minute. For convienence, reactor volume and temperature

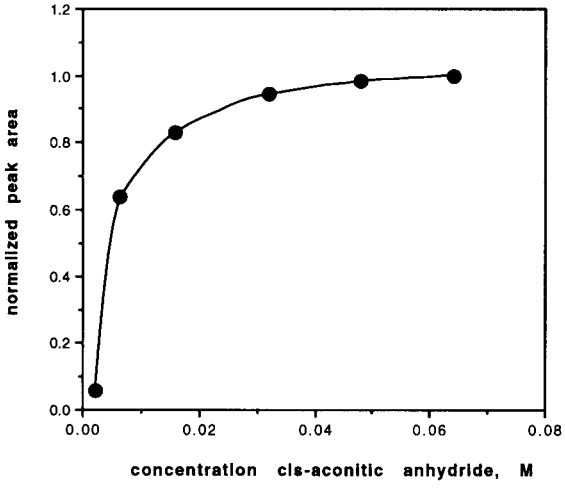

Fig. 2. Effect of reagent concentration on detector response with acetic anhydride–isopropyl acetate (1:1) as solvent. Experimental conditions as described in text.

were also held constant. Figure 2 portrays the effect of reagent concentration on response. A 1.0 mM standard was injected in triplicate into a series of reagent solutions prepared in a 1 : 1 ratio of acetic anhydride: isopropyl acetate. The concentration of *cis*-aconitic anhydride varied over the domain 2–64 mM. The response increased with reagent concentration, however, minimal increase in response was observed at *cis*-aconitic anhydride concentrations above 16 mM, suggesting complete reaction of tylosin with *cis*-aconitic anhydride. Discoloration of the reagent occured more quickly with excessive concentration of *cis*-aconitic anhydride, therefore 16 mM was selected as the optimal reagent concentration. The effect of solvent composition was studied by varying the ratio of acetic anhydride and isopropyl acetate with a constant *cis*-aconitic anhydride concentration of 16 mM. Over the domain 25–100% acetic anhydride, no significant effect was observed on detector response. At concentrations below 25% acetic anhydride, solubility of the reagent at 0°C was uncertain. Hexane and acetonitrile were substituted for isopropyl acetate with no significant effect on detector response. To evaluate the long-term stability of the reagent, a standard solution was injected at 5-min intervals over the course of 6 h. The reagent consisted of 16 mM *cis*-aconitic anhydride disolved in acetic anhydride–isopropyl acetate (1 : 1) and was stored at room temperature to enhance degradation. During the course of the experiment, the color of the reagent changed from pale yellow to a reasonably dark violet. The coefficient of variation observed was 0.8%, indicating stability of the reagent. This level of precision is comparable to LC [20] and is primarily limited by reproducibility of injection volume, consistent with the hypothesis that reaction of tylosin with *cis*-aconitic anhydride is essentially complete.

Figure 3 shows a typical FIA trace obtained for tylosin with the parameters detailed in the Experimental section. The first three injections were calibration standards and the other injections are actual samples. A value of 80 was obtained for the dispersion as defined by Ruzicka and Hansen [21]. A series of standards were prepared over the concentration domain 0.11–2.2 mM tylosin. Linear regression of the response obtained in duplicate for each standard gave a

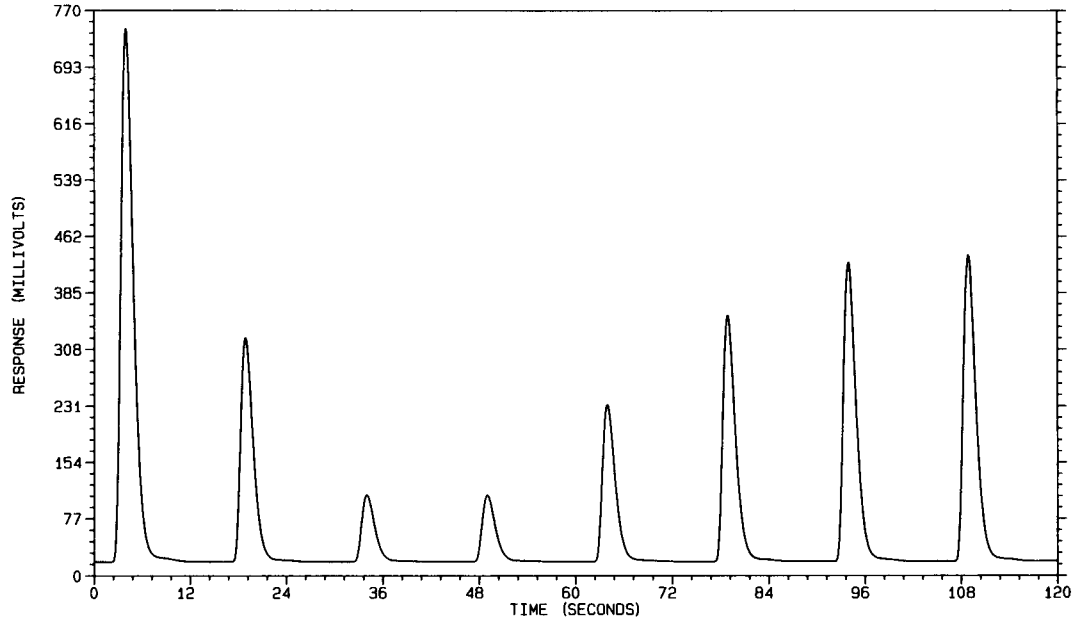

Fig. 3. Typical FIA trace. Injections 1, 2, and 3 are standard solutions at 0.805, 0.335, and 0.123 mM concentration, respectively. Subsequent injections are fermentation broth samples.

regression coefficient of 0.9998 with an offset corresponding to −0.03 mM. At concentrations in excess of 2.2 mM, the deviation from linearity appears to be related to limitations of the Beer–Lambert relation rather than limiting reagent, since an absorbance of 1.5 was observed for the 2.2 mM standard. The linear range of the method was extended to 11 mM by changing the detection wavelength from 525 nm to 560 nm.

To evaluate the precision of the method, a sample of fermentation broth was prepared seven times and analyzed. The coefficient of variation was 1.3%. The slight increase in variance relative to repetitive injections of standard reflects the heterogeneity of the sample matrix. The uncertainty is, however, quite acceptable. Spiking experiments were performed to evaluate the accuracy of the method. A sample of fermentation broth was spiked with a concentrated aqueous solution of tylosin over the domain 50–500% of initial tylosin concentration. The pertinent data are portrayed in Fig. 4. Over the concentration domain studied, the recovery ranged from 96.6–106.1%, indicating quantitative extraction of tylosin from the sample. To evaluate the effect of sample matrix, a model lipid, methyl oleate, was spiked into the sample over the domain 1–10 ×

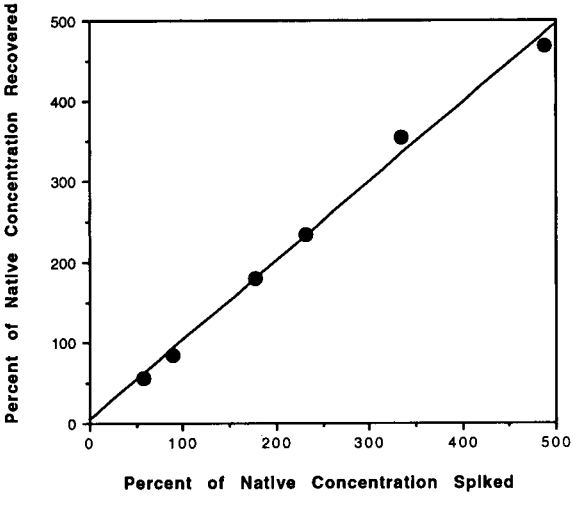

Fig. 4. Linear regression of recovery from spiked samples. Data are normalized relative to native concentrations for presentation purposes. Line: recovered = 0.981 · spiked + 4.14%, $r^2 = 0.994$.

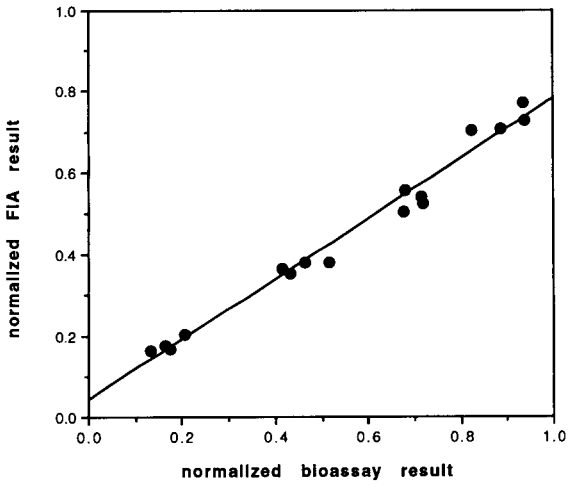

Fig. 5. Comparison of FIA and bioassay results for fermentation samples. Data are normalized for presentation purposes. Line: FIA = 0.739 · bioassay + 0.042, $r^2 = 0.981$.

the concentration of tylosin. Over this domain, the presence of methyl oleate did not affect the detector response. The effect of residual water was evaluated by diluting a standard prepared in acetonitrile with varying ratios of water and acetonitrile. Significant peak inversion was observed at water concentration as low as 0.3%. A set of fermentation broth samples were analyzed by the flow-injection analysis method and the method of Coleman. The data, normalized for presentation purposes, are well correlated as portrayed in Fig. 5. Linear regression of the data gave the equation FIA result = 0.739(bioassay result) + 0.042 (r^2 = 0.981). The intercept is essentially origin relative to the concentration regime studied. The slope of the line differ from the theoretical result of unity. This may be related to the occurrence of tylosin-related macrolides which differ in biological activity relative to tylosin and may react at different rates with *cis*-aconitic anhydride than tylosin. Similar treatment of the ranked assay results yields the equation ranked FIA result = 0.982(ranked bioassay result) + 0.0005. The near-unity slope indicates that the FIA assay is a viable means of rapidly screening fermentation broth samples.

To evaluate the applicability of the method to other tertiary amine-bearing antibiotics, stan-

TABLE 1

Relative response [a] of selected tertiary amine antibiotics

Antibiotic	Relative response [b]
Clindamycin	0.024
Erythromycin	0.824
Penicillin V	0.098
Tylosin	0.873

[a] Detector response relative to triethylamine on a molar basis.
[b] Average of three injections.

dards of clindamycin, erythromycin, penicillin V, and tylosin were prepared in acetonitrile and analyzed against a triethylamine standard. The data are presented in Table 1. Tylosin and erythromycin gave relative molar responses nearly equivalent to triethylamine. The tertiary amine moiety of tylosin and erythromycin is of the general formula NR_2R', where R represents a methyl substituent. Therefore, minimal steric hindrance is anticipated in the formation of the internal salt of *cis*-aconitic anhydride. The tertiary amine moieties of clindamycin and penicillin V contain a single methyl substituent and no methyl substituents, respectively. The relative detector response of the antibiotics suggests that steric hindrance toward internal salt formation is a significant aspect in the application of this method to other analytes. A detailed study of the stereoelectronic aspects of the reaction kinetics is beyond the scope of this study, however.

Conclusions

A rapid assay has been developed for the determination of tylosin in fermentation broth. The precision of the assay is comparable to that observed in LC. The specifity of the color-forming reaction affords excellent selectivity, thereby avoiding a chromatographic separation. The reaction appears to be applicable to a wide variety of tertiary amines, although the sensitivity varies considerably as a function of the stereoelectronic environment of the tertiary amine moiety.

REFERENCES

1 S. Okhuma, J. Parm. Soc. Jpn., 75 (1962) 1124.
2 M. Palumbo and S. Sacca, II Farmaco, 2 (1962) 65.
3 R.M. Silverstein, Anal. Chem., 35 (1963) 154.
4 M. Pesez and J. Bartos, Bull. Soc. Chim. Fr., (1964) 2333.
5 A.B. Groth and G. Wallerberg, Acta Chim. Scand., 20 (1966) 2628.
6 A.B. Groth and M.E. Dahlen, Acta Chim. Scand., 21 (1967) 291.
7 W.D. Langley, Anal. Chem., 39 (1967) 199.
8 G. Gubitz, R. Wintersteiger and A. Hartinger, J. Chromatogr., 218 (1981) 51.
9 I. Rubinstein, C.R. Martin and A.J. Bard, Anal. Chem., 55 (1983) 1590.
10 J.K. Leland and M.J. Powell, J. Electrochem. Soc., 137 (1990) 3127.
11 J.B. Noffsinger and N.D. Danielson, J. Chromatogr., 387 (1987) 520.
12 J.B. Noffsinger and N.D. Danielson, Anal. Chem., 59 (1987) 865.
13 N.D. Danielson, L. He, J.B. Noffsinger and L. Trelli, J. Pharm. Biomed. Anal., 7 (1989) 1281.
14 L. He, K.A. Cox and N.D. Danielson, Anal. Lett., 23 (1990) 195.
15 M.A. Targove and N.D. Danielson, J. Chromatogr. Sci., 28, (1990) 505.
16 M. Kudoh, I. Matoh and S. Fudano, J. Chromatogr., 261 (1983) 293.
17 S. Sass, J.J. Kaufman, A.A. Cardenas and J.J. Martin, Anal. Chem., 30 (1958) 529.
18 M.R. Coleman, J. Assoc. Off. Anal. Chem., 72 (1989) 454.
19 M.R. Coleman and D.H. Mowrey, J. Assoc. Off. Anal. Chem., 73, (1990) 927.
20 R.E. Majors, LC–GC, 16 (1992) 1190.
21 J. Ruzicka and E.H. Hansen, Flow Injection Analysis, Wiley, New York, 1981.

Analytica Chimica Acta, 281 (1993) 249–257
Elsevier Science Publishers B.V., Amsterdam

Rapid microwave assisted hydrolysis of formetanate

K. Dema-Khalaf, A. Morales-Rubio and M. de la Guardia

Department of Analytical Chemistry, Faculty of Chemistry, University of Valencia, 50 Dr. Moliner St., 46100 Burjassot (Valencia) (Spain)

(Received 28th January 1993; revised manuscript received 5th April 1993)

Abstract

A fast microwave-assisted hydrolysis procedure has been developed for the derivatization of formetanate previously to the flow-injection spectrophotometric determination of *m*-aminophenol by reaction with *p*-aminophenol. Formetanate is quantitatively hydrolyzed with 0.1 M NaOH in 150 s using a closed polytetrafluoroethylene reactor with 115 ml internal volume and a radiation power of 390 W. The above procedure has been applied, as a previous step, for the flow-injection spectrophotometric determination of formetanate in spiked water samples and accurate and precise results have been found. The method permits to obtain a limit of detection of 0.025 mg l^{-1} of formetanate. The relative standard deviation of five independent analyses of a sample containing 6 mg l^{-1} formetanate was 0.5%.

Keywords: Flow injection; Spectrophotometry; Aminophenol; Formetanate; Microwave-assisted hydrolysis; Waters

Formetanate (*m*-{[(dimethylamino)methylene]amino}phenyl methylcarbamate monohydrochloride) is an acaricide and insecticide product and very effective for the control of spider mites, rust mites, certain aphides, thrips, lygus bugs, leaf hoppers, slugs and snails on horticultural agronomic and ornamental plants. Also, it is specifically effective against organophosphate resistant mites [1–3]. Therefore, formetanate is widely used and analytical methods are required to determine formetanate and its degradation products in water. However, few data have been reported up till now on residue levels of this pesticide in ground water.

Liquid chromatography (LC) is the most commonly employed technique to determine formetanate residues [4–8]. Traditional gas chromatography (GC) cannot be used directly to determine formetanate due to the decomposition of the pesticide during the injection. However, GC has been employed after the hydrolysis of formetanate to *m*-aminophenol (MAP), which is brominated to give 2,4,6-tribromo-3-aminophenol which can be separated and detected by using electron capture detection [1].

Formetanate can be determined spectrophotometrically at 555 nm after hydrolysis to MAP and reaction with *N*-(1-naphthyl)ethylenediamine [1].

On the other hand, many studies have been carried out on the determination of MAP by LC [9–16], GC [17,18], thin-layer chromatography (TLC) [19–22], spectrophotometry [23–30] and spectrofluorometry [31–34] and, for the determination of formetanate a previous derivatization to obtain MAP is therefore very convenient. However, as has been reported previously [35–38], the hydrolysis of formetanate is a very slow process and requires the use of high NaOH concentrations and high temperature values in order to obtain quantitative results.

Correspondence to: M. de la Guardia, Department of Analytical Chemistry, Faculty of Chemistry, University of Valencia, 50 Dr. Moliner St., 46100 Burjassot (Valencia) (Spain).

The recent application of microwave ovens in chemistry [39,40] offers a good way for supplying high temperatures in a short time. Microwave assisted procedures have been developed to dry biological tissues [41] and inorganic samples [42] and to improve the sample digestion procedures by both wet [43–45] and dry ashing [46], providing very fast methods which can be applied for the on-line sample preparation in flow systems [47–49].

On the other hand, microwave assisted procedures can also be employed to accelerate organic reactions [50–53]. In particular, hydrolysis of different organic molecules can be accelerated by means of microwave irradiation in closed reactors [53–57].

In this work, a rapid microwave-assisted method for formetanate hydrolysis has been developed in order to accelerate this step of the formetanate analysis. The effect of experimental parameters on the hydrolysis efficiency, such as radiation power, digestion time, volume of reagents and NaOH concentration, have been studied, and the concentration of MAP determined by a flow injection spectrophotometric method based on the reaction of MAP with *p*-aminophenol (PAP) [58].

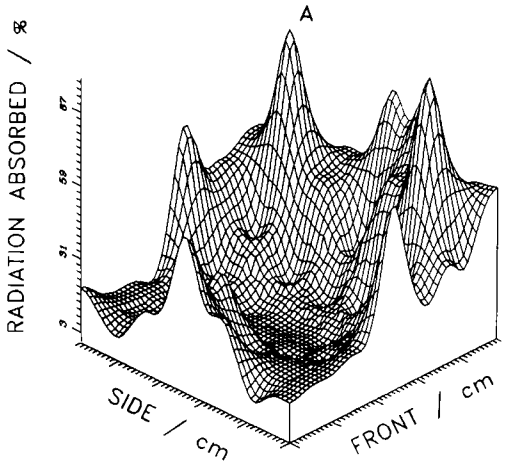

Fig. 1. Distribution of the microwave radiation into the cavity of the oven. The base of the oven has a surface of 30×30 cm^2, the door of the oven is located in the front part. Point A shows the maximum absorption of the radiation and was selected for the reactors.

EXPERIMENTAL

Apparatus

A domestic Balay Model Bahm-100 microwave oven with 2450 MHz frequency and 650 W maximum exit power was used to improve the formetanate hydrolysis. The microwave radiation into the cavity oven is not homogeneous, as can be seen in Fig. 1; for this reason, the best reactor position into the oven was established after several experiments [55] in order to obtain the highest yield of hydrolysis. Therefore, the inhomogeneity on the microwave field has not been compensated but used to achieve the maximum absorption of the magnetron power by the samples. Laboratory-made following the design indicated in the diagram of Fig. 2 polytetrafluoroethylene (PTFE) reactors, 115 ml internal volume, with 1 cm wall thickness and screw caps were used for the treatment of samples in the microwave oven.

A Hewlet Packard 8452 A diode array spectrophotometer, equipped with HP 89530 A MS DOS UV/V software with a response time of 0.1 s, was used to carry out the spectrophotometric determinations. A flow cell of 50 μl internal

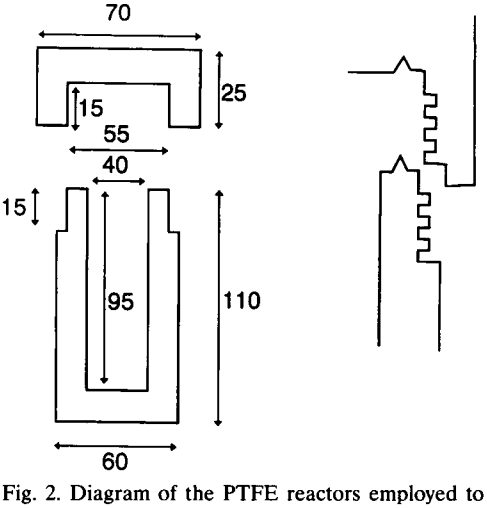

Fig. 2. Diagram of the PTFE reactors employed to carry out the alkaline hydrolysis of formetanate. Note: all the measurements are in mm and the detail corresponds to the screw cap.

volume and 1 cm pathlength was used for the measurements.

A four-channel flow injection (FI) manifold (Fig. 3) was employed to carry out the Fl spectrophotometric determination of MAP (obtained by microwave assisted hydrolysis of formetanate) by reaction with PAP. A Gilson P2 minipuls peristaltic pump was used to transport the carrier solutions.

As indicated in Fig. 3, channel A was used to transport PAP and channel B for the introduction of a potassium metaperiodate solution. Channel C was employed to transport samples and standard solutions by a carrier water flow in which 100 μl volumes were injected using a Rheodyne type 50 injection valve. Channel D provides the transport of sodium hydroxide solution.

The A and B channels were connected by a Y-shaped merging zone, in order to provide a good mixture of PAP and metaperiodate. A similar connection was made between channels C and D and a further connection was made to join the A/B channel and the C/D channel before the measurement zone.

Flexible vinyl chloride pump tubes of 1.52 i.d., which provide a carrier flow-rate of 2 to 4 ml min^{-1} in each channel, were used.

A coil of 45 cm in length (LR1) permitted us to obtain the benzoquinoneimine form of PAP from its oxidation by potassium metaperiodate. A second coil (LR2), also 45 cm in length, provides a suitable alkaline medium for the reaction of samples with PAP. Another reaction coil (LR3), 800 cm in length, provides a good reaction yield between MAP and the reactive quinoneimine in order to produce the blue dye which is measured at 576 nm [58]. All the tubes, which have been used to construct the reaction coils, are made of PTFE with an internal diameter of 0.8 mm.

Reagents

Formetanate hydrochloride was supplied by Riedel de Häen (Germany), *p*-aminophenol (PAP) was supplied by Fluka (Switzerland), *m*-aminophenol (MAP) from Aldrich (Germany), sodium hydroxide and potassium metaperiodate were obtained from Probus (Spain).

Stock solutions were prepared in demineralized distilled water as follows: 20 mg of formetanate hydrochloride was dissolved in 100 ml of distilled water, then 25 ml of this solution was diluted to 100 ml with distilled water. This solution was used in the same day to avoid the hydrolysis of formetanate.

PAP stock solution was freshly prepared each day by dissolving 0.0287 g in 250 ml of boiled and cooled distilled water.

Standard stock solution of MAP was prepared by dissolving 0.025 g in 250 ml of distilled water.

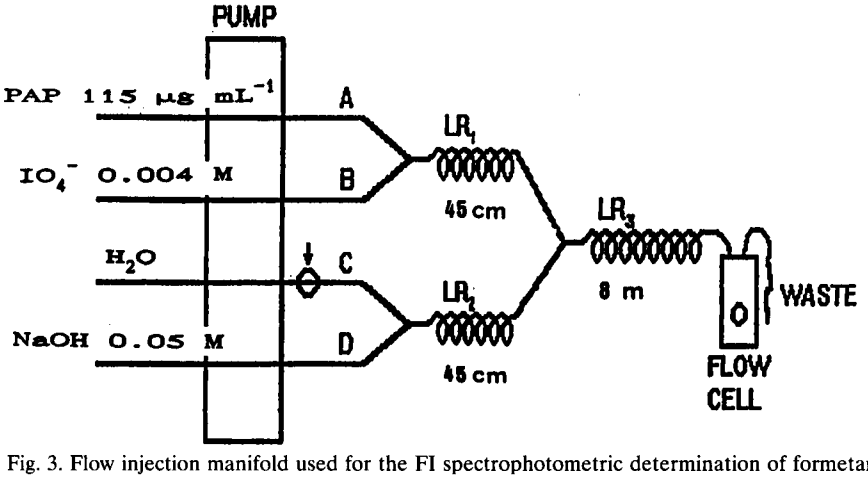

Fig. 3. Flow injection manifold used for the FI spectrophotometric determination of formetanate as MAP. LR1, LR2, LR3 are the reaction coils used to carry out the different steps of the reaction.

In all cases, an ultrasonic water bath was used to ensure a complete dissolution of the concerned compounds.

Conventional hydrolysis method

Aliquots of 10 ml of a 200 μg ml^{-1} solution of formetanate (which correspond to 84.8 μg ml^{-1} of MAP) were put into a series of 100 ml volumetric flasks and then, 2, 3, 5, 10 and 30 ml of 1 M aqueous NaOH solution were added and samples diluted up to the mark with distilled water in order to obtain 0.02, 0.03, 0.05, 0,1 and 0.3 M of NaOH respectively. All the flasks were put in a thermostatic water bath at 90°C. The absorbance measurements were carried out in the batch mode at 10-min intervals of time at a wavelength of 292 nm against 8.48 μg ml^{-1} of standard MAP solution.

Microwave assisted digestion method

0.02 g of formetanate was dissolved in distilled water and diluted to 100 ml. This stock solution was used to study the microwave assisted hydrolysis parameters. To study the effect of the experimental variables, on the alkaline hydrolysis in the microwave oven, different volumes of the stock solution were treated with the same volumes of several concentrations of NaOH, for 1–7 min, at various power levels.

After digestion, samples were diluted to 25 ml with distilled water and MAP was determined with PAP using FI spectrophotometry.

FI spectrophotometric determination of MAP

To control the hydrolysis of formetanate to MAP, 100 μl of the treated samples are injected

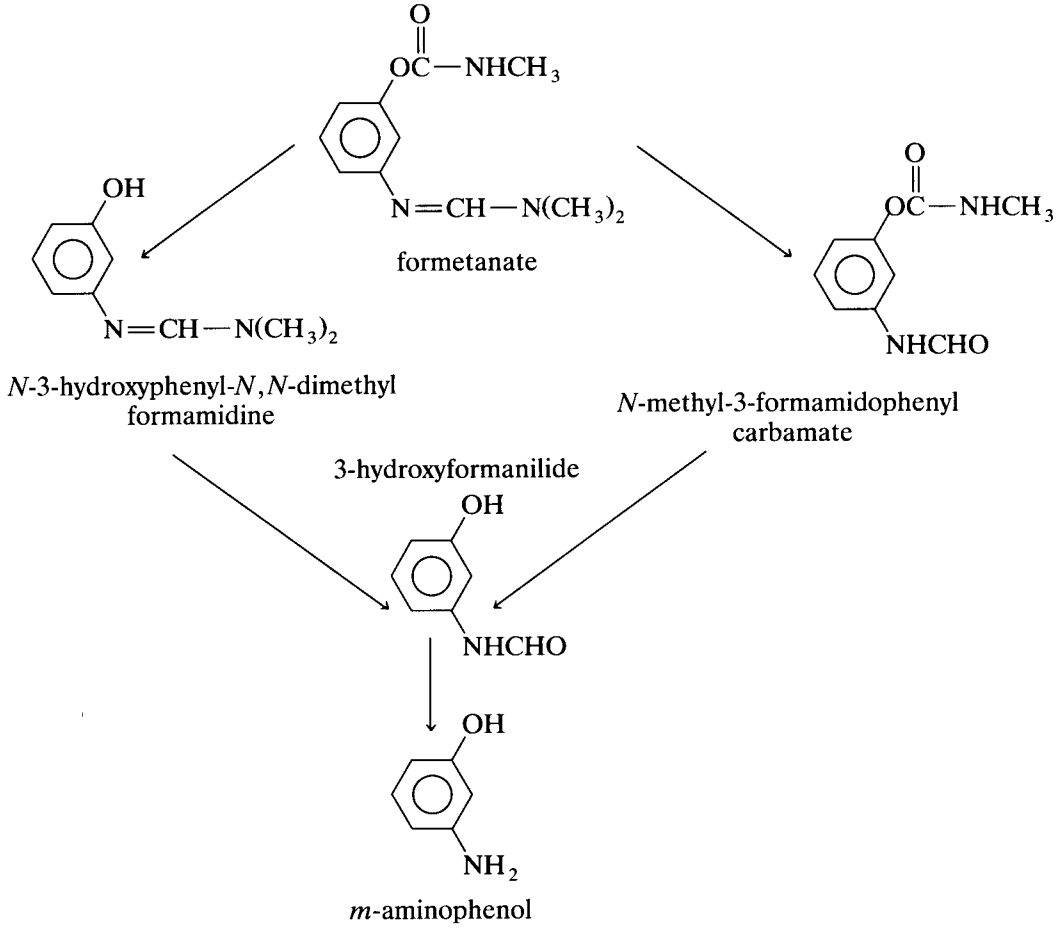

Scheme 1.

in the FI manifold of Fig. 3, using a carrier flow of 3.2 ml min^{-1} for each channel and the following concentrations of reagents: 115 $\mu g\ ml^{-1}$ PAP, 0.05 M NaOH and 0.004 M KIO_4. In the above conditions [58], a typical calibration line $A = 0.003 + 0.0132C$ (C in mg l^{-1} of MAP), with a regression coefficient $R = 0.9999$ was obtained for the concentration range from 2 to 8 mg l^{-1} and for the absorbance measurements at 576 nm.

RESULTS AND DISCUSSION

Hydrolysis of formetanate

Few papers reported on the hydrolysis of formetanate and similar compounds [35–38]. In these publications it was found that the hydrolysis rate of the *N*-methylcarbamoyl group of formetanate is affected by the protonated or non-protonated *N*,*N*-dimethylformamidine group. The suggested reaction mechanism of formetanate hydrolysis in a mixture of dioxane–water (4 : 1) at 60°C is shown in Scheme 1 [35].

It was mentioned also that, at the reaction conditions chosen, the subsequent hydrolysis of 3-hydroxyformanilide to MAP is very slow and that its velocity increases with increasing temperature. Therefore, several experiments about the effect of NaOH concentration and hydrolysis time, on the hydrolysis yield of formetanate to MAP, were carried out in a water bath at 90°C, and it has been found that a reaction time higher or equal to 2 h is necessary to obtain a hydrolysis yield of 95% in 0.02 M NaOH. This reaction time can be reduced by increasing the NaOH concentration by more than 15 times, but in strong alkaline conditions the spectrophotometric determination of MAP, by reaction with PAP, presents serious difficulties.

Microwave assisted hydrolysis of formetanate

In order to reduce the time required to carry out the complete hydrolysis of formetanate (using low NaOH concentrations) a series of experiments in closed PTFE reactors was carried out.

Effect of microwave parameters

The effect of experimental parameters on the hydrolysis of formetanate; such as the radiation power supplied, hydrolysis time, total volume of reagents into the reactor, and NaOH concentration, was studied. The percentage of hydrolysis efficiency was calculated from the quotient between the theoretical MAP concentration expected and that obtained after microwave-assisted hydrolysis.

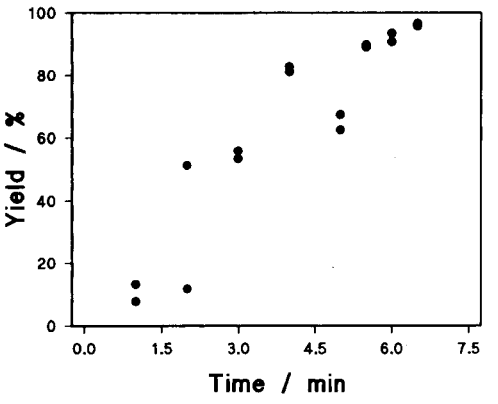

Fig. 4. Effect of the digestion time on the hydrolysis efficiency of formetanate for an applied power of 260 W (reaction conditions: 2 ml 0.1 M NaOH + 2 ml 200 mg l^{-1} formetanate).

Effect of the radiation power and time

Figures 4 and 5 show the effect of the digestion time on the hydrolysis efficiency at two different power levels. In these experiments the concentration of both formetanate and NaOH were kept constant.

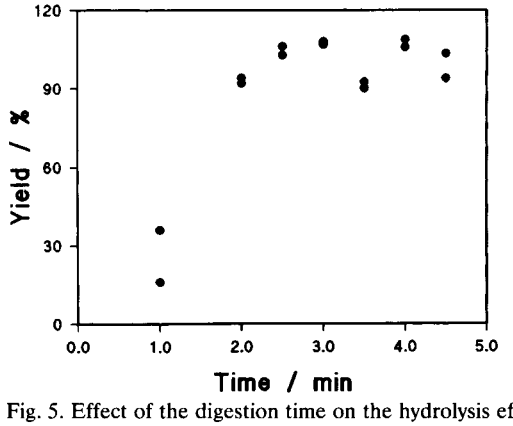

Fig. 5. Effect of the digestion time on the hydrolysis efficiency of formetanate for an applied power of 390 W (reaction conditions: 2 ml 0.1 M NaOH + 2 ml 200 mg l^{-1} formetanate).

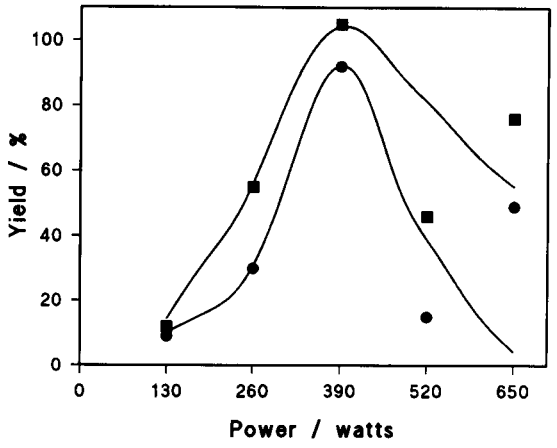

Fig. 6. Effect of the radiation power on the hydrolysis yield of formetanate to *m*-aminophenol. Measurements were carried out after a fixed irradiation time of 2 min (●) and 3 min (■), carrying out the hydrolysis of 2 ml 200 mg l^{-1} formetanate with 2 ml 0.1 M NaOH.

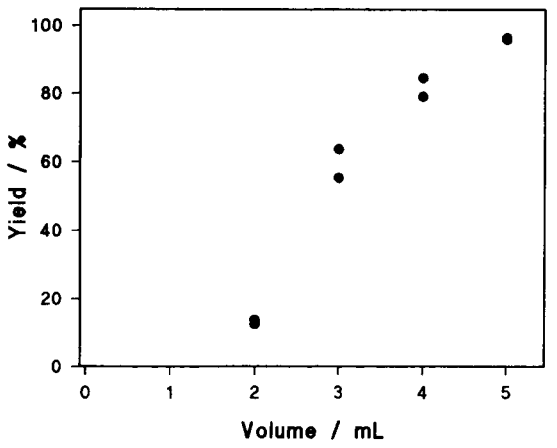

Fig. 7. Effect of the total volume of reagent on the hydrolysis efficiency of formetanate for 135 s and 390 W using 1:1 volumes of 0.1 M NaOH and 200 mg l^{-1} formetanate.

As can be seen, an increase in the exposure time provides an increase in the hydrolysis yield. At 40% power level (which corresponds to 260 W) the maximum hydrolysis yield is obtained after 390 s. However, at 390 W power, an appreciable increase in the hydrolysis efficiency is obtained and only 150 s is required to obtain a quantitative hydrolysis of formetanate.

On the other hand, the use of radiation power levels $\geq 80\%$ of the maximum exit power could cause leaks during the hydrolysis providing lower efficiency values (Fig. 6) and thus an irradiation power ≥ 520 W must be avoided. However, in order to provide the power supplied to the samples, no additional loading was introduced into the oven.

Effect of the total volume of reagent

Figure 7 shows the effect of the reagents volume on the hydrolysis yield of formetanate.

For this experiment, increasing volumes of a 100 mg l^{-1} solution of formetanate and identical volumes of 1 M NaOH were introduced into the reactor and then treated at 390 W during 135 s.

It is clear that the reaction yield increases when the total volume into the reactor increases. A volume of 4 ml was selected because 5 ml could cause leaks from the reactors.

Effect of NaOH concentration

Figure 8 shows the effect of NaOH concentration on the hydrolysis yield of formetanate at a power level of 390 W and an irradiation time of 150 s. An increase in the NaOH concentration provides an increase in the hydrolysis efficiency for concentrations between 0.025 and 0.1 M, but higher concentrations do not provide increases in the hydrolysis efficiency. Therefore a concentration of 0.1 M of NaOH was selected.

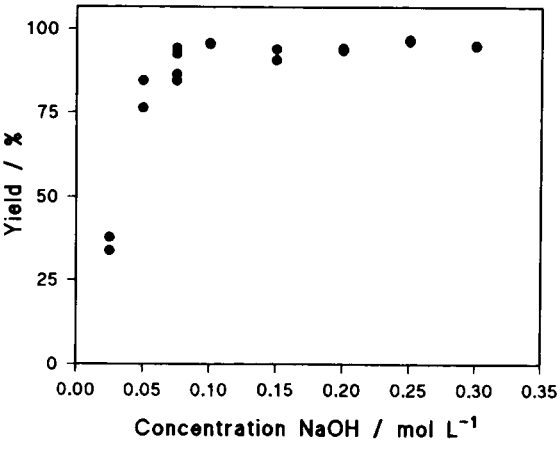

Fig. 8. Effect of NaOH concentration on the hydrolysis efficiency of formetanate using 2 ml NaOH, 2 ml 200 mg l^{-1} formetanate, 150 s and 390 W.

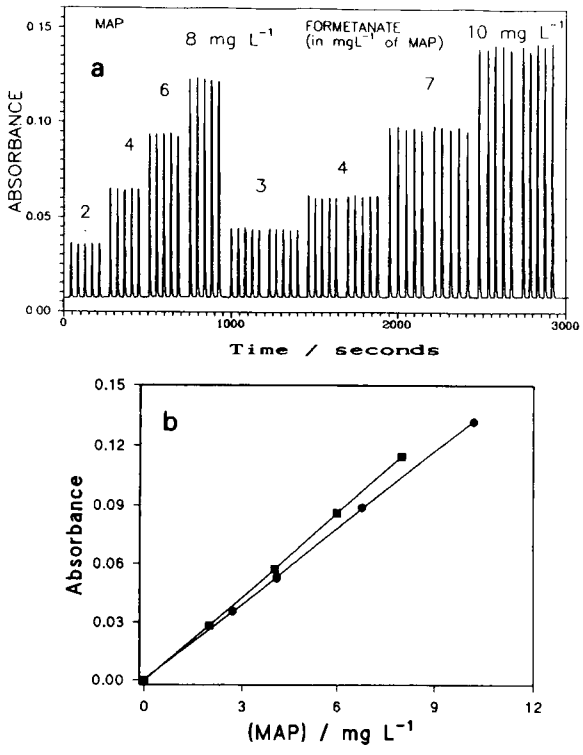

Fig. 9. (a) FI recording obtained for the determination of MAP by FI spectrophotometry, using PAP, and those corresponding to formetanate solutions after microwave assisted hydrolysis to MAP. The formetanate concentrations are expressed in mg l^{-1} of MAP theoretically obtained from the quantitation hydrolysis of formetanate. (b) Calibration lines obtained for MAP and formetanate solutions by FI spectrophotometry.

Recommended procedure for the microwave assisted hydrolysis

From the experiments carried out, the following procedure can be recommended to hydrolyze formetanate to MAP. Introduce 2 ml of a sample containing formetanate and 2 ml of a solution of 0.2 M NaOH into a 115-ml PTFE reactor, equipped with a hermetic screw cap. Close the reactor and introduce it into the microwave oven carrying the irradiation at 390 W for 150 s and cool down. Open the reactor and dilute to 25 ml with distilled water.

Analytical application of formetanate hydrolysis

Figure 9a shows the typical FI recording corresponding to a calibration for the MAP determination with PAP, and peaks found for different formetanate standards, previously hydrolyzed in a microwave oven (F). In Figure 9b the calibration line for both series of standards are shown which correspond to: MAP, $A = -0.0004 + 0.0143C$, $R = 0.999993$; F, $A = 0.0004 + 0.0130C$, $R = 0.99996$, where A is the absorbance peak height measured at 576 nm, C the MAP concentration in mg l^{-1} of directely injected or that corresponding to the quantitative hydrolysis of formetanate, expressed in mg l^{-1} of MAP and R is the regression coefficient.

From these data, the hydrolysis yield of formetanate can be evaluated from the quotient between the slope of both lines. In this case, a 91% hydrolysis yield can be obtained for the full range of formetanate concentrations considered. On the other hand, the good linearity of the formetanate solutions proves the good reproducibility of the microwave-assisted alkaline hydrolysis of the pesticide.

From the calibration data, the limit of detection can be established as 0.025 mg l^{-1} of formetanate, for $k = 3$ (a probability level of 99.86%), and the repeatability of the procedure corresponds to a relative standard deviation of 0.5% for five independent analysis of a sample containing 6 mg l^{-1}

In the above mentioned conditions, a series of water samples, spiked with known concentrations of formetanate, were hydrolyzed in the microwave oven and the obtained MAP determined by FI spectrophotometry with PAP [58]. Results found are summarized in Table 1, and, as it can

TABLE 1

Analysis of water samples spiked with known concentrations of formetanate

	Formetanate added (mg l^{-1})	Formetanate found (mg l^{-1})	Recovery (%)
Well water	2.71	3.04 ± 0.06	112
	4.07	4.33 ± 0.03	106
	6.78	7.12 ± 0.05	105
Tap water	2.74	2.87 ± 0.04	105
	4.11	4.18 ± 0.06	102
	6.85	7.05 ± 0.04	103

be seen the developed procedure, provides accurate and reproducible results.

Conclusions

The developed procedure for the hydrolysis of formetanate to MAP is a fast and reproducible way for the quantitative derivatization of formetanate, which can be applied as a previous step for the different methods of formetanate analysis which requires a previous hydrolysis.

As compared to the classical thermal hydrolysis at 90°C, and using a 0.1 M NaOH solution, the microwave assisted procedure is 16 times faster.

The authors thank the Spanish DGICYT for the financial support under project No. PB880351. Karim D. Khalaf wishes to thank the Spanish Institute of International Cooperation for the financial support to carry out the PhD Studies in Spain and A. Morales-Rubio acknowledges the Ministerio de Educación y Ciencia for the FPI grant.

REFERENCES

1 N.A. Jenny and K. Kossmann, Anal. Methods Pestic. Plant Growth, Regul., 12 (1978) 279.
2 B.F. Stone, P.W. Atkinson and C.O. Knowles, Pestic. Biochem. Physiol., 4 (1974) 407.
3 P.W. Atkinson and C.O. Knowles, Pestic. Biochem. Physiol., 4 (1974) 417.
4 J.F. Lawrence, L.G. Panopio, D.A. Lewis and H.A. Mcleod, J. Agric. Food Chem., 29 (1981) 722.
5 C.F. Aten and J.B. Bourke, J. Agric. Food Chem., 25 (1977) 1428.
6 T.K. Richard, J. Chromatogr., 185 (1979) 615.
7 G. Blaicher, W. Annhauser and H. Woidich, Chromatographia, 13 (1980) 438.
8 C.J. Miles and H.A. Moye, Anal. Chem., 60 (1988) 220.
9 S.H. Lee, T.S. Oh and K.H. Park, Taehan Hwahakhoe Chi., 34 (1990) 44.
10 S.N. Lanin, A.V. Ligaen and Y. Nikitin, Zh. Anal. Khim., 41 (1986) 1411.
11 L. Escade, D. Guillochon and D.J. Thomas, J. Chromatogr., 341 (1985) 373.
12 M.R. Detaevernier, W. Hoogewijis and D.L. Massart, J. Pharm. Biomed. Anal., 1 (1983) 331.
13 M.T. Bernabei, V. Ferioli, G. Gamberini and R. Cameroni, Atti Soc. Nat. Mat. Modena., 111 (1980) 35.
14 M. Goto, Y. Koyanagi and D. Ishii, J. Chromatogr., 20 (1981) 261.
15 J.L. Melvin, L.C. Bailey and T. Medwick, J. Chromatogr., 19 (1981) 146.
16 M. Maruyama and M. Kakemoto, Nippon Kagaku Kaishi, 12 (1987) 1646.
17 Y. Osaki and T. Matsueda, Bunseki Kagaku, 37 (1988) 253.
18 Y. Urushigawa, Z.Y. Yone, S. Mausanaga, F. Yamaguchi, M. Hirai and M. Tanaka, Kogai Shigen Kenkyusho Iho, 11 (1981) 83.
19 R.S. Dhillon, J. Singh, V.K. Gautam and B.R. Chabra, J. Chromatogr., 435 (1988) 256.
20 M. Blesova, J. Cizmarik and I. Majerikova, Chem. Pap., 42 (1988) 45.
21 M. Petrovic, M. Kastelan-Macan and A. Durrigi, Prehrambeno-Tehnol. Biotehnol. Rev., 27 (1989) 141.
22 C. Marutiou, V. Comam, A.D. Patrut, L. Romam and A. Gansca, J. Planar Chromatogr.-Mod. Tlc., 3 (1990) 435.
23 K. Nakashima, K. Muraki, S. Nakatsuji, S. Akiyama, T. Kaneda and S. Misumi, Analyst, 114 (1989) 501.
24 M. Ansheng and L. Xiulu, Yaowu Fenxi Zazhi, 9 (1989) 294.
25 A.l. Kostromin. D.G.Z. Badret, I.F. Abdullin and T.V. Yakimova, Zavod Lab., 55 (1989) 8.
26 C. Vetuschi and G. Rango, Spectrosc. Lett., 22 (1989) 51.
27 C. Vetuschi and G. Rango, Pharm. Acta Helv., 63 (1988) 290.
28 Y.I. Korenman and N.G. Sotnikova, Zh. Prikl. Khim. (Leningrad), 55 (1983) 2278.
29 R.T. Sane and A.Y. Dhamankar, Indian Drugs, 19 (1981) 74.
30 A. Mazzeo-Farina, M. Iorio and A. Laurenzi, Ann. Chim. (Rome), 71 (1981) 103.
31 K.W.Jr. Street and G. Schenk, J. Pharm. Sci., 68 (1979) 1306.
32 P.G. Sennikov, V.A. Kuznetsov, A.N. Egorchkin, M.A. Lopatin and Y.I. Korenman, Zh. Obshch. Kim., 50 (1980) 2761.
33 V.K. Phansalkar, A.V. Khedekar, A.S. Kalgaonkar and R.S. Pande, Indian J. Phys. B., 58B (1984) 487.
34 C. Gonzalez-Rojas and R.G.E. Morales, Spectrosc. Lett., 23 (1990) 243.
35 C. Alexander, S. Jaroslav and V. Miroslav, Collect. Czech. Chem. Commun., 45 (1980) 1065.
36 C. Alexander, S. Jaroslav and V. Miroslav, Collect. Czech. Chem. Commun., 43 (1978) 134.
37 M.L. Weiner, J. Org. Chem., 25 (1960) 2245.
38 M.J. Clark, M.W. Broks, S.A. Woods and W.M. Coli, J. Am. Soc. Hort. Sci., 112 (1987) 260.35
39 H.M. Kingston and L.B. Jassie (Eds.), Introduction to Microwave Sample Preparation. Theory and Practice. American Chemical Society, Washington, DC, 1988.
40 M. de la Guardia (Ed.), Empleo de los Hornos de Microondas en Quimica, Universidad de Valencia, Valencia, 1990.
41 K. Tee-Siew, Anal. Chem., 52 (1980) 1978.
42 J.A. Hesek and R.C. Wilson, Anal. Chem., 46 (1974) 8.
43 A. Abu-Samra, J.S. Morris and S.R. Koirtyohann, Anal. Chem., 47 (1975) 1475.

44 M. de la Guardia, A. Salvador, J.L. Burguera and M. Burguera, J. Flow Injection Anal., 5 (1988) 121.
45 H. Matusiewicz and R.E. Sturgeon, Prog. Anal. Spectrosc., 12 (1989) 21.
46 A. Morales-Rubio, A. Salvador and M. de la Guardia, Fresenius' J. Anal. Chem., 342 (1992) 452.
47 V. Carbonell, M. de la Guardia, A. Salvador, J.L. Burguera and M. Burguera, Anal. Chim. Acta, 238 (1990) 417.
48 V. Carbonell, A. Morales-Rubio, A. Salvador, M. de la Guardia, J.L. Burguera and M. Burguera, J. Anal. At. Spectrom., 7 (1992) 1085.
49 M. de la Guardia, V. Carbonell, A. Morales-Rubio and A. Salvador, Talanta, in press.
50 R. Gedye, F. Smith, K. Westaway, H. Ali, L. Baldisera, L. Laberga and J. Rousell, Tetrahedron Lett., 27 (1986) 279.
51 R.J. Giguere, T.L. Bray, S.M. Duncan and G. Majetich, Tetrahedron Lett., 27 (1986) 4945.
52 R.A. Abramovitch, Org. Prep. Proc. Int., 23 (1991) 683.
53 D.M.P. Mingos and D.R. Baghurst, Chem. Soc. Rev., 20 (1991) 1.
54 M. de la Guardia, A. Salvador, M.J. Gomez and Z.A. de Benzo, Anal. Chim. Acta, 224 (1989) 123.
55 A. Morales-Rubio, J. Cerezo, A. Salvador and M. de la Guardia, Microchem. J., in press.
56 S.H. Chiou and K.T. Wang, J. Chromatogr., 491 (1989) 424.
57 S.T. Chen, S.H. Chiou, Y.H. Chu and K.T. Wang, J. Peptide Protein Res., 30 (1987) 572.
58 K.D. Khalaf, J. Sancenón and M. de la Guardia, Talanta, in press.

Analytica Chimica Acta, 281 (1993) 259–264
Elsevier Science Publishers B.V., Amsterdam

Flow-injection determination of water in organic solvents by near-infrared spectrometry

Salvador Garrigues, Máximo Gallignani and Miguel de la Guardia

Department of Analytical Chemistry, University of Valencia, 50 Dr. Moliner St., 46100 Burjassot (Valencia) (Spain)

(Received 16th December 1992; revised manuscript received 15th March 1993)

Abstract

A flow-injection (FI) procedure was developed for the direct determination of water in organic solvents by using the O–H stretch absorbance band of water in the near-infrared (NIR) region. Dichloromethane was employed as a test solvent to study the influence of the flow parameters (carrier flow and sample injection volume) and time interval on the sensitivity and repeatability of the FI-NIR measurements. The developed procedure permits the determination of water in dichloromethane and isobutyl methyl ketone samples with limits of detection of 0.01 and 0.005% (v/v), respectively. Real and spiked samples of solvents were analysed by FI-NIR and accurate results were found. The method is rapid, it does not require any pretreatment of samples and it is free from contamination of samples by atmospheric humidity.

Keywords: Flow injection; Infrared spectrometry; Dichloromethane; Isobutyl methyl ketone; Organic solvents; Waters

The determination of the water content of organic solvents is currently carried out by the Karl Fischer coulometric method [1,2] or by gas chromatography [3,4]. However, the coulometric procedure gives poor precision and presents serious problems owing to slow reactions and interferences. On the other hand, the gas chromatographic procedures cannot be applied in the presence of inorganic electrolytes because salts are accumulated in the injection chamber.

For very low concentrations (of the order of a few μg ml^{-1}), a series of spectrophotometric procedures [5–13] have been proposed by using different reactions with inorganic and organic reagents. However, in general, these methods are slow and tedious, they require extensive sample handling and they show low reproducibility.

Correspondence to: M. de la Guardia, Department of Analytical Chemistry, University of Valencia, 50 Dr. Moliner St., 46100 Burjassot, Valencia (Spain).

Direct procedures, based on infrared (IR) measurements, provide fast and reproducible means for the determination of water in organic solvents in both the mid- [14,15] and near-IR (NIR) regions [15–20]. However, a series of precautions must be taken in order to avoid contamination of samples and reference solutions by water, specially when double-beam instruments are used.

In recent years, efforts have been made to avoid the principal drawbacks of the procedures for the determination of water by automation of the above methods using flow-injection (FI) analysis. This technique has been applied to the Karl Fischer procedure [21,22] and to spectrophotometric analysis [23]. However, no work has been reported on flow-injection analysis with NIR spectrometry.

The aim of this paper is to propose a simple and direct procedure for the routine determination of water in organic solvents. Two organic

solvents, one chlorinated solvent, dichloromethane (CH_2Cl_2), and one ketone, 4-methylpentan-2-one [isobutyl methyl ketone (IBMK)], were selected as test systems. Owing to a lack of previous experience with the FI automation of NIR procedures (only a few papers have been published on the use of NIR in liquid chromatography [24–26] and also on on-line determinations by using fibre-optics [27]), a systematic study of the effect of flow variables on the sensitivity and speed of water determination by FI-NIR was carried out.

EXPERIMENTAL

Apparatus and reagents

A Perkin-Elmer Lambda 9 double-beam UV–visible–NIR spectrophotometer equipped with a tungsten–halogen lamp source and a PbS detector was used for absorbance measurements in the NIR region. The spectrometer covers a wavelength range from 185 to 3200 nm and is equipped with a monochromator with 360 lines mm^{-1} to work in the NIR region. An Epson EL2 computer with a PECSS software package for UV–visible–NIR (release 4.01) controls the spectrometer and permits absorbance measurements to be made sequentially in the full region or at a fixed wavelength as a function of time. Optical glass cells of path length of 1 cm and 1 mm were employed for batch measurements and a quartz flow cell of path length 1 cm, with a volume of 30 μl, for the FI measurements.

For the determination of water content by the Karl Fischer procedure a Crison KF Model 431 titrator equipped with a Crison Model 738 burette was employed. Hydranal solvent and Hydranal Titrant 5 from Riedel-de Haën (Hannover) were used.

All the solvents employed were of analytical-reagent grade (Panreac, Spain), previously distilled and dried by using 4 Å molecular sieve from SDS (Peypin, France).

For absorbance measurements in the FI mode the two manifolds indicated in Fig. 1 were employed. In both instances a Rheodyne RS 50 PTFE rotary valve was used to introduce discrete volumes of samples into the flow cell. To avoid air bubbles, the injection coil was filled by aspiration using a Gilson P2 peristaltic pump. For the determination of water in CH_2Cl_2 a second peristaltic pump was used to transport a dry solvent carrier flow using solvent-resistant flexible Iso-Versinic tubing of 1.5 mm i.d.. However, for the IBMK analysis adequate flexible tubing could not be found so nitrogen gas pressure was employed to transport the carrier. In the latter instance a needle valve ensured a fixed pressure and a glass column packed with silica gel and a coloured indicator was employed to retain the water of the carrier gas. In both manifolds 0.8 mm i.d. PTFE tubing was employed.

General procedure

CH_2Cl_2 was employed to study the effect of the different FI and instrumental parameters on the determination of water by NIR spectrometry.

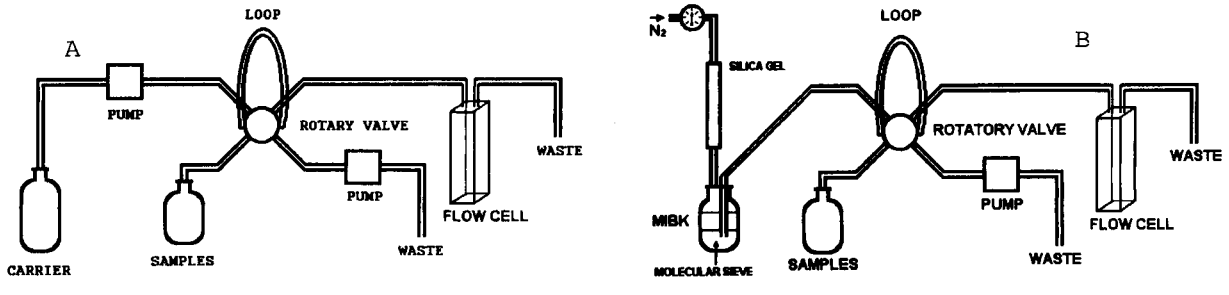

Fig. 1. Manifolds employed for the FI-NIR determination of water in (A) CH_2Cl_2 and (B) IBMK.

The effects of the injection volume, flow-rate and time interval were studied in a univariate mode and the optimum conditions were selected to obtain rapid, sensitive and reproducible measurements. Water was then determined in real saturated CH_2Cl_2 and IBMK samples and in a series of IBMK spiked samples with a known content of water. The results obtained were compared with those obtained by the Karl Fischer procedure.

Recommended procedure

From the results of experiments to determine the optimum conditions, the following procedure can be recommended for the determination of water in CH_2Cl_2.

Inject a volume of the order of 200 μl of sample in a carrier flow of 1.5 ml min^{-1} of dry CH_2Cl_2 and measure the absorbance at 1898 nm using a time interval of 0.3 s. Interpolate the peak-height values obtained on a calibration graph obtained using standard solutions of water in CH_2Cl_2. A sealed reference cell containing dry CH_2Cl_2, with molecular sieve, is used in all measurements in order to compensate for the background provided by the absorbance of the solvent.

RESULTS AND DISCUSSION

FI-NIR determination of water in dichloromethane

Pure water has an NIR absorption spectrum with five bands at 1940, 1450, 1190, 970 and 760 nm. The bands at 1450, 970 and 760 nm correspond to the first, second and third overtones of O–H stretch and those at 1940 and 1190 are combination bands involving O–H stretch and O–H bend [28]. Figure 2 shows the NIR spectrum of pure water in the range 800–2000 nm. All the above-mentioned bands are modified by hydrogen bonding when water is present in different types of solvents. The 1940-nm band provides, in general, the most selective measurement in order to determine water in organic solvents. In CH_2Cl_2 this band of water shifts to 1898 nm and can be employed for analytical purposes using the dry solvent in the reference beam.

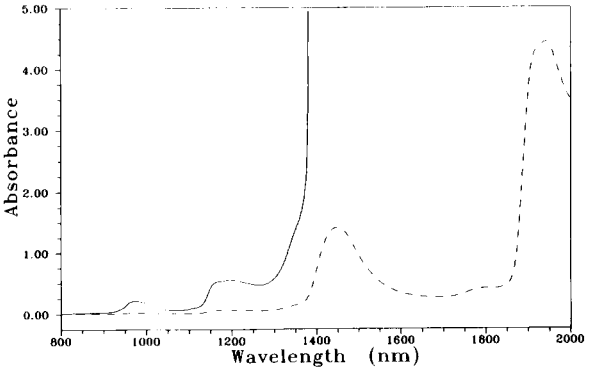

Fig. 2. NIR spectrum of pure water. The spectrum was obtained by using a 1-mm (dashed line) and a 1-cm (solid line) path length cell and carbon tetrachloride as reference.

The manifold shown in Fig. 1A was employed to determine the effect of the FI parameters on the analytical signals obtained at 1898 nm for the determination of water in CH_2Cl_2.

Effect of FI parameters

The effect of the sample injection volume on the absorbance measurements obtained for a water-saturated CH_2Cl_2 sample using a 1.5 ml min^{-1} carrier flow was studied, and it was found that the sensitivity of the absorbance measurements increases as the injection volume increases up to a volume of the order of 300 μl, and thereafter the absorbance tends to stabilize. In all instances reproducible measurements were obtained. However, the increase in the injection volume also increases the time required to obtain the corresponding FI recording and, as can be seen in Fig. 3, more than 24 s were necessary to obtain the full peak for an injection volume of 55 μl but only 15 and 14 s for volumes of 211 and 100 μl, respectively. Therefore, a sample injection volume of 211 μl was selected as a compromise between sensitivity and speed.

The carrier flow-rate has a small influence on sensitivity, as shown in Fig. 4. However, an increase in the carrier flow-rate also increases the sample throughput frequency; a flow-rate $\geq$ 1.5 ml min^{-1} provides a rapid analysis with a good sensitivity level.

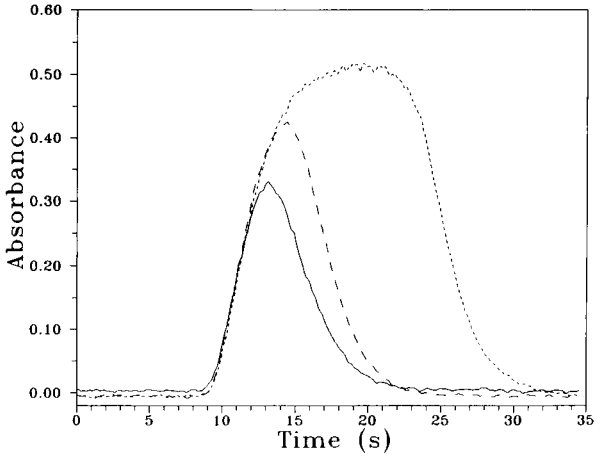

Fig. 3. Effect of sample injection volume on the FI peak: solid line, 100 μl; long dashed line 211 μl; short dashed line, 550 μl.

Effect of NIR parameters

The determination of water in CH_2Cl_2 by FI-NIR spectrometry is carried out at a fixed wavelength and using an automatically adjusted value of the slit. Hence the only parameter that can be modified is the time interval between two absorbance measurements.

Figure 5 shows that the use of short time intervals provides well defined FI peaks and that the use of time intervals > 2.5 s causes a loss of information about the absorbance of the injected sample, which can decrease the sensitivity of the FI measurements. On the other hand, the repeatability of the measurements decreases when the time interval is > 1 s. Concerning the sample frequency, it can be seen that the time interval does not modify the width of the FI peaks; the only problem caused by the use of short time intervals is the large number of data obtained for each experiment. A value of 0.3 s was selected.

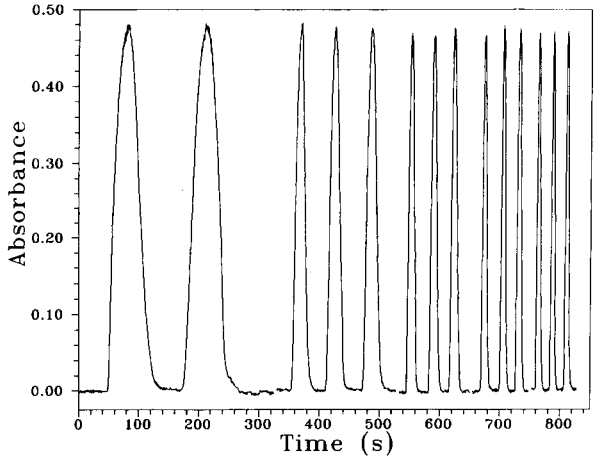

Fig. 4. Effect of carrier flow-rate on the sample throughput frequency for the determination of water in CH_2Cl_2 using an injection volume of 317 μl.

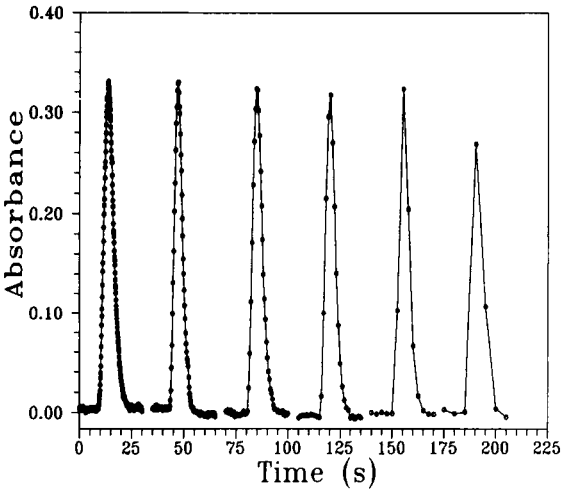

Fig. 5. Effect of the spectrophotometer measurement time interval on the FI recording obtained for a water-saturated CH_2Cl_2 sample. Carrier flow-rate, 1.5 ml min^{-1}; injection volume, 211 μl.

Analytical figures of merit of the determination of water in dichloromethane

Using the conditions in the recommended procedure, a typical regression line obtained for a water concentration range (C) between 0 and 0.2% (v/v) corresponds to

$$A = 0.002_7 + 2.34_6C$$

with a regression coefficient $r = 0.99990$ ($n = 9$), which gives a 3σ limit of detection of 0.01% (v/v) of water. The relative standard deviation (R.S.D.) for five independent measurements of a sample containing 0.1% (v/v) of water was 1.1% and 0.5% for a sample containing 0.2% (v/v) of water.

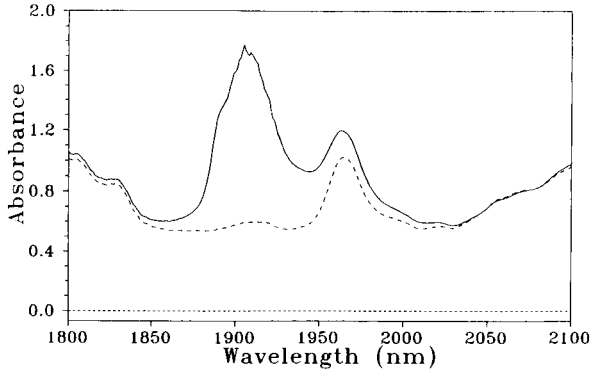

Fig. 6. NIR spectrum of (solid line) water-saturated IBMK and (long dashed line) dry IBMK using a reference of (short dashed line) CCl_4.

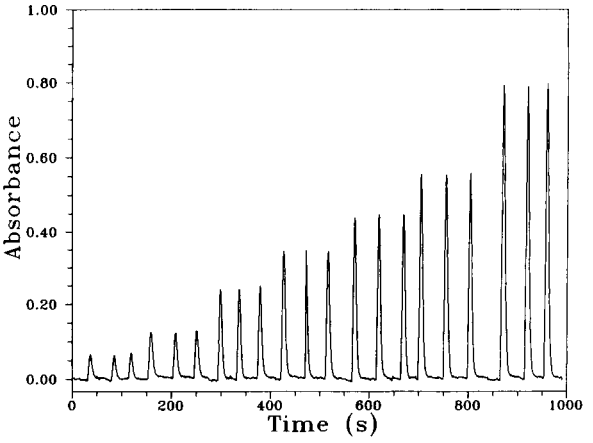

Fig. 7. FI recording obtained for different standard solutions of water in IBMK. Carrier flow-rate, 1.5 ml min^{-1}; sample injection volume, 211 μl; spectrophotometric measurement time interval, 0.3 s.

The developed procedure is rapid and provides a sample injection frequency of 257 h^{-1}.

FI-NIR determination of water in IBMK

The NIR spectrum of water in IBMK presents a well defined band at 1907 nm. As can be seen in Fig. 6, the spectrum of water-saturated IBMK, compared with that of dried IBMK, provides an absorbance range of 1.2 over which to carry out the direct measurement of the water content in this solvent.

Using the experimental conditions previously found for the determination of water in CH_2Cl_2, and taking into account that IBMK cannot be transported by using flexible Iso-Versinic or other flexible tubing, the manifold shown in Fig. 1B was employed for the determination of water in IBMK. In this instance a needle valve was employed to control the nitrogen pressure and to fix the transport carrier flow-rate.

Analytical figures of merit for the determination of water in IBMK.

Figure 7 shows a typical FI recording obtained for a series of water in IBMK standards. From these measurements a linear calibration graph is obtained up to a water concentration (C) of ca. 0.5% (v/v), corresponding to

$$A = 0.003_8 + 1.09C$$

with $r = 0.9998$ ($n = 9$). Under these conditions, the 3σ limit of detection was 0.005% (v/v) and the R.S.D. for five independent measurements of a sample containing 0.2% (v/v) of water was 0.6% and 0.3% for a sample containing 0.4% (v/v) of water. The sample injection frequency is 257 h^{-1}.

Determination of water in real and spiked IBMK samples

The solubility of water in IBMK is ca. 1.52% (v/v) measured at ambient pressure and temperature. Under these conditions, a water-saturated IBMK sample was analysed by FI-NIR spectrometry; a concentration of $1.54 \pm 0.02\%$ (v/v) was found from five independent analyses, which is identical with the value obtained using the Karl Fisher method.

TABLE 1

Determination of water added to IBMK samples

Water content (%, v/v)		Relative error (%)
Added	Found (mean ± S.D.) ($n = 5$)	
0.0750	0.0754 ± 0.0009	0.5
0.150	0.148 ± 0.002	−1.3
0.350	0.347 ± 0.004	−0.9
0.126	0.129 ± 0.002	2.4
0.262	0.260 ± 0.002	−0.8
0.374	0.370 ± 0.004	−1.1

A series of spiked samples of water in IBMK were prepared by dissolving known amounts of water in dry and previously analysed IBMK. The data in Table 1 indicate the good recovery of the FI-NIR procedure, which provides relative errors lower than 2.5% for the analysis of samples with water contents between 0.075 and 0.375% (v/v). A standard deviation of five independent measurements lower than 0.004% (v/v) was found in all instances. Hence it can be concluded that the developed procedure is accurate and precise.

Conclusions

The results obtained in this study indicate that the FI-NIR procedure developed for the determination of water in organic solvents is very rapid and does not require any pretreatment of samples, providing accurate and precise results. Compared with the batch procedure the method incorporates all the typical advantages of automated methods concerning to the use of small amounts of sample and saving of time. The use of a well designed manifold avoids the contamination of the carrier and samples by the atmospheric humidity and the fact that no other reagent is needed reduces the cost per analysis and avoids the need for tedious pretreatment of reagents.

The limits of detection for water in CH_2Cl_2 and IBMK are comparable to those found obtained using FI spectrophotometry [23]; only the lead tetraacetate method [5] provides a better sensitivity and limit of detection.

S. Garrigues acknowledges a grant from the Conselleria de Cultura, Educació i Ciència de la Generalitat Valenciana, for carrying out PhD studies. M. Gallignani acknowledges a grant from the Agencia Española de Cooperación Internacional for carrying out PhD studies and financial support of Los Andes University and CONICIT (Venezuela).

REFERENCES

1 E.W. Blank and R.M. Kelley, in F.J. Welcher (Ed.), Standard Methods of Chemical Analysis, Vol. III B, Van Nostrand, New York, 1966.
2 Metrohm KF-Processor/Dosimat, Int. Lab., March (1984) 64.
3 O.L. Hollis and W.V. Hayes, J. Gas Chromatogr., 4 (1966) 235.
4 R.J. Jasinski and S. Kirkland, Anal. Chem., 39 (1967) 1663.
5 C.D. Thompson, F.D. Bogar and R.T. Foley, Anal. Chem., 42 (1970) 1474.
6 C.L. Luke, Anal. Chim. Acta, 54 (1971) 447.
7 C.E. Matkovich and G.D. Christian, Anal. Chim. Acta, 60 (1972) 319.
8 A.A. Muk, T.V. Petrova and S.B. Savin, Zh. Anal. Khim., 28 (1973) 1777.
9 H. Langhals, Fresenius' Z. Anal. Chem., 305 (1981) 26.
10 A.T. Pilipenko, E.R. Falendysh and N.F. Falendysh, Otkrytiya Izobret, 26 (1985) 176.
11 A.T. Pilipenko, E.R. Folendysh, O.M. Drapailo and V.A. Zayats, Zh. Anal. Khim., 41 (1986) 94.
12 A.T. Pilipenko, O.M. Drapailo and E.R. Falendysh, Otkrytiya Izobret, 43 (1988) 184.
13 A.T. Pilipenko, E.R. Falendysh, O.M. Drapailo and V.A. Zayats, Zh. Anal. Khim., 44 (1989) 51.
14 A. Barbetta, W. Edgell, Appl. Spectrosc., 32 (1978) 93.
15 J. Ludvík, S. Hilgard and J. Volke, Analyst, 113 (1988) 1729.
16 H.F. Cordes and C.W. Tait, Anal. Chem., 29 (1957) 485.
17 D. Chapman and J. Nacey, Analyst, 83 (1958) 377.
18 H.G. Streim, E.A. Boyce and J.R. Smith, Anal. Chem., 33 (1961) 85.
19 R.L. Meeker, F.E. Critchfield and E.T. Bishop, Anal. Chem., 34 (1962) 1510.
20 R. Jasinski and S. Carroll, Anal. Chem., 40 (1968) 1908.
21 I. Nordin-Andersson, O. Åström and A. Cedergren, Anal. Chim. Acta, 162 (1984) 9.
22 Y.Y. Liang, Anal. Chem., 62 (1990) 2504.
23 M. Guzman, J.L. Pérez-Pavón, E. Rodríguez Gonzalo, C. Hatfield, J. Ruzicka and G.D. Christian, Analyst, 116 (1991) 1043.
24 E.W. Ciurczak and F.M.B. Weis, Spectroscopy, 2 (1987) 33.
25 E.W. Ciurczak and I.M. Vance, Spectroscopy, 3 (1988) 56.
26 E.W. Ciurczak and T.A. Dickinson, Spectroscopy, 6 (1991) 12.
27 A.F. Parisi, L. Nogueiras and H. Prieto, Anal. Chim. Acta, 238 (1990) 95.
28 B.G. Osborne and T. Fearn, Near Infrared Spectroscopy in Food Analysis, Longman, Harlow, 1988.

Analytica Chimica Acta, 281 (1993) 265–270
Elsevier Science Publishers B.V., Amsterdam

Near-infrared sensing utilising the evanescent field

A.R. Lennie and F. Kvasnik

Department of Instrumentation and Analytical Science, UMIST, P.O. Box 88, Manchester M60 1QD (UK)

(Received 5th October 1992; revised manuscript received 16th March 1993)

Abstract

A new fibre optic sensing system used to determine the water content of a solvent is described. The transduction mechanism is absorption of the evanescent field by the water with the consequent reduction of the transmitted optical power in an optical fibre. The viability of this sensing system was demonstrated on mixtures of water and acetone using 950-nm excitation which overlaps the O–H stretching overtone of water. A complex non-linear relationship between transmitted optical power, absorbant concentration and the length of the interaction region was observed and is discussed in detail.

Keywords: Infrared spectrometry; Acetone; Evanescent field; Fibre optic sensors; Waters

The near-infrared region of the electromagnetic spectrum offers interesting analytical possibilities, particularly for the determination of compounds containing OH, NH, or CH groups. Compounds having OH groups, for example, show strong absorption in the region of fundamental hydrogen stretching overtones at 2730–3100 nm, and at the first and second overtones at 1365–1550 and 910–1033 nm.

Near-infrared spectroscopy exploiting these OH absorption peaks is used to determine the water content of many process constituents. Conventional near-infrared absorption techniques have been used to determine the water content of aqueous mixtures of alcohols and other soluble solvents [1]. Such spectral information can also be obtained by internal reflection spectroscopy. This technique has been used to make infrared spectra measurements of solid materials [2] and measurements of real and imaginary parts of the refractive index of absorbing fluids using a rod photoreflectometer [3].

Correspondence to: F. Kvasnik, Department of Instrumentation and Analytical Science, UMIST, P.O. Box 88, Manchester M60 1QD (UK).

These spectroscopic techniques, however, are not readily adaptable to meet current requirements for remote chemical sensing and real-time continuous analysis [4]. One solution is to use optical fibres to interface conventional instruments to the process stream, another is to use the optical fibre as a transducer or sensor. The latter approach exploits the property of the evanescent field.

Analysis of total internal reflection phenomena based on wave theory predicts a phase shift of the reflected wave relative to the incident wave, and the existence of a standing electromagnetic wave in the lower refractive index medium [5]. The electric field amplitude of this wave decays exponentially from the reflecting interface into the lower refractive index material. This field is referred to as the evanescent field and can be described by

$$E(z) = E_0 \exp(-z/d) \qquad (1)$$

where z is the distance normal to the optical interface, E_0 the electric field amplitude of the propagating wave at the optical interface, and $E(z)$ the electric field amplitude in the rarer medium. The penetration depth, d, is defined as

the distance required for the electric field to fall to e^{-1} of its value at the surface. This penetration depth is about one tenth the wavelength of the light travelling in the denser medium near grazing incidence and increases to about one wavelength for incident angles about one degree greater than the critical angle. The depth of penetration becomes infinitely large as the angle of incidence approaches the critical angle. In approximate terms, only material located within one wavelength of an interface will have significant interaction with the evanescent field. In an optical fibre, the evanescent field around the fibre core is a superposition of component evanescent fields of the modes propagating within the fibre.

An absorbing medium placed in contact with the reflecting interface can extract energy from the evanescent wave and the amplitude of the total internal reflection decreases. For a fibre sensor operating by attenuation of the evanescent field by an absorbing gas, Tai et al. [6] defines the transmittance of light through the fibre by the following equation:

$$I = I_0 \exp(-\alpha r c L) \quad (2)$$

where I is the transmitted intensity, I_0 the incident intensity, α the absorption coefficient of the absorbing material, r the ratio of power of the evanescent wave to the total propagating power, c the concentration, and L the sensor length. This equation can be written in a manner of the Beer–Lambert relation such that

$$\log (I_0/I) = 0.4342 (\alpha r c L) \quad (3)$$

The ratio of power of the evanescent wave to the total propagating power, r, has been shown [7] to be a function of the optical fibre core radius, the core and cladding refractive indices, and the wavelength of the electromagnetic wave propagating in the optical fibre. In the case of an absorbing cladding, where the refractive index becomes a complex function, departures from linearity in Eqn. 3 will occur.

Applications for sensors utilising evanescent field absorption have already been demonstrated. These include determination of methane concentrations using the 3.392-μm excitation [6], and detection of dissolved dyes using white light [3] or an argon ion laser [7] as spectral sources. Recently, utilisation of the near-infrared spectral region between 1 and 4.5 μm for sensing using evanescent absorption has been demonstrated [8,9]. These experiments, using a Fourier transform near-infrared (FT-NIR) spectrometer coupled to the optical fibre, were aimed at monitoring various mixtures of solvents, such as toluene in cyclohexane, ethanol in chloroform, or acetonitrile in alcohol.

The water OH absorption band centred around 960 nm, where attenuation due to CH groups is at a minimum [10], coincides with the emission range of solid state incoherent light sources. This suggests the possibility of configuring a relatively simple and inexpensive optical system capable of determining the water content of organic solvents.

The purpose of the work presented here is to demonstrate the potential of such a system and to investigate its limitations. Experiments were carried out to establish the sensitivity of this technique for the determination of water in acetone.

EXPERIMENTAL

A high-power near-infrared light emitting diode (LED) with peak emission at 940 nm was used as the light source. A simple circuit consisting of a 5-V power supply and a 55-Ohm resistor in series with the LED gave a continuous current of 67 mA through the LED, within the specified maximum forward continuous current.

The curved front surface of the LED was filed flat and polished to aid coupling of light via a microscope objective into the optical fibre. The LED was then fitted into a matt black plate. A Photodyne silicon photodiode detector was used to measure to LED light output.

The peak emission wavelength and the full width half maximum (FWHM) of the LED were 935 and 40 nm, respectively. An interference filter with a bandpass of 10 nm centred at 950 nm was used to select from this spectrum a narrow band of wavelengths corresponding to the absorption band of water.

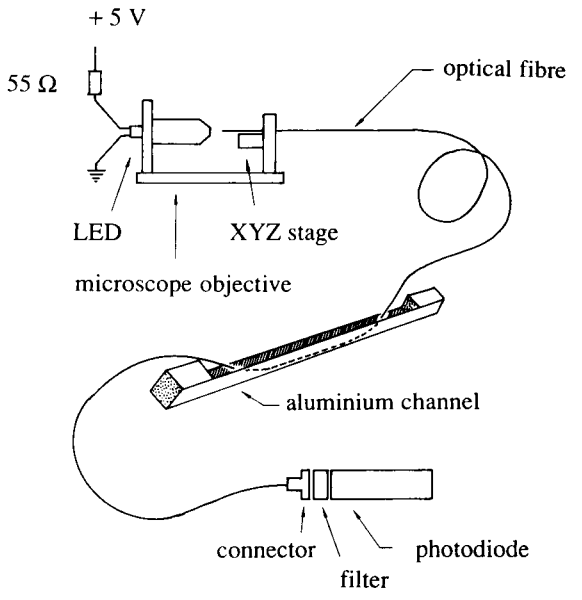

Fig. 1. Experimental configuration for absorption measurements utilising the evanescent field of the optical fibre.

The transmittance of water and acetone mixtures was measured by placing a standard cuvette between the LED and the detector. Three sets of measurements of acetone and water mixtures, ranging from pure acetone to pure water, were taken. The transmittance of each mixture was normalised to the value obtained with pure acetone present in the cuvette.

Evanescent absorption measurement

Figure 1 shows the experimental arrangement for the measurements of the evanescent field absorption. A 20 × microscope objective was used to efficiently launch the light into the fibre, ensuring that the light fully filled the numerical aperture of the fibre. The fibre itself was secured by a magnetic bar into a V-grove in a steel block to an XYZ stage. This allowed small positional adjustments to be made in order to achieve maximum light coupling efficiency into the fibre. The plastic coating and polymer cladding of the optical fibre were stripped back 2 cm from each end of the silica fibre core, and the optical fibre end-face was cleaved. At the other end of the fibre, the fibre was mounted in a connector and the protruding silica core was then cleaved. The fibre ends were examined under a microscope to check that the cleaved ends were clean since the light coupling into and out of the fibre is very dependent on the quality of these faces. The fibre connector was then attached to the detector.

The optical fibres used had a core diameter of 200 μm, and were 1.5 m in length. Each fibre had sections of silica core exposed by peeling off the plastic coating with a scalpel. The soft polymer cladding underneath this coating was then carefully scraped off and the exposed core cleaned by several washings with acetone. Five lengths of optical fibre with exposed cores of 10, 20, 30, 40 and 50 cm were prepared in this fashion.

For measuring absorbance of light from the fibre core, an aluminium channel was constructed to contain liquid in which the exposed fibre core could be immersed. Aluminium angle 1 m in length was supported at both ends in order to hold the extrusion with sides at 45° to the vertical thus forming a channel. Each end of this channel was stopped using a square sectioned piece of aluminium clamped into the channel with a silicone rubber seal to prevent loss of liquid.

Evanescent sensing of solvent–water mixtures

To measure changes in light throughput of an optical fibre when the exposed fibre core was immersed in absorbing water and solvent mixtures, seven solutions of water in acetone were prepared with concentrations of 2.6, 5.1, 7.2, 9.3, 15.9, 20.8 and 24.7 mol l^{-1} of water.

The exposed core of optical fibre was immersed in the set solution contained in the aluminium channel. To overcome surface tension effects which tended to lift the fibre out of the test solution, the fibre was immersed by careful tensioning at each end of the exposed section with small weights. Measurements of the transmitted power through the optical fibre were then taken.

For each length of exposed core, the fibre was first exposed to pure acetone and the transmitted power measured. The acetone was then removed from the channel and the channel dried. This procedure was repeated for each solution working from lower to higher concentrations of water.

Three cycles of readings were made for each

length of exposed fibre working from pure solvent through to progressively higher water concentrations. After the final prepared solution had been added and the reading taken, a further aliquot of deionised water was added to the 24.7 mol l^{-1} solution. Again the measurements of the transmitted optical power were normalised to the values obtained with only pure acetone surrounding the exposed core.

RESULTS AND DISCUSSION

The measurements of transmittance of a cuvette containing mixtures of acetone and water demonstrated a linear relationship (slope −0.0045, intercept 0.984, and correlation coefficient 0.997) between the transmittance and the concentration of water (mol l^{-1}) in accordance with the Beer–Lambert law.

In our experiments with the exposed optical fibre the pure acetone surrounding the fibre acts as a non-absorbing fibre cladding. With a refractive index less than that of the fibre silica core, acetone does not hinder total internal reflection of light in the silica core. The refractive index of acetone–water mixtures is not significantly different from that of pure acetone hence any changes

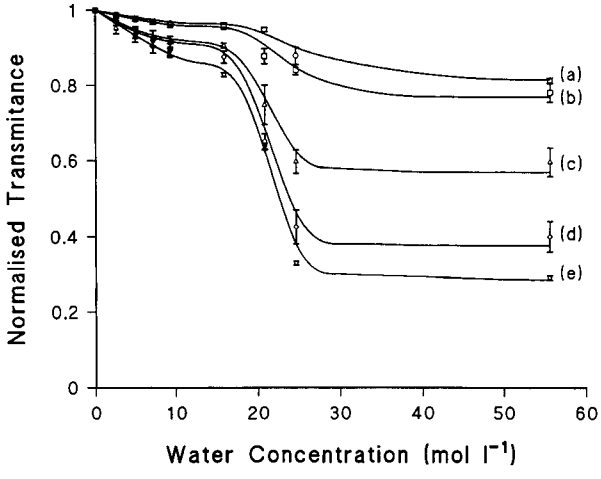

Fig. 2. Normalised transmittance of water and acetone mixtures as a function of water concentration for different lengths of sensing fibre. Exposed core: (a) 10; (b) 20; (c) 30; (d) 40; and (e) 50 cm.

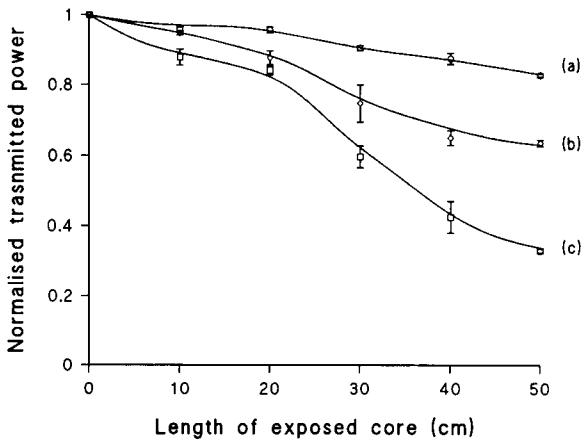

Fig. 3. Dependance of normalised transmitted optical power on the length of exposed optical fibre core length for different concentrations of water in acetone: (a) 15.9; (b) 20.8; and (c) 24.8 mol l^{-1}.

in the transmittance properties of the fibre immersed in these mixtures may not be attributed to changes in the refractive index of the cladding. Previous reported work with evanescent optical fibre sensors had shown a linear relationship between absorbance and concentration [6]. Our results, presented in Fig. 2, confirm this relationship until the concentration of water reaches approximately 20 mol l^{-1} after which a rapid decrease in the intensity of the transmitted light is observed.

At approximately 25 mol l^{-1} of water, the transmitted power curve levels off and subsequently shows little change with concentration. The narrow concentration range over which the level of transmitted power changes rapidly does not appear to vary significantly with the length of exposed fibre core. However, the degree of attenuation of guided light is dependent on the length of exposed core in contact with the absorbing solution.

A plot of exposed fibre length against transmitted optical power for 15.9, 20.8 and 24.7 mol l^{-1} water in acetone is given in Fig. 3. This shows a non-linear relationship between transmitted optical power and length of fibre core. Since only a fraction of the transmitted power in an optical fibre is carried in the evanescent field, there will be a limit to how much light can be absorbed

from this field. If little or no mode mixing occurs, then the low order modes will be essentially unaffected by interaction with an absorbing solution as the length of exposed core is increased. Therefore the reduction in transmitted optical power would be expected to approach a constant value as the length of exposed optical fibre increases (Fig. 3).

At very short lengths of exposed fibre, the maximum amount of light that could be absorbed by the evanescent field should be similar to the fraction of light carried in the cladding. The experimental results indicate that approximately 10% of optical power is flowing in the cladding of the multimode fibre.

The current theoretical models [11–13] for interpreting the relationship between the transmitted power in the optical fibre, the length of exposed fibre and the attenuation characteristics of the cladding medium predict a linear relationship between the evanescent absorbance and both the exposed fibre length and the concentration of the absorber. For fibre lengths shorter than 24 cm and low concentration of absorbing species, there is good agreement between these theoretical predictions and the experimental results in this work and those presented in Ref. 12. However, the current theoretical models cannot account for the rapid change in value of the transmitted power observed in our experiments when the concentration of water in acetone reaches approximately 20 mol l^{-1}. Theoretical work by Harrick [2] on attenuated total internal reflectance in the presence of an absorbing material in the optically less dense medium shows reflectance to have a minimum for a certain value of absorbance. The position and the depth of this minimum depends on the angle of incidence, polarization of light and the value of absorption coefficient of the absorbing medium. A study by Kapany and Pontarelli [3] of rod reflectometry produced similar results.

Harrick [2] predicts a region of approximately linear fall in reflectance with absorption coefficient, then a rapid decrease to a minimum reflectance. With a further increase of absorption coefficient, the reflectance increases again. A similar behaviour has been observed in our experiments. The transmitted power observed when the fibre was immersed in pure water was found to drop with the addition of a small amount of acetone. In each case the values of transmitted power reduced to those observed with 50 mol l^{-1} concentrations of water shown in Fig. 2.

The core–cladding interface of a multimode optical fibre is more complex than the experimental systems investigated by Harrick, and Kapany and Pontarelli, where the angle of incidence of the polarized monochromatic light on the dielectric interface was controlled. The bandwidth of the light source used in our studies was considerably wider than that used in their work. A theoretical model would need to take this into consideration as well as being able to take into account the large number of modes, supported by the multimode optical fibre, each corresponding to different polarizations and angles of incidence. The power distribution between various modes would also be essential for the model. The development of such a model was outside the scope of the present study.

Conclusion

Our experiments confirm that detection of absorbing liquids in non-absorbing solvents by evanescent field absorption in the near-infrared is possible using a rather simple apparatus. At low concentrations of an absorbing liquid in a non-absorbing solvent, the relationship between transmitted power and concentration is linear in a good agreement with current theoretical models. This linear relationship may be exploited to determine the concentration of an absorbing species in a non-absorbing solvent. However, the reported existence of a non-linear region, in which there are rapid changes in transmitted optical power with concentration, merit further investigation. At wavelengths longer than 950 nm, the concentrations at which these changes occur may differ from those obtained in this experimental work.

The first overtone of the water absorption at 1450 nm is approximately 100 times stronger then the second at 975 nm, used in these studies. There may be some benefit in working at the longer wavelength since the penetration of the

evanescent field into the liquid would be greater. Furthermore, the rapid decrease in the transmitted power accompanying the addition of a small amount of acetone to the pure water observed in our experiments may be far more pronounced at 1450 nm since this phenomenon is a strong function of the absorption coefficient as shown by Harrick [2]. Possible increases in sensitivity need to be balanced against the difficulty of obtaining suitable, low-cost, light sources and detectors.

The advantage of using an optical fibre system similar to that described in this experimental work is the potential simplicity of the optical configuration. The optical fibre lends itself to implementation of remote sensing systems, hence in the future, evanescent field sensors are likely to be found in systems controlling industrial processes.

REFERENCES

1 R.A. Nyquist, M.A. Lengers, M.L. McKelvey, R.R. Papenfuss, C.L. Putzig and L. Yurga, Anal. Chem., 62 (1990) 223R.
2 N.J. Harrick, Internal Reflection Spectroscopy, Wiley Interscience, New York, 1967.
3 N.S. Kapany and D.A. Pontarelli, Appl. Opt., 2 (1963) 1043.
4 J.E. Freeman, A.G. Childers, A.W. Steele and G.M. Hieftje, Anal. Chim. Acta, 177 (1985) 121.
5 J.M. Senior, Optical Fibre Communications: Principles and Practice, Prentice-Hall, London, 1985.
6 H. Tai, H. Tanaka and T. Yoshino, Opt. Lett., 12 (1987) 437.
7 P.H. Paul and G. Kychakoff, Appl. Phys. Lett., 51 (1987) 12.
8 M.D. DeGrandpre and L.W. Burgess, Proceedings of the ISA, Houston, TX, 1988, ISA Transactions, 28 (1988) 71.
9 M.D. DeGrandpre and L.W. Burgess, Appl. Spectrosc., 44 (1990) 273.
10 I. Murray, in C.S. Creaser and A.M.C. Davies (Eds.), Analytical Applications of Spectroscopy, Royal Society of Chemistry, London, 1988, p. 9.
11 A.W. Snyder and J.D. Lowe, Optical Waveguide Theory, Chapman and Hall, London, 1983, p. 126.
12 V. Ruddy, B.D. MacCraith and J.A. Murphy, J. Appl. Phys., 67 (1992) 6070.
13 G. Stewart, J. Norris, D.F. Clark and M. Tribble, I. Andonovic and B. Culshaw, SPIE Proc. No. 990 (1988) 188.

Analytica Chimica Acta, 281 (1993) 271–280
Elsevier Science Publishers B.V., Amsterdam

General voltammetric method for studying metal complexation in macromolecular systems

Miquel Esteban and José M. Díaz-Cruz

Departament de Química Analítica, Facultat de Química, Universitat de Barcelona, Av. Diagonal 647, 08028 Barcelona (Spain)

(Received 23rd December 1992; revised manuscript received 8th March 1993)

Abstract

A general method is proposed for the investigation of metal–macromolecule interactions by means of the voltammetric reduction of the metal ion in the presence of the macromolecule. The method considers two extreme cases: the absence or presence of electrodic adsorption. In the absence of electrodic adsorption, the method integrates some specific procedures previously developed to minimize the effects of variations in pH (and of other protolytic parameters) and adsorption of metals by cell components on the voltammetric response. A procedure for evaluating hydrodynamic conditions in anodic stripping voltammetry is also integrated in the data treatment. Some guidelines and procedures are given in order to account for the electrodic adsorption of the macromolecule and the induced adsorption of the metal ion. Either complexation and adsorption parameters or only complexation parameters can be estimated by means of a rigorous numerical or a semi-empirical method, respectively.

Keywords: Voltammetry; Complexation; Metal–macromolecule complexes; Macromolecules

In recent years, voltammetric titration procedures, in particular by stripping voltammetry, have been widely used in environmental metal speciation analysis [1,2]. A large number of references concerning heavy metal speciation analysis in systems with large ligands such as humic and fulvic acids, polysaccharides and synthetic polyelectrolytes are available [2,3].

Theoretical studies on the interpretation of experimental data concerning the voltammetric reduction of a metal ion in the presence of ligands with diffusion coefficients other than that of the metal ion are scarce, especially in comparison with studies devoted to systems with equal diffusion coefficients. Extensive theoretical and experimental studies in this field are urgently needed.

Adsorption of reactants at the electrode/solution interface is a well known phenomenon which may be the result of surface activity of the reacting species themselves, or due to a surface-active electroinactive component in the sample which induces adsorption of the reactant. For the above-mentioned complex systems, experimental evidence is available for the adsorption of a variety of macromolecular ligands and the induced adsorption of the metal ion, with the formation of the metal complex in the adsorbed phase [4].

In order to understand the voltammetric reduction of a metal ion in a metal–macromolecular ligand system, a model should be formulated considering the different phenomena occurring simultaneously. This model should incorporate at

Correspondence to: M. Esteban, Departament de Química Analítica, Facultat de Química, Universitat de Barcelona, Av. Diagonal 647, 08028 Barcelona (Spain).

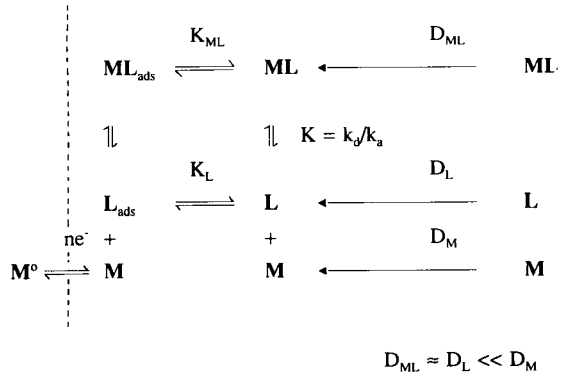

Fig. 1. Simplified model for the reduction of a metal ion in the presence of a macromolecular ligand. K = Formation constant of the complex ML; k_a, k_d = kinetic rate constants for the association–dissociation of the complex; K_{ML} = adsorption constant of the complex; K_L = adsorption constant of the ligand; D_i = diffusion coefficient of species ($D_L \approx D_{ML} \ll D_M$.

least an elementary system of an electroactive metal ion and an electroinactive 1:1 complex for which the diffusion coefficients are unequal, the rate constants of association–dissociation have finite values and both the ligand and the complex can be adsorbed on the electrode surface. This can be illustrated by means of Fig. 1. This model has not been rigorously solved, and only some partial approaches have been modelled and mathematically formulated.

The high complexity inherent in voltammetric measurements in macromolecule–metal systems and also recent findings in this field lead to difficulties in proposing and/or choosing a global experimental procedure for their study.

The aim of this paper is to propose, in the light of recent findings, guidelines and a global procedure for the experimental study of metal–macromolecular ligand systems. The global method proposed here incorporates some different methodological improvements obtained separately in the study of various particular aspects of the subject.

COMPLEXATION IN ABSENCE OF ELECTRODIC ADSORPTION

Theoretical basis

The simultaneous effects of finite association–dissociation kinetics and different diffusion coefficients of M, L and ML have been analysed [5–7]. A rigorous solution has been described for the limiting current [5]. The solution is formulated in the Laplace domain and is valid for a stationary planar electrode. It must be noted that it is restricted to the case with an excess of ligand. It is fully rigorous with respect to the values of the association–dissociation rate constants, thus including any stability constant of the complex [5]. However, in such an approach electrodic adsorption phenomena are not considered.

For the labile case an exact analytical solution

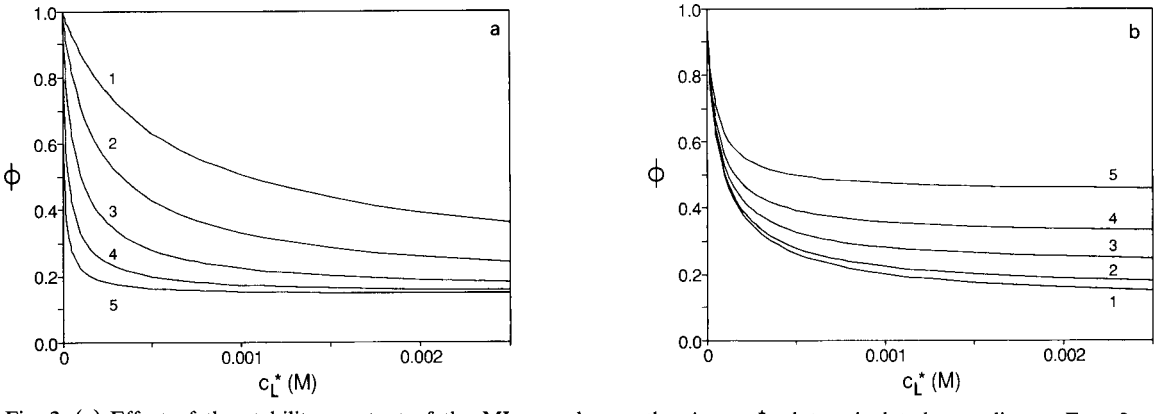

Fig. 2. (a) Effect of the stability constant of the ML complex on the ϕ vs. c_L^* plots calculated according to Eqn. 2, $\epsilon = 0.02$; log K = (1) 3.5, (2) 4.0, (3) 4.5, (4) 5.0 and (5) 5.5. (b) Effect of the parameter ϵ ($= D_{ML}/D_M$) on the ϕ vs. c_L^* plots calculated from Eqn. 2. Log $K = 4.5$; ϵ = (1) 0.01, (2) 0.02, (3) 0.05, (4) 0.1 and (5) 0.2.

is available for the limiting current in the time domain. It is formulated by means of the normalized current ϕ, defined as

$$\phi = I/I_0 = \frac{\text{limiting (or peak) current measured in presence of ligand}}{\text{limiting (or peak) current measured in absence of ligand}} \quad (1)$$

which is related to the formation constant of the complex, K ($= c^*_{ML}/c^*_M c^*_L$), by [5,6]

$$\phi = \left(\overline{D}/D_M\right)^{1/2} = (1 + \epsilon K c^*_L)^{1/2}/(1 + K c^*_L)^{1/2} \quad (2)$$

where

$$\overline{D} = (c^*_M D_M/c^*_T) + (c^*_{ML} D_{ML}/c^*_T) \quad (3)$$

$$c^*_T = c^*_M + c^*_{ML} \quad (4)$$

$$\epsilon = D_{ML}/D_M \quad (5)$$

D_i and c^*_i are the diffusion coefficient and the bulk concentration of species i respectively, $\overline{D}$ is the mean diffusion coefficient of the complex system and c^*_T is the total concentration of the metal in solution.

The value of c^*_L where the sensitivity of ϕ to K has a maximum can be found by solving $d(d\phi/dK)/dc^*_L = 0$, which for very small values of $\epsilon (= D_{ML}/D_M)$ approaches the condition $Kc^*_L \approx 1$. That is, ϕ is most sensitive to K at $c^*_L \approx 1/K$. For additional mathematical details, see the Appendix of [8].

Figure 2a shows that the first part of the ϕ vs. c^*_L curves (low c^*_L values) appears to be the part most sensitive to K, although the condition of large excess of ligand cannot be fulfilled, in some instances, in that region.

Analogously, Fig. 2b shows that for determining ϵ (i.e., the ratio D_{ML}/D_M, which allows the calculation of the diffusion coefficient of the complex, D_{ML}, if D_M is known), the region at high c^*_L values is preferable, because from Eqn. 2 it can be deduced that for $Kc^*_L \gg 1$, ϕ approaches the limiting value $\epsilon^{1/2}$ [8].

Still for labile systems, the potential shift ΔE (i.e., the difference between the half-wave or peak potentials in the presence and absence of ligand) can be related to K through the equation [7]

$$F_0 = \exp[-(nF/RT)\Delta E - \ln \phi] = 1 + Kc^*_L \quad (6)$$

which is written in terms of the well known Leden function of order zero (F_0).

In principle, Eqns. 2 and 6 should be applicable to direct current polarography (DCP), normal-pulse polarography (NPP), reverse-pulse polarography (RPP) and differential-pulse polarography (DPP).

Further, analysis of Eqns. 2 and 6 shows that, in principle, the most convenient experimental procedure for determining ϵ and K is through successive additions of aliquots of a ligand-containing solution to a metal ion solution. In this way, sets of ϕ vs. c^*_L and F_0 vs. c^*_L data are obtained.

As a consequence, this model appeared to be extremely useful for the interpretation of voltammetric results for macromolecule–metal systems, particularly labile systems, but it is restricted to the cases without electrodic adsorption and in the presence of excess ligand, sufficient to consider negligible transport of ligand. Polarographic studies with different polyelectrolytic ligands confirmed the validity and usefulness of this model [9–11].

However, from the point of view of environmental studies, the most important technique is anodic stripping voltammetry (ASV). In the case of ASV with a hanging mercury drop electrode (HMDE), the complexity of the hydrodynamic conditions during the pre-electrolysis step has prevented a rigorous theoretical solution of the problem, the efforts of Buffle and co-workers [12–15] being especially notable.

As a consequence, Eqn. (2) does not need to be satisfied, as it was deduced for the semi-infinite linear diffusion case. The application of the above model to ASV data has been carried out by postulating the validity of a modified form of Eqn. 2, based on the introduction of a parameter p instead of 1/2 [16]:

$$\phi = \frac{I_{peak}\ (\text{with L})}{I_{peak}\ (\text{without L})} = \left(\frac{\overline{D}}{D_M}\right)^p = \left(\frac{1 + \epsilon K c^*_L}{1 + K c^*_L}\right)^p \quad (7)$$

In principle, the empirical parameter p depends only on the hydrodynamic conditions during the pre-electrolysis step, which are not clearly defined. It may be expected to range between 1/2 (semi-infinite linear diffusion conditions, as described above) and 2/3 (which corresponds to laminar convective diffusion, by analogy with the Levich equation for the rotating disc electrode [17]). This first approach has become very useful for interpreting ASV experiments [8,16,18].

However, all these investigations indicated the necessity for methodological experimental studies in order to apply this model under optimum experimental conditions. Further, such studies

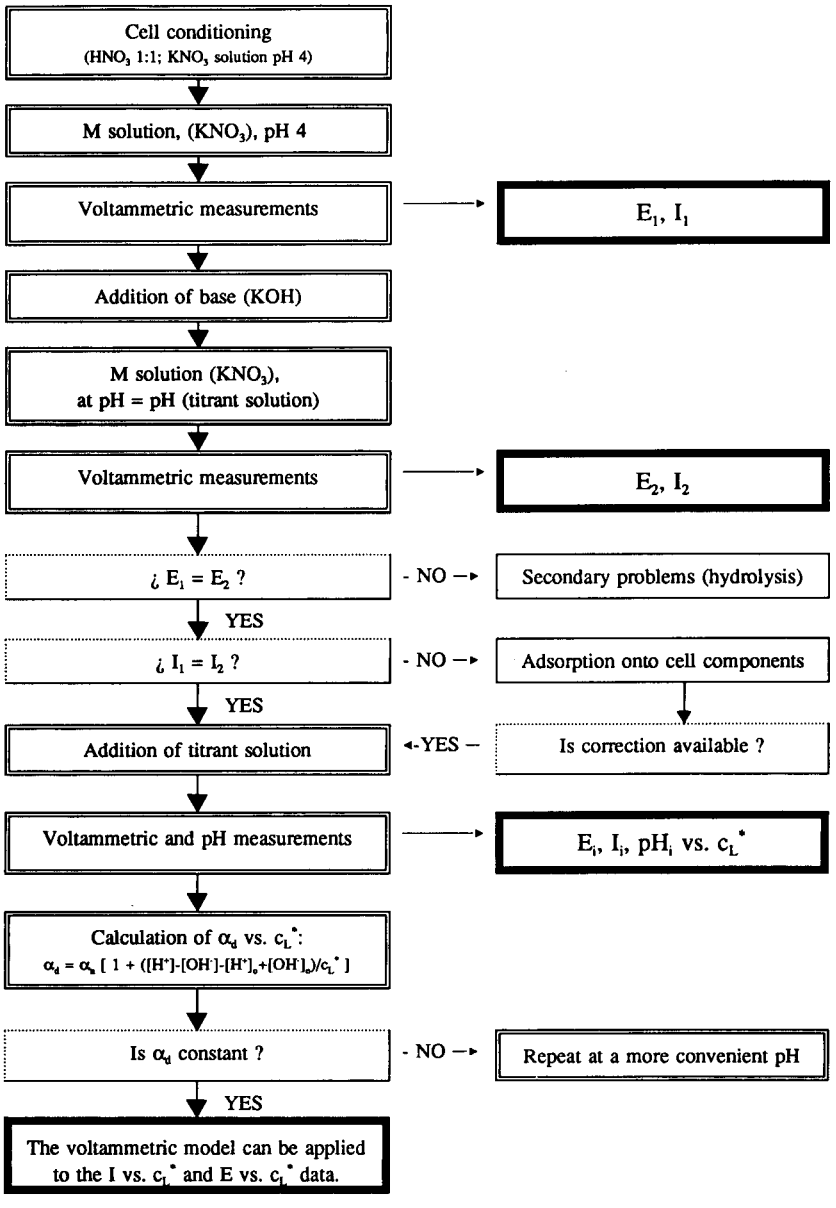

Fig. 3. Flow chart for the method proposed for voltammetric titrations of metal ion solutions with macromolecular ligand solutions.

showed the occurrence of electrodic adsorption phenomena, the extension of such phenomena being dependent on the experimental conditions and the technique used.

Tests to characterize the metal–macromolecule system: choice of conditions to minimize electrodic adsorption phenomena

In order to determine whether the voltammetric behaviour of a particular system can be explained by the model of De Jong and co-workers [5–7], the fulfillment, by the particular experimental system, of the assumed hypothesis of the model must be tested. M–L systems at different metal-to-ligand ratios, with excess of ligand, were studied by various techniques at several pulse times, scan rates, initial potentials and pre-electrolysis times (depending on the technique) in order to test the electrochemical reversibility, the lability of the complex and the presence of induced reactant adsorption.

The major complication in most of the systems studied is the electrodic adsorption of the macromolecule and the induced adsorption of the metal ion, which is mainly noted in NPP, and also DPP. The NPP response is usually characterized by both a decrease in the limiting current and the appearance of a peak in the current response, which progressively decreases with increasing pulse time (t_p) values. Further, the initial potential in NPP is a powerful variable influencing reactant adsorption phenomena. Simultaneously, RPP is characterized by normal-shaped waves, whereas DPP usually shows wider peaks than those expected in the absence of induced reactant adsorption [4]. It should be noted that the absence of NPP peaks does not necessarily imply the absence of adsorption phenomena.

When induced reactant adsorption seems to be present (because of the effects seen in NPP and DPP), RPP and DPASV are usually the more appropriate techniques in order to avoid or, at least, minimize adsorption phenomena. Systematic study by some techniques should allow the selection of the most suitable technique for further studies. Subsequently, voltammetric titrations can be performed, by means of the techniques chosen, in order to obtain ϕ vs. c_L^* and F_0 vs. c_L^* data (free from electrodic adsorption interferences) to determine ϵ, p and K.

Proposed method for voltammetric titrations

Figure 3 summarizes the proposed method for voltammetric titrations, which has been tested to be valid for metal–polycarboxylic acid systems in the absence of electrodic adsorption.

The metal ion solution is first placed in the voltammetric cell, which has been previously treated with HNO_3 (1 + 1) for 24 h and then with KNO_3 solution at the same concentration to be used in the further experiments and at pH 4. In this way, the cell surface is cleaned of metal ions, but excessive activation of the cell surface is avoided. The above metal ion solution contains a fixed KNO_3 concentration, as a supporting electrolyte, and a certain amount of HNO_3 to adjust its pH close to 4. This ensures the absence of losses of metal by adsorption on the cell materials. After degassing, some voltammetric responses are recorded until they are reproducible. These measurements yield the limiting or peak current I_1 and the half-wave or peak potential E_1.

The pH of the metal ion solution is then adjusted (by addition of KOH or HNO_3) to the pH of the titrant polyacid solution. Voltammetric measurements are again taken until the signal becomes reproducible, the values of I_2 and E_2 being obtained. At this point, the peak potential E_2 should coincide with E_1. If not, undesirable phenomena such as hydrolysis of the metal ion could be involved. If the currents I_1 and I_2 are equal, no secondary phenomena are present and the experiment can continue. If $I_1 > I_2$, adsorption of the metal ion on the voltammetric cell is involved, which event titration results will be useful only if any of the possible data treatments described in Fig. 4 is suitable for correcting for the effects of adsorption in the system considered. This point will be discussed later.

If secondary phenomena are absent, the titration is then performed by adding aliquots of the titrant solution to the metal ion solution to the cell and making voltammetric and pH measurements after each new addition. This produces a

set of I_i, E_i and pH_i values as functions of the ligand concentration c_L^*.

In order to determine whether the acidic conditions have been kept reasonably constant during the titration, the constancy of the degree of dissociation α_d is tested. For the experimental conditions normally used, an accurate calculation of α_d from pH measurements is possible by means of the approximate expression

$$\alpha_d = \alpha_n\{1 + ([H^+] - [OH^-] - [H^+]_0 + [OH^-]_0)/c_L^*\} \quad (8)$$

where α_n is the degree of neutralization of the macromolecule, $[H^+]_0$ and $[OH^-]_0$ are the initial concentrations of H^+ and OH^- species, respectively, in the metal ion solution before titration and $[H^+]$ and $[OH^-]$ are the actual concentrations of H^+ and OH^- species at each particular point.

This equation summarizes the two equations obtained previously [19] for an acidic or basic initial pH in the presence of a large excess of ligand. If α_d remains constant, the results will be valid. In contrast, the titration must be repeated at a more suitable initial pH value if reliable K values are required [19].

Data treatment

Figure 4 shows a flow chart including some aspects to be considered in the rigorous treatment of the data obtained by voltammetric titrations, which needs previous knowledge of the experimental system. On the one hand, it is necessary to know whether adsorption–desorption of the metal ion on the cell materials is significant and, if so, determine the influence of the polyelectrolyte on this process. On the other hand, in ASV the hydrodynamic conditions during the

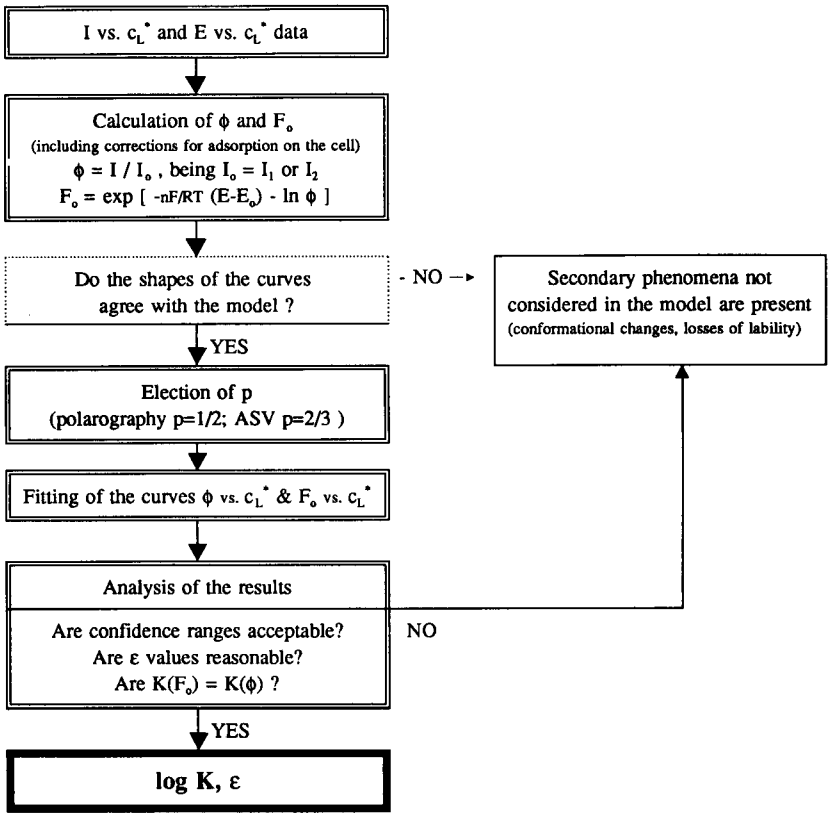

Fig. 4. Flow chart for the treatment of data obtained by voltammetric titrations.

voltammetric measurements must be taken into account, i.e., an estimation of the parameter p which appears in Eqn. 7 is necessary.

Estimation / correction of adsorption of the metal ion on the cell. The preliminary tests showed the presence or absence of losses of metal by adsorption on the cell materials. If adsorption occurs, experiments involving solution exchange are carried out to determine the role of the ligand in this process [20]. They are based on measuring I_1, E_1, I_2 and E_2 (in the absence of ligand), and E and I at different fixed concentrations of the ligand, in the same way as in the voltammetric titrations mentioned above (see Fig. 3). In the same cell the solution is then replaced with another containing only KNO_3 at the same concentration as before, and at an acidic pH able to desorb the metal ions previously adsorbed. Voltammetric measurements on this new solution yield the current I_{ad} and the potential E_{ad}. In all instances, measurements must be repeated until constant values are obtained, in order to approach the equilibrium state. If the experiments performed with metal ions in the absence of polyacid show the absence of hydrolysis of the metal (by verifying $E_1 = E_2 = E_{ad}$) and the quantitative recovery of the metal ion adsorbed on cell materials (by verifying $I_1 = I_2 = I_{ad}$), the results obtained in the presence of polyacid will allow the calculation of the amount of metal ion desorbed by the macromolecular ligands.

In this kind of experiment, the corrected ϕ function (ϕ_{corr}) can be defined in the form

$$\phi_{corr} = I/(I_1 - I_{ad}) \qquad (9)$$

In this way, ϕ_{corr} verifies Eqns. 2, 6 and 7, since ϕ_{corr} accounts for the total concentration of the metal in the bulk solution.

Depending on the ability of the polyacidic ligands to dissolve the adsorbed metal ion, the corrected normalized current ϕ_{corr} can be similar to the normalized currents ϕ_1 or ϕ_2, defined in the form $\phi_1 = I/I_1$ and $\phi_2 = I/I_2$. It can be assumed that $\phi_{corr} = \phi_1$ when the ligand, even at very low concentrations, is able to desorb quantitatively the adsorbed metal ion. In contrast, if desorption is only significant at very high ligand concentrations, $\phi_{corr} = \phi_2$ will be achieved. In most systems, however, an intermediate situation is observed, where $\phi_{corr} = \phi_2$ in the first part of the titration (high ϕ values) and $\phi_{corr} = \phi_1$ in the last part of the experiment (ϕ close to the limiting value ϵ^p).

The comparison of the functions ϕ_{corr}, ϕ_1 and ϕ_2, obtained in the experiments with solution exchange over a particular system, permits a more convenient definition of ϕ (ϕ_2 or ϕ_1) to be used in the treatment of the data obtained (for the same or similar systems) by means of voltammetric titrations without solution change. In this way, the experiments are much faster and more useful than those with solution exchange, but they do not allow the calculation of ϕ_{corr}. In the most general case, that of intermediate ability of the ligand to desorb the metal, the first part of the ϕ vs. c_L^* curve (where $\phi_{corr} \approx \phi_2$) is the most sensitive to the formation constant (K) values, whereas the limiting part (where $\phi_{corr} \approx \phi_1$) mostly depends on ϵ. Hence, in such systems, the strategy should be the use of ϕ_2 to calculate K and the use of ϕ_1 to calculate ϵ.

Estimation of the hydrodynamical parameter p. A knowledge of the hydrodynamic conditions is important for an accurate choice of the value of the parameter p. In polarographic techniques, the mass transfer is controlled by diffusion; then $p = 1/2$ and Eqn. 2 is valid. In ASV, the a priori choice of p is not clear, as the hydrodynamic conditions in the pre-electrolysis step are poorly defined.

A simple semi-empirical method has been proposed for evaluating the parameter p in ASV over metal–polyelectrolyte systems, i.e., in Eqn. 7 [21]. The method is based on the comparison between polarographic and stripping voltammetric currents measured in the same system. It follows from Eqn. 2 (as applied to polarographic data) and Eqn. 7 (as applied to ASV data) that

$$\ln \phi_{pol} = \frac{1}{2p} \ln \phi_{ASV} \qquad (10)$$

where ϕ_{pol} and ϕ_{ASV} denote the normalized currents measured by polarography (DCP, NPP, RPP

or DPP) and ASV, respectively. Equation 10 allows p to be calculated from the slope of the ln ϕ_{pol} vs. ln ϕ_{ASV} plots referred to the same particular system.

The results obtained with polycarboxylic acids [21] suggest that the hydrodynamic conditions are similar to convective laminar diffusion. Then, a fixed value of $p = 2/3$ can usually be assumed for the fitting of ϕ vs. c_L^* data obtained from ASV.

Nevertheless, if the hydrodynamic conditions in special experiments do not seem to fit either of the two cases mentioned above, the application of the method to the determination of p is recommended before the performance of any voltammetric titration.

The value of the χ^2 function, the analysis of residuals and the confidence ranges for the parameters K and ϵ ($= D_{ML}/D_M$) fitted will provide arguments to decide whether or not the experimental results agree with the model and, as a consequence, the reliability of the parameters can be determined. The lack of reasonable agreement would suggest the presence of secondary phenomena in the system studied, which are not considered in the voltammetric model, such as conformational changes of the macromolecule and loss of lability of the complex during the titration.

COMPLEXATION IN THE PRESENCE OF ADSORPTION PHENOMENA

In many instances experimental evidence is available for the adsorption of the ligand and the induced adsorption of the metal ion, with the formation of the metal complex in the adsorbed phase [4]. This is usually present in the case of metal–macromolecule systems. As a consequence, the availability of some approach to cope with this problem is of great interest.

Theoretical basis

Recently, theoretical efforts have been made to include adsorption phenomena in voltammetric models concerning metal complexation with unequal diffusion coefficients. A model has been proposed for the interpretation of the NPP reduction of a metal ion in a labile metal–polyelectrolyte system, in the presence of an excess of ligand, and including both the polyelectrolyte adsorption and the induced adsorption of the metal ion [22–24]. Langmuirian adsorption isotherms for the ligand and the complex have been assumed.

In the particular case of adsorption parameters independent of the applied potential, the model yields a general equation for the response function of NPP, which is given by

$$I_{NPP} = nFA\left(\frac{\delta}{1+\delta}\right)\left\{\sqrt{\frac{\bar{D}}{\pi}}\left[\frac{c_T^*}{\sqrt{t_d}} + \frac{c_T(0,t_0)}{\sqrt{t_p}} - \int_0^{t_0}\frac{c_T'(0,\tau)}{\sqrt{t_d-\tau}}\,d\tau\right] - \left(\frac{d\Gamma_{ML}}{dt}\right)_{t=t_d}\right\} \quad (11)$$

where $\bar{D}$ and c_T have the same meaning as before, Γ_{ML} is the adsorbed concentration of the complex, t_d and t_p are the drop and pulse time, respectively, $t_0 = t_d - t_p$, the prime (′) notation means the first derivative respect to time and δ is a potential function defined in the form

$$\delta(t) = \sqrt{\frac{D_{M^0}}{\bar{D}}}\cdot\frac{1}{1+K'}\cdot\exp\left\{-\frac{nF}{RT}[E(t)-E_0]\right\} \quad (12)$$

where $K' = Kc_L^*$, D_{M^0} is the diffusion coefficient of the metal atom in the amalgam and E_0 is the equilibrium potential of the metal.

Equation 11 allows one to understand and to simulate characteristic NPP curves with induced reactant adsorption phenomena, including the maxima at the onset of the wave and the depletion of the limiting currents. Equation 11 can be divided into two parts, a sigmoidal contribution, $(I_{NPP})_{sigm}$, and a peak contribution, $(I_{NPP})_{peak}$:

$$I_{NPP} = (I_{NPP})_{sigm} + (I_{NPP})_{peak} \quad (13)$$

$$(I_{NPP})_{sigm} \equiv \frac{c(K)\,e^{ax}}{1+c(K)\,e^{ax}}[(I_{NPP})_{lim}] \quad (14)$$

$$(I_{NPP})_{peak} \equiv \frac{c(K)\ e^{ax}}{1+c(K)\ e^{ax}}\left[-nFA\left(\frac{d\Gamma_{ML}}{dt}\right)_{t=t_d}\right] \quad (15)$$

where $a = nF/RT$, $x = -[E(t_d) - E_0]$, $(I_{NPP})_{lim}$ is the limiting value of the current, and $(d\Gamma_{ML}/dt)_{t=t_d}$ indicates the time variation of the surface concentration of the complex at the drop time (t_d). The parameter $c(K)$ is related to the stability constant, K, of the complex by

$$c(K) \equiv \sqrt{\frac{D_{M^0}}{D_M}}\ \frac{1}{\sqrt{(1+\epsilon K')(1+K')}} \quad (16)$$

where $K' = Kc_L^*$.

Proposed method for the estimation by normal-pulse polarography of complexation and adsorption parameters

If preliminary tests show the presence of non-negligible adsorption phenomena in NPP (see above), the model described above can be applied to fit experimental NPP curves.

A systematic procedure was proposed in order to improve the fitting of the numerical results to experimental data avoiding a cumbersome and computationally expensive optimization process. The process based on the use of the general equation (Eqn. 11) was described in detail elsewhere [24]. This equation implicitly contains some parameters such as the adsorption constant of the complex, K_{ML}, the adsorption constant of the ligand, K_L, and the maximum surface concentration averaged for both species L and ML, Γ_m (for more details, see [24]). The main steps of the fitting process are as follows.

The decreasing part of the NPP peak can be used to evaluate K_{ML}. Then, with the value found for K_{ML}, the fit of the rising part of the peak will be used to evaluate K. Finally, with the K and K_{ML} values found, K_L and Γ_m can be evaluated from a more accurate fit of the limiting current zone and the peak maximum. After the full fitting sequence, some small modifications to the parameters can be observed. Usually, a second iterative process in the same sequence yields improved and satisfactory parameters.

However, this procedure, although optimized, is time consuming and requires of computational facilities.

Proposed method for the estimation by normal-pulse polarography of only complexation parameters

As mentioned, Eqn. 11 can be split into two contributions. The peak contribution $(I_{NPP})_{peak}$ (Eqn. 15) depends on the stability constant K and on the set of adsorption parameters of the ligand and the complex. Hence, to obtain the value of the stability constant from this contribution, the values of the adsorption parameters and the model for the adsorption isotherms of the complex and the ligand must be known. On the other hand, the sigmoidal contribution $(I_{NPP})_{sigm}$ (Eqn. 14) depends only on the stability constant of the complex, because $(I_{NPP})_{lim}$ can be found from the experimental full NPP wave.

When only complexation parameters are required, a simpler semi-empirical method has been developed [25], which is based on fitting the full wave, by means of a simple non-linear regression analysis, by writing the peak contribution $(I_{NPP})_{peak}$ in the form of a semi-empirical expression.

The most appropriate semi-empirical function is of the type

$$I_{NPP} = \frac{c\ e^{ax}}{1+c\ e^{ax}}[(I_{NPP})_{lim} - \beta] + \frac{q\ e^{ax}}{1+q\ e^{ax}}\left[\beta + \frac{r\ e^{ax}}{(1+s\ e^{ax})^2}\right] \quad (17)$$

where β, q, r and s are empirical parameters without physical meaning and c is an estimate of the stability constant (K) through the expression $c(K)$ defined in Eqn. 16. Thus c contains only the information on complexation, which is the main interest in the present simpler approach. Moreover, this approach requires only a personal computer and well tested commercial or laboratory-written programs for non-linear fitting.

The accuracy of the semi-empirical Eqn. 17 was tested by simulated curves, and applied to experimental results for the Cd(II)–polymethacrylate complex. Formation constants obtained

from the parameter c by means of the semi-empirical approach were in satisfactory agreement with those obtained from $c(K)$ by means of the rigorous numerical procedure. It should be mentioned that the accuracy of the data obtained from the semi-empirical approach is not satisfactory enough for NPP curves with high adsorption peaks. However, as the height of the peaks can be experimentally controlled by choosing the appropriate pulse times and ligand concentrations, a proper choice of these variables greatly improves the applicability of the method and the quality of the results.

Conclusion

In trace metal speciation analysis of natural samples or metal complexation studies under conditions as similar as possible to those of natural media, voltammetric techniques are valuable tools. However, because of the complexity inherent in measurements and interpretation in voltammetry, especially when several simultaneous phenomena have a role, great methodological efforts are still necessary. In particular, when macromolecular ligands are present (and their ubiquity is well known), additional theoretical and experimental difficulties arise.

The general method proposed here, covering different experimental and theoretical aspects, can be applied within systematic studies with model solutions which are necessary in order to establish guidelines and to illustrate the many problems associated with using modern voltammetric techniques in speciation studies. The method proposed can be selected, as a first choice, to start voltammetrically the investigations with metal–macromolecule systems.

The financial support of the Spanish Ministry of Education and Science (DGICYT Project PB90-0821) and of the Institut d'Estudis Catalans is gratefully acknowledged. The authors thank H.P. van Leeuwen, M.A.G.T. van den Hoop, E. Casassas, J. Puy, F. Mas and C. Ariño for their contributions and useful comments.

REFERENCES

1 C.J.M. Kramer and J.C. Duinker (Eds.), Complexation of Trace Metals in Natural Waters, Nijhoff-Junk, The Hague, 1984.
2 J. Buffle, Complexation Reactions in Aquatic Systems: an Analytical Approach, Horwood, Chichester, 1988, Chap. 9.
3 H.P. van Leeuwen, R. Cleven and J. Buffle, Pure Appl. Chem., 61 (1989) 255, and references cited therein.
4 H.P. van Leeuwen, J. Buffle and M. Lovric, Pure Appl. Chem., 64 (1992) 1015, and references cited therein.
5 H.G. de Jong, H.P. van Leeuwen and K. Holub, J. Electroanal. Chem., 234 (1987) 1.
6 H.G. de Jong and H.P. van Leeuwen, J. Electroanal. Chem., 234 (1987) 17.
7 H.G. de Jong and H.P. van Leeuwen, J. Electroanal. Chem., 235 (1987) 1.
8 M.A.G.T. van den Hoop, F.M.R. Leus and H.P. van Leeuwen, Collect. Czech. Chem. Commun., 56 (1991) 96.
9 M. Esteban, E. Casassas, H.G. de Jong and H.P. van Leeuwen, Anal. Chim. Acta, 229 (1990) 93.
10 J.M. Díaz-Cruz, C. Ariño, M. Esteban and E. Casassas, Electroanalysis, 3 (1991) 299.
11 A.M. Nadal, C. Ariño, M. Esteban and E. Casassas, Electroanalysis, 3 (1991) 309; 4 (1992) 757.
12 J. Buffle, J. Electroanal. Chem., 125 (1981) 273.
13 A.M. Mota, J. Buffle, S.P. Kounaves and M.L. Simoes Gonçalves, Anal. Chim. Acta, 172 (1985) 13.
14 J. Buffle, A.M. Mota and M.L. Simoes Gonçalves, Port. Electrochim. Acta, 3 (1985) 293.
15 J. Buffle, J.J. Vuilleumier, M.L. Tercier and N. Parthasarathy, Sci. Total Environ., 60 (1987) 75.
16 M. Esteban, H.G. de Jong and H.P. van Leeuwen, Int. J. Environ. Anal. Chem., 38 (1990) 75.
17 V.G. Levich, Physicochemical Hydrodynamics, Prentice-Hall, Englewood Cliffs, NJ, 1962.
18 H.P. van Leeuwen, Colloids Surf., 51 (1990) 359.
19 J.M. Díaz-Cruz, M. Esteban, M.A.G.T. van den Hoop and H.P. van Leeuwen, Anal. Chim. Acta, 264 (1992) 163.
20 J.M. Díaz-Cruz, M. Esteban, M.A.G.T. van den Hoop and H.P. van Leeuwen, Anal. Chem., 64 (1992) 1796.
21 J.M. Díaz-Cruz, C. Ariño, M. Esteban and E. Casassas, J. Electroanal. Chem., 333 (1992) 33.
22 F. Mas, J. Puy, J.M. Díaz-Cruz, M. Esteban and E. Casassas, J. Electroanal. Chem., 326 (1992) 299.
23 J. Puy, F. Mas, J.M. Díaz-Cruz, M. Esteban and E. Casassas, J. Electroanal. Chem., 328 (1992) 271.
24 J. Puy, F. Mas, J.M. Díaz-Cruz, M. Esteban and E. Casassas, Anal. Chim. Acta, 268 (1992) 261.
25 F. Mas, J. Puy, J.M. Díaz-Cruz, M. Esteban and E. Casassas, Anal. Chim. Acta, 273 (1993) 297.

Analytica Chimica Acta, 281 (1993) 281–290
Elsevier Science Publishers B.V., Amsterdam

On-line monitoring of cobalt in zinc plant electrolyte by differential pulse adsorptive stripping voltammetry

Robert I. Mrzljak, Alan M. Bond, Terence J. Cardwell and Robert W. Cattrall

Centre for Scientific Instrumentation, Department of Chemistry, La Trobe University, Bundoora, Victoria 3083 (Australia)

Roger W. Knight [1]

Department of Chemical and Analytical Sciences, Deakin University, Geelong, Victoria 3217 (Australia)

O. Michael G. Newman, Bruce R. Champion and John Hey

Pasminco Metals - EZ, Hobart, Tasmania 7001 (Australia)

Andrzej Bobrowski

Institute of Materials Science, School of Mining and Metallurgy, 30-059 Krakow (Poland)

(Received 17th February 1993)

Abstract

Two methods that have now been used routinely for several years for on-line monitoring of cobalt in zinc plant electrolyte by adsorptive stripping voltammetry (ADSV) are described in which interference from the very high background zinc concentration is overcome. The first method combines ADSV of cobalt as its dimethylglyoxime complex at a hanging mercury drop electrode with in situ matrix exchange. This method utilises a bottom-drain flow-through cell to overcome problems associated with the high density of zinc electrolyte and enables cobalt to be determined down to 9 $\mu g\ l^{-1}$ in plant electrolyte solutions which contain 150 $g\ l^{-1}$ zinc. This method is therefore suitable for low-purity electrolyte. However, in highly purified zinc electrolyte the matrix exchange technique lacks the required sensitivity for cobalt determination and a second technique known as catalytic differential pulse ADSV is employed which has a detection limit of 0.25 $\mu g\ l^{-1}$ cobalt in zinc plant electrolyte. The catalytic technique again utilises a bottom-drain flow-cell, but involves formation of the α-benzil dioxime complex rather than that with dimethylglyoxime. Addition of nitrite enhances the cobalt signal and eliminates the need for matrix exchange. Both methods have been adapted for use in on-line voltammetric analysers at Pasminco Metals-EZ. The conditions used for efficient removal of cobalt during the purification process almost invariably result in removal of nickel to levels where possible interference from the presence of high nickel concentrations does not occur in the practical situation.

Keywords: Differential pulse polarography; Stripping voltammetry; Cobalt; On-line monitoring; Zinc

Correspondence to: A.M. Bond, Centre for Scientific Instrumentation, Department of Chemistry, La Trobe University, Bundoora, Victoria 3083 (Australia).

[1] Present address: Australian Trade Commission, World Trade Centre, Melbourne, Victoria 3005 (Australia).

On-line methods for determining trace metals in zinc plant electrolyte are important for maintaining electrolyte quality and ensuring high current efficiency in the final electrolytic step in

which zinc is cathodically reduced to metal. However, the high specific gravity of the electrolyte, the presence of an extremely large concentration of zinc and the harsh operating conditions in the plant have limited the application of on-line methods. Recently at the Pasminco Metals-EZ (PMEZ) zinc plant (Risdon, Tasmania, Australia), on-line voltammetric analysers have been developed [1,2], which are routinely used for the determination of cadmium, lead, antimony and copper by anodic stripping voltammetry. Methods for other metals are now required and in this paper studies on the development of an on-line method for the determination of cobalt are described. The presence of cobalt in the zinc electrolyte leads to decreased current efficiency and, hence, lower power efficiency during the deposition process. The maximum concentration allowable in the zinc electrolyte, so that its effect is minimal, is 0.3 mg l^{-1} cobalt. Consequently very sensitive methods are required for the determination of cobalt.

The determination of cobalt by voltammetry at stationary mercury electrodes and polarography at mercury drop electrodes have been reported by many workers [3–7]. To overcome the problems associated with irreversibility and poor sensitivity of stripping methods due to the low solubility of cobalt in mercury [8,9], many workers have employed complexing agents and monitored the adsorption wave of the cobalt complex formed. For example, dimethylglyoxime (DMG)-sensitized polarography has been used to determine cobalt in solutions containing large excesses of other metals [10] and in plant materials and sewage sludges [6]. The determination of cobalt as water-soluble dithiocarbamate complexes using polarography [11] and liquid chromatography with amperometric detection [12] have also been reported as has the determination of cobalt as its DMG complex by adsorptive stripping voltammetry (ADSV) at a hanging mercury drop electrode, in biological materials [5], in sea water [13] and in simulated pressurised water reactor coolant [14].

A range of off-line voltammetric methods has been described for the determination of cobalt in the presence of a large excess of zinc. Geissler and Da Maia [15] developed a method for determining cobalt in zinc plant solutions in a supporting electrolyte which contained 0.1 M sodium citrate and 0.1 M ammonium chloride with 0.08% DMG. It was found that cobalt could be determined in the presence of zinc up to a Co:Zn ratio of $1:10^4$ using this supporting electrolyte. However, this falls short of the required Co:Zn ratio of $1:10^6$, which occurs in purified zinc plant electrolyte. Schmidt et al. [16] improved the sensitivity for cobalt in this system by adding the surfactant 1-benzylsulfonyl-(*N*-morpholino)ethane (BME) to the supporting electrolyte. BME was found to selectively retard the zinc reduction without inhibiting the reduction of the cobalt–DMG complex, thereby giving increased peak separation and improved sensitivity. Bobrowski [17] developed a method in which cobalt could be determined in solutions containing zinc concentrations 10^7 times higher than cobalt. α-Benzil dioxime was used as the complexing agent which forms a 2:1 complex with cobalt in the same manner as DMG. The complex adsorbs onto the mercury electrode surface when a potential is applied and the reduction potential was found to be $-0.98(\pm 0.01)$ V (vs. Ag/AgCl). The sensitivity and resolution relative to the interfering zinc process may be further increased by the addition of the nitrite ion to the supporting electrolyte [17,18]. This technique is called catalytic adsorptive stripping voltammetry and appears to have both the sensitivity and selectivity necessary for the determination of cobalt in zinc plant electrolyte.

The aim of this study was to develop voltammetric methods that are suitable for on-line determination of cobalt in both low-purity and high-purity zinc electrolyte and apply the methods in a plant situation. The first method described uses on-line matrix exchange and can be used to determine cobalt in low-purity zinc electrolyte. The second method uses adsorptive catalytic voltammetry for the ultra-trace determination of cobalt in high-purity zinc electrolyte. The two methods were initially developed and tested in the laboratory and then applied to on-line voltammetric analysers now used [2] in the Pasminco Metals-EZ zinc plant to monitor metal impurities present in process streams.

EXPERIMENTAL

Reagents

All reagents were of analytical-reagent grade purity. Mercury metal was Aristar grade (B.D.H., Poole, UK) and cobalt standard was AAS grade (May & Baker, Dagenham, UK). A stock dimethylglyoxime solution was prepared by dissolving the appropriate amount in 96% ethanol. A 10^{-3} M stock α-benzil dioxime (Ajax Chemicals, Melbourne) solution was prepared by dissolving 0.024 g of α-benzil dioxime in a solution of 20 ml of 0.5 M sodium hydroxide and 80 ml of 96% ethanol, with gentle heating. Sodium nitrite was recrystallised from water before use. All solutions were made using NANO-pure water (16 MΩ cm, Barnstead, Dubuque, IA) and nitrogen gas was of high-purity grade.

Instrumentation

A BioAnalytical Systems (BAS 100) electrochemical analyser was used in conjunction with an EG&G Princeton Applied Research (PAR) Model 310 static mercury drop electrode (SMDE) in the laboratory based studies to develop the on-line version of the matrix exchange method. A three-electrode cell arrangement was used with a large hanging mercury drop with an area of 2.4 mm^2 as the working electrode, Ag/AgCl (3 M KCl) as the reference electrode, and platinum wire as the auxiliary electrode. The samples in the off-line version were conveyed to the cell by a Masterflex pump (Cole-Parmer Instruments, Chicago, IL). In the matrix exchange method, the zinc electrolyte sample is injected directly over the hanging mercury drop electrode (HMDE) from the attached flow adaptor [1]. During the injection period the potential is fixed for a period of time at a value where adsorption of the Co–DMG complex occurs. After flowing over the electrode, residual plant electrolyte sample sinks to the bottom of the cell because of its greater specific gravity than the receiving solution in the cell. This leaves relatively uncontaminated solution around the electrode after the equilibration step, thereby minimising the zinc interference for the cobalt determination which is made in the receiving electrolyte. The contaminated electrolyte is drained from the cell and replaced with fresh electrolyte between each experimental determination.

For the laboratory based development of optimal conditions for the catalytic method, a Metrohm 646 VA Processor and 647 VA stand (Herisau, Switzerland) were used. The voltammograms were recorded in a three-electrode system with a hanging mercury drop with an area of 0.45 mm^2 as the working electrode, an Ag/AgCl (3 M KCl) reference electrode and a glassy carbon rod auxiliary electrode.

For the on-line matrix exchange (Fig. 1) and catalytic methods (Fig. 2), a titro-analyser, Applikon ADI 2020 [Applikon Dependable Instruments (ADI), Schiedam, Netherlands] was modified into a voltammetric configuration by Pasminco Metals-EZ (Fig. 3). To develop a voltammetric analyser the ADI 2020 was fitted with a Metrohm multi-mode electrode used in the hanging mercury drop mode, communications processor, voltammetric processor, potentiostat and solenoid driver cards (PMEZ). The titro-analyser provides sample and reagent handling as in the standard configuration of the ADI 2020. The communications processor is programmed to con-

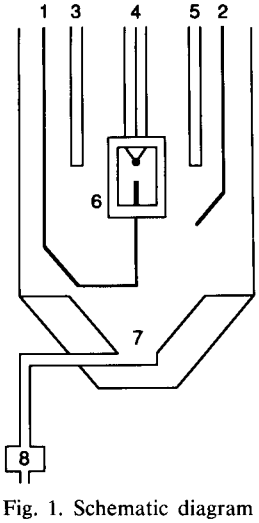

Fig. 1. Schematic diagram of the bottom-drain flow-through cell used for the on-line matrix exchange voltammetric method. (1) Sample inlet line; (2) nitrogen purge line; (3) reference electrode; (4) Metrohm hanging mercury drop electrode; (5) auxiliary electrode; (6) PAR 310 flow adaptor; (7) sample electrolyte drain to waste; (8) control valve.

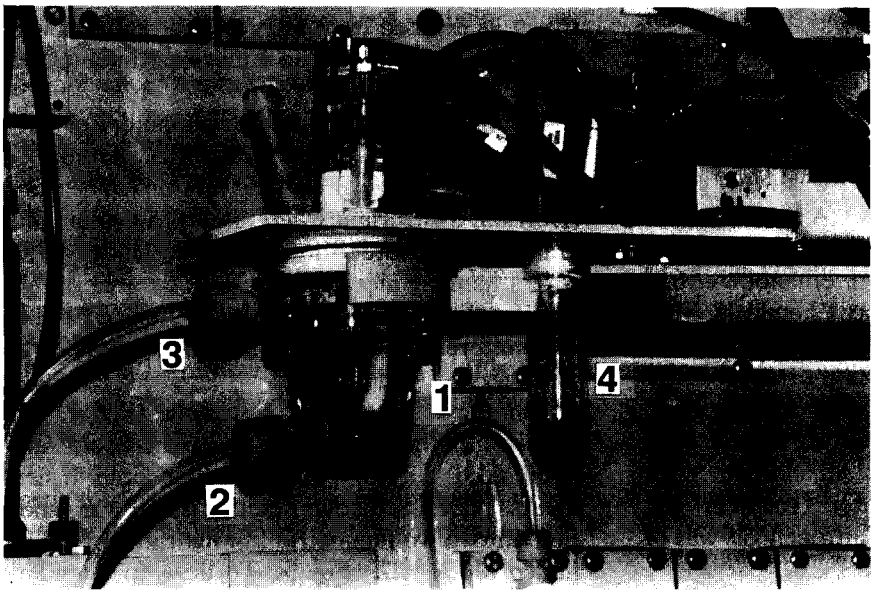

Fig. 2. Photograph of the bottom-drain flow-through cell used for the on-line catalytic method. (1) A cell consisting of a Metrohm hanging mercury drop electrode, Ag/AgCl reference electrode, glassy carbon rod electrode, nitrogen purge line and a PTFE stirrer; (2) waste removal and wash line; (3) overflow line; (4) nitrogen gas wash vessel.

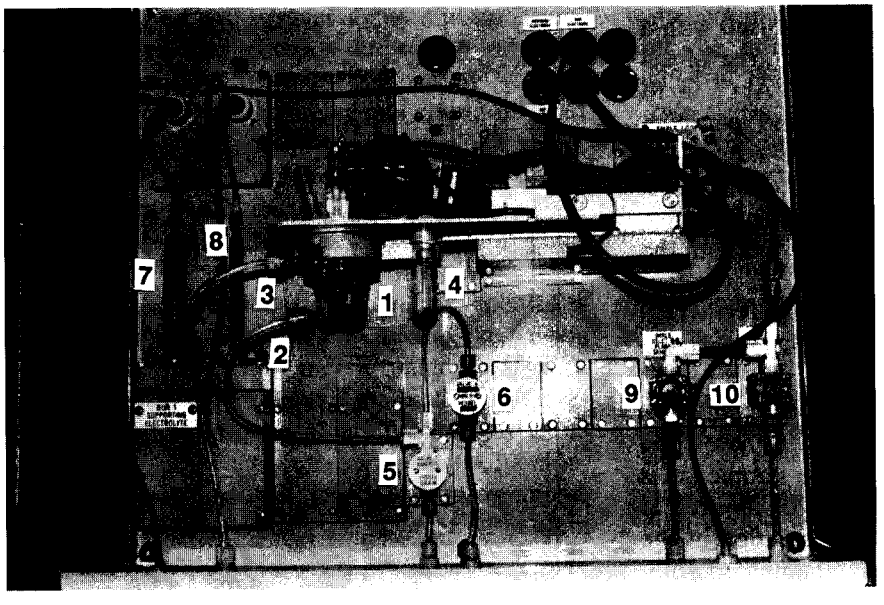

Fig. 3. Photograph of the voltammetric configuration and plumbing arrangement used for the on-line catalytic method. (1–4) as in Fig. 2; (5) valve controlling waste removal and cleaning solution; (6) valve controlling clean water throughput; (7) burette for supporting electrolyte delivery to cell; (8) burette for cobalt standard delivery, used in self calibrating system; (9, 10) valves controlling throughput of sample electrolyte to sample loop and waste.

vert the current measurements for each analyte's peak height from the voltammetric processor to four 20-mA signals for transmission to the process control system. The voltammetric processor is programmed to handle all the electrode signals via the potentiostat and to dispense and dislodge the mercury drops via the solenoid driver and the HMDE system. The voltammetric form of the analyser is now commercially available from ADI and the solution sampling system developed at PMEZ, which enables the zinc plant electrolyte to be automatically transferred to the ADI 2020 system, is also available from Palfreyman Instrumentation, Collinsvale, Tasmania, Australia.

Procedures

Laboratory experiments initially used to provide optimal electrolytes for use in the on-line methods were carried out at (20 ± 1)°C in the presence of 150 g l^{-1} zinc sulfate as the electrolyte. For on-line experiments, zinc electrolyte sampled directly from the plant was used.

(a) Matrix exchange method. The technique of differential pulse adsorptive stripping voltammetry with in situ matrix exchange was adopted in the initially described method. For the adsorption step, zinc electrolyte was diluted 1:5 with 0.5 M trisodium citrate, 0.4% (v/v) ammonia and 5×10^{-4} M dimethylglyoxime at pH 6.4 and then reduced after matrix exchange using the parameters and electrolyte described below. For the off-line method, dilution was achieved with a pipette. For on-line measurements, the zinc plant electrolyte is automatically sampled from the desired process reactor or stream, automatically filtered, diluted with 0.05% H_2SO_4 to avoid precipitation in the sample delivery lines that may otherwise occur during the cooling of the plant electrolyte and then pneumatically transported to the analyser. Once the sample has been received at the voltammetric analyser site, the analytical procedure is started using the operating parameters entered into the control unit. A volume of 900 μl of sample diluted 1:5 in the electrolyte used for the adsorption step was delivered by means of a burette system at a rate of 11 ml min^{-1} directly onto the mercury drop in the measurement cell (Fig. 1), which contains receiving electrolyte composed of 0.1 M trisodium citrate, 0.1 M ammonium chloride, 0.04% (v/v) ammonia and 3×10^{-3} M dimethylglyoxime at pH 8.4. Consequently adsorption of the Co–DMG complex takes place in the pH 6.4 medium in the presence of a very high concentration of zinc, whereas stripping occurs in the pH 8.4 medium which contains very little zinc. The injected sample after passing the electrode, sinks to the bottom of the cell because of its greater specific gravity than the receiving electrolyte and the only zinc present during the stripping is the residual amount left after matrix exchange.

During sample delivery the potential of the mercury drop was held at -0.6 V for 5 s and then for a further 10 s with all flow stopped after the adsorptive deposition period was complete. A scan in the negative potential direction using the differential pulse waveform gave rise to a cobalt peak at $-0.98(\pm 0.01)$ V vs. Ag/AgCl. Results were transmitted to the computer for processing. Prior to the next determination, fresh receiving electrolyte was introduced into the top of the cell to replace contaminated electrolyte which is drained from the bottom of the cell. A cell drainage of 25 ml per run was found to be suitable. No interference was encountered from the presence of nickel in plant electrolyte. The nickel–DMG complex is reduced at $-0.87(\pm 0.01)$ V vs. Ag/AgCl in the matrix exchange method and if present at very high concentrations, relative to cobalt levels, could, cause interferences. However, in plant electrolyte nickel levels were found to be too low to cause interferences with the cobalt determination.

The instrumental parameters were as follows: initial potential, -0.6 V; final potential, -1.1 V; nitrogen purge time, 300 s; deposition time, 5 s; equilibration time, 10 s; drop size, 2.4 mm^2 (off-line), 0.45 mm^2 (on-line); pulse time, 50 ms; pulse amplitude, -50 mV; ramp step, -3 mV; scan rate, 10 mV s^{-1}.

(b) Catalytic method. The technique of catalytic differential pulse ADSV was used directly without matrix exchange for this method. For the laboratory tests, a volume of 200 μl of sample was pipetted into a cell containing 20 ml of supporting electrolyte of composition 1.3×10^{-5} M

α-benzil dioxime, 1.0 M ammonium chloride, 0.5 M sodium nitrite and 1.3% (v/v) ammonia at pH 9.4 and the determination was then carried out using the instrumental parameters listed below. For the on-line measurements, the zinc electrolyte was automatically transported from the plant to the voltammetric analyser in the same way as described for the matrix exchange method. The operating parameters were entered into the control unit when the sample was received and the analytical procedure started. The cell was washed twice with water and drained from the bottom outlet (Fig. 2) to ensure no residual contamination from the previous run. A volume of 20 ml of catalytic supporting electrolyte, described above, was combined with 200 μl of acidified plant electrolyte sample from a sample loop and transferred to the analysis cell. The solution was purged with nitrogen for 3 min to remove interfering oxygen. A new mercury drop was then formed at the HMDE and a potential of −0.5 V was applied to the drop. After a 10-s equilibration period, a negative potential scan of the voltage using the differential pulse waveform, yielded a peak at −0.98(±0.01) V which corresponds to the reduction of adsorbed cobalt complex. Results of the experiment were transmitted to the central computer for processing. The cell was drained, flushed and refilled with water and the cycle recommenced for the determination of cobalt in the next sample delivered from the process stream.

The instrumental parameters were as follows: initial potential, −0.5 V; final potential, −1.2 V; nitrogen purge time, 300 s; deposition time, 0 s; equilibration time, 10 s; drop size, 0.45 mm^2 (off- and on-line); pulse time, 50 ms; pulse amplitude, −50 mV; ramp step, −2 mV; scan rate, 10 mV s^{-1}.

(c) Spectrophotometric method. The laboratory reference method used for the determination of cobalt, was a spectrophotometric method involving formation of a soluble red complex with sodium 1-nitroso-2-hydroxynaphthalene-3,6-disulfonate (cobalt-nitroso-R salt) in an acetate–acetic acid medium and measurement of the absorbance at 500 nm [19]. This method was used to validate the data obtained on-line by the voltammetric procedure.

RESULTS AND DISCUSSION

Laboratory matrix exchange method

Prior to implementing the matrix exchange method, extensive tests on the laboratory based system were conducted to determine optimal conditions for the cobalt determination. Results of these investigations are summarised below. The major difficulty to be overcome in determining cobalt by adsorption voltammetry in zinc plant electrolyte is the interference caused by the zinc reduction wave which occurs at potentials close to that of the cobalt response (Fig. 4). Zinc is in fact present at a 10^6 or greater concentration excess over cobalt in plant electrolyte. The method of in situ matrix exchange may be used to minimize the zinc interference. This concept has been demonstrated by Bond et al. [1] in determining cadmium, copper, lead and antimony in zinc plant electrolyte. The interference also may be

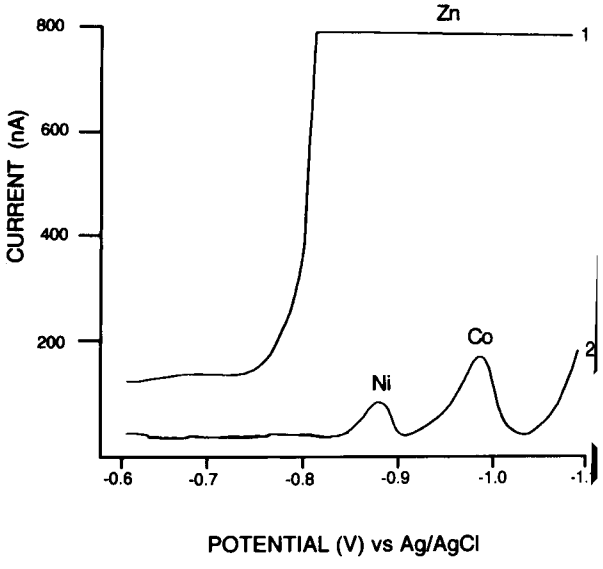

Fig. 4. Comparison of voltammograms obtained for the determination of cobalt in purified zinc plant electrolyte using (1) a static cell and (2) the bottom-drain cell incorporating the matrix exchange procedure.

reduced by adding the zinc complexing reagent sodium citrate to the supporting electrolyte, as suggested by Geissler and Da Maia [15]. Additionally, via use of the matrix exchange method it is possible to further discriminate against interfering processes via the ability to independently vary the chemical composition of diluent and receiving electrolyte.

Another benefit of using in situ matrix exchange in the flowing solution mode is the decreased time required for the determination of low concentrations of cobalt because of the efficiency of the accumulation. The deposition time is 5 s for this method while, for a static cell, the deposition time required to determine the same concentration could be anything up to 10 min. Furthermore, while it was found necessary to perform a 300-fold dilution of the zinc plant electrolyte to enable the determination of cobalt in a static cell, this level of dilution is not required for matrix exchange with the bottom-drain cell. A dilution ratio of 1 part zinc plant electrolyte to 5 parts diluent containing 0.05 M trisodium citrate, 0.4% ammonia buffer and 5×10^{-4} M DMG was found to be ideal because it lowers the zinc concentration to some extent whilst retaining a sufficiently large difference between the specific gravities of the sample electrolyte and the receiving electrolyte to allow efficient operation of the cell.

The bottom-drain flow-cell combination also provides the opportunity of decreasing the concentration of trisodium citrate required to shift the zinc reduction to sufficiently negative potentials. This minimizes the decrease in the cobalt response which occurs with increasing concentration of this reagent [15]. Better sensitivity for cobalt can therefore be achieved whilst retaining the discrimination from zinc. Another advantage of the matrix exchange method is the ability to vary the pH of the diluent and receiving electrolyte. The optimum pH for determining cobalt is between 8 and 9, but basic precipitates are also formed in this pH region in zinc plant electrolyte. To overcome this problem, in situ matrix exchange is adopted where the diluent pH is adjusted to 6.4 to suppress the formation of precipitates but still allowing complexation of the cobalt

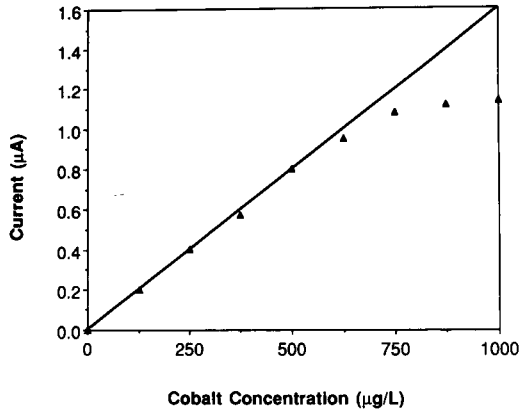

Fig. 5. Cobalt calibration graph obtained with the on-line matrix exchange method. For the linear region: slope = 0.002; intercept = −0.001; standard deviation = 0.01; correlation coefficient = 0.999.

with dimethylglyoxime so that adsorption may occur on the mercury electrode at this pH. The reduction is then performed at pH 8.4 after the zinc electrolyte has been removed by matrix exchange to achieve excellent sensitivity (Fig. 4). Finally, since the bottom-drain flow-cell is operated with a diluted zinc electrolyte sample and a short deposition time, saturation coverage of the mercury drop occurs at a higher concentration than with a standard cell. This extends the linear analytical range and the upper detection limit for cobalt to 600 $\mu g\ l^{-1}$ which allows the range of interest for low-purity zinc electrolyte to be covered. Beyond 600 $\mu g\ l^{-1}$, saturation coverage of the electrode occurs and curvature of the calibration graph is observed, as shown in Fig. 5.

Laboratory catalytic method for the determination of cobalt

As was the case for the matrix exchange method, before implementing the on-line method laboratory based measurements were conducted. Some initial laboratory based experiments confirmed the work of Bobrowski and co-workers [17,18] that cobalt could be determined by adsorptive stripping voltammetry at levels below 1 $\mu g\ l^{-1}$ in the presence of many interfering ions using α-benzil dioxime. This method was applied to purified zinc plant electrolyte using a supporting electrolyte composed of 1.3×10^{-5} M α-ben-

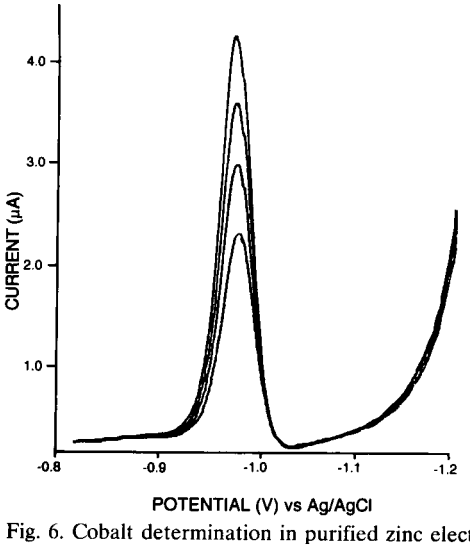

Fig. 6. Cobalt determination in purified zinc electrolyte using catalytic voltammetry and 5 $\mu g\ l^{-1}$ additions of a cobalt standard in a static cell.

zil dioxime, 1.0 M ammonium chloride, 0.5 M sodium nitrite and 1.3% (v/v) ammonia. The major benefit obtained with this catalytic method is that it is so much more sensitive and specific for cobalt that there is no need to use matrix exchange to eliminate zinc interference. The mechanism of this process is not completely understood. The complexation, adsorption and reduction of the cobalt–benzil dioxime complex accumulated by adsorption gives rise to high sensitivity. Addition of nitrite to the supporting electrolyte results in a further 10-fold increase in sensitivity. Nitrite is a strong oxidising agent and is believed to play a role in the regeneration of Co^{2+} by oxidising the electrochemically reduced form, hence giving rise to a catalytic effect [17].

The concentration of ammonium chloride is crucial in minimizing the interference of the zinc reduction wave. Higher concentrations shift the zinc reduction wave to more negative potentials. This is believed to be due to the formation of zinc–chloride complexes. A concentration of 1.0 M ammonium chloride was chosen because it gave peak potential separations of 250 mV for the cobalt and zinc reduction processes. Figure 6 shows clearly that excellent separation of the cobalt and zinc reduction peaks has been achieved even though the ratio of cobalt to zinc is in the order of $1:10^6$.

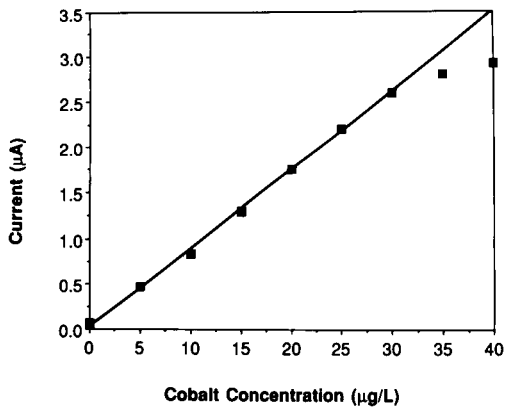

Fig. 7. Cobalt calibration graph obtained with the on-line catalytic method. For the linear region: slope = 0.089; intercept = 0.018; standard deviation = 0.04; correlation coefficient = 0.999.

The linear range for the determination was found to extend from the detection limit of 0.25 $\mu g\ l^{-1}$ to 30 $\mu g\ l^{-1}$. This range is achieved by keeping the adsorption time to a minimum and using large drop sizes. A drop size of 6 (0.45 mm^2) on the Metrohm MME was the largest stable drop size that could be obtained in the supporting electrolyte. The adsorption time used was 10 s, which was in fact the equilibrium period before commencement of the negative potential direction scan. Above a concentration of 30 $\mu g\ l^{-1}$, saturation of the electrode occurs which leads to curvature of the calibration graph, as seen in Fig. 7. Results obtained with the voltammetric method show excellent agreement with the colorimetric results obtained by shift chemists at Pasminco Metals-EZ laboratories [19] in the off-line mode (Table 1) and on-line mode (Fig. 8).

TABLE 1

Off-line cobalt results obtained for low-purity zinc electrolyte and high-purity zinc electrolyte samples

Sample	Voltammetric result [a] ($mg\ l^{-1}$)	Spectrophotometric result ($mg\ l^{-1}$)
Low-purity zinc electrolyte	2.35	2.3
High-purity zinc electrolyte	0.30	0.30

[a] Voltammetric catalytic method with an error of 5% ($n = 5$).

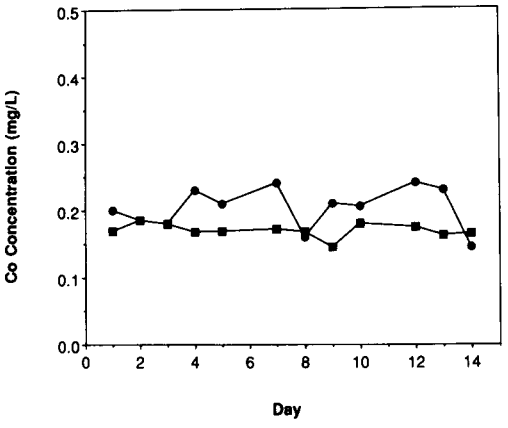

Fig. 8. Comparison of cobalt results obtained over a two-week period with the on-line voltammetric analyser using: (●) the catalytic method ($n = 5$) and (■) the off-line laboratory based spectrophotometric method.

On-line determination

The matrix exchange and catalytic methods have been incorporated into the on-line monitoring program developed at the Pasminco Metals-EZ zinc refining plant using the procedures described in the experimental section. The cobalt methods have been used routinely for the last 3 years. A cobalt determination is performed on zinc electrolyte in both purification tanks and purified electrolyte samples three times an hour, 24 hours a day. The results are transferred to a central computer which graphically displays the levels in a central processing room located in the purification section of the plant. The decision as to whether further purification of the electrolyte is required is based on the result, and so high accuracy is essential. The supporting electrolyte is made up in 20-l batches which last for two weeks. The electrode set-up is reliable and requires very little maintenance, with the only manual input being the changing of the electrode capillary and the filling of the reservoir with mercury. A self-calibrating system fully eliminates operator intervention. Figure 8 shows a graphical comparison of cobalt results obtained from an on-line analyser and the off-line manual spectrophotometric methods performed by shift chemists at the plant. The agreement is excellent with the minor discrepancies being attributable to different sampling locations in the tanks, rather than problems with the chemistry.

Conclusions

Results obtained over a three-year period have shown that cobalt can be monitored routinely in an on-line mode in zinc plant electrolyte using differential pulse adsorptive stripping voltammetry with an error of approximately $\pm 4\%$, based on comparisons with a reference off-line spectrophotometric method. The method has been adapted for on-line monitoring of zinc electrolyte in purification tanks and purified zinc electrolyte samples. The main objective, which was to perform routine on-line cobalt determinations continually, with high precision and with minimal operator intervention, has been achieved. The catalytic method is required to determine cobalt in purified zinc electrolyte where the cobalt levels are of the order of 0.3 mg l^{-1}. The other technique investigated, flow-based differential pulse ADSV with in situ matrix exchange, can be used to determine cobalt in zinc electrolyte from purification tanks where the cobalt concentrations are higher and in the milligram per litre range. The catalytic technique may also be used for low-purity zinc electrolyte, provided levels lie within the linear calibration range.

Financial support provided by Pasminco Metals-EZ and the Australian Research Council is gratefully acknowledged and R.I.M. is grateful for the award of an Australian Postgraduate Research Award (Industry).

REFERENCES

1 A.M. Bond, R.W. Knight and O.M.G. Newman, Anal. Chem., 60 (1988) 2445.
2 A.M. Bond, R.W. Knight, B.R. Champion and O.M.G. Newman, Extraction Metallurgy, Inst. of Mining and Metallurgy, London, 1989, pp. 301–313.
3 Y. Inokuma, Jpn. Pat. Appl., 85-52664 (1985).
4 H. Chen and R. Neeb, Fresenius' Z. Anal. Chem., 314 (1983) 657.
5 S.B. Adeloju, A.M. Bond and M.H. Briggs, Anal. Chim. Acta, 164 (1984) 181.
6 S.B. Adeloju and T. Tran, Anal. Lett., 19 (1986) 1633.

7 P.K. Agasyan, E.A. Osipova and G.V. Prokhorova, Zavodsk. Lab., 49 (1983) 11.
8 S.P. Kounaves and J. Buffle, J. Electroanal. Chem., 216 (1987) 53.
9 E.S. Pilkington, C. Week and A.M. Bond, Anal. Chem., 48 (1976) 1665.
10 R.G. Clem, G. Litton and L.D. Ornelas, Anal. Chem., 45 (1973) 1306.
11 A.M. Bond and G.G. Wallace, J. Liq. Chromatogr., 6 (1983) 1799.
12 M. Uto, Y. Itoh and M. Sugawara, Fresenius' Z. Anal. Chem., 32 (1985) 68.
13 L. Huynh and N.E. Whitehead, Oceanologica Acta, 9 (1986) 433.
14 K. Torrance and C. Gatford, Talanta, 32 (1978) 273.
15 M. Geissler and R. DaMaia, Fresenius' Z. Anal. Chem., 330 (1988) 624.
16 T. Schmidt, M. Geissler, G. Werner and H. Emons, Fresenius' Z. Anal. Chem., 330 (1988) 712.
17 A. Bobrowski, Anal. Chem., 61 (1989) 2178.
18 A. Bobrowski and A.M. Bond, Electroanalysis, 3 (1991) 157.
19 A.I. Vogel, Quantitative Inorganic Analysis, Longman, London, 3rd. edn., 1961, p. 795.

Analytica Chimica Acta, 281 (1993) 291–297
Elsevier Science Publishers B.V., Amsterdam

Study of uranyl(VI) ion reduction at various ionic strengths of sodium perchlorate

Renata Djogić and Marko Branica

Centre for Marine Research Zagreb, "Rudjer Bošković" Institute, POB 1016, 41001 Zagreb (Croatia)

(Received 24th August 1992; revised manuscript received 16th March 1993)

Abstract

To determine the number of water molecules involved in the electrode reaction of the uranyl(VI)–(V) redox pair, square-wave voltammetric measurements of uranyl(VI) ion reduction in non-complexing $NaClO_4$ media at pH 2 and different ionic strengths between 0.1 and 8.5 mol l^{-1} were performed. The available literature water activity data were compared and taken into account. The loss of two water molecules was established.

Keywords: Voltammetry; Uranyl(VI)

The purpose of this work was to evaluate how the change in the supporting, non-complexing electrolyte concentration affects the dehydration of the uranyl(VI)–(V) redox pair from measurements of square-wave voltammetric (SWV) peak potential shifts.

A frequently used concept in describing the state of the ions in solution is the so-called "solvation" or "hydration" number. Conway [1] distinguished water molecules simply geometrically coordinated as inevitable neighbours of the ions and those which in the time average are in some way physically or chemically associated with the ions. Bockris [2] defined a primary solvation number (permanently associated with the ion) and secondary hydration number (larger number of water molecules affected by the ion). Koryta and Dvorak [3] differentiate between the primary hydration region (close vicinity of the ion where water molecules are strongly electrostatically bound to it, causing a loss of rotation ability) and a region further from the ion with a more or less distorted water structure. Regions even further away retain the original water structure.

In acidic non-complexing media, uranyl(VI) ion is hydrated with six molecules of water, $UO_2(H_2O)_6^{2+}$ [4]. The polarographic behaviour of uranyl(VI) ion in aqueous solutions containing non-complexing agents has been the subject of numerous studies [5]. The general conclusion of the electrode reaction study corresponding to the first polarographic wave (at potentials of ca. −0.2 V vs. SCE) is that a one-electron reduction of the uranyl(VI)ion (UO_2^{2+}) results in the formation of the uranyl(V) ion (UO_2^{+}). The reversible nature of this electrode reaction was recognized.

In this paper, the electrochemical reduction of the uranyl(VI) ion in dilute to highly concentrated perchlorate media at a hanging mercury drop electrode is described. Attempts are made to explain the SW peak potential shift to positive values with increasing ionic strength.

Correspondence to: R. Djogić, Centre for Marine Research Zagreb, "Rudjer Bošković" Institute, POB 1016, 41001 Zagreb (Croatia).

EXPERIMENTAL

Solutions were prepared from analytical-reagent grade chemicals. A uranium perchlorate stock standard solution was prepared and standardized gravimetrically [6].

All measurements were made using a PAR 384B polarographic analyser and a standard polarographic cell (50 cm^3) with a three-electrode system: a hanging mercury drop electrode (surface area 2.20 ± 0.05 mm^2) as the working electrode, an Ag/AgCl–saturated NaCl reference electrode and a platinum wire counter electrode. In the set of measurements in which the reference electrode was provided with a salt bridge, the solution inside the bridge was of the same ionic strength as the electrolyte solution in the polarographic cell. Square-wave voltammograms were recorded at a frequency of 50 Hz, pulse height 50 mV and scan increment 2 mV.

The PAR 384 was connected with an HP 9816 S technical computer together with an HP 9121D double-disk drive, an HP 82986A graphics printer and an HP 7475A six-pen plotter, as described previously [7]. The software package 384-Allmet [8] for communication between the computer system and the PAR 384B for graphical presentation and evaluation of electrochemical data was used.

For the study of uranyl(VI) ion reduction at pH 2, the experiment was designed as follows. Starting with uranyl(VI) ion in aqueous acidic solution, the reduction peak potential was measured after successive additions of 9.25 mol l^{-1} $NaClO_4$ [acidified to pH 2 with $HClO_4$ and the same uranyl(VI) ion concentration] until an ionic strength of 5 mol l^{-1} had been reached. A new solution of the same uranyl(VI) ion concentration in acidified $NaClO_4$ (9.25 mol l^{-1}) medium was then placed in the polarographic cell and measurements after successive dilutions with acidified aqueous solution of the same uranyl(VI) concentration were repeated until an ionic strength of 5 mol l^{-1} had been reached. In this way the uranyl(VI) ion concentration and acidity were kept constant throughout the measurements and only the ionic strength was varied. During the experiment the pH electrode was immersed in the measuring solution and the pH was maintained constant.

RESULTS AND DISCUSSION

Square-wave voltammetric measurements were made in order to study the influence of ionic strength on the reduction of the hydrated uranyl(VI) ion in non-complexing media. The measurements were made using dilute to highly concentrated $NaClO_4$ solutions. Sodium perchlorate was selected owing its small complexing abil-

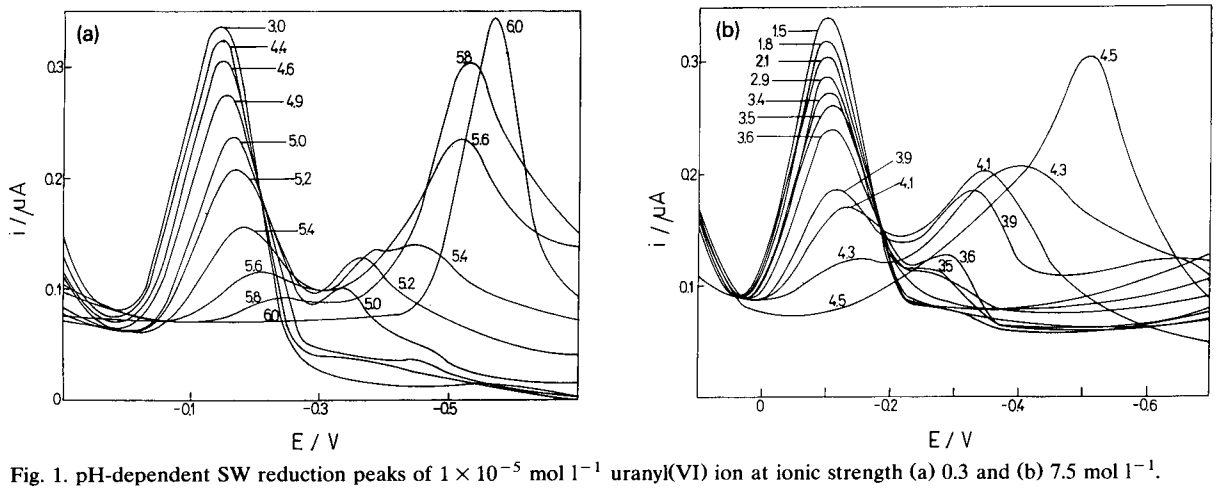

Fig. 1. pH-dependent SW reduction peaks of 1×10^{-5} mol l^{-1} uranyl(VI) ion at ionic strength (a) 0.3 and (b) 7.5 mol l^{-1}.

ity and high solubility. A pH value of 2 and a concentration of uranyl(VI) ion of 1×10^{-5} mol l^{-1} were kept constant throughout the measurements. The reduction of uranyl(VI) ion under these conditions is a single-electron reversible process [9]. A low pH was used because at ionic strength 7.5 mol l^{-1} the uranyl(VI) hydrolysis starts at pH values higher than 2.

Uranyl(VI) hydrolysis at different ionic strengths

The hydrolysis of hydrated uranyl(VI) ion in the pH range 1.5–6.5 was studied at different ionic strengths. Depending on the acidity of the solution and the ionic strength (0.1 and 5.0 mol l^{-1}), the first reduction peak occurs in the pH range 1.5–5 and the second between pH 3.4 and 5 (Fig. 1). The first reduction peak is ascribed to the reduction of hydrated and labile hydrolysed uranyl(VI) ion to uranyl(V) ion [10]. On increasing the pH of the solution, OH^- ions are produced by the protolysis of one of the coordinated water molecules and the uranyl(VI) hydrolytic species are reduced at more negative potentials (in the range -0.3 to -0.5 V vs. Ag/AgCl).

The dependence of the normalized currents of the first peak on pH and ionic strength is shown in Fig. 2. It can be seen that in highly concentrated 7.5 mol l^{-1} $NaClO_4$ solution, the normalized peak current decreases at pH > 2. The dependence of the peak potential on the pH of the solution is shown in Fig. 3. Up to pH 4 and an electrolyte concentration of 4 mol l^{-1}, there is no pronounced shift of the peak potential. However,

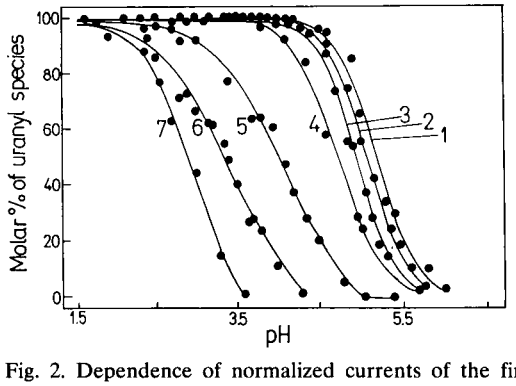

Fig. 2. Dependence of normalized currents of the first SW peak on pH and ionic strengths. Ionic strength: (1) 0.1; (2) 0.3; (3) 2; (4) 3.0; (5) 4.0; (6) 7; (7) 7.5 mol l^{-1}.

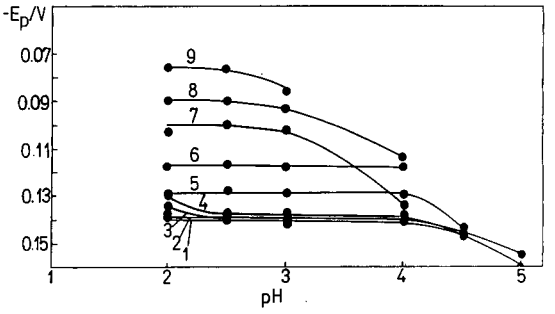

Fig. 3. Dependence of first SW peak potential on pH at different ionic strengths. Ionic strength: (1) 0.1; (2) 0.3; (3) 0.5; (4) 2; (5) 3; (6) 4; (7) 5; (8) 7.5; (9) 8.75 mol l^{-1}.

with a highly concentrated electrolyte the peak potential shifts to negative values, i.e., the hydrolysis of the hydrated uranyl(VI) ion is detected at pH 2.5. This indicates that at higher ionic strengths, more pronounced interactions between uranyl(VI) ion and OH^- ligands, i.e., the hydrolysis of the dehydrated uranyl(VI) ions, start at lower pH values. From these results it could be concluded that uranyl(VI) ion in aqueous solution shows a strong interaction with water molecules. The hypothesis is that the hydration number of uranyl(VI) ions plays a role in the reduction mechanism.

According to literature data [11], the stability of uranyl(V) ion increases with decreasing acidity and an optimum stability can be predicted for the pH range 2–4. In other words, the rate of disproportionation decreases with decreasing acidity [11]. During the experiments, in order to avoid the precipitation and polymerization of uranyl(VI) hydrolysis products, the uranyl(VI) ion concentration must be kept as low as possible.

Overall process

At pH 2, with an increase in the ionic strength the SW peak potential shifts in the positive direction (Fig. 3) and the shift is linear in the experiment performed with the reference electrode immersed directly in the solution (Fig. 4a). By regression analysis the slope is 6.6×10^{-3} with a standard error of 3.0×10^{-4} (for 23 measuring points). However, to reduce the liquid junction potential to the smallest possible value, another series of measurements were performed with the

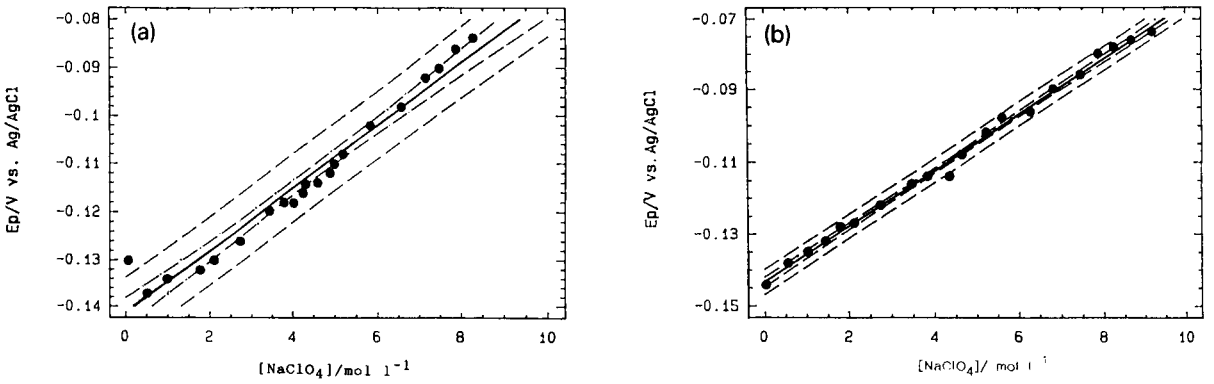

Fig. 4. SW peak potential shift of the uranyl(VI) ion reduction peak (1×10^{-5} mol l^{-1} UO_2^{2+}) with variation in the concentration of $NaClO_4$ at pH 2. (a) without salt bridge; (b) with salt bridge. Straight lines have been fitted (solid lines) with a 95% confidence interval.

reference electrode connected through a salt bridge (Fig. 4b). The "new" slope is 7.8×10^{-3} with a standard error of 1.2×10^{-4} (for 20 measuring points). The difference between these two sets of experiments is small but is significant from the statistical point of view.

The observed SW peak potentials plotted as a function of the square root of the ionic strength are shown in Fig. 5, showing that the SW peak potential varies between wide limits when the ionic strength is altered. Curve 1 in Fig. 5 represents the experiment with the reference electrode connected with the bulk through the bridge containing the cell solution without uranyl(VI) ion.

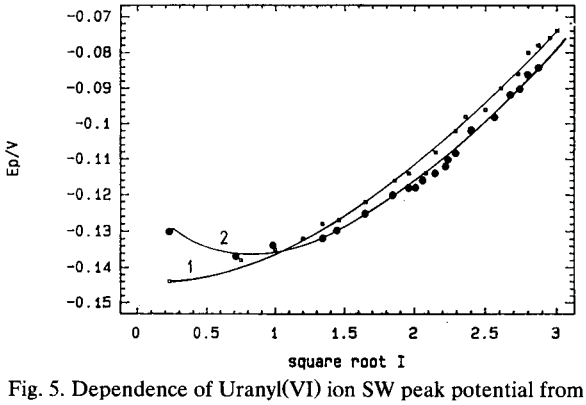

Fig. 5. Dependence of Uranyl(VI) ion SW peak potential from Fig. 4 on square root of ionic strength. Line 1, experiment with reference electrode connected with bulk throughout the bridge; line 2, reference electrode immersed directly in the solution.

Curve 2 is obtained with the reference electrode immersed directly in the solution. At ionic strengths less than 1 mol l^{-1} a considerble E_p potential shift between curves 1 and 2 exists. For ionic strengths higher than 1 mol l^{-1} an almost constant difference between curves 1 and 2 is recorded, which can be ascribed to the liquid junction potential. The peak current at pH 2 depends almost linearly on the ionic strength (Fig. 6). This means that under such experimental conditions the disproportionation of uranyl(V) ion is not significant. An increase in the ionic strength usually increases the viscosity of the solution, which, in turn, should decrease the rate of diffusion of the electroactive species to the electrode. This is reflected in the lowering of the observed SW peak current [12].

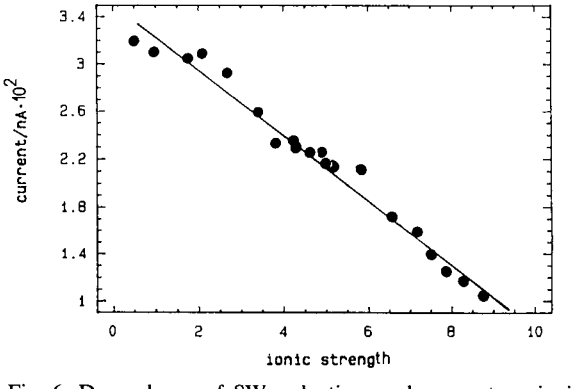

Fig. 6. Dependence of SW reduction peak current on ionic strength of the solution at pH 2.

Activity of water in sodium perchlorate solutions

Different literature data [13–21] for the dependence of the water activity, a_w, on sodium perchlorate concentration are presented in Fig. 7. According to Galus and co-workers [14,15], a_w decreases almost linearly with increase in sodium perchlorate concentration. Data presented by Andreu et al. [13] and Jindal et al. [19] differ significantly from those of Galus and co-workers. Values given by Robinson and Stokes [18] and Durst and Hume [20] were recalculated from molality to molarity of $NaClO_4$ [21] and they fit very well the values for a_w of Andreu et al. [13] and Rush and Johnson [17]. The activity of water for each experimentally used ionic strength was taken from line 2 in Fig. 7.

Hydration number

The number of water molecules involved in the electrode reaction can be calculated as described by Andreu et al. [13]. However, there is a difference on comparing their data with the present results as the uranyl(VI) ion and its reduction product, uranyl(V) ion are both water soluble, whereas Zn(II) is reduced to an amalgam. Considering the electrode reaction

$$[UO_2(H_2O)_m]^{2+} + e^- \rightleftharpoons [UO_2(H_2O)_n]^{+} + (m-n)H_2O$$

one should take into account the change in hydration of both ions. Hydration may be formally

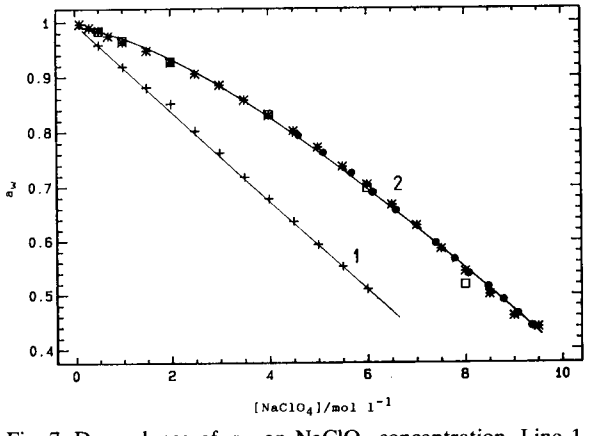

Fig. 7. Dependence of a_w on $NaClO_4$ concentration. Line 1 (+): a_2 data from [14,15]. Line 2: (*) a_w data from [13,18,20,21]; (□) a_w data from [19]; (●) a_w data from [17].

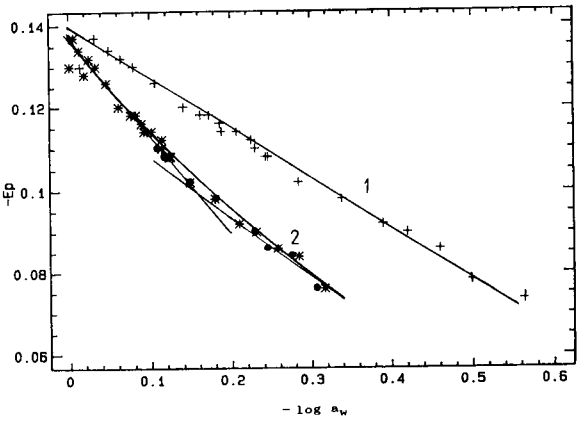

Fig. 8. Linear regression of E_p (from Fig. 4a) vs. the logarithm of the water activity. Reference electrode connected directly with the electrolyte solution. Line 1 (+): a_w data from [14,15]; line 2: (*) a_w data from [13,18,20,21]; (●) a_w data from [17].

considered as a special case of a complex formation reaction. These procedures were worked out for the determination of the coordination numbers of reversible reaction systems and may be adapted to the determination of the difference in hydration numbers $(m-n)$ [22].

However, this calculation with respect to hydration is valid only under the assumption that the activity coefficients of uranyl(VI) and uranyl(V) ions are not significantly different, leading to a ratio $a(UO_2^{2+})/a(UO_2^{+}) \approx 1$ for the calculation of E_p at the same lonic strength.

From the slope of the reversible SW peak potential versus the logarithm of the water activity (Figs. 8 and 9), the difference in the number of water molecules $(m-n)$ involved in the electrode reaction of pH 2 was obtained.

Taking into account the a_w data of Galus and co-workers [14,15], the slope appears to be constant from 0.1 to 8.74 mol l^{-1} $NaClO_4$ and equals $(m-n) \times (0.0591/n)$ [22], from which the difference in the number of water molecules participating in the electrode reaction was determined (Fig. 8). From the regression analyses the slope is 0.11 with a standard error of 2.4×10^{-3}. The slope corresponds to $m-n = 1.9$ water molecules. From the a_w data taken from line 2 in fig. 7, a similar plot was constructed (Fig. 8). From linear regrfession analysis it follows that a linear relationship exists up to $-\log a_w = 0.16$, which cor-

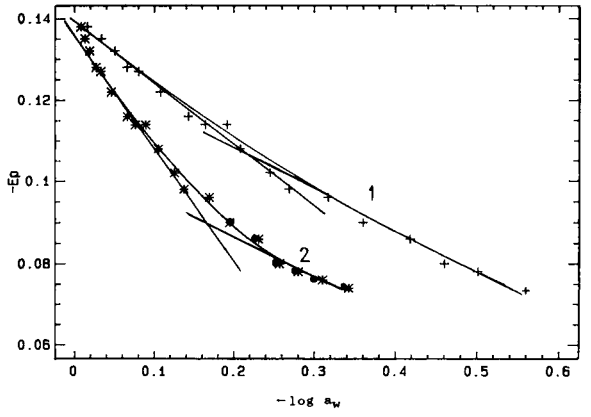

Fig. 9. Linear regression of E_p (from Fig. 4b) vs. the logarithm of the water activity. Reference electrode connected through the bridge with the electrolyte solution. Line 1 (+): a_w data from [14,15]. Line 2: (*) a_w data from [13,18,20,21]; (•) a_w data from [17].

responds to about 5.8 mol l^{-1} $NaClO_4$. The slope of this line gives a hydration difference number $(m-n)$ for the UO_2^{2+}–UO_2^+ couple of 4.1. Above 5.8 mol l^{-1} the hydration difference number decreases gradually to 2.3, indicating desolvation at low water activities.

The slope of the plot obtained from the measurements performed with the reference electrode connected through the bridge with the cell solution and using the a_w data of Galus and co-workers appears to be 0.12 with a standard error of 5.5×10^{-3}, and corresponds to $m-n=2$ water molecules. This plot can be divided into two parts at low ionic strengths the slope is 2.3 and at higher ionic strengths it is 2.0 (Fig. 9, line 1). The plot constructed from the a_w data taken from line 2 in Fig. 7 shows a linear relationship up to $-\log a_w = 0.16$, which corresponds to about 5.6 mol l^{-1} $NaClO_4$. The hydration difference number for UO_2^{2+}–UO_2^+ is 4.5 and above 5.6 mol l^{-1} it decreases gradually to 2.0, indicating progressive desolvation (Fig. 9, line 2).

Elving and Krivis [12] found that on increasing the perchlorate concentration in the $HClO_4$ solution, E_p shifts to more positive values and they ascribed this to junction potential effects. Our experimental data do not show a significant difference between the results obtained with and without a bridge for the reference electrode. Hence, comparing Figs. 8 and 9, lines 1 and 2 have nearly the same slope in both instances, which leads to the conclusion that the liquid junction potential is not of great importance for the E_p shift.

As the hydration difference number is a small value and taking into account the specific structure of uranyl ions [4], probably this method measures the primary hydration difference number.

One can conclude that in aqueous $NaClO_4$ solutions in the ionic strength range 0.1–5.6, the hydration difference number of the uranyl(VI)–(V) couple $(m-n)$ varies between 1.9 and 4.5 because the literature data for a_w differ considerably for this region. At higher ionic strengths the time-average number of water molecules with which the central ion interacts calculated from all available a_w literature data is ca. 2.

From the results obtained according to the different data for water activity, some further speculations can be made, namely that line 2 (Figs. 8 and 9) indicates a more complex nature of the dehydration processes of the uranyl(VI) ion than line 1. The greater slope of line 2, which corresponds to the region of more dilute solutions, could be ascribed to the total effects of dehydration from the outer and primary hydration spheres. In the region of higher ionic strengths, the slope of line 2 becomes 2.0 which is identical with that of line 1 over its entire range and could be ascribed to dehydration from the primary hydration sphere only. This means that line 1 shows only the energetically stronger effect of dehydration from the primary hydration sphere, which is described by the following proposed expression:

$$[UO_2(H_2O)_6]^{2+} + e^- \rightleftharpoons [UO_2(H_2O)_4]^+ + 2H_2O$$

In addition, line 2 also takes into account the influence of dehydration of the outer sphere, which particularly occurs in dilute solutions.

Conclusions

In aqueous $NaClO_4$ solutions the uranyl(VI)–(V) hydration difference number $(m-n)$ de-

pends on the a_w data which were used in the calculations. Taking into the account the a_w data of Galus and co-workers over the entire ionic strength range, the uranyl(VI)–(V) hydration difference number is 2.0. However, considering other above mentioned sets of a_w data, the hydration difference number varies from 4.5 to 2.0 and provides further insight into the dehydration processes. It seems that at lower ionic strengths the greater energy loss is partly caused by the uranyl outer sphere of water. Hence both lines 1 and 2 in Figs. 8 and 9 can be ascribed to the same processes of loss of two water molecules in the dehydration reactions.

The financial support of the Ministry of Science, Technology and Informatics of the Republic Croatia, under Project 1-07-011, Physical Chemistry of Trace Metals in Aquatic Systems, is gratefully ackowledged.

REFERENCES

1 B.E. Conway, Ionic Hydration in Chemistry and Biophysics, Elsevier, Amsterdam, 1981.
2 J.O'M. Bockris, Q. Rev. Chem. Soc. 3 (1949) 173.
3 J. Koryta and J. Dvorak, Principles of Electrochemistry, Wiley, New York, 1987.
4 L.V. Volodko, A.I. Komiak and D.S. Umreiko, Uranilovie Soedinenia, BGU Lenin, Minsk, 1981.
5 L. Sipos, Lj. Jeftic, M. Branica and Z. Galus, Electroanal. Chem., 32 (1971) 35, and referenced cited therein.
6 Gmelins Handbuch der Anorganischen Chemie, No. 55 Verlag Chemie, Weinheim/Bergstr., Berlin, 8th edn., 1936, p. 136.
7 M. Branica, I. Pizeta and I. Maric, J. Electroanal. Chem., 214 (1986) 95.
8 I. Pizeta and M. Branica, J. Electroanal. Chem., 250 (1988) 293.
9 R. Djogic, L. Sipos and M. Branica, Limnol. Oceanogr., 31 (1986) 1122.
10 R. Djogic and M. Branica, Electroanalysis, 4 (1992) 151.
11 K.A. Kraus, F. Nelson and G.L. Johnson, J. Am. Chem. Soc., 71 (1949) 2510.
12 P.J. Elving and A.F. Krivis, J. Inorg. Nucl. Chem., 11 (1959) 234.
13 R. Andreu, M. Sluyters-Rehbach, A.G. Remijnse and J.H. Sluyters, J. Electroanal. Chem., 134 (1982) 101.
14 M. Zielinska-Ignaciuk and Z. Galus, J. Electroanal. Chem., 50 (1974) 41.
15 E. Malyszko, and Z. Galus, Roczn. Chem., 46 (1972) 2291.
16 M. Saakes, M. Sluyters-Rehbach and J.H. Sluyters, J. Electroanal. Chem., 259 (1989) 265.
17 R.M. Rush and J.S. Johnson, J. Phys. Chem., 72 (1968) 767.
18 R.A. Robinson and R.H. Stokes, Electrolyte Solutions, Butterworths, London, 1965.
19 H.L. Jindal, K. Matsuda and R.J. Tamamushi, J. Electroanal. Chem., 90 (1978) 185.
20 R.A. Durst and D.N. Hume, Anal. Chim. Acta, 251 (1991) 3.
21 Š. Komarsky-Lovrić, M. Lovrić and M. Branica, J. Electrochem. Soc., 140 (1993) in press.
22 D.C. Crow, Polarography of Metal Complexes, Academic, London, 1969.

Analytica Chimica Acta, 281 (1993) 299–304
Elsevier Science Publishers B.V., Amsterdam

Catalytic determination of copper in blood plasma using flow-injection biamperometry

Jacek Michałowski

Institute of Chemistry, Warsaw University Branch, Białystok (Poland)

Marek Trojanowicz

Department of Chemistry, University of Warsaw, Pasteura 1, 02-093 Warsaw (Poland)

(Received 25th November 1992; revised manuscript received 15th March 1993)

Abstract

A method for the determination of copper based on the catalytic effect of Cu(II) on the oxidation of thiosulphate by Fe(III) is described. Fe(II) formed in this reactiton in the presence of an excess of Fe(III) allows the use of amperometric detection with two polarized platinum wire electrodes. At a polarizing voltage of 80 mV a linear dependence of current intensity on Cu(II) concentration is obtained in the range of Cu(II) concentrations present in blood plasma. In determinations with a sampling rate of 70 h^{-1} a satisfactory agreement was obtained between the results of flow-injection analysis with biamperometric detection and flame atomic absorption spectrometry.

Keywords: Amperometry; Catalytic methods; Flow injection; Blood; Copper; Plasma

Because of the very complex matrix composition, the determination of copper in blood serum and plasma or in whole blood is most frequently carried out using atomic spectrometric methods, requiring expensive equipment, such as atomic absorption spectrometry with electrothermal [1–7] or less often flame atomization [8,9], inductively coupled plasma (ICP) atomic emission spectrometry [10,11], ICP–mass spectrometry [12] or energy-dispersive x-ray fluorescence spectrometry [13]. New reagents for the selective determination of copper in serum or whole blood are also often reported [14–17]. Much more seldom are reported determinations with the use of gas [18] or ion [19] chromatography.

Copper is the most commonly determined element using catalytic methods, mainly with the use of oxidation reactions [20]. The catalytic effect of Cu(II) on the oxidation of thiosulphate by Fe(III) was employed for practical analytical purposes in two studies [21,22], where spectrophotometric detection of the thiocyanate complex of Fe(III) was utilized.

Amperometric detection with two identical working electrodes, polarized with a small potential difference, is based on the measurement of current intensity, which is observed in the presence of two forms of a reversible redox couple in solution. Direct determination of one of the components of a redox couple is rarely used, owing to insufficient selectivity. A much broader application can be found for indirect biamperometric detection with the use of an indicating redox couple. The most often used indicating system so far in flow-injection biamperometry is the iodide–iodine couple, exploited for the determination of nitrate and nitrite [23], residual chlorine [24] and acids [25] and for the catalytic determi-

Correspondence to: M. Trojanowicz, Department of Chemistry, University of Warsaw, Pasteura 1, 02-093 Warsaw (Poland)

nation of molybdenum [26]. A hexacyanoferrate(III)–hexacyanoferrate(II) indicating system was successfully used for the simultaneous determination of sucrose and sugars [27].

In this study, the flow-injection catalytic determination of copper was investigated with the Fe(III)–Fe(II) couple as the indicating system in the presence of thiosulphate. The intensity of the current in the biamperometric detection system in the presence of an excess of Fe(III) is proportional to the concentration of Fe(II) formed and indirectly to the copper(II) concentration in injected solutions. The measuring set-up is instrumentally simple and was successfully employed for the determination of copper in blood plasma samples.

EXPERIMENTAL

The measuring system consisted of a Minipuls 2 multi-channel pump (Gilson), a Rheodyne Model 5020 low-pressure rotary injection valve and a flow cell connected to a PLP-225C a.c./d.c. polarograph (Zalmed, Warsaw), which was in turn connected to a TZ 4620 potentiometric strip-chart recorder (Laboratorní Přístroje, Prague).

The flow cell used was the same as described previously [26]; the platinum electrodes were 0.6 mm i.d. and 13 mm long. A constant polarizing voltage was applied from the polarograph and controlled using a V541 digital voltmeter (Meratronik, Warsaw). The optimized system used is outlined in Fig. 1. The manifold was made of polypropylene tubing of 0.7 mm i.d. with laboratory-made Perspex connectors.

AAS measurements with electrothermal atomization (ETAAS) were performed using a Philips PU 9100 spectrometer and measurements with flame atomization (FAAS) using an AAS 1 spectrometer (Zeiss, Jena).

RESULTS AND DISCUSSION

Optimization of flow-injection system

The catalysis by Cu(II) of the oxidation of thiosulphate by iron(III) is well known. The rate constants defined by the equations

$$-\mathrm{d}[Fe^{3+}]/\mathrm{d}t = k_1[Fe^{3+}][S_2O_3^{2-}]$$

$$-\mathrm{d}[Fe^{3+}]/\mathrm{d}t = k_2[Cu^{2+}][Fe^{3+}][S_2O_3^{2-}]$$

are $k_1 = 1.44 \times 10^4$ l mol^{-1} min^{-1} and $k_2 = 2.1 \times 10^9$ l mol^{-1} min^{-1} [28]. This behaviour can be exploited for the indirect biamperometric determination of copper using the Fe(III)–Fe(II) indicating system. In continuously delivered Fe(III) solution the production of Fe(II) due to the addition of Cu(II) to the solution results in a current flow in the biamperometric detection system.

Because the copper concentration in blood is within the range 0.7–1.6 mg l^{-1} [29], for such a concentration range the conditions of biamperometric flow-injection analysis in the set-up shown in Fig. 1 were optimized. In initial optimization measurements Cu(II) solutions were injected into a carrier stream of distilled water, which was merged with combined streams of iron(III) nitrate and sodium thiosulphate and then through the reaction coil was delivered to the detector. Preliminary measurements indicated that such a configuration of the flow-injection system is more advantageous than that with simultaneous injection of Cu(II) solution into the carrier stream of HCl and thiosulphate into the Fe(III) solution stream, as in the latter system a much larger signal was observed from the non-catalysed reaction of thiosulphate oxidation by Fe(III).

The magnitude of the signal and the stability of the baseline in the measuring system investi-

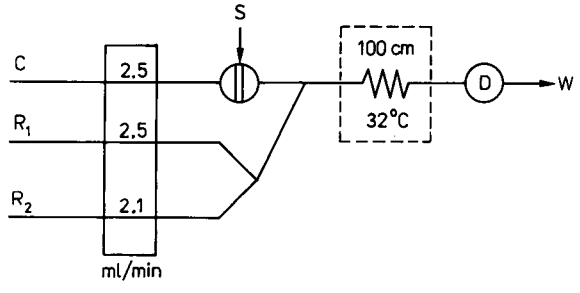

Fig. 1. Schematic diagram of optimized flow-injection system used. S = Sample injection point; D = biamperometric detector; C = carrier solution of 0.11 M HCl with 6.7% trichloroacetic acid; $R_1 = 0.02$ M iron(III) nitrate solution; $R_2 = 0.28$ M sodium thiosulphate solution.

gated are affected by numerous experimental parameters, which were separately optimized for injections of 0.7 mg l^{-1} Cu(II) solution. With an increase in the polarizing voltage from 10 to 100 mV almost linear increase in the magnitude of the signal was observed (Fig. 2). Above 100 mV the changes in signal magnitude were much smaller. As an increase in signal magnitude was associated with a significant increase in the baseline noise, for further studies 80 mV was adopted the as optimum polarizing voltage.

The concentration levels of the two substrates of the catalytic reaction employed have a significant influence on the sensitivity of detection. The effect of Fe(III) concentration was examined in the range 5–30 mM. The signal increased up to 20 mM and this value was adopted as the optimum. Then, using this concentration of iron(III), the effect of thiosulphate concentration was examined in the range 0.1–0.45 M. The largest peak height was obtained at a concentration of 0.28 M.

As one would expect in a catalytic determination, and as was reported previously using the same catalytic system with spectrophotometric detection [22], an increase in temperature in the reaction coil should lead to a larger signal. With the present system, however, this was observed only up to 35°C and at higher temperatures a decrease in the flow-injection peak height was observed (Fig. 3), which can be attributed to a higher rate of non-catalysed reactions taking place. The effect of Cu(II) addition in such a circumstance is less pronounced. Similarly to the influence of the increase in polarizing voltage, an increase in temperature in the reaction coil is accompanied by deterioration of the baseline stability. As a compromise, 32°C was taken as the optimum temperature.

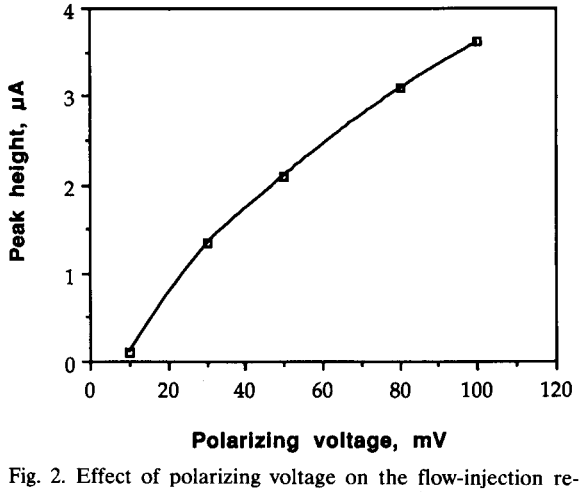

Fig. 2. Effect of polarizing voltage on the flow-injection response obtained for injections of 0.7 mg l^{-1} Cu(II) solution.

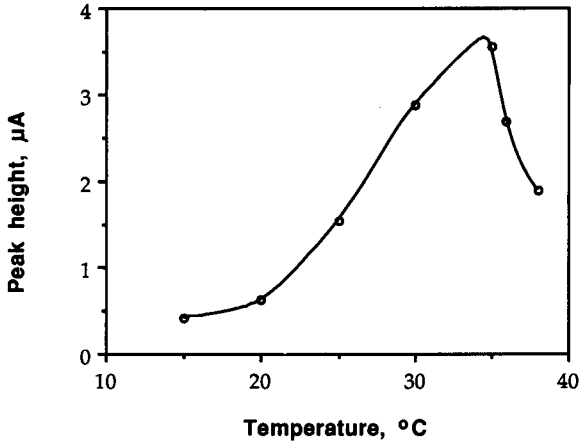

Fig. 3. Effect of temperature in the reaction coil on the flow-injection response obtained for injections of 0.7 mg l^{-1} Cu(II) solution.

Other factors affecting the response of the detection systems examined included the length of the reaction coil, the flow-rate of the carrier stream and the sample injection volume. An increase in reaction coil length from 100 to 250 cm resulted in a small increase in the signal magnitude, with an increased time of return of the signal value to the baseline level. For coils longer than 250 cm, a decrease in signal magnitude was observed. A 100-cm reaction coil was used in further work.

A monotonous decrease in flow-injection peak height was recorded with increasing flow-rate of the carrier stream in the range 1.3–3.8 ml min^{-1}. Owing to the opposite effect of these changes on the dynamic characteristics of the response, a flow-rate 2.5 ml min^{-1} was selected for the final configuration, which allows a sampling frequency of 70 h^{-1}.

Usually in flow-injection analysis an increase in sample volume leads to an increase in the

sensitivity of detection. The effect of this parameter was examined in the range 50–300 μl. As an increase in injection volume from 200 to 300 μl produced only a 10% increase in the signal magnitude, a 200-μl injection volume was considered to be sufficient.

An example of the results obtained with the optimized set-up for Cu(II) concentrations in the range 0.2–0.8 mg l^{-1} is shown in Fig. 4. The calibration graph obtained from this measurement was linear and can be described by equation $y = -0.191 + 4.56x$ with a correlation coefficient value of 0.9998 ($n = 24$), where y is the signal height (μA) and x is the Cu(II) concentration (mg l^{-1}). Figure 4 also illustrates the good signal reproducibility for the same sample of blood plasma.

Owing necessary pretreatment of plasma samples described below, in the final configuration of the flow-injection set-up the water in carrier stream was replaced with 0.11 M hydrochloric acid containing 6.7% trichloroacetic acid. These conditions were used to obtain the recording shown in Fig. 4 and also to study the effect of several potential inorganic interfering species (Table 1) by comparing the flow-injection responses obtained for the injection of Cu(II) solutions without and with interfering species. The tolerance limit adopted was the concentration of interferent causing deviations of the signal magnitude of $< 5\%$. For all the species examined, the tolerated concentrations were lower than or equal to the upper levels normally present in blood serum. Measurements of standard Cu(II) solutions without and with preliminary oxygen removal with argon showed no interference from the dissolved oxygen.

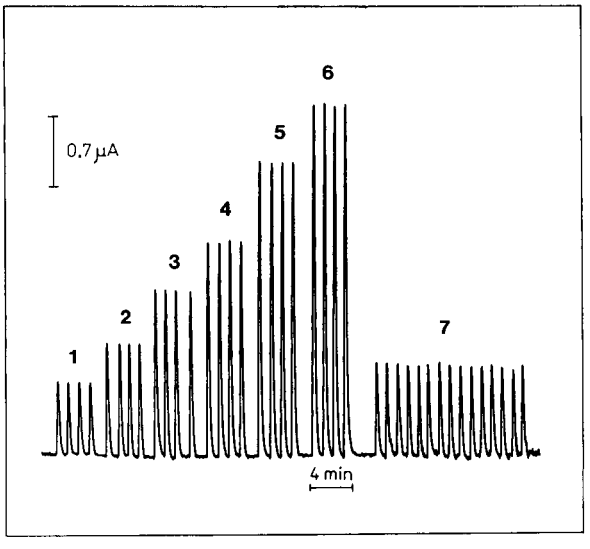

Fig. 4. Flow-injection response obtained in the optimized set-up for injections of (1) 0.2, (2) 0.3, (3) 0.4, (4) 0.5, (5) 0.7 and (6) 0.8 mg l^{-1} Cu(II) solutions and (7) multiple injections of blood plasma sample.

TABLE 1

Concentrations of interfering species causing an error in flow-injection biamperometric determination of 0.2 mg l^{-1} Cu(II) not exceeding $\pm 5\%$.

Interferent	Level in human blood serum (mg l^{-1})	Tolerated concentration (mg l^{-1})
Chloride	3300–3600 [a]	4500
Chromate		0.15
Al(III)	0.13–0.17 [b]	0.2
Cd(II)	0.001–0.005 [b]	0.1
Cr(III)	0.03 [b]	0.1
Co(II)		0.1
Fe(II)	0.6–1.5 [a,c]	1.0
Mn(II)	0.01–0.02 [b]	0.1
Ni(II)		0.1
Pb(II)	< 0.5 [a]	0.3
Zn(II)	0.5–1.5 [a]	1.4

[a] According to [29]. [b] According to [22]. [c] Total iron.

Determination of copper in blood plasma samples

For biamperometric flow-injection determination of Cu(II) in human blood plasma samples, the samples were pretreated according to procedure described by Gubler et al. [30], which was successfully employed previously for spectrophotometric determination with diethyldithiocarbamate. The copper was liberated from the proteins by incubation for 10 min with hydrochloric acid, followed by precipitation of proteins with 20% trichloroacetic acid. The pretreated samples were centrigfuged for 5 min at 2300 g and the supernatant solution was injected into the flow-injection system.

The results of biamperometric flow-injection analysis were compared with those of ETAAS

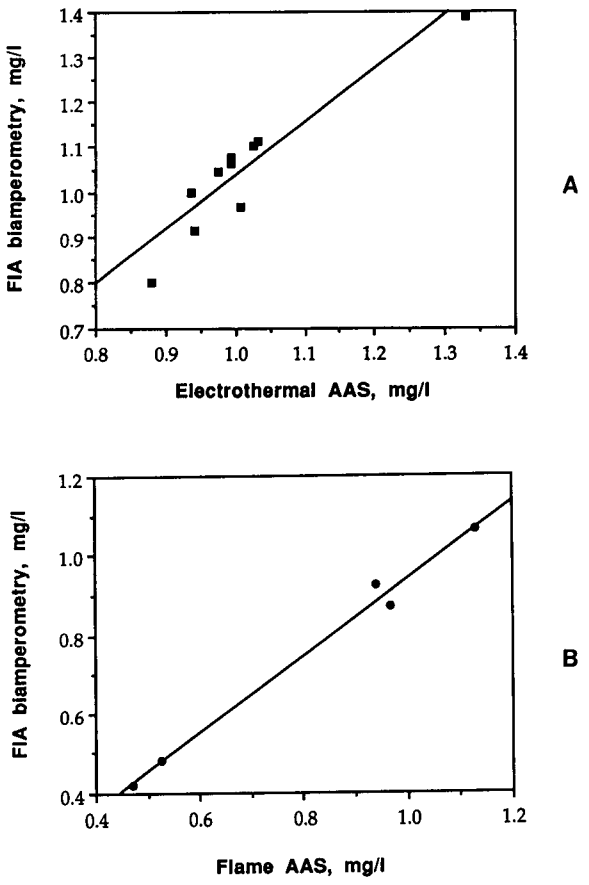

Fig. 5. Correlation plots obtained for results of Cu(II) determination in two sets of blood plasma samples by flow-injection biamperometry vs. (A) ETAAS and (B) FAAS.

determinations under the conditions reported by Glenn et al. [2]. For determinations without precipitation of proteins from plasma with trichloroacetic acid the results of flow-injection analysis were 20–50% lower than those given by ETAAS. For samples with proteins removed, the agreement was much better (Fig. 5A), although the correlation coefficient obtained was not very satisfactory (0.869, $n = 10$).

A much better correlation was obtained between results of flow-injection analysis and FAAS (Fig. 5B). In this instance only partial deproteinization of samples was carried out by adding to 1 ml of plasma sample 50 μl of concentrated nitric acid and distilled water up to total volume 1.5 ml. After centrifugation the sample solution was aspirated to the spectrometer and injected into the flow-injection system. The correlation coefficient obtained was 0.990 ($n = 5$). The precision of the AAS determination as relative standard deviation was 5.9% ($n = 11$), whereas that for flow-injection biamperometry was 2.6% ($n = 15$).

Conclusions

Although the level of copper in blood plasma is in the range detectable by d.c. polarography, the developed method of electrochemical detection is simpler and it extends a variety of previously presented applications of biamperometric detection in flow-injection analysis. The proposed method for the determination of copper in blood plasma can be considered to be an attractive alternative to numerous other methods, as it does not require expensive instrumentation or expensive reagents. A relatively high level of copper present in plasma allows amperometric determination with a signal magnitude in the range of microamps. Routinely used precipitation of proteins is the only sample pretreatment required for this complex matrix. From the study of interferences and the good agreement with the results of AAS determination it is evident that the proposed method is sufficiently selective for routine applications.

REFERENCES

1 J.P. Matousek and B.J. Stevens, Clin. Chem., 17 (1971) 363.
2 M. Glenn, J. Savory, L. Hart, T. Glenn and J. Winefordner, Anal. Chim. Acta, 57 (1971) 262.
3 R.A.A. Muzzarelli and R. Rocchetti, Talanta, 22 (1975) 683.
4 P. del Castilho and R.F.M. Herber, Anal. Chim. Acta, 94 (1977) 269.
5 H. Kamel, J. Teape, D.H. Brown, J.M. Ottaway and W.E. Smith, Analyst, 103 (1978) 921.
6 S. Levi and W.C. Purdy, Clin. Biochem., 13 (1980) 253.
7 A. Taylor and T.N. Bryant, Clin. Chim. Acta 110 (1981) 83.
8 N. Weinstock and M. Uhleman, Clin. Chem., 27 (1981) 1438.
9 T. Makino and K. Takahara, Clin. Chem., 27 (1981) 1445.
10 Z. Minzhi and R.M. Barnes, Appl. Spectrosc., 38 (1984) 635.

11 E.S. Dipietro, M.M. Bashor, P.E. Stroud, B.J. Smarr, B.J. Burgess, W.E. Turner and J.W. Neese, Sci. Total Environ., 74 (1988) 249.
12 H. Vanhoe, C. Vandecasteele, J. Versieck and R. Dams, Anal. Chem., 61 (1989) 1851.
13 H.H. Sky-Peck and B.J. Joseph, Clin. Biochem., 14 (1981) 126.
14 A. Barua, Y.S. Varma, B.S. Garg, R.P. Singh and I. Singh, Analyst, 106 (1981) 799.
15 T. Makino and J.I. Itoh, Clin. Chim. Acta, 111 (1981) 1.
16 T. Makino, Clin. Chim. Acta, 185 (1985) 7.
17 A. Abe, S. Yamashita and A. Noma, Clin. Chem., 35 (1989) 552.
18 S.K. Aggarwal, M. Kinter and D.A. Herold, Anal. Biochem., 194 (1991) 140.
19 C.N. Ong, H.Y. Ong and L.M. Chua, Anal. Biochem., 173 (1988) 64.
20 D. Perez-Bendito and M. Silva, Kinetic Methods in Analytical Chemistry, Horwood, Chichester, 1988, Chap. 2.
21 V.I. Vershinin and G.L. Bukhbinder, C.A., 92 (1980) 51398t.
22 S.M. Ramasamy and H.A. Mottola, Anal. Chim. Acta, 127 (1981) 39.
23 M. Trojanowicz, W. Matuszewski, B. Szostek and J. Michalowski, Anal. Chim. Acta, 261 (1992) 391.
24 W. Matuszewski and M. Trojanowicz, Anal. Chim. Acta, 207 (1988) 59.
25 W. Matuszewski, A. Hulanicki and M. Trojanowicz, Anal. Chim. Acta, 194 (1987) 2669.
26 M. Trojanowicz, A. Hulanicki, W. Matuszewski, M. Palys, A. Fuksiewicz, T. Hulanicka-Michalak, S. Raszewski, J. Szyller and W. Augustyniak, Anal. Chim. Acta, 188 (1986) 165.
27 J. Michalowski, A. Kojlo, M. Trojanowicz, B. Szostek and E.A.G. Zagatto, Anal. Chim. Acta, 271 (1993) 239.
28 K.B. Jacimirski, Kinetyczne Metody Analizy Chemicznej, WNT, Warsaw, 1965.
29 J.B. Henry (Ed.), Clinical Diagnostics and Management by Laboratory Methods, Saunders, Philadelphia, 18th edn. 1991.
30 C.J. Gubler, M.E. Lahey, H. Ashenbrucker, G.E. Cartwright and M.M. Wintrobe, J. Biol. Chem., 196 (1952) 209.

Analytica Chimica Acta, 281 (1993) 305–314
Elsevier Science Publishers B.V., Amsterdam

Determination of iron(III) and titanium(IV) as their Solochrome Violet RS complexes by constant-current stripping potentiometry

Part 1. Automated single-point calibration method for iron(III)

Daniel Jagner, Lars Renman and Svana H. Stefansdottir

Department of Analytical and Marine Chemistry, University of Göteborg and Chalmers University of Technology, S-412 96 Göteborg (Sweden)

(Received 14th January 1993; revised manuscript received 20th March 1993)

Abstract

An automated constant-current stripping potentiometric method for the determination of iron(III) as its Solochrome Violet RS complex is described. The instrumentation is based on a stripping potentiometry unit, a sample changer, a burette system and a conventional three-electrode system with a mercury film electrode. The method can be utilised over a large concentration range [0–500 $\mu g\ l^{-1}$ iron(III)], by an automated adaption of the experimental conditions to the concentrations found in the samples. A single-point calibration procedure with calibration for three different concentration ranges is used. The possibility for normalisation of the electrode response to compensate for variations in hydrodynamic conditions and electrode area is demonstrated. Using this normalisation, the reproducibility is better than 5% for samples at the 15 $\mu g\ l^{-1}$ iron(III) level. For higher concentrations (65 and 300 $\mu g\ l^{-1}$), the corresponding values are 2.9 and 3.5%, respectively. The applicability of the method for the determination of titanium(IV) is discussed. The method is applied to the determination of iron(III) in tap water and rain water samples.

Keywords: Potentiometry; Batch system; Calibration; Iron; Titanium; Waters

Determination of iron by electrochemical stripping techniques has previously been performed using either precipitation of hydrated iron(III) oxide [1] or adsorption of various organic ligand complexes such as iron–catechol [2,3] and iron(III)–Solochrome Violet RS (SVRS) and similar complexes [3–5] on a mercury electrode followed by cathodic stripping. It has also been shown that SVRS can be employed in the determination of titanium(IV) [6]. Adsorptive stripping applications have in common that the useful concentration range for a given analytical procedure is limited by the non-linear response obtained due to electrode surface saturation and/or competitive adsorption from the reagent used. One previously described approach for overcoming non-linear response problems is the use of short electrolysis/strip cycles, where the results from many such cycles are added together before evaluation of the results [5]. For applications employ-

Correspondence to: L. Renman, Department of Analytical and Marine Chemistry, University of Göteborg and Chalmers University of Technology, S-412 96 Göteborg (Sweden).

ing SVRS, the poor resolution between the reagent and the titanium(IV)–SVRS complex poses additional problems.

Automation of electrochemical stripping techniques has hitherto mostly been achieved by different flow system approaches [7]. Though versatile, such systems may suffer from functional anomalies, such as leakage and problems with gas bubbles introduced with the flowing solutions, formed by electrode reactions, or formed by spontaneous degassing at the mixing point of solutions with different viscosity or salt contents and hence different solubilities for gases. When a system for batch mode stripping analysis can be automated by the use of a sample changer, many of these anomalies can be avoided. One of the most prominent qualities of the flow system approach, namely that the electrode system can be kept under potentiostatic control at all times is, however, not readily realised in a batch mode system, and may therefore cause variations in electrode response. As demonstrated in this work, a proper treatment and continuous re-conditioning of the working electrode can overcome this problem, and allow a simpler and more time-efficient single-point calibration approach for quantification, as opposed to the more often used standard addition method.

An inherent advantage in automated analytical systems with a moderate degree of sophistication is that some performance check can be built into the system. This can permit analytical procedures which adapt themselves to conditions set by the samples. In adsorptive electrochemical stripping applications, this is of considerable interest, as linear response over large concentration ranges can seldom be achieved. This work describes a method for the adsorptive stripping potentiometric determination of the SVRS complexes of iron(III) which is adaptive to the point that different concentration ranges are handled and the appropriate analytical conditions are automatically selected for each sample. The method's applicability to the determination of titanium(IV), and the possibility of normalising electrode response for variations in hydrodynamic conditions is also discussed.

EXPERIMENTAL

Instrumentation

A PSU20 potentiometric stripping unit, a SAC80 sample changer and an ABU93 triburette system (Radiometer, Copenhagen), all interfaced to an IBM-compatible personal computer and controlled by the TAP2 Trace Talk program (Radiometer) were used for all experiments. All control of instrumental parameters, including electrolysis potentials, electrolysis times, stirring, stripping current magnitudes, stripping measurements, evaluation of stripping signals, calculation of sample concentrations and logical decision making, as well as control of sample changer and burettes were pre-programmed into the TAP2 program and automatically executed without operator assistance. To avoid contamination from ambient air, the autosampler was placed in a laboratory-built case. The electrode system consisted of a laboratory-constructed 2-mm diameter glassy-carbon (Hochtemperatur-Werkstoffe, Meitingen, Germany) disk electrode, a saturated calomel reference electrode (K436, Radiometer), and a platinum counter electrode with a salt bridge (P736, Radiometer). The inner solution of the platinum electrode assembly was 0.1 M nitric acid. A digital ammeter was connected to the counter electrode to allow an estimation of the electrolysis current during electrode plating and potentiostatic preconcentration.

All potentials given below are vs. the saturated calomel electrode. Unless otherwise stated, all potentiostatic preconcentrations and stripping measurements were performed in stirred solutions.

Reagents and solutions

Stock solutions of 1 mM Solochrome Violet RS (SVRS, Pfaltz and Bauer, Waterbury, CT) in Milli-Q water (Millipore, Bedford, MD) were prepared daily. A 4 M sodium acetate (p.a. grade, Merck) solution was prepared in Milli-Q water and purified by elution through a Chelex column. A sample matrix modifying solution was prepared by mixing 600 g of the 4 M sodium acetate solution with 27.3 ml of a 10000 mg l^{-1} Hg(II)

solution. A 5 mg l^{-1} iron(III) solution in 0.1 M nitric acid was used for preparation of standard solutions. The mercury plating solution used was 100 mg l^{-1} Hg(II) in 0.1 M nitric acid.

Sample preparation

All samples were acidified to 0.1 M nitric acid on sampling. On analysis, 1.1 ml of the sample matrix modifying solution and an aliquot of the SVRS reagent, the amount of which depended on the concentration range investigated, were added to 20 ml of the acidified sample through two of the burettes in the triburette system. This resulted in a final sample pH of 4.5, a mercury(II) concentration of 25 mg l^{-1}, and SVRS concentrations in the range of 20–90 mM.

Electroanalytical procedures

Prior to each batch of analyses, the glassy-carbon electrode was polished with a soft paper tissue and rinsed with ethanol and water. It was then plated from the 100 mg l^{-1} mercury(II) solution by electrolysis at −0.2 to −0.8 V (20 s at each 0.1-V interval) in a non-stirred solution followed by electrolysis for 4 min at −1.0 V with stirring. Between each sample analysis, the electrodes were rinsed for 5 s in a beaker containing the plating solution at a potential of −1.0 V and in a second beaker also containing the plating solution for 20 s at a potential of −1.0 V. When the electrodes were moved from one solution to another, the potentiostat was turned off.

Depending on the concentration ranges investigated, three different measurement procedures were used. When different concentration ranges were investigated in the same batch of analyses, all samples were first subjected to a measurement for the 30–100 μg l^{-1} iron(III) concentration range. The result thus obtained was then used, if necessary, to select the appropriate procedure for a lower or higher concentration range. The experimental conditions used for the different iron(III) concentration are summarised in Table 1.

Procedure for the 30–100 μg l^{-1} iron(III) range

A volume of 1.1 ml of the sample matrix modifying solution and 0.4 ml of the SVRS stock solution was added to each 20 ml sample, resulting in a sample pH of 4.5, a mercury(II) concentration of 25 mg l^{-1} and a SVRS concentration of 20 mM. The sample was then subjected to a pulsed electrolysis/stripping procedure consisting of electrolysis at −0.45 V for 0.3 s followed by stripping with a reducing current of 40 μA until a potential of −0.9 V was reached. The electrolysis potential was then kept at −1.5 V for 1 s prior to the next electrolysis/stripping cycle. A number of 20 of such electrolysis/stripping cycles were used for electrode conditioning prior to the analytical measurement, which consisted of 40 such cycles. The results from the 40 stripping measurements were accumulated in the PSU20 unit before transfer to the personal computer for subsequent evaluation. After a digital filtration of the stripping curve, the iron(III) peak was automatically located and integrated at a peak potential of approximately −0.65 V.

Procedure for the 0–30 μg l^{-1} iron(III) range

The sample, that had previously been analysed by the 30–100 μg l^{-1} iron(III) range procedure, was electrolysed at 0 V for 10 s and −0.45 V for 1 s prior to stripping with a 40-μA reducing current until a potential of −0.9 V was reached.

TABLE 1

Experimental conditions for different iron(III) concentration ranges

Iron(III) concentration range (μg l^{-1})	SVRS reagent concentration (μM)	Electrolysis potential (V vs. SCE)	Electrolysis time (s)	Number of electrolysis/stripping cycles
0– 30	20	0.0	10	20
		−0.45	1	
30–100	20	−0.45	0.3	40
100–500	90	−0.45	0.3	40

The electrode was then held at −1.5 V for 1 s prior to the next electrolysis/stripping cycle. Ten such electrolysis/stripping sequences were used as electrode conditioning prior to the analytical measurement which consisted of 20 such electrolysis/stripping cycles. The accumulated results from these 20 measurements were then evaluated as described above.

Procedure for the 100–500 μg l^{-1} iron(III) range

To the sample, which had previously been subjected to the measurement for the 30–100 μg l^{-1} iron(III) concentration range, a further 1.6 ml of the SVRS stock solution were added, resulting in a total SVRS concentration of 90 mM. After a reaction time (see below), the sample was then subjected to the same analytical measurement as for samples in the 30–100 μg l^{-1} iron(III) concentration range.

Analytical procedure

Two beakers with 25 ml of the mercury plating solution, serving both as plating and rinsing solution, were placed in two positions on the autosampler. Three beakers with 20-ml aliquots of 30, 100 and 500 μg l^{-1} iron(III) standards in 0.1 M nitric acid were placed in three other positions on the autosampler and the remaining positions were used for up to fifteen 20-ml samples. If all three concentration ranges described above were investigated, the following analytical procedure was performed:

The working electrode was first plated with mercury as described above.

Volumes of 1.1 ml sample matrix modifier and 0.4 ml of the SVRS reagent solution were added to the 100 μg l^{-1} standard which was then analysed as for the 30–100 μg l^{-1} iron(III) range described above. The result from this calibration measurement was saved in the computer for later use.

The 30 μg l^{-1} standard was prepared in the same way as the 100 μg l^{-1} standard, and this solution was subjected first to the measurement for the 30–100 μg l^{-1} iron(III) range, the result of which was discarded, and then subjected to the measurement for the 0–30 μg l^{-1} iron(III) range. The result from this calibration measurement was saved in the computer for later use.

Volumes of 1.1 ml of the sample matrix modifier and 2.0 ml of the SVRS reagent solution were added to the 500 μg l^{-1} iron(III) standard. It was then left to stand until a complete run-through of all samples with measurements for the 30–100 μg l^{-1} iron(III) range had been performed.

After the calibration measurements, each sample was then subjected to the procedure for the 30–100 μg l^{-1} iron(III) range. Using the result from the 100 μg l^{-1} calibration solution, the sample concentration was then calculated. For samples found to be below 30 μg l^{-1} in concentration, the measurement procedure for lower concentrations was invoked. For samples with iron(III) concentrations found to be higher than 100 μg l^{-1}, additional SVRS reagent was added as described above, and the sample was left to stand until the first run-through of all samples had been completed.

After the run-through of all samples, the results obtained were checked to determine if any samples required analysis for concentration ranges above 100 μg l^{-1}. If this was the case, the 500 μg l^{-1} standard and the samples found to be above 100 μg l^{-1} in iron(III) were then subjected to final measurements for this concentration range.

Through a simple user-configuration, a prompt from the controlling TAP2 program, one or two of the concentration ranges could be excluded in the analysis of a batch of samples.

RESULTS AND DISCUSSION

Potentiostatic deposition, linear range, and single-point calibration procedure

It has previously been shown that a sample pH of 4.5 is optimum with regard to formation and adsorption of the iron(III)–SVRS complex [4,5], and this was confirmed by the present work. Of a number of metal ion forming complexes with SVRS, only iron(II) and tin(IV) can be shown to give an appreciable interference at this pH [4,5].

The linear response range for the iron(III)–SVRS system can be widely manipulated by an appropriate selection of reagent concentration and potentiostatic deposition potential and deposition time. It has been previously stated that accumulation potentials above −0.3 V result in broad and unsymmetrical peaks, and deposition potentials around −0.4 V have therefore been suggested [4,5]. This is true when high reagent concentrations (above 20 mM) and long deposition times are used. The efficiency of the adsorptive accumulation can, however, be greatly enhanced by the use of a high deposition potential. In fact, deposition potentials of up to +0.2 V can be used on a mercury film electrode to achieve a multifold increase in adsorption efficiency. At this potential, oxidation of the mercury film will, however, start to occur, and potentials above +0.1 V are therefore not recommendable. This high potential also promotes the adsorption of the uncomplexed reagent to such an extent that linearity for the iron(III) complex is impaired due to competitive adsorption. For this reason, deposition at this high potential requires a low reagent concentration and must not be performed for longer times. By the use of the pulsed electrolysis/stripping procedure in samples containing 20 mM reagent, and with the electrolysis time not exceeding 10 s, as described for low iron(III) concentration samples above, the reagent interference could be avoided and linear response and appreciably improved sensitivity could be obtained for samples with iron(III) concentrations up to 30 $\mu g\ l^{-1}$. Figure 1a shows an example of a calibration graph for this concentration range.

For higher iron(III) concentrations, non-linearity occurs also due to saturation of the electrode surface by the iron(III)–SVRS complex itself. Thus, to extend the linear response range, a pulsed electrolysis with very short electrolysis times, 0.3 s, and a deposition potential of −0.45 V, where adsorption of the reagent does not occur, was used. This electrolysis time was the shortest possible to achieve with the instrumentation used. Because of the analytical procedure used, with low reagent concentrations required for the low iron(III) concentration samples, the upper limit for the concentration range with this

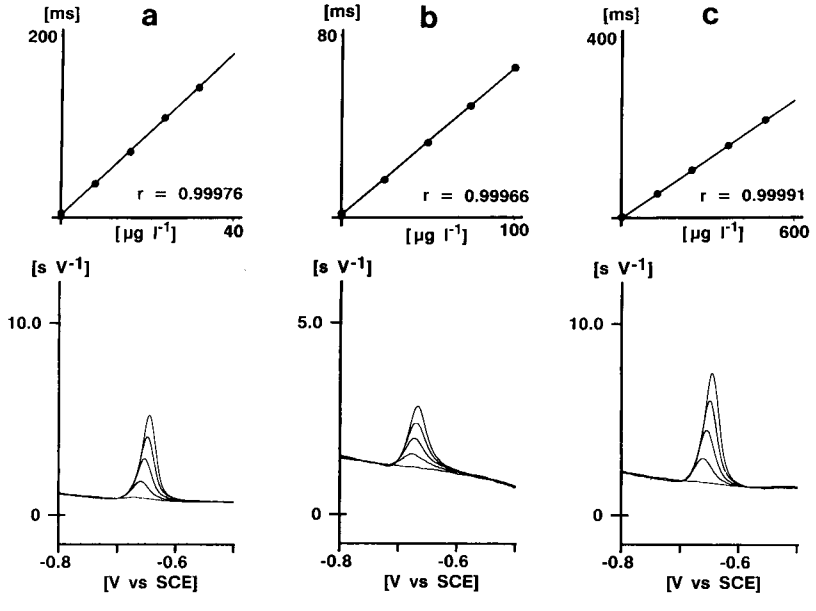

Fig. 1. Stripping curves and linearity for (a) iron(III) in the range from 0 to 35 $\mu g\ l^{-1}$, 20 mM SVRS and electrolysis for 10 s at 0 V and 1 s at −0.45 V and stripping repeated 20 times; (b) iron(III) in the range from 0 to 100 $\mu g\ l^{-1}$, 20 mM SVRS and electrolysis for 0.3 s at −0.45 V and stripping repeated 40 times, and (c) iron(III) in the range from 0 to 500 $\mu g\ l^{-1}$, 90 mM SVRS and electrolysis for 0.3 s at −0.45 V and stripping repeated 40 times. Stripping current 40 μA in all measurements.

short electrolysis procedure was about 150 $\mu g\ l^{-1}$ if no further addition of reagent was made. Figure 1b shows a calibration graph for the 0–100 $\mu g\ l^{-1}$ concentration range obtained using this measuring procedure. For iron(III) concentrations above 100 $\mu g\ l^{-1}$ the reagent concentration was increased to 90 mM. With the same measuring procedure this allowed determination of samples with concentrations above 500 $\mu g\ l^{-1}$ iron(III) with maintained linear response, as is shown in Fig. 1c. With even higher reagent concentrations, linear response can be maintained beyond 5 mg l^{-1} iron(III).

Due to the non-linear response characteristics of the adsorptive stripping technique, use of the standard addition technique for calibration was not considered for this application, as an optimised standard addition procedure should use additions that give a multi-fold increase in response [8]. Obviously, this is not suitable for methods with narrow linear response ranges. Furthermore, standard addition and calibration graph techniques are more time-consuming than the single-point calibration technique used in the present method. As shown below, the reproducibilities obtained warrants the use of the single-point calibration.

Working electrode stability

When calibration procedures other than the standard addition technique is used, it is essential that a stable electrode response is maintained. To achieve this in the present application, mercury(II) must be added to the samples. It was found that the mercury(II) concentration should not be below 20 mg l^{-1}, and preferably higher. Higher concentrations do, however, demand a larger stripping current and therefore result in a decreased sensitivity. The selection of the mercury(II) concentration is therefore a trade-off between electrode stability and sensitivity, and it was found that 25 mg l^{-1} was an acceptable compromise. It should be noted that between each sample analysed, the electrode was re-plated for a short period (20 s) in a 100 mg l^{-1} mercury(II) solution. It should also be noted that after each stripping measurement, the electrode potential was kept at -1.5 V for 1 s. This served the purpose of desorbing reagent reduction products and other adsorbed species, and was necessary in keeping the electrode response stable. If any of these measures were omitted, the electrode response deteriorated rapidly.

In this context it should also be emphasized that both the potentiostatic depositions and the stripping measurements were performed in stirred solutions. This was necessary for two reasons. First, if stirring was not used to facilitate removal of reaction products from the electrode, the response deteriorated rapidly. Second, with the use of up to 40 electrolysis/stripping cycles for each measurement, the time required to stop and restart the stirring between each cycle became forbiddingly long.

Though used for several thousand measurements, the glassy-carbon electrode was rarely polished by other means than with a soft paper tissue. In fact, the same electrode could be used for several months without other polishing, and when polished with a diamond paste, the electrode required extensive use before satisfactory backgrounds were again obtained. This phenomenon has also been observed in other applications where glassy-carbon has been used as substrate for mercury and gold films. Two tentative explanations for this behaviour can be suggested. First, since glassy carbon is a porous material, it is possible that sites inside pores are plated only after prolonged use. Polishing of the electrode with a diamond paste then recreates a new set of such poorly accessible sites. Second, the fact that the counter electrode is kept in a separate compartment with a salt bridge hinders reaction products formed at the counter electrode to reach the working electrode surface and thus prevents detrimental effects from these [9].

Normalization of analytical signal. Reproducibility

In anodic stripping potentiometry, often referred to as potentiometric stripping analysis, the magnitude of the stripping curve background caused by charging/discharging of capacitive ion layers and reactions on the electrode surface is affected by the diffusion rate of oxidants to the electrode surface [10]. If an oxidising constant

current is applied during the stripping measurement, the flux of oxidants to the electrode and the applied current concord in lowering the magnitude of the background. In cathodic stripping applications, where a reducing current is applied, diffusion of oxidants to the working electrode during the stripping measurement may influence the background appreciably.

The principal electrode reactions involved in the present application are summarised in Fig. 2. As obvious, reducible species will diffuse to the working electrode throughout the whole potential range used. This means that during a stripping measurement starting at −0.45 V and ending at −0.9 V, mercury(II), SVRS and dissolved oxygen diffusing to the electrode will consume some of the applied current and thus contribute to the magnitude of the background. By monitoring the electrolysis current, it can be shown that at a potential of −0.5 V, the diffusion-controlled reduction of mercury(II) and SVRS provide the main contributions to the stripping curve background.

Assuming that linear conditions prevail, i.e. that saturation of the electrode surface does not occur, the amount of iron(III)–SVRS complex, M, accumulated during potentiostatic deposition, will be determined by normal diffusion laws according to

$$M = k_1 \frac{CD}{d} A t_{dep} \quad (1)$$

where C is the bulk concentration of the complex, D its diffusion coefficient, d the diffusion layer thickness, A the electrode surface area, and t_{dep} the deposition time. Under constant-current stripping conditions the stripping time, t_{strip}, will then be determined by [11]

$$t_{strip} = k_2 \frac{M}{(i_{strip} - i_o)} \quad (2)$$

where i_{strip} is the magnitude of the applied current and i_o is the amount of this current lost by side reactions due to diffusion of reducible species to the electrode and reactions at the electrode substrate surface. Provided that the condition

$$i_{strip} \gg i_o \quad (3)$$

is fulfilled, small variations in the diffusion layer will not influence t_{strip} noticeably in this respect. If small variations in the electrode surface area or the diffusion layer thickness do occur, and all other experimental conditions are kept constant, a combination of Eqns. 1 and 2 give

$$t_{strip} = k_3 \frac{A}{d} \quad (4)$$

Thus, variations in the electrode surface area or the diffusion layer thickness, e.g. due to variations in positioning of the electrode in the sample vessel, will be pronounced as variations in the analytical signal. As discussed above, the reduction of mercury(II) and SVRS are the main con-

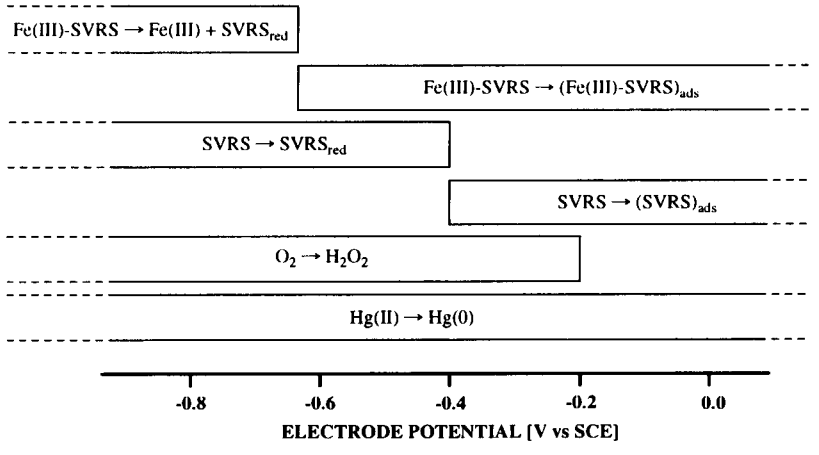

Fig. 2. Principal electrode reactions during potentiostatic deposition and constant-current stripping for the iron(III)–SVRS complex.

tributors to the stripping curve background at potentials around −0.5 V. Since these reactions are diffusion-controlled in the same way as the potentiostatic deposition of the analyte, the background will vary in the same way as the stripping time for the iron(III)–SVRS complex according to Eqn. 4. The magnitude of the background can therefore serve as an internal standard allowing for correction for variations in the diffusion layer thickness. In accordance with this, the stripping curve background in the potential range from −0.55 to −0.5 V was used to normalise the analytical signal by dividing the iron(III)–SVRS stripping peak area by the integrated background area. The reproducibility of the over-all analytical procedure was estimated for the three different concentration levels by analysing ten identical samples at each level. The results, with and without background normalisation of the iron(III)–SVRS stripping peak area, are summarised in Table 2. As obvious, normalisation gives an appreciable improvement in the reproducibility.

Determination of iron(III) in tap water and rain water samples. Detection limit

The applicability of the method was investigated by analysis of various tap water and rain water samples. The results obtained, together with the result obtained in the determination of the same samples by graphite furnace atomic absorption spectrometry (GFAAS) are shown in Table 3. The results shown are those obtained after normalisation of the stripping peak areas as described above. As evident, the results obtained do not significantly differ from those obtained by the GFAAS.

TABLE 2

Reproducibility of the analytical procedures for different iron(III) concentration levels
[Found values are given with standard deviation and C.V. in percent (10 determinations)]

Iron(III) taken ($\mu g\ l^{-1}$)	Iron(III) found ($\mu g\ l^{-1}$)	Iron(III) found after normalisation [a] ($\mu g\ l^{-1}$)
15	16.5 ± 1.8 (11%)	15.9 ± 0.8 (4.8%)
65	64.4 ± 3.1 (4.8%)	65.8 ± 1.9 (2.9%)
300	289 ± 19.5 (6.7%)	318 ± 11.0 (3.5%)

[a] For details see text.

TABLE 3

Determination of iron(III) in tap water and rain water samples

Sample	Number of determinations	Iron(III) found by present method ($\mu g\ l^{-1}$)	Mean found	Iron(III) by AAS ($\mu g\ l^{-1}$)
Tap water 1	3	28.1, 30.2, 30.1	29.5	28.8
Tap water 2	3	59.6, 57.7, 58,5	58.6	60.0
Tap water 3	3	131, 125, 125	127	127
Rain water 1	2	18.6, 17.5	18.1	19.2
Rain water 2	2	31.3, 31.0	31.2	34.4
Rain water 3	2	21.6, 19.8	20.7	21.5

As obvious from Table 3, the results obtained for low-concentration samples show a tendency of underestimating the iron(III) concentration. This is due to a blank from the reagent amounting to about 1 $\mu g\ l^{-1}$ at 20 mM SVRS. With the single-point calibration procedure used, this will pronounce itself as an underestimation of the iron(III) concentration, but can, of course, be corrected for. Because of the reagent blank, the practical detection limit is circa 1 $\mu g\ l^{-1}$.

Determination of titanium(IV)

Because of the poor separation between the reagent and titanium(IV) complex stripping peaks, the applicability of the present method to the determination of titanium is severely limited. Using a reagent concentration of 7.5 mM, and a pulsed electrolysis/stripping procedure similar to the one for low iron(III) concentrations, with potentiostatic adsorption at 0 V for 3 s with stirring and 10 s without stirring followed by 1 s at −0.29 V prior to stripping, the reagent interference can be avoided, as can be seen from the example given Fig. 3. With this procedure, titanium can be determined in concentrations up to 30 $\mu g\ l^{-1}$. For higher concentrations, a non-linear response is obtained.

A major problem with this procedure is, however, that the potential for reduction of the reagent prior to the stripping measurement must be controlled with extreme care. A small deviation from this potential, or a minor change in the

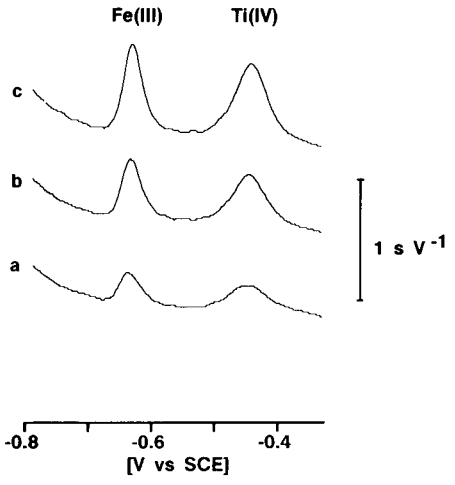

Fig. 3. Determination of titanium(IV) and iron(III) by electrolysis for 3 s at 0 V with stirring and 10 s without stirring and 1 s at −0.29 V followed by stripping with a current of 32 μA (repeated four times): (a) 5, (b) 10, and (c) 15 μg l^{-1} each of iron(III) and titanium(IV). Reagent concentration 7.5 mM.

sample pH, will result either in an incomplete removal of the reagent, or a reduction of the titanium complex before the measurement is started. An additional problem is that in the presence of high concentrations of iron(III) or other ions forming complexes with the reagent, there will not be enough reagent available. Furthermore, at this low reagent concentration, the titanium–SVRS complex formation requires a 10-min reaction time, which makes the method less suitable for automation. The risk for interference from other metals forming complexes with SVRS can be decreased, and the reaction time shortened by using a higher reagent concentration, but this results in a more severe linearity problem due to competitive adsorption and the reduction of the adsorbed reagent prior to the stripping measurement is much less reliable.

Conclusions

It has been demonstrated that problems with non-linear response in adsorptive stripping potentiometry can be overcome by the accumulation of the results from many short electrolysis/strip cycles before evaluation, and by using an automated adaption of the experimental conditions to the analyte concentrations found in the samples. Although this allows iron(III) to be determined as its SVRS complex in a wide concentration range, it does not solve the problem with interference from the reagent in the determination of titanium(IV), and the usefulness of the method to the determination of titanium(IV) is therefore limited.

As also demonstrated, normalisation of the electrode response can be used to improve the reproducibility of the measurements. This has also been shown useful in several anodic stripping applications where an internal standard has been added to the samples as, for example, in the determination of lead in wine [12].

Although extrapolations to other applications and techniques cannot be generalised, it is suggested that most of the operations for extending the linear working range and improving the reproducibility described in the present work should be applicable to most adsorptive stripping applications, also in voltammetry. A moderately demanding prerequisite for using the operations described is, however, that computerised instrumentation is used. Although most modern stripping voltammetry and stripping potentiometry instruments are controlled by personal computers, the software available is often suprisingly simple, lacking even the simplest tools for automating the steps in an analysis method or for manipulating the results obtained. For the present work, all instrument control and data manipulations could be performed with the Radiometer TAP2 program. This program will be described in a future publication.

Multivariate calibration offers an alternative solution to solving some of the problems addressed in the present paper. As described elsewhere [13], both non-linearity and interference problems can be overcome by a partial least-squares regression calibration procedure.

REFERENCES

1 Kh.Z. Brainina and E.M. Roizenblat, Zh. Anal. Khim., 18 (1963) 1392.
2 C.M.G. van den Berg and Z. Qianghuang, J. Electroanal. Chem., 177 (1984) 269.

3 J. Wang and S. Mannino, Analyst, 114 (1989) 643.
4 J. Wang and J.S. Mahmoud, Fresenius' Z. Anal. Chem., 327 (1987) 789.
5 Chi Hua, D. Jagner and L. Renman, Talanta, 35 (1988) 597.
6 J. Wang and J.S. Mahmoud, J. Electroanal. Chem., 208 (1986) 383.
7 J. Wang, Stripping Analysis, VCH, Deerfield Beach, FL, 1985.
8 M.J. Gardner and A.M. Gunn, Fresenius' Z. Anal. Chem., 325 (1986) 263.
9 K.G. McLaren and G. E. Batley, J. Electroanal. Chem., 79 (1977) 169.
10 J. Mortensen and D. Brietz, Anal. Chim. Acta, 131 (1981) 159.
11 Chi Hua, D. Jagner and L. Renman, Anal. Chim. Acta, 197 (1987) 257.
12 D. Jagner, L. Renman and Y. Wang, Electroanalysis, in press.
13 D. Jagner, L. Renman and S.H. Stefansdottir, Anal. Chim. Acta, 281 (1993) 315.

Analytica Chimica Acta, 281 (1993) 315–321
Elsevier Science Publishers B.V., Amsterdam

Determination of iron(III) and titanium(IV) as their Solochrome Violet RS complexes by constant-current stripping potentiometry

Part 2. Partial least-squares regression calibration procedure for iron(III) and titanium(IV)

Daniel Jagner, Lars Renman and Svana H. Stefansdottir

Department of Analytical and Marine Chemistry, University of Göteborg and Chalmers University of Technology, S-412 96 Göteborg (Sweden)

(Received 14th January 1993; revised manuscript received 20th March 1993)

Abstract

An automated method for the determination of iron(III) and titanium(IV) as their Solochrome Violet RS complexes by constant-current stripping potentiometry and partial least-squares (PLS) regression calibration is described. The multivariate calibration procedure overcomes the problem of completely overlapped titanium(IV) complex and reagent stripping peaks and allows prediction of iron(III) and titanium(IV) concentrations from data obtained under non-linear response conditions. For iron(III), accuracy and precision at the 15 and 65 $\mu g\ l^{-1}$ concentration levels are 13.2 ± 2.1 mg l^{-1} (16%) and 67.5 ± 4.6 mg l^{-1} (6.8%), respectively. For titanium(IV) the corresponding values are 14.6 ± 7.3 mg l^{-1} (50%) and 69.5 ± 7.9 (11%). Limitations in the applicability of PLS to electrochemical stripping applications are discussed.

Keywords: Potentiometry; Calibration; Iron; Partial least-squares regression; Titanium

Electrochemical stripping applications based on adsorption of organic analytes or metal chelates often suffer from limitations imposed by non-linearity in response or overlap of the stripping peaks of the analytes and/or the chelating reagent. Examples of this are given in the determination of iron(III) as its Solochrome Violet RS (SVRS) complex, which has been described in a number of applications based on stripping voltammetry [1,2] and constant-current stripping potentiometry [3]. SVRS has also been used for the determination of titanium(IV) by stripping voltammetry [4]. It has been shown that an automated adaption of the experimental conditions to the iron(III) concentrations found in the samples can be used to overcome problems with non-linear response [5].

A major problem involved in using the SVRS reagent for the determination of titanium is the poor resolution between the reagent and reagent–titanium(IV) complex stripping peaks. As a consequence of this, the reagent concentration must be kept low, and the adsorption potential must be chosen and controlled with extreme care. This limits the applicability of the method to a

Correspondence to: L. Renman, Department of Analytical and Marine Chemistry, University of Göteborg and Chalmers University of Technology, S-412 96 Göteborg (Sweden).

narrow concentration range and makes the method sensitive to small variations in experimental conditions or sample composition, and the interference from e.g. iron(III) can be severe due to the low reagent excess used [5].

Multivariate calibration techniques [6,7], as opposed to classical univariate techniques such as standard addition or calibration graph methods, can offer solutions to these problems. An early attempt to apply multivariate data analysis in electrochemical stripping applications was made by Gerlach and Kowalski [8] who tried to solve the problem of copper–zinc intermetallic complex formation in stripping voltammetry by using a multivariate standard addition procedure. Calibration by partial least-squares (PLS) regression has most succesfully been applied to spectroscopic methods, where problems with non-linearity, spectral interferences and light scattering have been overcome [7]. PLS regression has recently been used in the determination of lead(II) and thallium(I) by stripping voltammetry, where a stripping peak overlap occurs [9]. The present paper describes the application of PLS regression calibration to the constant-current stripping potentiometric determination of the SVRS complexes of iron(III) and titanium(IV) with the objective of resolving overlapping stripping peaks and solve problems of non-linear response.

EXPERIMENTAL

Instrumentation

A PSU20 potentiometric stripping unit, a SAC80 sample changer and two ABU93 triburette systems (Radiometer, Copenhagen), all interfaced to an IBM-compatible personal computer and controlled by the TAP2 Trace Talk program (Radiometer) were used for all experiments. All control of instrumental parameters, including electrolysis potentials, electrolysis times, stirring rates, stripping current magnitudes and control of stripping measurements, sample changer, and burettes, as well as the complete calibration designs were pre-programmed into the TAP2 program and automatically executed without operator assistance. To avoid contamination from ambient air, the sample changer was placed in a laboratory-built case.

The electrodes used were laboratory-constructed three-in-one combination electrodes consisting of a 1- or 2-mm diameter glassy-carbon rod inserted in a porous plug in contact with a 0.5 M hydrochloric acid inner solution in which a silver wire and a silver chloride-coated silver wire were used as counter and reference electrodes, respectively. All potentials given below are versus this Ag/AgCl reference electrode. The design of this electrode has been described in detail elsewhere [10].

Multivariate calibration calculations were performed with the Unscrambler software package (CAMO A/S, Trondheim). The data obtained from the PSU20 instrument, where a potential resolution of 2 mV and time resolution of 33 μs is obtained, were converted to a format suitable for the Unscrambler program prior to calculations.

Reagents and solutions

Stock solutions of 0.4 mM Solochrome Violet RS (SVRS, Pfaltz and Bauer, Waterbury, CT) in Milli-Q water (Millipore, Bedford, MD) were prepared daily. A 4 M sodium acetate (p.a. grade, Merck) solution was prepared in Milli-Q water and was used without further purification. A sample matrix modifying solution was prepared by mixing 600 g of the 4 M sodium acetate solution with 27.3 ml of a 10000 mg l^{-1} Hg(II) solution. Standard solutions of 1 mg l^{-1} of iron(III) and titanium(IV) in 0.1 M nitric acid were used for preparation of calibration solutions and simulated samples. The mercury plating solution was 100 mg l^{-1} Hg(II) in 0.1 M nitric acid.

Preparation of standard and sample solutions

Calibration and simulated sample solutions were prepared by mixing appropriate volumes of the iron and titanium standard solutions with 0.1 M nitric acid to a final volume of 18 ml. Prior to analysis, 1 ml of the sample matrix modifying solution and 1 ml of the SVRS solution were added to the samples. This resulted in a pH of approximately 4.5, a mercury(II) concentration of 25 mg l^{-1} and an SVRS concentration of 20 mM.

Analytical procedure

Prior to each set of measurements, the glassy-carbon electrode was polished with a soft paper tissue and rinsed with ethanol and water. It was then plated from the 100 mg l^{-1} mercury(II) solution by electrolysis at −0.2 to −0.8 V (20 s at each 0.1-V interval) in a non-stirred solution followed by electrolysis for 4 min at −1.0 V with stirring. Between each measurement, the electrode was rinsed for 5 s in a beaker containing the plating solution at a potential of −1.0 V and in a second beaker also containing the plating solution for 20 s at a potential of −1.0 V. When the electrode was moved between samples, potentiostatic control was maintained through the drop hanging under the porous plug of the combination electrode [10].

For each sample the following procedure was used:

Standard solutions and nitric acid were added to the sample beaker while the electrode potential was kept at −1.0 V. After the addition of the matrix modifier and the reagent, the potential was lowered to −1.4 V. Each stripping measurement consisted of potentiostatic deposition in a stirred solution for 5 s at +0.05 V followed by 10 s without stirring. The stripping was then performed with a constant current of 10 or 40 μA (for 1- and 2-mm electrodes, respectively) until a potential of −1.05 V was reached. The stirrer was then started and a potential of −1.4 V was applied for 1 s. Prior to the analytical measurement, ten such electrolysis/stripping cycles were performed to allow time for the complex formation and to condition the electrode. The analytical measurement consisted of 20 such stripping measurements, the results of which were summed together in the PSU20 instrument prior to transfer of the data to the controlling computer for further treatment.

The data acquired with the PSU20 instrument, where a time resolution of 33 ms and a potential resolution of 2 mV is obtained, were converted to a format suitable for the Unscrambler software package. This resulted in data matrices with up to 500 response variables for each measurement.

A calibration data set obtained from nine solutions covering the 0–100 μg l^{-1} concentration range for both iron(III) and titanium(IV) was used. Figure 1 shows a graphical representation of the calibration design and the composition of the simulated samples. Unless otherwise stated, PLS regression analysis was performed simultaneously for iron(III) and titanium(IV) using nine cross validation segments, one for each of the nine standards used in the calibration model.

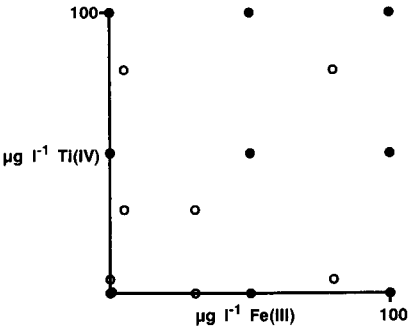

Fig. 1. Composition of (●) calibration solutions and (○) simulated samples.

RESULTS AND DISCUSSION

Measurement conditions

The determination of iron(III) with SVRS can be achieved with high reproducibility, and by appropriate adaption of experimental parameters, can be applied over a wide concentration range using a classical calibration approach [5]. For titanium(IV), the applicability of the method is severely limited by the poor resolution between the SVRS and the titanium(IV)–SVRS complex stripping peaks. To avoid this interference, a low reagent concentration must be used and adsorption of reagent during potentiostatic deposition must be avoided. The use of a low reagent concentration limits the applicable concentration range and makes the procedure sensitive to interferences from other species forming complexes with SVRS, such as iron(III). The reaction time required for formation of the titanium(IV)–SVRS complex at low reagent concentrations makes the procedure less suitable for automated analysis. In addition, the electrolysis potential required to avoid adsorption of the reagent without reduction

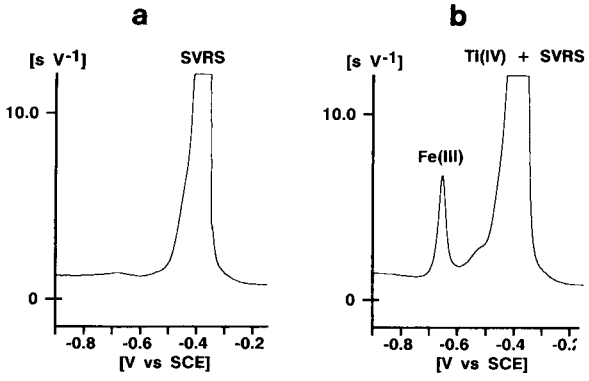

Fig. 2. Stripping curves obtained from (a) blank solution and (b) solution containing 50 μg l^{-1} titanium(IV) and 50 μg l^{-1} iron(III). 20 electrolysis/stripping cycles consisting of electrolysis at +0.05 V for 5 s with stirring and 10 s without stirring followed by stripping with a current of 40 μA (2-mm electrode) and electrolysis at −1.4 V for 1 s. SVRS concentration, 20 mM.

of the titanium(IV) complex must be selected and controlled with extreme care. Alternatively, adsorbed reagent can be reduced prior to stripping, but this requires the same extreme care in potential control, and makes the procedure extremely sensitive to small variations in experimental conditions [5]. The influence of sample pH and reagent concentration, and possible interferences has been discussed in detail elsewhere [1–5].

In the procedure used in the present work, a relatively high reagent concentration (20 mM) was used, and no explicit attempt to avoid reagent adsorption was made. This made it possible to use an adsorption potential of +0.05 V, where adsorption of the complexes is most efficient. An example of a measurement performed by the described procedure is shown in Fig. 2, where the overlap between the reagent and titanium complex stripping peaks is evident.

PLS calibration – selection of reponse variables

PLS regression analysis is an empirical method for correlating a set of measured variables (in this case the stripping time at each 2-mV interval) to a set of "known" variables (the analyte concentrations). This is performed by a partial least-squares optimised extraction of a number of vectors that most significantly transfers the measured variables into the known variables. Each consecutively determined vector is named a "factor", and the total set of factors used to provide the equation for transferring measured variables to known variables is called the "model". The model extracted from the calibration data can, if a significant fit is obtained, be used on data from unknown samples and their concentrations thus be predicted.

For each consecutive factor, the explained variance in measured and known variables can be calculated. The quality of a model can be judged from the accumulated explained variances and the number of factors required to achieve an acceptable explained variance. If too large a number of factors is required to achieve this, the model becomes overfitted, i.e. the model is too well adapted to the calibration data and thus not suitable for prediction of unknown samples. In the present work, the optimum number of factors for a calibration model was determined by cross validation [7] with the highest number of validation segments possible, i.e. by using the data for each individual standard solution separately.

Unlike other regression analysis methods, PLS regression allows covariation in the measured variables. This means that a few number of known variables can be correlated to a large number of randomly chosen measured variables. In the present application, the concentrations of the two analytes [iron(III) and titanium(IV)] are correlated to the stripping curve data at the maximum resolution obtainable, i.e. with up to 500 measured variables.

An inherent property of the PLS regression calibration is that outlier results, which when a univariate calibration technique is used may pass unnoticed, can be detected. Not only outliers with respect to the concentration range used for the calibration, but also with respect to deviating sample matrices, can be detected.

For the present application, the PLS regression analysis on a calibration data set (cf. Fig. 1) typically reached an optimum for 3–4 factors where the variance in iron(III) and titanium(IV) concentrations was explained to 98–99%. Using these model factors on the simulated samples, predicted values for the titanium and iron concentrations were obtained as shown by the exam-

ples in Fig. 3. As is obvious, the prediction of iron concentrations is substantially better than for titanium, and for low titanium concentrations, the predicted values are less than satisfactory.

A number of reasons can be given for the difference in behaviour between the iron and titanium analytes. Most obvious, there is less influence from the reagent on the iron stripping peak. Because of the overlap between the titanium complex and reagent stripping peaks, variations in the size of the reagent peak will influence the modelling of the titanium response. As some reagent is consumed by formation of the iron(III) complex, the shape of the overlapped reagent and titanium(IV) complex peak is influenced not only by the reagent and titanium(IV) concentrations, but also by the iron(III) concentration, and a complex pattern of dependencies therefore exist. Furthermore, the potential shifts associated with varying analyte concentrations, and non-linearity of the reagent and analyte responses make a successful modelling difficult. For these reasons, the selection of a potential range for calibration will influence the outcome, and hence the model's ability to predict sample concentrations. For the results shown in Fig. 3, only a part of the overlapping reagent and titanium complex peaks was included in the calibration, i.e. data in the potential range from −0.9 to −0.4 V was used (cf. Fig. 2).

An evidence for the dependence of the iron(III) concentration on the overlapped reagent–titanium(IV) complex stripping peaks is given by the results of different calibration approaches on the same data set. Thus, calibration for and prediction of iron(III) concentrations (using the data in the potential range from −0.9 to −0.55 V) can be successfully made without

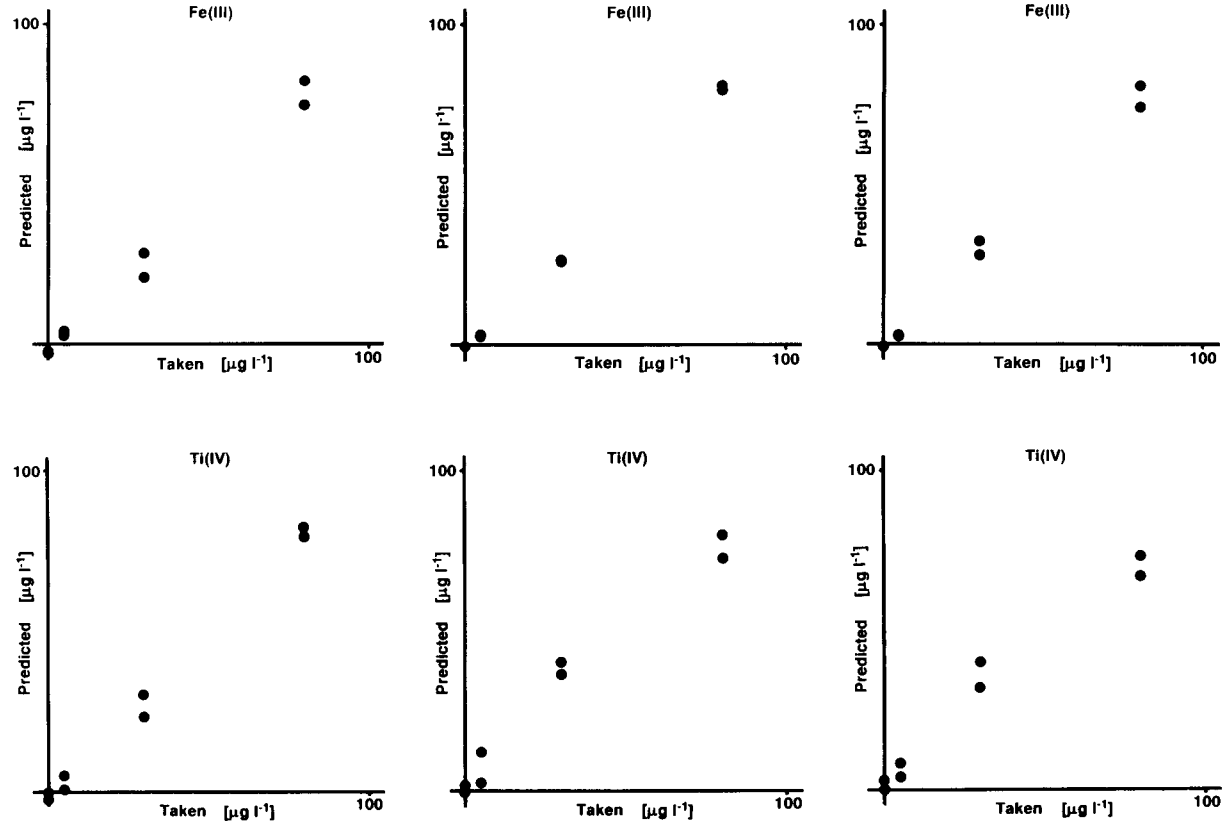

Fig. 3. Predicted vs. taken concentration for iron(III) and titanium(IV) from three different calibrations and predicitions in the concentrations range 0–100 mg l^{-1}. Composition of standards and samples as shown in Fig. 1.

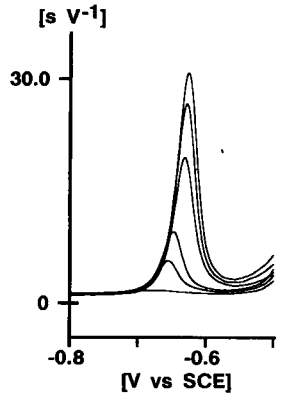

Fig. 4. Potentiograms from samples containing 0, 50, 100, 200, 300 and 400 $\mu g\ l^{-1}$ iron(III). Experimental parameters as in Fig. 2.

including the titanium(IV) data and concentration values in the model. Attempts to calibrate for titanium(IV) without including the iron(III) data is, however, much less reliable.

Contrary to spectrophotometric applications, where shifts in absorption wavelengths often are small or negligible, the potential shift of the stripping peaks associated with the changes in analyte concentrations sets a practical limit for the PLS technique in electrochemical stripping applications, even if there are no obvious interferences. Even though the PLS technique can compensate for non-linearity in response [7], it is vulnerable to positional variations in the response variables. Data with moderate potential shifts can be correctly modelled, provided that there still is a peak overlap between the measurements at the highest and lowest concentrations. An example of the potential shift is given in Fig. 4, where the stripping curves for a number of iron(III) samples in a large concentration range are shown. Using the data shown in Fig. 4 for a calibration and prediction on a number of samples gave results as shown in Fig. 5a. After a manual adjustment of the potential scale for each measurement, results were obtained as shown in Fig. 5b. This adjustment improves modelling in that fewer factors are required to reach the same degree of explained variance, but is, of course, of little practical use. As shown in Fig. 6, equally acceptable results can be obtained for an analogous treatment of samples containing 0–400 $\mu g\ l^{-1}$ titanium(IV) when no iron(III) is present in the samples. In the latter case, adjustment of the potential scale can, of course, not be made.

Conclusions

The accuracy and precision in the PLS calibration approach was estimated by analysing samples where either of the iron(III) or titanium(IV) concentration was kept constant while the other was varied randomly. The results obtained are summarised in Table 1. The results obtained for iron(III) do not compare favourably with what

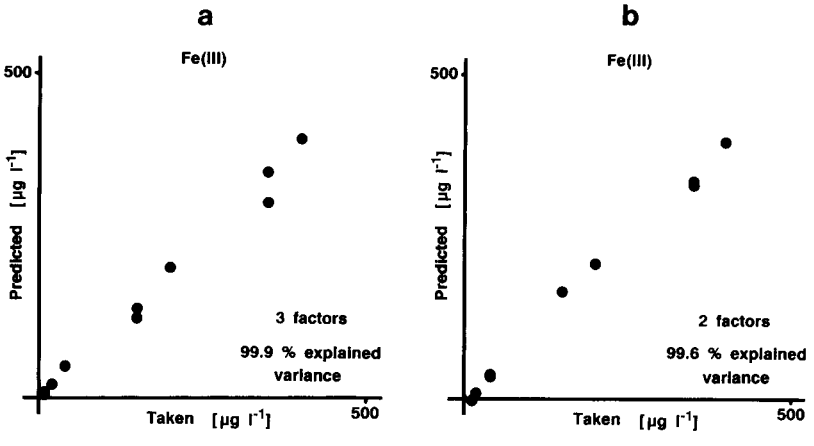

Fig. 5. Predicted vs. taken iron(III) concentration for samples in the concentration range 0–400 $\mu g\ l^{-1}$ (a) without potential scale adjustment and (b) after potential scale adjustment. Calibration based on data shown in Fig. 4. No titanium(IV) is present in the samples.

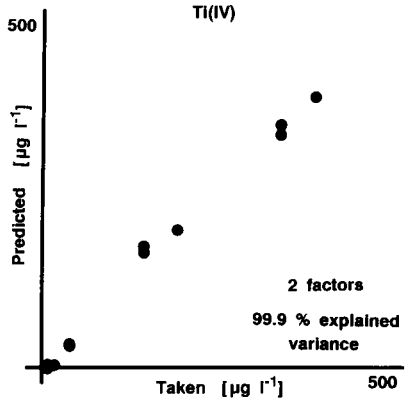

Fig. 6. Predicted vs. taken concentration for samples in the concentration range 0–400 mg l^{-1} titanium(IV). Calibration based on samples containing 0, 50, 100, 200, 300 and 500 μg l^{-1} titanium(IV). No iron(III) present in the samples.

can be obtained by a univariate calibration approach. As has been shown previously [5], a single-point calibration can provide accurate results in the determination of iron(III). To apply the latter technique to samples in a large concentration range where non-linear response occurs, the experimental conditions must, however, be adapted to the individual samples [5]. As shown in the present work, the PLS regression calibration affords a means for avoiding this adaption. For titanium(IV), the problem of a severe stripping peak overlap can be resolved, but due to this overlap, the detection limit is not comparable to that of iron(III). Obviously, no comparable data exist for a univariate calibration in the determination of titanium(IV).

Though not evident from the present work, results obtained from other stripping potentiometry applications indicate that PLS calibration can be useful in solving problems resulting from formation of intermetallic compounds and in improving detection limits [11], and that samples of different origins and of different matrices can be identified. A practical consequence of improved detection limits is that the analysis time for a given application can be shortened. Although the number of standards required for a PLS regression calibration can be quite large, it still compares favourably with standard addition calibrations. Coupled with the possibilities for resolving overlapped stripping peaks and the outlier detection capabilities of the PLS regression technique, its application to stripping analysis applications can become of major importance, especially when automated instrumentation can be used.

TABLE 1

Accuracy and precision for PLS calibration
[Found values are given with standard deviation and C.V. in percent (8 determinations)]

Taken ($\mu g\, l^{-1}$)	Found by PLS calibration ($\mu g\, l^{-1}$)
Iron(III)	
15	13.2 ± 2.1 (16%)
65	67.5 ± 4.6 (6.8%)
Titanium(IV)	
15	14.6 ± 7.3 (50%)
65	69.5 ± 7.9 (11%)

REFERENCES

1 J. Wang and J.S. Mahmoud, Fresenius' Z. Anal. Chem., 327 (1987) 789.
2 J. Wang and S. Mannino, Analyst, 114 (1989) 643.
3 Chi Hua, D. Jagner and L. Renman, Talanta, 35 (1988) 597.
4 J. Wang and J.S. Mahmoud, J. Electroanal. Chem., 208 (1986) 383.
5 D. Jagner, L. Renman and S.H. Stefansdottir, Anal. Chim. Acta, 281 (1993) 305.
6 K.R. Beebe and B.R. Kowalski, Anal. Chem., 59 (1987) 1007A.
7 H. Martens and T. Naess, Multivariate Calibration, Wiley, Chichester, 1989.
8 R.W. Gerlach and B.R. Kowalski, Anal. Chim. Acta, 134 (1982) 119.
9 A. Henrion, R. Henrion, G. Henrion and F. Sholz, Electroanalysis, 2 (1990) 309.
10 D. Jagner, L. Renman and Y. Wang, Electroanalysis, 4 (1992) 267.
11 D. Jagner, L. Renman and S.H. Stefansdottir, Electroanalysis, in press.

Analytica Chimica Acta, 281 (1993) 323–326
Elsevier Science Publishers B.V., Amsterdam

Enzyme electrode for the successive detection of hypoxanthine and inosine

Toshio Yao

Department of Applied Chemistry, College of Engineering, University of Osaka Prefecture, 1-1 Gakuen-cho, Sakai, Osaka 593 (Japan)

(Received 18th December 1992; revised manuscript received 4th March 1993)

Abstract

An enzyme electrode for the successive detection of hypoxanthine and inosine was constructed by co-immobilizing nucleoside phosphorylase and xanthine oxidase on a Nafion-coated platinum disc electrode. The successive responses for hypoxanthine and inosine were obtained in 0.1 M borate buffer (pH 7.5) without and with phosphate, respectively. The calibration graphs for hypoxanthine and inosine were linear up to 2×10^{-4} M. The sensor could be used repeatedly for at least 20 days without deterioration of the response.

Keywords: Amperometry; Biosensors; Enzymatic methods; Enzyme electrodes; Fish; Hypoxanthine; Inosine

Over the past 10 years, a variety of biosensors have been developed by combining the specificity of enzyme catalysis with the sensitivity of various electrodes. Such biosensors have been successfully employed for various purposes [1], particularly the highly selective assay of one analyte in complex mixtures with minimum pretreatment.

Inosine and hypoxanthine are intermediate metabolites in successive catabolic steps of purine nucleotides. Further, their concentrations have frequently been used as indicators of fish freshness because they increase on prolonged storage. The determination of fish freshness is important for the quality control of fish products in the food processing industries. Therefore, the development of a simple and rapid method without pretreatment or complicated procedures is desirable for the assay of inosine and hypoxanthine.

Recently, an enzyme sensor consisting of a xanthine oxidase-immobilized membrane and an oxygen electrode has been developed for the assay of hypoxanthine [2–4]. Further, a few xanthine oxidase-immobilized electrodes have likewise been proposed for hypoxanthine assay, on the basis of the use of hydroxymethylferrocene [5] as an alternative electron acceptor to oxygen and the detection of uric acid produced by the enzymatic reaction [6]. However, an enzyme sensor that can detect successively inosine and hypoxanthine has still not been reported. Their successive detection is more important than the detection of hypoxanthine alone for a more exact estimation of freshness.

In this paper, a bienzyme electrode involving nucleoside phosphorylase and xanthine oxidase is proposed for the successive detection of inosine and hypoxanthine. Nucleoside phosphorylase and xanthine oxidase catalyse the enzymatic reactions shown in reactions 1 and reaction 2, respectively.

$$\text{inosine} + \text{phosphate} \xrightarrow{\text{nucleoside phosphorylase}} \text{hypoxanthine} + \text{ribose-1-phosphate} \quad (1)$$

$$\text{hypoxanthine} + 2O_2 \xrightarrow{\text{xanthine oxidase}} \text{uric acid} + 2H_2O_2 \quad (2)$$

Correspondence to: T. Yao, Dept. of Analytical Chemistry, College of Engineering, University of Osaka Prefecture, 1-1 Gakuen-cho, Sakai, Osaka 593 (Japan).

However, reaction 1 does not occur for inosine in buffer solution without phosphate, because phosphate is required as a co-substrate. Therefore, it is expected that the first response will be obtained for hypoxanthine in buffer solution without phosphate and the second response for inosine by adding an excess of phosphate. A bienzyme electrode was constructed by immobilizing an enzyme layer on a Nafion-coated platinum electrode to exclude electroactive, anionic species such as urate and L-ascorbate, to enhance the selectivity for the detection of hypoxanthine and inosine.

EXPERIMENTAL

Reagents

All reagents were of analytical-reagent grade unless stated otherwise and distilled water was used throughout. Xanthine oxidase (EC 1.2.3.2, 1.2 U mg^{-1} protein, from buttermilk), nucleoside phosphorylase (EC 2.4.2.1, 13.4 U mg^{-1} protein, from bacteria) and bovine serum albumin (BSA, 96–99% albumin) were obtained from Sigma (St. Louis, MO), Nafion [5% (w/v) solution] from Aldrich (Milwaukee, WI) and inosine, hypoxanthine and glutaraldehyde (20% solution) from Wako (Osaka).

Construction of the enzyme electrode

Prior to the Nafion coating, a platinum disc electrode (3 mm in diameter) was polished with 0.3-μm alumina particles, then washed with distilled water in an ultrasonic bath and allowed to air dry. The same end of the electrode was modified by coating the disc and its surrounding with 5 μl of the 5% Nafion solution. The film was allowed to dry in air for 1 h. The enzyme electrode was then constructed by cross-linking the two enzymes (xanthine oxidase and nucleoside phosphorylase) and BSA with glutaraldehyde on the Nafion-coated surface of the electrode. The method was similar to that described previously [7,8] and was as follows. Xanthine oxidase (1.5 U), nucleoside phosphorylase (11 U) and 20 μl of 10% (w/v) aqueous BSA were added to 20 μl of 0.02 M borate buffer (pH 7.0). A 20-μl portion of a 4% (v/v) solution of glutaraldehyde was added and mixed well. A 12-μl aliquot of this solution was spread over the Nafion film of the electrode. The membrane was allowed to form for 3 h at room temperature, open to the air. Then a nylon net (mesh size 71 μm) was placed on the enzyme membrane with an O-ring. The completed enzyme electrode was stored in borate buffer (pH 7.5, 0.1 M) at 4–5°C when not in use.

Apparatus and procedures

The measurements were made by immersing the bienzyme electrode in a measuring cell thermostated at 30 ± 0.2°C containing 5 ml of borate buffer (pH 7.5, 0.1 M), with constant stirring. A constant potential of +0.60 V (vs. Ag/AgCl) was then applied to the electrode by using a Yanagimoto (Kyoto) P-8 polarograph coupled to a chart recorder. When a steady baseline had been obtained, 500 μl of the sample solution were added from a microsyringe. A steady-state response to hypoxanthine was first obtained and then an additional response to inosine was obtained on adding 200 μl of 0.25 M sodium dihydrogenphosphate solution. The bienzyme electrode could be reused immediately.

RESULTS AND DISCUSSION

Experiments were first done to establish the optimum conditions for the successive detection of hypoxanthine and inosine using the bienzyme electrode, especially pH and co-substrate concentration.

On injection of 500 μl of sample solution containing hypoxanthine and inosine into 0.1 M borate buffer (pH 7.5) without phosphate, the current rapidly increased and a plateau corresponding to the steady-state response was reached within 2 min. The current was proportional to the concentration of hypoxanthine and was not related to the concentration of inosine in the sample solution. This means that only reaction 2 occurs in the enzyme layer of the electrode. In fact, this bienzyme electrode gave no signal with inosine in the borate buffer in the absence of phosphate. However, by adding 200 μl of phos-

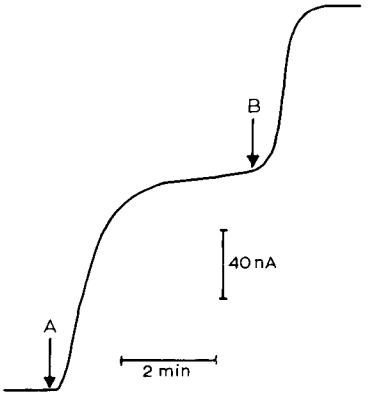

Fig. 1. Typical response to hypoxanthine and inosine. A response to hypoxanthine was obtained by adding 500 μl of the sample solution (containing 1.0 mM each of hypoxanthine and inosine) to 5 ml of borate buffer (pH 7.5, 0.1 M) at point A. Further, by adding 200 μl aliquot of 0.25 M phosphate at point B, an additional response was obtained for inosine.

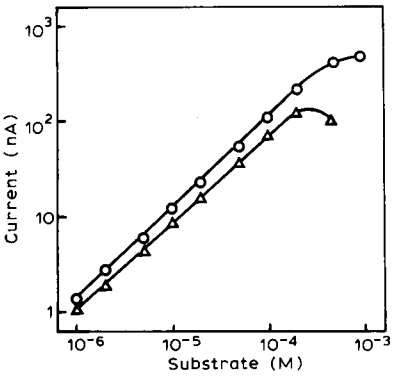

Fig. 2. Typical calibration graphs for (○) hypoxanthine and (△) inosine.

phate solution after a steady-state response for hypoxanthine had been obtained, an additional steady-state response was obtained within 1 min. This additional response is based on the occurrence of the successive enzymatic reactions (reactions 1 and 2) induced by the addition of phosphate. A typical response for hypoxanthine and inosine is shown in Fig. 1.

The influence of the concentration of phosphate, the co-substrate of nucleoside phosphorylase, on the electrode sensitivity for inosine was tested. As the phosphate concentration was increased from 0 to 10 mM, the electrode sensitivity for inosine increased, as would be expected from reaction 1, but the increase was slight at higher phosphate concentrations. Therefore, a 200-μl volume of 0.25 M phosphate was added to the borate buffer for the detection of inosine, after a steady-state response for hypoxanthine had been obtained. The effect of the pH of the borate buffer (0.1 M) was also investigated. The maximum response was obtained at pH 7–8 for both hypoxanthine and inosine. Therefore, 0.1 M borate buffer (pH 7.5) was selected for subsequent work.

Nafion film fitted on the electrode is negatively charged [9,10], thereby tending to exclude anionic species such as urate and L-ascorbate. In practice, the bienzyme electrode modified with a Nafion film gave no signal for uric acid and L-ascorbic acid below 0.5 mM. Hence the prepared bienzyme electrode can detect only hydrogen peroxide of the end-products produced by reaction 1. Therefore, the selectivity for the detection of hypoxanthine and inosine could be enhanced by preparing the immobilized enzyme layer on a Nafion film fitted on the electrode.

Figure 2 shows typical calibration graphs for hypoxanthine and inosine obtained by the recommended procedure. The graphs were linear up to 2×10^{-4} M, above which the sensitivity to inosine decreased. The limits of detection (signal-to-noise ratio = 3) were 5×10^{-7} and 8×10^{-7} M for hypoxanthine and inosine, respectively. The relative standard deviations for five replicate

TABLE 1

Results for the successive determination of hypoxanthine and inosine in mixtures of hypoxanthine, inosine, uric acid and L-ascorbic acid

Taken (10^{-5} M)				Found (10^{-5} M)	
Hypoxanthine	Inosine	Uric acid	L-Ascorbic acid	Hypoxanthine	Inosine
1.00	5.00	10	10	0.98	5.31
5.00	5.00	10	10	4.92	4.93
10.00	5.00	10	10	9.97	4.86
5.00	1.00	20	20	5.09	1.03
5.00	10.00	20	20	5.10	9.89
1.00	10.00	20	20	0.98	10.03
10.00	1.00	20	20	10.12	0.96

measurements were 0.5–1.2 and 0.8–2.2% for hypoxanthine and inosine, respectively.

Some typical results are given in Table 1. The presence of uric acid and L-ascorbic acid did not interfere with the successive detection of hypoxanthine and inosine. Clearly this bienzyme electrode was useful for the successive detection of hypoxanthine and inosine in the presence of urate and L-ascorbate as electroactive species.

The long-term stability of the bienzyme electrode was investigated; measurements were made ten times a day for 30 days. The electrode response was almost constant for the first 22 days, but subsequently the sensitivity to inosine gradually decreased because of the instability of nucleoside phosphorylase in the co-immobilized enzyme layer.

In conclusion, the bienzyme electrode based on the combined use of a co-immobilized nucleoside phosphorylase–xanthine oxidase layer and a Nafion film, although it cannot be employed for the analysis of different samples, can be used as a relatively sensitive and highly selective sensor for the successive detection of hypoxanthine and inosine, especially for the estimation of fish freshness.

REFERENCES

1 G.J. Moody and J.D.R. Thomas, Sel. Electrode Rev., 13 (1991) 113.
2 E. Watanabe, K. Toyama, I. Karube, H. Matsuoka and S. Suzuki, J. Appl. Microbiol. Biotechnol., 19 (1984) 18.
3 E. Watanabe, H. Endo, T. Hayashi and K. Toyama, Biosensors, 2 (1986) 235.
4 M. Suzuki, H. Suzuki, I. Karube and R.D. Schmid, Biosensors; Applications in Medicine, Environmental Protection and Process Control, GBF Monogr., 13 (1989) 107.
5 H. Okuma, H. Takahashi and S. Sekimukai, Anal. Chim. Acta, 244 (1991) 161.
6 E. Gonzalez, F. Pariente, E. Lorenzo and L. Hernandez, Anal. Chim. Acta, 242 (1991) 267.
7 T. Yao, Anal. Chim. Acta, 148 (1983) 27.
8 T. Yao, H. Yamamoto and T. Wasa, Anal. Chim. Acta, 236 (1990) 437.
9 J. Wang, P. Tuzhi and T. Golden, Anal. Chim. Acta, 194 (1987) 129.
10 D.S. Bindra and G.S. Wilson, Anal. Chem., 61 (1989) 2566.

Analytica Chimica Acta, 281 (1993) 327–333
Elsevier Science Publishers B.V., Amsterdam

Cobalt phthalocyanine as a mediator for the electrooxidation of glucose oxidase at glucose electrodes

I. Rosen-Margalit

Department of Molecular Microbiology and Biotechnology, Faculty of Life Sciences, Tel-Aviv University, Tel-Aviv (Israel)

A. Bettelheim

Nuclear Research Center–Negev, P.O.B. 9001, Beersheva 84190 (Israel)

J. Rishpon

Department of Molecular Microbiology and Biotechnology, Faculty of Life Sciences, Tel-Aviv University, Tel-Aviv (Israel)

(Received 18th January 1993; revised manuscript received 23rd March 1993)

Abstract

A method for the construction of a highly stable enzyme electrode is described. A new mediator, cobalt phthalocyanine, a biocompatible material, was immobilized together with the enzyme glucose oxidase in a colloidal graphite emulsion matrix. The resulting glucose electrode was characterized. The electrode retains its full activity for long periods (more than 11 months). The response to glucose is high, fast and independent of pH (5–8) or oxygen partial pressure. The linear range obtained (0–5 mM) can be extended by the introduction of a dialysis membrane and can thus be adjusted to the measurement of glucose concentrations in the range of medical interest. The electrode was tested successfully on serum samples.

Keywords: Amperometry; Enzymatic methods; Cobalt phthalocyanine; Enzyme electrodes; Glucose

In the last two decades, the development of cheap and reliable enzyme electrodes for industrial and medical applications has attracted major efforts. The lack of a direct electrical communication of redox enzymes with the electrode and the disadvantages of oxygen as an electron acceptor from oxidases such as glucose oxidase (GOD) led to the use of various redox mediators in such electrodes.

Electron acceptors for glucose oxidase that have been described previously include ferrocene derivatives [1–11], benzoquinone [12–20], tetrathiafulvalene (TTF) [21], hexacyanoferrate [22], hexacyanoruthenate [23], rhodium compounds [24], manganese porphyrin [25] and others [26]. A major obstacle with mediator-based enzyme electrodes is the lack of long-term stability. Other drawbacks are low electron transfer efficiency and dependence on oxygen partial pressure, the latter being especially relevant in in vivo measurements and in measurements in anaerobic systems.

Phthalocyanines are a group of benzoporphyrins that have strong pigmenting power, forming a family of dyes [27]. Some phthalocyanines and, in particular, copper phthalocyanines, have acquired a long safety record during years of extensive use as industrial pigments and dyes.

Correspondence to: J. Rishpon, Department of Molecular Microbiology and Biotechnology, Faculty of Life Sciences, Tel-Aviv University, Tel-Aviv (Israel).

Copper and other paramagnetic metals, such as cobalt, nickel and iron, make the dye photoinactive. The dark toxicity of these materials is also insignificant [28]. Electrodes using cobalt phthalocyanine (without enzymes) have been investigated [29–33], mainly with regard to their catalytic oxygen reduction activity [29,33] or the possibility of decreasing the effective oxidation or reduction potential of various reactions (e.g., gluthation [32]). Cobalt phthalocyanine-modified electrodes (with no enzymes) had also been used as catalysts for the determination of hydrazine, thiols, oxalic acid, α-keto acids, carbohydrates, ribonucleosides, alditols and aldonic, uronic and aldaric acids [34]. Cobalt phtalocyanine was used as a mediator with an acetylcholineesterase electrode for the determination of organophosphate [35].

In this work, the use of cobalt phthalocyanine as a redox mediator in a glucose electrode based on glucose oxidase was tested. The electrodes were prepared according to a novel method in which the mediator and enzyme are both embedded in a colloidal graphite emulsion matrix [36].

EXPERIMENTAL

Glucose oxidase (EC 1.1.3.4) (Cat. No. G-2133) from *Aspergillus niger*, Type VII lyophilized powder (150 000 units g^{-1} solid), was purchased from Sigma (St. Louis, MO). A glucose kit (Cat. No. 510A was obtained from Sigma. D-Glucose (Cat. No. 10117), was purchased from BDH (Poole, UK). Horse serum was obtained from Biological Industries (Bethaemek, Israel). Cobalt phthalocyanine (β-form) (Aldrich), colloidal graphite emulsion (Dag. 568y) (Acheson), absolute ethanol and *N*,*N*-dimethylformamide (DMF) (Merck) were used without further purification. All other chemicals were of analytical-reagent grade.

Preparation of the electrode

The method for electrode preparation is based on previous work in which vinylferrocene was used as a mediator [36]. A volume of 100 μl of colloidal graphite emulsion was mixed with an equal volume of cobalt phthalocyanine emulsion in ethanol (100 mg ml^{-1}) or in DMF (10 mg ml^{-1}). The use of DMF instead of ethanol as a solvent for the mediator (DMF is a better solvent for cobalt phthalocyanine) improved the reproducibility of the electrodes. After mixing, 20 μl of a glucose oxidase solution [100 mg ml^{-1} in 0.1 M phosphate buffer (pH 6)] were added and the solution was mixed vigorously. A 10-μl volume of this mixture was applied to glassy carbon disc electrodes (0.3 cm diameter) shrouded in PTFE. After evaporation of the solvents (within a few minutes), the electrodes were ready for use. In some instances the electrode was covered with a dialysis membrane (molecular weight cut-off 3500) held by a polypropylene ring. When not in use, the electrodes were stored at 4°C in phosphate buffer solution (pH 6).

Electrochemical measurements

A conventional three-electrode cell was used with a platinum as counter electrode and a KCl–saturated calomel electrode (k-401, Radiometer, Copenhagen). The cell was thermostated (25°C) and deaerated with argon before and during the experiments. The measurements were performed with an IIT Model 303-C potentiostat including a multiplexer and programmer (Technicon, Haifa, Israel), an *X*–*Y* recorder (Model 3086, Yokogawa, Japan), an Ims S-100 64K microcomputer equipped with Tecmar A/D and D/A units, Model 8253 PIT timer unit and a Model 8253 PPI parallel port.

The electrode response to glucose was measured amperometrically. A high sensitivity and a better signal-to-noise ratio were obtained by the use of repetitive potentiostatic pulses and integration of the current, as explained elsewhere [37]. In this mode the electrode is connected and disconnected repetitively and the current during the connection period is sampled and integrated. The resulting response is expressed in charge units. The time intervals used were 10 and 0.5 s for the disconnection and connection stages, respectively. The electroenzymatic activities of the various electrodes prepared were measured by dipping the electrode in a thermostated (25°C) buffer solution containing all the essential components for the enzymatic reaction, except the

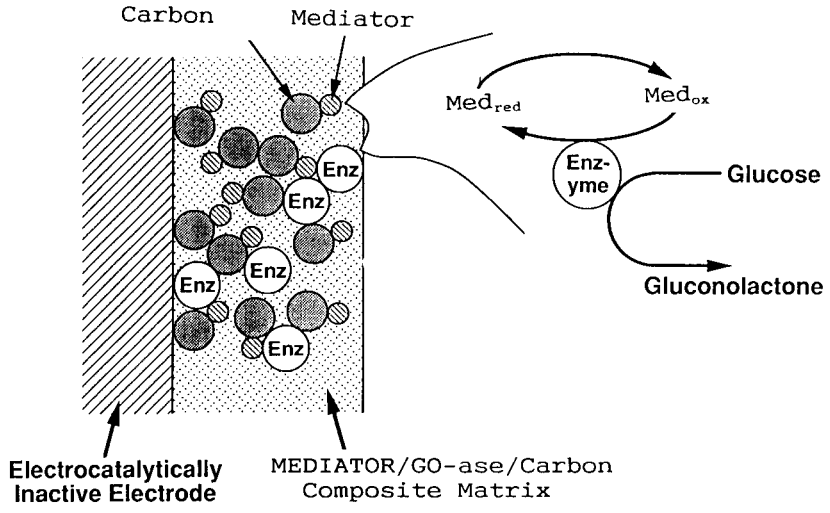

Fig. 1. Schematic diagram of the composite CoPhtC–GOD electrode.

substrate (glucose). The electrode current at the appropriate potential was recorded until a steady value was obtained (a few minutes). The substrate was then added and the difference in current recorded.

RESULTS AND DISCUSSION

The proposed structure of the composite phthalocyanine–glucose oxidase enzyme electrode is shown in Fig. 1. This structure assures good contact between all the components and leads to a better efficiency of the enzyme reaction and electron transfer. Moreover, as the phthalocyanine is insoluble in water and the enzyme is strongly adsorbed on the carbon particles, these two components are closely confined to the electrode and do not leach out to the solution.

A voltammogram of a colloidal graphite emulsion-based cobalt phthalocyanine–glucose oxidase electrode, with and without glucose, is shown in Fig. 2. In the absence of glucose, no peak is observed in the tested potential range and this appears also to be the case in the absence of glucose oxidase. The reduction of dissolved Co(III) PhtC in an organic solvent [38] and that of adsorbed Co(III) tetrasulphonate PhtC on pyrolytic graphite in aqueous acid [28] has been reported to take place in the range +0.7 to +0.8 V. However, a prewave for the adsorbed CoPhtC was observed at about +0.4 V [29], which might arise from the stabilization of the Co(III) oxida-

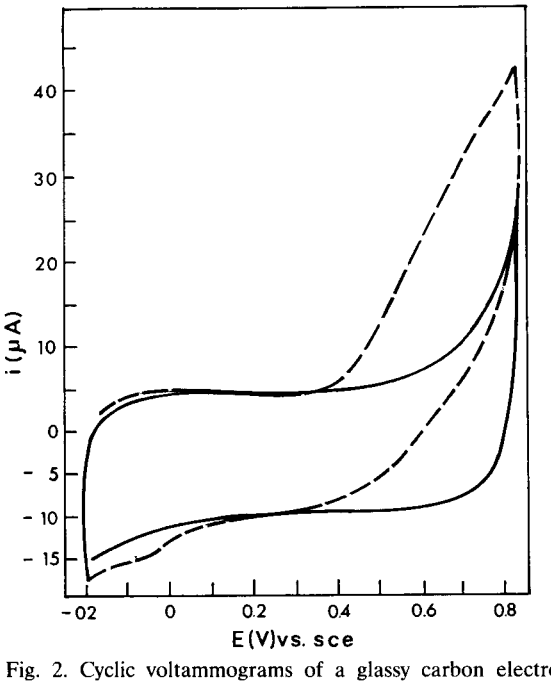

Fig. 2. Cyclic voltammograms of a glassy carbon electrode coated with a colloidal graphite emulsion containing glucose oxidase and cobalt phthalocyanine. Measurement conditions: deaerated 0.1 M phosphate buffer (pH 6); scan rate, 5 mV s^{-1}. Solid lines, buffer only; dashed lines, with 23.5 mM glucose.

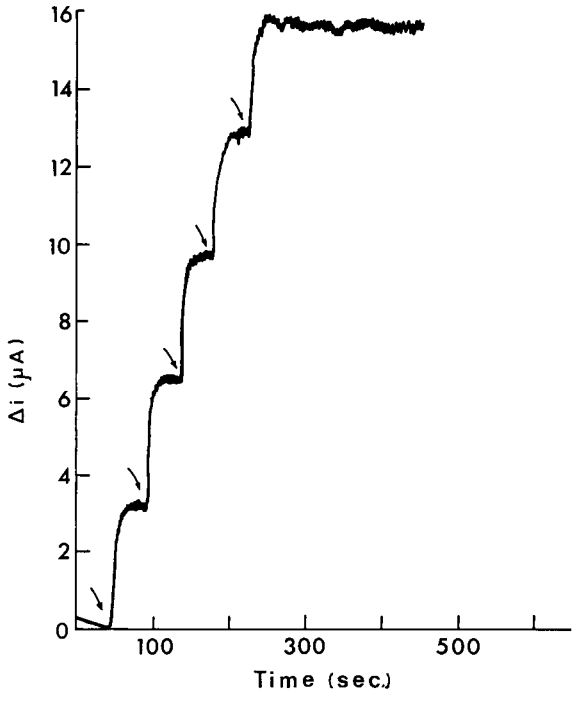

Fig. 3. Electrode response to successive additions of glucose. The electrode was biased at +0.7 V in phosphate buffer (pH 6). Arrows show the successive addition of 1 mM glucose.

tion state relative to that of Co(II) owing to interactions with functionalities in the carbon matrix [39]. With the addition of glucose, a large increase in anodic current, starting at 0.4 V (vs. SCE) is observed (Fig. 2). It is therefore suggested that Co(III) PhtC mediates electron transfer between glucose oxidase and the electrode through oxidation of the reduced form of the enzyme. A similar mechanism was proposed for the electrooxidation of glucose by glucose oxidase and the mediator by the Mn(III)–Mn(IV) tetra(*o*-aminophenyl)porphyrin couple [25].

Fig. 3 shows the response of the electrode at a constant potential of 0.7 V vs. SCE for successive additions of glucose (1 mM each time). The very fast response (10 s) and the linear range (up to 5 mM) can be seen. At higher concentrations saturation was observed and above 10 mM the current was no longer sensitive to glucose addition. However, as shown in Fig. 4, the linear range can be extended by covering the electrode with a

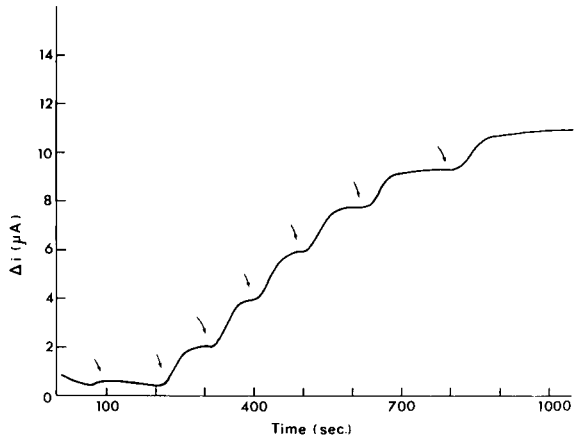

Fig. 4. Response to glucose addition of a membrane-covered electrode. Arrows show the addition of 5 mM glucose. Other conditions as in Fig. 3.

dialysis membrane (molecular weight cut-off 3500). The response time with the membrane is increased by a factor of 5, and can still be considered fast.

Higher responses (higher currents by a factor of 20) and better sensitivity (Fig. 5) were achieved by using potentiostatic pulses according to the scheme described under Experimental. This high current amplification is specifically related to the immobilized redox mediator. The mechanism for

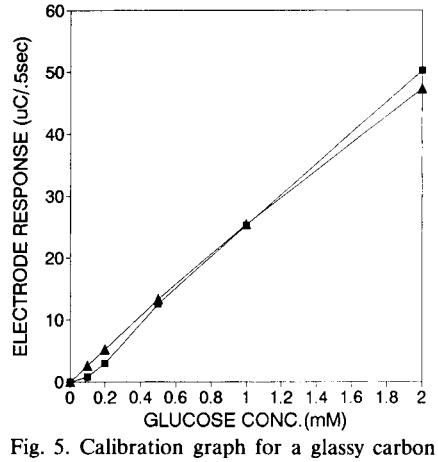

Fig. 5. Calibration graph for a glassy carbon CoPhtC/GOD electrode to glucose additions. Measurement conditions: deaerated 0.1 M phosphate buffer (pH 6); +0.7 V vs. SCE (0.5 s connection, 10 s disconnection). ▲ = Freshly prepared electrode, ■ = after 11 months of storage.

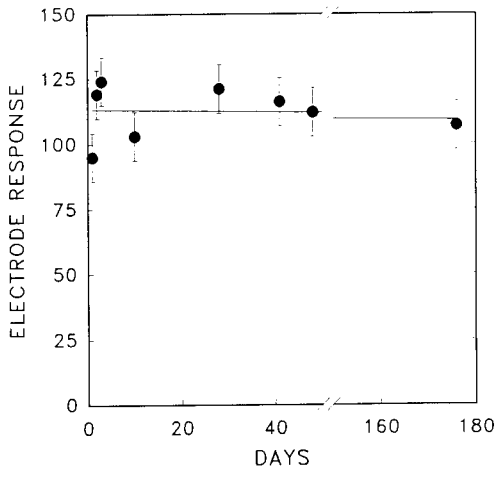

Fig. 6. Storage stability of a glassy carbon/CoPhtC/GOD electrode. Measurement conditions: deaerated 0.1 M phosphate buffer (pH 6); 0.6 V vs. SCE (0.5 s connection, 10 s disconnection); 23.5 mM glucose.

the oxidation of glucose by glucose oxidase involves a reduction of the enzyme by glucose and its reoxidation by the oxidized form of the mediator. During the delay time, the electrode is disconnected and the enzyme reduced by the glucose can be effectively reoxidized by the Co(III) PhtC immobilized on the electrode. The reduced mediator, Co(II) PhtC, which does not diffuses from the electrode, is completely oxidized when the anodic potential is applied, resulting in high currents.

The long-term stability of the electrode was remarkable. The time dependence of the electrode response to low substrate concentrations (diffusion-controlled enzyme reaction) and high substrate concentrations (kinetically controlled enzyme reaction) are shown in Figs. 5 and 6. Electrodes stored at 4°C for 11 months and then tested retained their full activity and the high sensitivity at low glucose concentrations had not been affected (Fig. 5). The activity at high substrate concentrations was also unaffected as well. The electrode retained its full activity during 6 months of intensive operation. During this period, no leaching of the mediator or loss of enzyme activity was observed. Apparently the mediator coimmobilized with the enzyme is present in a sufficient amount to prevent hydrogen peroxide formation completely. Hydrogen peroxide causes deactivation of the enzyme [40] and is a primary reason for the loss of activity of glucose electrodes based on glucose oxidase [41].

The effects of buffer concentration, pH and temperature on the electrode response to glucose additions were studied. The optimum buffer concentration was found to be 0.1 M. At lower buffer concentrations the current decreased and higher buffer concentration did not have any effect on the current. In the pH range 5–8, the response to glucose was not dependent on pH. Variation of the temperature from 25 to 37°C did not have any effect on the electrode response. As the rates of enzymatic reactions are generally temperature and pH dependent, these results suggest that the rate-determining step is the mediator reaction at the electrode and not the enzymatic reaction. The electrode response was also independent of oxygen concentration and similar results were obtained in both its presence and absence (argon atmosphere). This could probably be related to the large excess of accessible mediator (in conditions under which the oxygen does not compete) [42].

Measurements were also made in biological media, e.g., horse serum. For this measurement

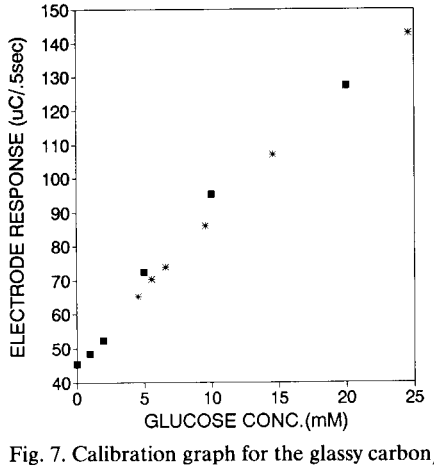

Fig. 7. Calibration graph for the glassy carbon/CoPhtC/GOD membrane-covered electrode. ■ = Glucose added to horse serum; * = measurements performed in phosphate buffer immediately after the measurement in the horse serum. The background current was not subtracted.

the membrane-coated electrode was used and Fig. 7 shows the calibration graph obtained with the serum (by adding glucose to the serum) compared with a similar measurement using a buffered aqueous solution. The original glucose concentration in the serum was determined spectrophotometrically (glucose kit) and found to be 4.6 mM (see Fig. 7). The result obtained with the electrode is identical and apparently the serum had no effect on the electrode performance. The calibration graph with phosphate buffer was obtained immediately after the measurement with serum. No fouling of the electrode or the dialysis membrane was observed.

Conclusions

Cobalt phthalocyanine is an advantageous mediator for glucose oxidase when both are immobilized together on a carbon electrode. The introduction of phthalocyanine into graphite emulsion-based enzyme electrodes results in improved long-term stability (more than 11 months) compared with other mediated electrodes [11,43,44]. During this period no leakage of the mediator was observed. The latter feature is particularly relevant to in vivo measurements. Cobalt phthalocyanine is biocompatible and commercially available. The response to glucose is high and fast (5–10 s) and does not depend on oxygen partial pressure, pH or temperature. Although the high anodic working potential (0.7 V) can cause some difficulties in measurements performed in biological fluids, no such problems were observed in serum measurements when using a protective membrane and short pulses of the anodic potential.

REFERENCES

1 A.E.G. Cass, G. Davis, G.D. Francis, H.A. Hill, W.J. Aston, I.J. Higgins, E.V. Plotkin, L.D.L. Skott and A.P.F. Turner, Anal. Chem., 56 (1984) 667.
2 A.E.G. Cass, G. Davis, M.J. Green and H.A.O. Hill, J. Electroanal. Chem., 190 (1985) 117.
3 M.A. Lange and J.Q. Chambers, Anal. Chim. Acta, 175 (1985) 89.
4 A.P.F. Turner, Ann. N.Y. Acad. Sci., Enzyme Eng. 8, 501 (1985) 551.
5 K. DiGleria, H.A.O. Hill, C.J. McNeil and M.J. Green, Anal. Chem., 58 (1986) 1203.
6 E.J. D'costa, I.J. Higgins and A.P.F. Turner, Biosensors, 2 (1986) 71.
7 J.E. Frew, M.J. Green and H.A.O. Hill, J. Chem. Technol., 36 (1986) 357.
8 D.J. Claremont, C. Pentom and J.C. Pickup, J. Biomed. Eng., 8 (1986) 272.
9 M.J. Green and H.A.O. Hill, J. Chem. Soc., Faraday Trans. 1, 82 (1986) 1237.
10 D.J. Claremont, I.E. Sambrook, C. Penton and J.C. Pickup, Diabetologia, 29 (1986) 817.
11 W. Schuhmann, H. Wohlschlager, R. Lannert, H.L. Schmidt, U. Loffler, H.D. Wiemhofer and W. Gopel, Sensors Actuators, B1 (1990) 571.
12 T. Ikeda, I. Katasho, M. Kamei and M. Senda, Agric. Biol. Chem., 48 (1984) 1969.
13 C. Bourdillon, J.M. Laval and D. Thomas, J. Electrochem. Soc., 133 (1984) 706.
14 T. Ikeda, H. Hamada, K. Miki and M. Senda, Agric. Biol. Chem., 49 (1985) 541.
15 T. Ikeda, H. Hamada and M. Senda, Agric. Biol. Chem., 50 (1986) 883.
16 C. Bourdillon, R. Lortie and J.M. Laval, Biotechnol. Bioeng., 31 (1988) 553.
17 T. Ikeda, K. Miki, F. Fushimi and M. Senda, Agric. Biol. Chem., 51 (1987) 747.
18 F.W. Scheller, R. Hintsche, B. Neumann and D.V. Bogdanovskaya, Stud. Biophys., 132 (1989) 93.
19 T. Ikeda, F. Matsushita and M. Senda, Agric. Biol. Chem., 54 (1990) 2912.
20 J. Hu and A.P.F. Turner, Anal. Lett., 24, No. 10 (1991) 15.
21 A.P.F. Turner, S.P. Hendry and M.F. Cardosi, BioTech 87, 1987, p. 125.
22 D.W. Harak and H.A. Mottola, Biosensors Bioelectron., 6 (1991) 589.
23 A.L. Crumbliss, H.A.O. Hill and D.J. Page, J. Electroanal. Chem., 206 (1986) 327.
24 J. Wang and L. Angnes, Anal. Chem., 64 (1992) 456.
25 J. Rishpon, I. Rosen-Margalit, R. Harth, D. Ozer and A. Bettelheim, J. Electroanal. Chem., 307 (1991) 293.
26 P.N. Bartlett, P. Tebbutt and R.G. Whitaker, Prog. React. Kinet., 16 (1991) 55.
27 N.Y. Sax and R.J. Lewis, Hawlyey's Condensed Chemical Dictionary, Van Nostrand Reinhold, New York, 11th edn, 1987.
28 I. Rosenthal, Photobiology, 53 (1991) 658.
29 J. Zagal, R.K. Sen and E.B. Yeager, J. Electroanal. Chem., 83 (1977) 207.
30 M.K. Halbert and R.P. Baldwin, Anal. Chim. Acta, 187 (1986) 89.
31 S. Kim, X. Xu, I.T. Bue, Z. Wang and D.A. Scherson, Anal. Chem., 62 (1990) 2647.
32 S.A. Wring and J.P. Hart, Talanta, 38 (1991) 1257.
33 R. Jiang and S. Dong, J. Electroanal. Chem., 246 (1988) 101.

34 R.P. Baldwin and K.N. Thomson, Talanta, 38 (1991) 1.
35 P. Skladal and M. Mascini, Biosensors Bioelectron., 7 (1992) 335.
36 I. Rosen-Margalit and J. Rishpon, Biosensors Bioelectron., submitted.
37 I. Rosen-Margalit and J. Rishpon, J. Electroanal. Chem., 258 (1989) 27.
38 J. Manassen and A. Bar-ilan, J. Catal., 17 (1970) 86.
39 A. Bettelheim, R.J.H. Chan and T. Kuwana, J. Electroanal. Chem., 99 (1979) 391.
40 K. Bucholtz and B. Godelmann, Biotechnol. Bioeng., 20 (1978) 1201.
41 P.H.W. Tse and D.A. Gough, Biotechnol. Bioeng., 29 (1987) 705.
42 J.M. Dicks, S. Hattori, I. Karube, A.P.F. Turner and T. Yokozawa, Ann. Biol. Clin., 47 (1989) 607.
43 J.W. Chen, D. Belanger and G. Fortier, in P. Edleman and J. Wang (Editors), ACS Symposium Series, Vol. 487, American Chemical Society, Washington, DC, 1992, p. 31.
44 P.D. Hale, L.I. Boguslavsky, N.Y. Inagaki, H.I. Karan, H.S. Lee and T.A. Skotheim, Anal. Chem., 63 (1991) 677.

Analytica Chimica Acta, 281 (1993) 335–339
Elsevier Science Publishers B.V., Amsterdam

Microelectrochemical cell containing chloroplast membranes as a fast bioassay for catalase determination

Robert Carpentier and D. Christopher Goetze [1]

Centre de Recherche en Photobiophysique, Université du Québec à Trois-Rivières, C.P. 500, Trois-Rivières, Québec G9A 5H7 (Canada)

(Received 21st December 1992; revised manuscript received 18th March 1993)

Abstract

A three-electrode photoelectrochemical cell has been found to be an excellent catalase biosensor. The cell contains a sample of easily prepared photosynthetic membranes and produces a photocurrent via the electrochemical degradation of hydrogen peroxide at its working electrode. The cell is shown in this report to be very sensitive to the enzymatic action of catalase, even in small quantities, and is capable of providing a rough estimate of the amount of contaminating catalase present in a sample. Furthermore, individual assays are fast (~ 5 min), allowing a large number of replicates to be performed quickly.

Keywords: Amperometry; Biosensors; Catalase; Hydrogen peroxide; Photosynthesis

Catalase is a relatively abundant enzyme involved in detoxification processes in almost all eucaryotic cells. Specifically, it degrades hydrogen peroxide in a reaction generating oxygen [1,2]:

$$2H_2O_2 \xrightarrow{\text{catalase}} 2H_2 + O_2$$

Consequent of its nature and abundance is the fact that catalase is a common contaminant in many laboratory and commercial preparations of cellular products and enzymes. While many procedures exist to remove unwanted catalase, it would be advantageous to have a simply performed, fast assay for the presence of the enzyme. This would save the time and expense of unnecessary precautionary purification measures, especially in the case of a commercial product of unassured or uncertain quality where catalase is likely to be present.

A microphotoelectrochemical cell using chloroplast membranes was recently developed in this laboratory. In this cell, a current is photogenerated following photosynthetic electron transport in the thylakoid membranes [3]. The reduced species formed during this electron transport are oxidized by electroactive mediators that reduce a working platinum electrode [4]. This cell was demonstrated to have a great potential for the detection of phytotoxic compounds like heavy metals and herbicides that inhibits the photosynthetic electron transport [5,6]. The inhibitory effect results in a decreased photocurrent in proportion to the inhibitor concentration.

Lately, it was shown that in the absence of exogenously added electroactive mediators the remaining photocurrent generated by the photosynthetic membranes was due to the reduction of solvated oxygen [7]. The reduction of oxygen produces superoxide ions that dismutate spontaneously or enzymatically, due to the presence of

Correspondence to: R. Carpentier, Centre de Recherche en Photobiophysique, Université du Québec à Trois-Rivières, C.P. 500, Trois-Rivières, Québec G9A 5H7 (Canada)

[1] Present address: Department of Botany, University of British Columbia, Vancouver, British Columbia V6T 2B1 (Canada).

membrane-bound superoxide dismutase, to hydrogen peroxide [8,9]. The latter is oxidized by the working platinum electrode when the cell is kept under proper potentiostatic control [10].

Here, the above properties of the thylakoid-based photoelectrochemical cell are used for the detection of catalase. This approach applies the principle that the H_2O_2-mediated photocurrent is inhibited in proportion to the enzyme concentration owing to the degradation of H_2O_2 by catalase. The potential usefullness of this system as a fast bioassay for catalase determination is discussed.

EXPERIMENTAL

Isolation of thylakoid membranes

Thylakoid membranes were prepared from deveined spinach leaves as described previously [7] and resuspended in 330 mM sorbitol, 50 mM *N*-tris(hydroxymethyl)-methyl-2-aminoethanesulfonic acid–NaOH (pH 7.5), 2 mM $MgCl_2$, 1 mM NH_4Cl and 2 mM ethylenediaminetetraacetic acid. Chlorophyll (Chl) was determined according to Arnon [11] and the membranes were used at 250 μg Chl/ml unless otherwise specified.

Electrochemical measurements

Photoelectrochemical measurements were performed in the microelectrochemical cell described in Fig. 1 (see also Ref. 4). The cell uses a three-electrode system (platinum working and counter electrode and a calomel reference electrode) and is kept under an imposed potential of 750 mV (EG&G Princeton Applied Research Model 362 scanning potentiostat). The current is monitored on a chart recorder. For cyclic voltammetry measurements, the electrode system was connected to an EG&G Princeton Applied Research Model 273 scanning potentiostat-galvanostat, used in conjunction with a Recorder Co. Model 200 *X–Y* recorder. The voltammograms were obtained at a scan rate of 5 mV/s.

The cell microchamber (80 μl) was filled with a suspension of thylakoid membranes and equilibrated at 23°C and 750 mV vs. saturated calomel electrode (SCE). Then, illumination was provided on the top of the cell using a glass fiber-optic guide connected to a quartz hallogen illuminator (white light, 220 mW/cm^2). Bovine liver catalase (2 600 units/mg) obtained from Sigma (St. Louis, MO) was added to the thylakoid samples at the specified concentration before their introduction into the cell.

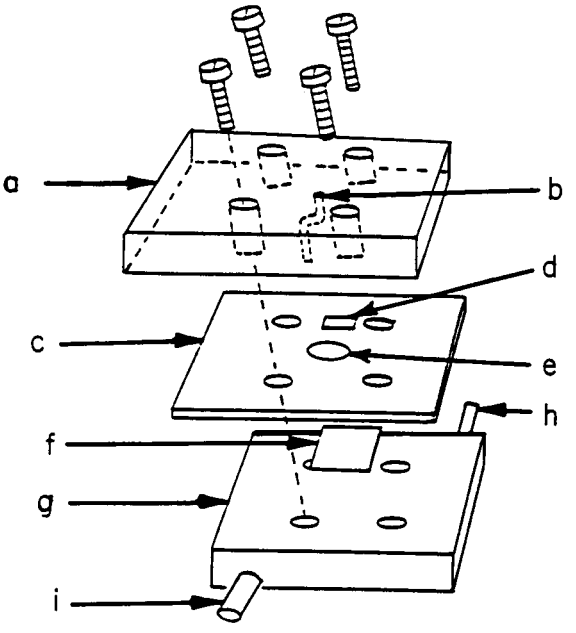

Fig. 1. Diagram of the microelectrochemical cell: (a) transparent plexiglass cover (6×5×1 cm); (b) inlet for a saturated calomel reference electrode; (c) rubber gasket (6×5×0.1 cm); (d) platinum foil counter electrode (1×0.2 cm); (e) cell microchamber (0.1×1 cm diameter); (f) platinum foil working electrode (1×1 cm); (g) stainless steel base (6×5×1 cm) with inlet (h) and outlet (i) for thermostated water circulation.

RESULTS

The induction kinetics of the photocurrent produced by the thylakoid membranes in the microphotoelectrochemical cell are shown in Fig. 2. Upon illumination, there is a gradual increase of photocurrent until a maximum is reached, after about 30 s (Fig. 2A). It was previously demonstrated that the induction rate is limited by the diffusion of the electroactive species produced at the photosynthetic membranes [12]. As mentioned above, it was shown that the photocurrent

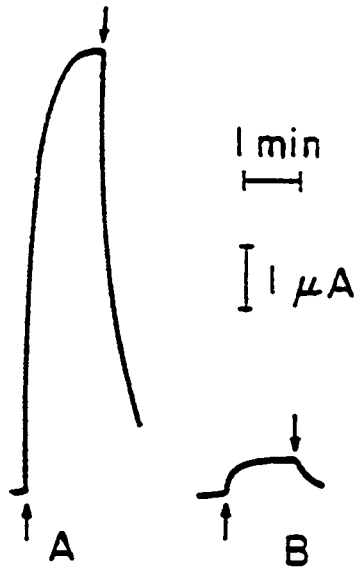

Fig. 2. Photocurrent (anodic) induction traces with the cell filled with thylakoid membranes at a Chl concentration of 250 μg/ml; (A) thylakoids alone, (B) thylakoids with the addition of 2000 units/ml catalase. Up and down arrows indicate light on and off, respectively. Measured photocurrents varied between ±5%.

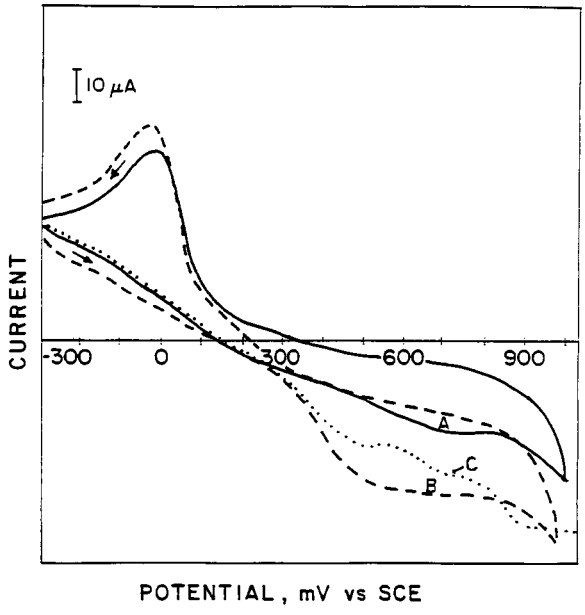

Fig. 3. Current–potential curves of thylakoid membranes kept in the dark (trace A) or during illumination (trace B). Trace C was obtained with thylakoids in the dark but with the addition of 0.01% H_2O_2. Anodic currents are represented on the lower part of the figure.

originates from the reduction of dissolved oxygen by the thylakoid membranes [7]. After light absorption by photosystem II and photosystem I, the intramembranous electron transport that occurs generates reduced species at the level of photosystem I which are able to reduce oxygen and lead to the formation of hydrogen peroxide [9,13]. The photocurrent is strongly inhibited by catalase which specifically degrades hydrogen peroxide before it can react with the platinum working electrode (Fig. 2B).

The properties of the photocurrent are further studied in Fig. 3. The cyclic voltammograms of the thylakoid-containing cell are presented before and during illumination. During illumination, a strong photocurrent with an onset potential above 250 mV can be seen. The photocurrent tends towards a limiting value of 20 μA that remains constant between 500 and 800 mV. The polarographic wave is characterized by a half-peak potential ($E_p/2$) of 310 mV corresponding to the value found for hydrogen peroxide added in the dark (Fig. 3, trace C).

The inhibitory action of catalase shown in Fig. 2B is detailed in Fig. 4. The inhibition increases with the concentration of catalase. This effect is almost optimal when the enzyme concentration reaches 200 units/ml (77 μg/ml) but at 2000 units/ml more than 90% of the photocurrent is

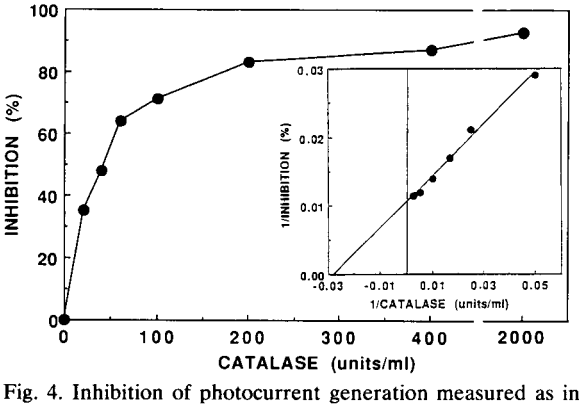

Fig. 4. Inhibition of photocurrent generation measured as in Fig. 2 at various catalase concentrations. Inset: double reciprocal plot of the data showing that 50% inhibition is obtained at 36 units/ml catalase; correlation factor = 0.993.

inhibited. The remaining current found at the latter catalase concentration is mostly due to a direct reaction of light with the platinum electrode that produces a weak photocurrent which is not related to the H_2O_2-mediated effect (see Ref. 7). The photocurrent was inhibited by 50% at 36 units/ml catalase (Fig. 4, inset).

Figure 4 demonstrates that catalase can be detected at concentrations as low as 20 units/ml (3.8 μg/ml) but the detection would be less precise above 200 units/ml. The concentration of hydrogen peroxide in the cell did not influence the range of sensitivity for catalase determination. In Fig. 5, the amount of hydrogen peroxide produced is varied by using various concentrations of thylakoid membranes on a Chl basis. It is clear that the photocurrent increases with Chl concentration which corresponds to the production of higher concentrations of hydrogen peroxide if more membranes are present (Fig. 5A). However, the inhibitory action of catalase (500 units/ml) was similar (83 ± 3%) at any Chl concentration used (Fig. 5B). Higher Chl concentrations are thus preferred because of the greater electrochemical signal produced under these conditions.

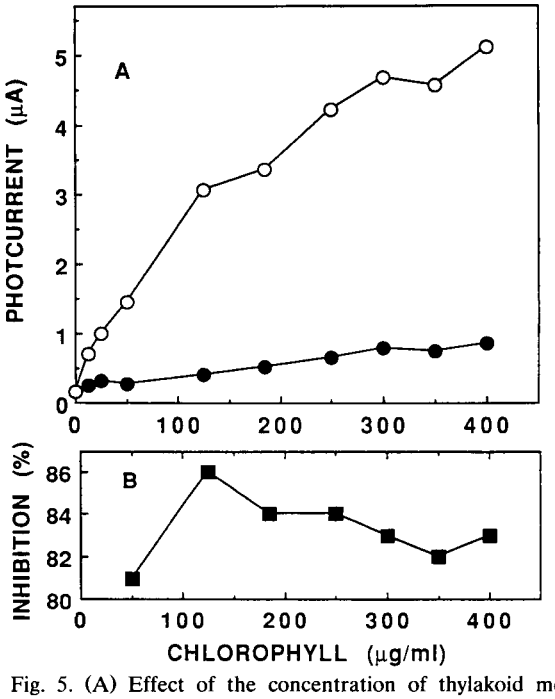

Fig. 5. (A) Effect of the concentration of thylakoid membranes (on a Chl basis) on the photocurrent generated without (○) and with (●) 500 units/ml catalase. (B) Percentage of inhibition of the photocurrent by catalase at various Chl concentrations calculated from the data in Fig. 5A.

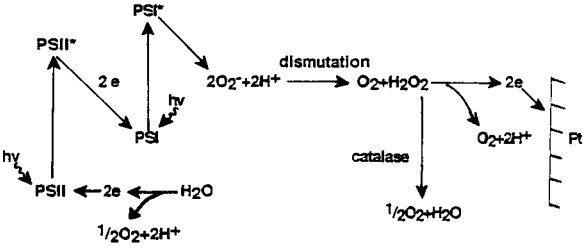

Scheme 1.

DISCUSSION

In the above data, the potential of a thylakoid-based microphotoelectrochemical cell for use as a catalase bioassay is demonstrated. The mechanism of photocurrent generation and catalase inhibition is depicted in Scheme 1. The H_2O_2-mediated photocurrent is reduced in proportion to the degradation of H_2O_2 by catalase without interference with the process leading to H_2O_2 formation by the thylakoid membranes.

Curiously, the amount of H_2O_2 produced by various concentrations of thylakoid membranes did not influence the percentage of inhibition by catalase. Usually, the degradation of H_2O_2 by catalase is a first order reaction that depends on substrate concentration [1]. However, in the usual catalase assays, H_2O_2 is present in the mM range. Here, the rate of H_2O_2 production in the electrochemical cell can be estimated from independent oxygen uptake measurements to about 5 mmol/ml · h (results not shown). Thus, at this very low H_2O_2 concentration a change in thylakoid concentration is seemingly insignificant in terms of the H_2O_2/catalase ratio. The above indicates that precise determination of Chl concentration in the cell is not required though higher concentrations will produce a stronger signal. On the other hand, the response of the cell strongly depends on the wavelength of illumination in agreement with the absorption spectrum of thyla-

koid membranes [14]. Thus, a better photocurrent intensity is obtained with white light which covers the whole absorption spectra of thylakoids that spans between 400 and 700 nm. The photocurrent also increases with light intensity untill the photosystems become light saturated [12].

In contrast with the usual spectrophotometric determination of catalase where the measurement of H_2O_2 degradation at 240 nm is used, light scattering problems should not influence the present detection system. This advantage is especially important when catalase must be determined in blood or tissues where the scattered light in the UV region is added together with the strong absorbance of the detergents used for solubilization. Furthermore, this bioassay should allow the measurement of large amounts of sample owing to the short measuring time (~ 5 min) and to the very small volume required (80 μl) for each sample.

Rather low concentrations of catalase could be detected. In fact, the assay was sensitive enough to monitor the presence of less than 10 units/ml (3.8 μg/ml) of the bovine liver catalase. A trace similar to Fig. 4 can be used as a calibration curve to determine unknown catalase concentrations. A dilution of the sample would be necessary if the enzyme concentration is too high.

In the present report, we have used a free suspension of thylakoid membranes. The biological material has a rather short active life-time in the electrochemical cell and the thylakoid samples must be changed for each measurement. However, thylakoids immobilized in a cross-linked albumin–glutaraldehyde matrix were also used advantageously for herbicide detection in the photoelectrochemical [5]. The immobilized preparations were characterized by a greater stability of their biological functions [15–17]. Since catalase does not interfere directly with the thylakoid membrane, the use of immobilized membranes should permit repetitive measurements in various catalase samples using the same membranes.

This work was supported in part by grants to R.C. from Natural Sciences and Engineering Research Council of Canada (NSERC).

REFERENCES

1 H. Aebi, Methods Enzymol., 105 (1984) 121.
2 M.L. Salin, Physiol. Plant., 72 (1988) 681.
3 R. Carpentier and M. Mimeault, Biotechnol. Lett., 9 (1987) 111.
4 M. Mimeault and R. Carpentier, Biochem. Cell Biol., 66 (1988) 436.
5 R. Carpentier, C. Loranger, J. Chartrand and M. Purcell, Anal. Chim. Acta, 249 (1991) 55.
6 M. Purcell and R. Carpentier, Water Poll. Res. J. Canada, 25 (1990) 175.
7 D.C. Goetze and R. Carpentier, Photochem. Photobiol., 52 (1990) 1057.
8 M. Brunori and G. Rotilio, Methods Enzymol., 105 (1984) 22.
9 K. Asada and M. Takahashi, in D.J. Kyle, C.B. Osmond and C.J. Arntzen (Eds.), Photoinhibition, Elsevier, Amsterdam, 1987, pp. 227–287.
10 A. Agostiano, D.C. Goetze and R. Carpentier, Photochem. Photobiol., 55 (1992) 449.
11 D.I. Arnon, Plant Physiol., 24 (1949) 1.
12 M. Mimeault and R. Carpentier, Bioelectrochem. Bioenerg., 22 (1989) 145.
13 J.M. Robinson, Physiol. Plant., 72 (1988) 666.
14 A. Agostiano, D.C. Goetze and R. Carpentier, Electrochim. Acta, 38 (1993) 757.
15 M.F. Cocquempot, B. Thomasset, J.N. Barbotin, G. Gellf and D. Thomas, J. Appl. Microbiol. Biotechnol., 11 (1981) 193.
16 B. Thomasset, J.-N. Barbotin, D. Thomas, T. Thomasset, A. Vejux and J. Jeanfils, Biotechnol. Bioeng., 25 (1983) 2453.
17 M.A. De la Rosa, K.K. Rao and D.O. Hall, Photobiochem. Photobiophys., 11 (1986) 173.

Analytica Chimica Acta, 281 (1993) 341–346
Elsevier Science Publishers B.V., Amsterdam

Application of an iodide ion-selective electrode to the determination of anionic polyelectrolytes and colloids with a cationic surfactant

J.-M. Séquaris and P. Kalabokas [1]

Institute of Applied Physical Chemistry, Research Centre (KFA) Jülich, P.O. Box 1913, D-52425 Jülich (Germany)

(Received 26th January 1993; revised manuscript received 6th April 1993)

Abstract

The analytical application of an iodide solid-state ion-selective electrode is described for the titration, in the low mg l^{-1} range, of polyanions with hexadecylbenzyldimethylammonium chloride, a cationic surfactant. Reliable calibration graphs were obtained at concentrations up to 10 mg l^{-1}. The feasibility of the titration method for determining the charge density of natural colloids such as humic acids and clays is also shown. The effects of surfactant concentrations of up to 30 mg l^{-1} on the polyanion titration show that anionic surfactants are co-titrated.

Keywords: Ion selective electrodes; Colloids; Humic acids; Iodide; Polyelectrolytes

The important role played by anionic polyelectrolytes and colloids in industrial processes [1] and in the speciation analysis of environmental chemicals [2] requires the development of methods for their detection and determination. Specific determinations in complex matrices need time-consuming preparation methods and expensive investment in equipment for, e.g., gel permeation chromatography (GPC) and liquid chromatography (LC). However, for rapid and accurate analyses of product classes, under known solution conditions, simpler handling techniques are sufficient. Thus automated photometric [3] and electrokinetic [4] methods have recently been introduced for the determination of polyelectrolytes and colloids.

In this paper, it is shown that the application of a more common potentiometric method can also give very satisfactory results by constructing reliable calibration graphs in the low mg l^{-1} range for solutions of anionic polyelectrolytes. Rapid information on the ionization density of strongly negatively charged natural colloids such as clays and humic acids can also be obtained. This determination is based on a briefly reported method [5] that revealed the potential of the iodide ion-selective electrode (ISE) as a detector for the end-point of the titration of an anionic polyelectrolyte, potassium poly(vinyl sulphate), with tetradecylbenzyldimethylammonium chloride (zephiramine), a long-chain cationic surfactant. The feasibility of various ISEs as sensors in the potentiometric titration of many inorganic and water-soluble organic anions with quaternary

Correspondence to: J.-M. Séquaris, Institute of Applied Physical Chemistry, Research Centre (KFA) Jülich, P.O. Box 1913, D-52425 Jülich (Germany).

[1] Present address: Department of Applied Physics, University of Athens, 33, Ippokratous Str., 10680 Athens (Greece).

ammonium halides has also been demonstrated [6,7].

EXPERIMENTAL

Chemicals

Surfactants. Hexadecylbenzyldimethylammonium chloride (purum) (HBDACl), tetraethylene glycol monododecyl ether (> 98%) ($C_{12}EO_4$), sodium dodecyl sulphate (> 99%) (NaDS) and sodium dodecyl benzensulphonate (80–85%) (NaDBS) were obtained from Fluka.

Polymers. Potassium poly(vinyl sulphate) (MW 245 000) (KPVS) was obtained from Serva, polyacrylic acid (MW 250 000) (PAA) from Aldrich and sodium copolymer (MW 219 000) based on acrylic acid (70%) and maleic acid (30%) (NaCP) from BASF. Calculated charge densities (milliequivalents per gram of polyelectrolyte) for KPVS, PAA and NaCP were 6.17, 13.89 and 11.18 meq/g, respectively.

Soil colloids. Humic acid was obtained from Aldrich. Sodium montmorillonite and sodium kaolinite were prepared from bentonite (Süd-Chemie) and kaolin (Serva), respectively. The cation-exchange capacities for montmorillonite and kaolinite were 98.1 and 4.1 meq per 100 g, respectively. Parabraun soil (B horizon) was collected at Merzenhausen, near Jülich (Germany).

Solutions of 10 mg l^{-1} humic acid, 50 mg l^{-1} sodium montmorillonite, 200 mg l^{-1} sodium kaolinite and 200 mg l^{-1} Parabraun soil (B horizon) in 0.001 M $NaNO_3$ sodium nitrate solution (pH 10) were prepared for titrations.

Other chemicals were of analytical-reagent grade from Merck. Solutions were prepared with triply distilled water.

Apparatus

Potentiometric measurements were performed with a Titroprozessor 670 coupled to a Dosimat 665 from Metrohm. A solid-state iodide ion-selective electrode (I^-/ISE) and an Ag/AgCl double-junction reference electrode from Metrohm were used as the iodide indicator and reference electrode, respectively. A PTFE cell and Model 649 magnetic stirrer from Metrohm were used for potentiometric titrations. Potentiometric pH titrations of PAA (1 g l^{-1}) and humic acids (100 mg l^{-1}) were performed with an Orion Model 960 Autochemistry system.

Procedure for potentiometric colloidal titration

Monotonic titrations under stirring conditions were performed by adding 5–10-μl aliquots of an HBDACl titrant solution (0.5 g l^{-1}) to a PTFE cell (25 ml) containing polyelectrolytes and colloids in 1×10^{-3} M electrolyte ($NaNO_3$, NaCl) solutions (pH 10). Titration began after a conditioning time of 5 min for the I^-/ISE detector system. Incremental addition of titrant took place after a potential drift lower than 3 mV min^{-1} or a maximum waiting time of 91 s.

RESULTS AND DISCUSSION

Principle of potentiometric colloidal titration

Titrant. According to different workers, a successful colloid titration is based on the highly cooperative binding of the titrant to the investigated colloid. Thus, a stoichiometric neutralization at the end-point can frequently be measured by the reaction between oppositely charged polyelectrolytes [3,8]. In a similar way, the cooperative electrostatic binding of ionic surfactants to oppositely charged polyelectrolytes or other amphiphilic molecules can be used for analytical purposes. In the case of the neutralization of an anionic polyelectrolyte by a cationic surfactant, the driving force for this cooperative binding is not only electrostatic but also of a hydrophobic nature [9]. Indeed, the initial electrostatic binding, favoured by a local high electric field around the polyanions, is reinforced for successive fixations by interactions between the carbon chains of primarily bound surfactant molecules. By analogy with the formation of surfactant micelles in solution, this cooperative molecular clustering is enhanced in the case of long-chain surfactants. Therefore, a cationic surfactant such as HBDACl is required for an effective neutralization titration.

It should be noted that possible competitive interactions of divalent and trivalent cations can

be suppressed by adding a strong complexing agent such as EDTA. Up a concentration of 3×10^{-3} M, no deleterious effects of EDTA on the electrode sensitivity to HBDACl were observed.

End-point indicator. From an electrostatic point of view, it can be considered that the iodide anion in the presence of excess of other anions does not bind to negatively charged colloids. Variations of its activity in solution occur only after interactions with positively charged titrants. Iodide has thus been proposed as an indicator for the end-point of neutralization titrations [5,10]. This activity change can be readily detected at concentrations as low as 10^{-7} M with an I^-/ISE. In this work an iodide ion trace concentration of 3×10^{-6} M was generally chosen.

End-point detector. In Fig. 1, typical potentiometric titration curves of PAA with HBDACl are shown. Potential changes of the I^- ISE (curves 1–3) are plotted against the volume of titrant solution added. The end-point of titration is determined by means of tangents on both sides of the curve break point.

Successive repetition of the titration (curves 2 and 3), after washing but without any prior intense polishing of the electrode surface, revealed an enhanced potential break at the end-point of about 30 mV, which improves its detection. This electrode sensitivity to HBDACl persists after immersing the electrode in the electrolyte solution (curve 0). As reported by other workers [6,11], this result confirms the sensitivity of the I^-/ISE system to interactions with quaternary ammonium ions. In the present case, a strong interaction of the free HBDACl or the less soluble HBDA–polyanion neutral complex with the AgI/Ag_2S sensing membrane of the solid-state ISE is to be expected. This can result in a modification of the electrochemical properties through a displacement of the determining potential ions Ag^+ and I^-, as is known for the adsorption of organic cations on AgI colloids [12]. It follows that the end-point detection involves complex interfacial reaction mechanisms [11] rather than a weak complexation between HBDACl and I^- in bulk solution [5]. Rinsing with distilled water and cleaning the electrode by touching with a soft adsorbent paper tissue maintain the sensitivity of detection for days without any deterioration of the reproducibility of the titration.

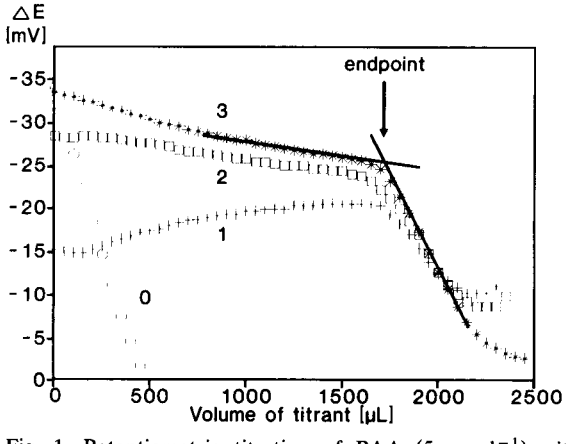

Fig. 1. Potentiometric titration of PAA (5 mg l^{-1}) with HBDACl (0.5 g l^{-1}) in the presence of iodide ion indicator (3×10^{-6} M) in 1×10^{-3} M $NaNO_3$ at pH 10. ○ = Electrolyte support; + = PAA, first potentiometric titration run; □ and * = PAA, repeated potentiometric titration runs (see text).

Sample solutions. For an effective quantitative charge neutralization process, a low supporting electrolyte concentration of 10^{-3} M was chosen. End-point volumes of titrant can be measured in the presence of $NaNO_3$ and NaCl salts. Further, a titration at pH 10, where most acidic functions are totally ionized, also allowed calibration graphs for polyanions to be obtained under optimum electrostatic interactions.

Calibration graphs for polyanions

In order to evaluate the titration procedure, calibration graphs for three different polyanion samples were constructed. In Fig. 2, the sample concentrations expressed in molar concentrations of HBDACl are plotted against the concentration of polyanions in mg l^{-1}. Straight-line relationships hold, obtained with a high correlation coefficient ($r = 0.999$) for the investigated concentration range up to 5 or 10 mg l^{-1}. In Table 1, the characteristics of the computed regression lines are reported. The different slope values are to be correlated with the charge densities of the corresponding polyanions KPVS, PAA and NaCP (see Experimental). Considering a slight excess of HB-

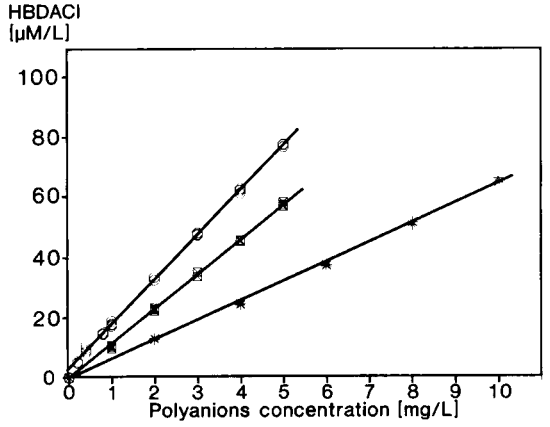

Fig. 2. Calibration graphs for polyanions. * = KPVS in 1×10^{-3} M $NaNO_3$; ⊠ = NaCP in 1×10^{-3} M NaCl; ○ = PAA in 1×10^{-3} M $NaNO_3$. Other conditions as in Fig. 1. See also Table 1.

DACl to fulfill the neutralization conditions, satisfactory agreement exists between the experimental and calculated values. The ratios of the slopes in Table 1 to the corresponding charge densities are found to be 1.07, 1.04 and 1.05 for PAA, NaCP and KPVS, respectively, i.e., close to the stoichiometric 1:1 reaction of neutralization.

The precision of the potentiometric titration was also evaluated for a 2 $mg^{-1}L$ PAA solution by running seven replicate titrations. An average value of 33.3 ± 0.8 μM was obtained, which gives

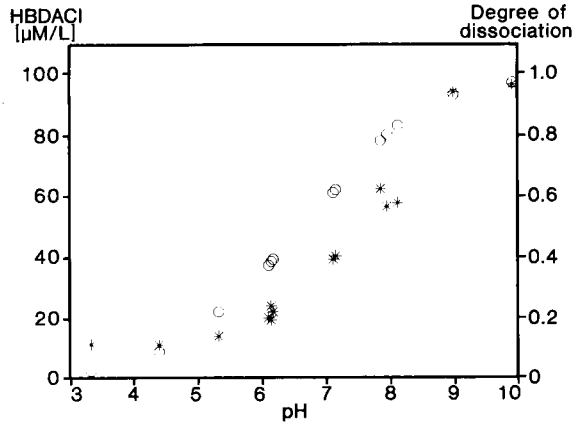

Fig. 3. Effect of the pH on the potentiometric determination of PAA (6 mg l^{-1}) in 1×10^{-3} M $NaNO_3$. * = End-point concentration of HBDACl (other conditions as in Fig. 1); ○ = degree of dissociation of PAA (see Experimental).

TABLE 1

Regression data from calibration graphs for polyanions and anionic surfactants (see also Fig. 2 and Fig. 5)

Compound	Slope (10^{-3} M HBDACl g^{-1})	Intercept (10^{-6} M HBDACl l^{-1})	Standard error (10^{-6} M HBDACl l^{-1})	
PAA ($n=29$)	14.85 ± 0.08	3.07 ± 0.20	0.70	0.999
NaCP ($n=17$)	11.63 ± 0.10	−0.74 ± 0.31	0.67	0.999
KPVS ($n=12$)	6.50 ± 0.08	−0.65 ± 0.48	0.95	0.999
NaDBS ($n=13$)	3.52 ± 0.07	2.84 ± 1.32	2.71	0.997
NaDBS in NaCP solution ($n=22$)	3.61 ± 0.06	34.39 ± 1.05	2.73	0.997
NaDS ($n=10$)	3.87 ± 0.09	4.51 ± 1.49	2.92	0.997

a relative standard deviation of better than 3%. Further the lowest PAA concentration that can be detected is 0.2 $mg^{-1}L$. PAA and CP are weak polyacids whose degree of dissocation depends on the solution pH. Thus, it can be seen from Fig. 3 that for PAA the required HBDACl concentration to reach the end-point of the titration rises drastically with increasing pH or the degree of ionization of carboxylic groups. Maximum binding of HBDACl is observed at pH 10 for a completely dissociated PAA. On the other hand, with strong polyacid KPVS, readily dissociated at acidic pH, an increase in titrant consumption of less than 10% is only measured from pH 3 to 10.

Effects of anionic and non-ionic surfactants.

Because more and more industrial applications are combining surfactants and polymers [13], the effects of surfactants on the titration process were investigated. In Fig. 4, the titration of 3 mg l^{-1} NaCP solution containing 10 mg l^{-1} of $C_{12}EO_4$ does not show any effect of the non-ionic surfactant (curves 1 and 2) on the location of the end-point volume. On the other hand, the same concentration of anionic surfactant NaDS (curve 3) induces a shift of the end-point volume to

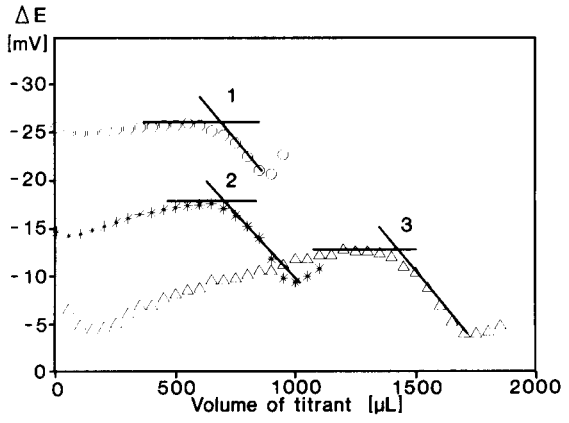

Fig. 4. Effects of surfactants on the potentiometric titration of NaCP (3 mg l^{-1}) in 1×10^{-3} M NaCl. ○ = Without surfactant; ∗ = 10 mg l^{-1} $C_{12}EO_4$; △ = 10 mg l^{-1} NaDBS. Other conditions as in Fig. 1.

higher values. This result makes it clear that not only NaCP but also the anionic surfactant is titrated. It must be noted that with anionic surfactant solutions a better reproducibility of the results is obtained by polishing the electrode surface with powdered alumina prior to each run. This results in lower potential breaks of about 10 mV amplitude, which are sufficient, however, for detecting the end-point of titration.

The additive effect of anionic surfactants in the titration of NaCP is illustrated in Fig. 5. Two parallel straight lines result from plotting in the

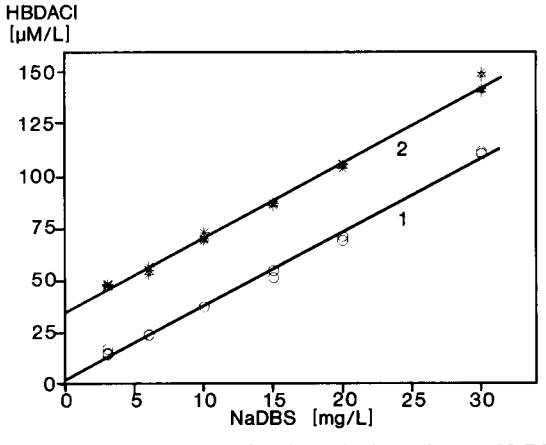

Fig. 5. Calibration curves for the anionic surfactant NaDBS. ○ = In the absence and ∗ = in the presence of NaCP (3 mg l^{-1}). Other conditions as in Fig. 4.

absence (line 1) or presence (line 2) of 3 mg l^{-1} NaCP the end-point HBDACl concentration against increasing NaDBS concentrations up to 30 mg l^{-1}. In Table 1, regression analysis data indicate the additive nature of this titration: similar slope values for lines 1 and 2 and intercept value of line 2 matching the NaCP concentration in the mixture.

In the same way, a calibration graph for the anionic surfactant NaDS can be obtained whose linear regression analysis data are also reported in Table 1. The ion-pair formation between oppositely charged surfactants is thus probed by the I^-/ISE sensor system [6] while the presence of a neutral charged non-ionic surfactant is not detected.

Titration of soil colloids.

An important chemical property of soil is its cation-exchange capacity (CEC) [14]. Thus, a rapid knowledge of the maximum amount of exchangeable cations can be estimated from the neutralization titration of negatively charged binding sites, which are mostly located on two common soil colloids: clay minerals and soil humus. In Table 2, data for the colloid titrations are reported for sodium kaolinite and sodium montmorillonite, two extensively distributed clays, and for a commercial humic acid sample. Values, measured at pH 10, were calculated per 100 g of dry material, as usually reported for CEC data. There is good agreement between the end-point HBDACl concentrations, also expressed as cationic surfactant binding capacities (CSBC), and available CEC data for clays (see Experimental).

TABLE 2

Cationic surfactant binding capacity (CSBC) of soil colloids (see also Experimental).

Soil colloid	CSBC (10^{-3} M HBDACl per 100 g)	
Humic acid (Aldrich)	463 ±25	(n = 3)
Sodium montmorillonite	93 ± 3	(n = 3)
Sodium kaolinite	4.2± 0.3	(n = 4)
B-horizon Parabraun soil	28 ± 1.0	(n = 3)

The titration of the Aldrich humic acid also gave a CSBC value that agrees with the proton binding capacity of 409 ± 12 meq per 100 g measured by the Gran method. This method has been used to determine the content of carboxylic groups in polycarboxylate [15]. However, the present results with the I^-/ISE were obtained at much lower concentrations (10 mg l^{-1}) such as are usually found in natural waters. For comparison, the CSBC result is reported for Parabraun soil (B horizon) with a composition of clays and humic acids of up to 25% and 0.6%, respectively. When the CSBC of Parabraun soil is calculated using the data in Table 2, a fair approximation is obtained with a high CSBC for clays, as is the case for sodium montmorillonite.

In conclusion, the end-point sensor properties of a commercially available I^-/ISE system with respect to a long-chain quaternary ammonium surfactant such as HBDACl offers a convenient method for titrating not only anionic surfactants but also anionic polyelectrolytes and colloids. With a modern potentiometer connected to an automatic titration device, the magnitude of the potential end-point break is not a limiting factor for the sensivity. Thus, in the framework of a research programme on the environmental behaviour of detergent components, this method is routinely applied in this laboratory for establishing adsorption isotherms of polycarboxylic acids at soil mineral components.

The authors are indebted to C. Walraf for her skilful technical assistance.

REFERENCES

1 D. Myers, in Surfaces, Interfaces, and Colloids: Principles and Applications, VCH, New York, 1991, Chap. 14.
2 E. Tipping, Chem. Ind. (London), (1988) 485.
3 K.-H. Wassmer, U. Schroeder and D. Horn, Makromol. Chem., 192 (1991) 553.
4 J.P. Fischer and E. Nölken, Prog. Colloid Polym. Sci., 77 (1988) 180.
5 N. Ishibashi, K. Kina and K. Tamura, Anal. Lett., 8 (1975) 867.
6 W. Selig, Microchem. J., 25 (1980) 200.
7 W. Selig, Microchem. J., 36 (1987) 42.
8 H. Terayama, J. Polym. Sci., 8 (1952) 243.
9 K. Hayakawa and J.C.T. Kwak, in D.N. Rubingh and P.M. Holland (Eds.), Cationic Surfactants: Physical Chemistry, Dekker, New York, 1991, p. 189.
10 K. Ueno and K. Kina, J. Chem. Educ., 62 (1985) 627.
11 S.A. Khan and B.G. Reuben, J. Appl. Electrochem., 15 (1985) 200.
12 A. de Keizer and J. Lyklema, J. Colloid Interface Sci., 75 (1980) 171.
13 M. Hunter, D.M.L. da Motta Marques, J.N. Lester and R. Perry, Environ. Technol. Lett., 9 (1988) 1.
14 R.L. Donahue, R.W. Miller and J.C. Shickluna, in Soils: an Introduction to Soils and Plant Growth, Prentice, Hall, Englewood Cliffs, NJ, 1983, p. 86.
15 F. Blockhaus, J.-M. Séquaris and M.J. Schwuger, Tenside Detergents, 28 (1991) 447.

Analytica Chimica Acta, 281 (1993) 347–351
Elsevier Science Publishers B.V., Amsterdam

Spectrofluorimetric determination of traces of zinc with the cadmium–$\alpha,\beta,\gamma,\delta$-tetrakis(4-sulphophenyl)-porphine complex

Shukuro Igarashi and Takao Yotsuyanagi

Department of Molecular Chemistry and Engineering, Faculty of Engineering, Tohoku University, Aoba, Aramaki, Aoba-ku, Sendai 980 (Japan)

(Received 4th December 1992; revised manuscript received 12th March 1993)

Abstract

A highly sensitive spectrofluorimetric method for the determination of zinc was established by using the metal ion substitution reaction of the cadmium–$\alpha,\beta,\gamma,\delta$-tetrakis(4-sulphophenyl)porphine (H_2P^{4-}) complex with zinc ion. The zinc complex, ZnP^{4-}, was quantitatively formed within 3 min at room temperature in the pH range 10–11. The relative fluorescence intensity ratio, $F(ZnP^{4-})/F(CdP^{4-})$, was 37.0 at $\lambda(em) = 604$ nm [$\lambda(ex) = 422$ nm]. The calibration graph was linear over the concentration range 5–100 ng Zn^{2+} ml^{-1} in sample solution. The detection limit (signal-to-noise ratio = 3) was 0.15 ng Zn^{2+} ml^{-1} and the relative standard deviation was 1.39% for 16.6 ng Zn^{2+} ml^{-1} (ten determinations). Results are given for the application of the method to the determination of Zn^{2+} in tap water.

Keywords: Fluorimetry; Complexation; Waters; Zinc

In the last two decades, water-soluble porphines have been synthesized and their function as highly sensitive chromogenic reagents for metal ions have been demonstrated [1–10]. In addition, the fluorimetric properties of metal–porphine complexes have also been studied in aqueous solution at room temperature, and methods for the fluorimetric determination of magnesium [11] and the quenched fluorimetric determination of copper(II) [12] have been proposed. Onoue et al. [13] established a unique delayed fluorimetric method for zinc [13], but the procedure is fairly complicated and it requires some modifications of conventional apparatus.

Water-soluble porphines have a serious drawback as chelating reagents for metal ions, viz., the rate of complexation is very slow [14]. In order to overcome this rate problem, several acceleration methods have been proposed [1–10], including heating, addition of auxiliary complexing agents (catalyst method) and application of metal ion substitution reactions. Grant and Hambright [15] studied metal ion substitution reactions of metal–porphine complexes in organic solvents [15]. The above acceleration methods in aqueous solution have been applied to the spectrophotometric determination of manganese(II) [16] and mercury(II) [17].

In this work, the metal ion substitution reaction of the cadmium–$\alpha,\beta,\gamma,\delta$-tetrakis(4-sulphophenyl)porphine (H_2P^{4-}) complex (CdP^{4-}) with zinc(II) ion was studied and conditions were established for the quantitative formation of the ZnP^{4-} complex within 3 min at room tempera-

Correspondence to: S. Igarashi, Department of Molecular Chemistry and Engineering, Faculty of Engineering, Tohoku University, Aoba, Aramaki, Aoba-ku, Sendai 980 (Japan).

ture. Based on this reaction and the characteristics of the fluorescence spectra of ZnP^{4-} and CdP^{4-} complexes, a simple and highly sensitive spectrofluorimetric method for zinc(II) was developed.

EXPERIMENTAL

Apparatus

All fluorescence measurements were made with a Model FP-4 spectrofluorimeter (Japan Spectroscopic) using 10-mm square quartz cells. The spectrofluorimeter was equipped with a 150-W xenon lamp source and an R106 photomultiplier detector. A Model HM-5A pH meter (Toa Dempa) was used for pH measurements.

Reagents

The reagent, H_2P^{4-} ($C_{44}H_{34}N_4O_{20}S_6 \cdot 12H_2O$), was prepared from tetraphenylporphine (TPP) by sulphonation [18]; TPP was synthesized from pyrrole and benzaldehyde in propionic acid under reflux [19].

Standard H_2P^{4-} solution (10^{-3} mol l^{-1}) was prepared by dissolving 1.35 g of H_2P^{4-} in distilled water and diluting to 1 l. Standard zinc(II) solution (0.01 mol l^{-1}) was prepared by dissolving 0.654 g of zinc in hydrochloric acid and diluting to 1 l with distilled water, and was standardized by EDTA titration.

Recommended procedure

An aliquot of 0.5 ml of 1×10^{-4} mol l^{-1} H_2P^{4-} solution, 1 ml of 1×10^{-4} mol l^{-1} $CdCl_2$ solution, 1 ml of 0.01 mol l^{-1} 2,2′-bipyridyl solution and 2 ml of buffer solution (pH 10.2; 0.1 mol l^{-1} sodium borate–1 mol l^{-1} sodium hydroxide) were placed in a 50-ml amber-coloured volumetric flask. After the mixture had been allowed to stand for 3 min at room temperature, 40 ml of sample solution containing up to 4 μg of Zn^{2+} were added and the mixture was diluted to the mark with water. After 5 min, the fluorescence intensity of the solution was measured at λ(em) = 604 nm with an excitation wavelength of λ(ex) = 422 nm. The sensitivity of the spectrofluorimeter was set by adjusting the fluorescence intensity to 100 with 1.4×10^{-4} mol l^{-1} *N,N′*-dimethylamino-*m*-nitrobenzene in a mixed solvent [benzene–hexane (30 + 70, v/v)] at (ex) = 422 nm and λ(em) = 604 nm.

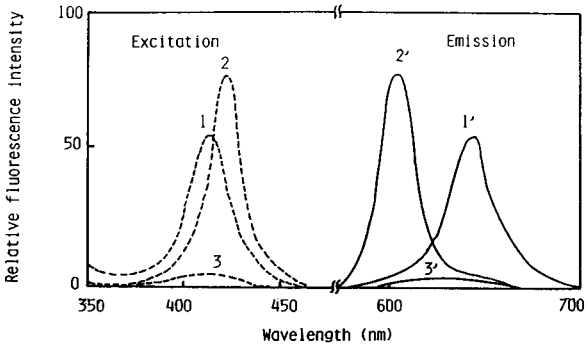

Fig. 1. Excitation and emission spectra of aqueous H_2P^{4-}, ZnP^{4-} and CdP^{4-} solutions at pH 9.3. 1 and 1′, H_2P^{4-}; 2 and 2′, ZnP^{4-}; 3 and 3′, CdP^{4-}.

RESULTS AND DISCUSSION

Composition of the complex and fluorescence spectra

The compositions of the complexes were established to be ZnP^{4-} and CdP^{4-} by the mole-ratio method. Excitation and emission spectra (uncorrected) of the free base form (H_2P^{4-}), ZnP^{4-} complex, and CdP^{4-} complex are shown in Fig. 1. The excitation spectra correspond well to the absorption spectra of each species, and the Soret band of ZnP^{4-} (at 423 nm, molar absorptivity $\epsilon = 6.3 \times 10^5$ l mol^{-1} cm^{-1}) overlaps with that of the reagent (at 413 nm, $\epsilon = 5.1 \times 10^5$ l mol^{-1} cm^{-1}). Therefore, it is difficult to determine zinc(II) with high sensitivity by using the change in the absorption spectra. However, the emission spectra of H_2P^{4-} and the ZnP^{4-} complex are well separated and allow the direct determination as shown in Fig. 1, curves 1′ and 2′ [λ(em) = 640 nm for H_2P^{4-} and λ(em) = 604 nm for ZnP^{4-}]. Moreover, when the metal ion substitution reaction was used according to the recommended procedure, the fluorescence intensity of the reagent blank was decreased markedly by using the CdP^{4-} complex [λ(em) = 633 nm], which

shows a lower fluorescence intensity than that of H_2P^{4-} [λ(em) = 640 nm]. The relative fluorescence intensity ratio, $F(ZnP^{4-})/F(CdP^{4-})$, was 37.0 at λ(em) = 604 nm [λ(ex) = 422 nm].

Influence of pH

The influence of pH on the complex formation of zinc(II) with H_2P^{4-} is shown in Fig. 2 (line 1). The ZnP^{4-} complex was quantitatively formed and gave a constant fluorescence intensity over the pH range 8.3–11.0. On the other hand, the complex once produced in this pH range was kinetically inert and was not dissociated at least for 12 h at pH down to 4.0. At pH above 12.4, the fluorescence intensity decreased owing to the hydrolysis of the ZnP^{4-} complex (Fig. 2, line 2):

$$ZnP^{4-} + H_2O \overset{K_a}{\rightleftharpoons} [Zn(OH)P]^{5-} + H^+ \quad (1)$$

The dissociation of one proton (H^+) was confirmed from relative fluorescence intensity (RFI) versus pH curve and the acid dissociation constant (K_a) was calculated as $pK_a = 13.2$ at 25°C. By considering the condition where both the CdP^{4-} and ZnP^{4-} complexes could exist as stable species, the pH adopted for the determination was 10.2. Both the CdP^{4-} and ZnP^{4-} complexes are light sensitive and are easily decomposed even under the room light conditions. Therefore, the complexations were carried out in an amber-coloured volumetric flask, in which they were stable for at least 12 h.

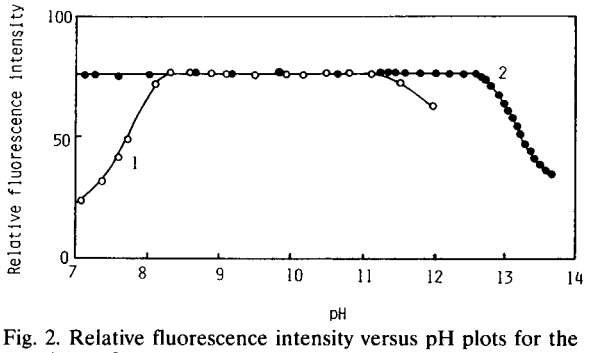

Fig. 2. Relative fluorescence intensity versus pH plots for the H_2P^{4-}–Zn^{2+} system. (1) Reaction mixture of H_2P^{4-} and Zn^{2+}; (2) ZnP^{4-} complex. $[Zn^{2+}]_{Total} = [H_2P^{4-}]_{Total} = 1 \times 10^{-6}$ mol l^{-1}.

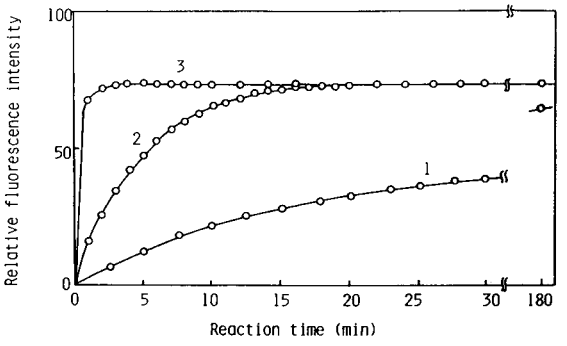

Fig. 3. Reaction time versus relative fluorescence intensity plots for the H_2P^{4-}–Cd^{2+}–Zn^{2+} system at 25°C. $[Zn^{2+}]_{Total} = [H_2P^{4-}]_{Total} = 1 \times 10^{-6}$ mol l^{-1}; pH = 10.2 (0.1 mol l^{-1} borate–1 mol l^{-1} NaOH buffer solution). (1) Reaction of H_2P^{4-} and Zn^{2+}; (2) reaction of H_2P^{4-} and mixture of bpy and Zn^{2+}; $[bpy]_{Total} = 2 \times 10^{-4}$ mol l^{-1}; (3) metal ion substitution reaction of CdP^{4-} complex and Zn^{2+}; $[bpy]_{Total} = 2 \times 10^{-4}$ mol l^{-1}.

Rate of complex formation

The relationship between reaction time and relative fluorescence intensity of the zinc(II)–H_2P^{4-} mixture at pH 10.2 is shown in Fig. 3. All of the acceleration methods are effective, as follows. (a) Heating: the ZnP^{4-} complex was quantitatively formed even at room temperature, but it took more than 3 h (Fig. 3, line 1). In a boiling water-bath (95–100°C) it was formed within 10 min. (b) Addition of auxiliary complexing agents: heterocyclic nitrogen bases, 2,2′-bipyridyl(bpy) and 1,10-phenanthroline, accelerated the complexation:

$$Zn^{2+} + n(bpy) \rightleftharpoons [Zn(bpy)_n]^{2+} \quad (2)$$

$$[Zn(bpy)_n]^{2+} + H_2P^{4-} \rightleftharpoons ZnP^{4-} + n(bpy) + 2H^+ \quad (3)$$

Molar fractions of zinc(II)–bpy complexes calculated from stability constants [20] were compared with the relative fluorescence intensity of the ZnP^{4-} complex, measured at the reaction time of 10 min (Fig. 4). Figure 4 indicates that the active species in this reaction system should be $[Zn(bpy)]^{2+}$ and $[Zn(bpy)_2]^{2+}$. At a bpy concentration of 2×10^{-5}–1×10^{-4} mol l^{-1}, the ZnP^{4-} complex was quantitatively formed within 20 min (Fig. 3, line 2) at room temperature. (c) Applica-

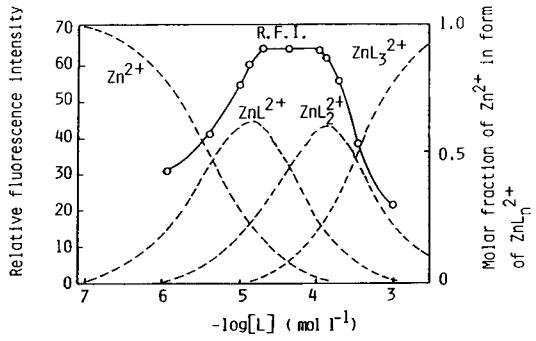

Fig. 4. Relative fluorescence intensity of H_2P^{4-}–Zn^{2+}–bpy mixture and molar fraction of Zn^{2+} in the form of $[ZnL_n]^{2+}$ as a function of $-\log[L]$ (L = bpy). The relative fluorescence intensity was measured after a reaction time of 10 min. $[Zn^{2+}]_{Total} = [H_2P^{4-}]_{Total} = 1 \times 10^{-6}$ mol l^{-1}.

tion of metal ion substitution reaction: when 2×10^{-6} mol l^{-1} Cd^{2+} was added in the reaction system, the ZnP^{4-} complex was formed within 20 min at room temperature. Moreover, the CdP^{4-} complex reacted with Zn^{2+} to form the ZnP^{4-} complex quantitatively, within 3 min at room temperature (Fig. 3, line 3). Therefore, in the recommended procedure, 1 ml of 0.01 mol l^{-1} bpy was added as a auxiliary complexing agent in order to prepare beforehand the CdP^{4+} complex at room temperature.

Calibration

The calibration graph was linear over the concentration range 5–100 ng Zn^{2+} ml^{-1} in the sample solution. The detection limit (signal-to-noise ratio = 3) was 0.15 ng Zn^{2+} ml^{-1} and the relative standard deviation was 1.4% for 16.6 ng Zn^{2+} ml^{-1} (ten determinations). This method (determination range 5–100 ng ml^{-1}) is more sensitive than the $\alpha,\beta,\gamma,\delta$-tetrakis(1-methylpyridyl-4-yl)porphine (TMPyP) method [2] (12–240 ng ml^{-1}) and the quinolin-8-ol method [21] (0.4–12 μg ml^{-1}).

Influence of foreign metal ions

The tolerance limits for foreign metal ions are summarized in Table 1. The tolerance limits for method B (the recommended procedure) are better on the whole than that of the method A. Especially Cd^{2+}, Hg^{2+}, Pd^{2+} and Fe^{3+} were tolerated up to 100 μg in method B. In method A, bpy is expected to act not only as an accelerating agent as shown in Eqns. 2 and 3, but also as a masking agent for other metal ions. The effective concentration of bpy is restricted in the appropriate range as shown in Fig. 4. The only metal ions for which the tolerance limits in method A are higher than those in method B are Co^{2+} and Cu^{2+}. This result cannot be understand on a simple equilibrium basis, as the bpy concentration in method A is lower than that in method B ($[bpy] = 2 \times 10^{-4}$ mol l^{-1}). Hence both Co^{2+} and Cu^{2+} should be incorporated into the porphine ring by the accelerating effect of CdP^{4-} complex.

An effective pretreatment method, namely dithizone extraction, was reported previously for

TABLE 1

Tolerance limits (μg per 50 ml) [a] of foreign metal ions in the determination of zinc(II) [b]

Method A [c]					Method B [c]					Method C [c]
1000	100	10	1	< 1	1000	100	10	1	< 1	100
Ba^{2+}	Al^{3+}	Ag^{+}	Cu^{2+}	Cr^{3+}	Al^{3+}	Ag^{+}	Ni^{2+}	Co^{2+}	Cr^{3+}	Cu^{2+}
Ca^{2+}	Ga^{3+}	Co^{2+}	Fe^{2+}	Cd^{2+}	Ba^{2+}	Cd^{2+}	Sn^{2+}		Cu^{2+}	Cr^{3+}
WO_4^{2-}	Mg^{2+}	In^{3+}	Fe^{3+}		Ca^{2+}	Fe^{3+}	Fe^{2+}			Co^{2+}
	VO^{2+}	Ni^{2+}	Hg^{2+}		Ga^{3+}	Hg^{2+}				Fe^{2+}
	VO_3^{-}		Pb^{2+}		Mg^{2+}	In^{3+}				Ni^{2+}
			Sn^{2+}		MoO_4^{2-}	Pb^{2+}				Sn^{2+}
					VO^{2+}	VO_3^{-}				
					WO_4^{2-}					

[a] Deviations of ±4% were allowed in the relative fluorescence intensity. [b] Zinc(II) taken: 0.83 μg per 50 ml. [c] Method A: this method is modified from the recommended procedure in two respects: no addition of $CdCl_2$ and addition of 1 ml of 0.01 mol l^{-1} 2,2′-bipyridyl solution. Method B: recommended procedure. Method C: zinc(II) was separated by dithizone extraction and then determined by method B.

TABLE 2

Determination of zinc(II) in tap water

Sample No. [a]	Concentration of zinc(II) (ng ml^{-1})	
	Proposed method [b]	Atomic absorption spectrometry [c]
1	48.1	45.8
2	20.9	19.6
3	248.4	255.0

[a] These tap water samples were collected from different outlets in the laboratory. [b] The relative standard deviation for sample No. 2 was 1.1% (five determinations). [c] The relative standard deviation for sample No. 2 was 6.1% (five determinations).

the spectrophotometric determination of zinc(II) with TMPyP [2], where Zn^{2+} was selectively separated from diverse ions. The method is as follows: 25 ml of sample solution containing less than 4 μg of zinc(II) are placed in a 50-ml sample vial and 1 ml of 0.1 mol l^{-1} citrate solution, 2 ml of 0.1 mol l^{-1} thiocyanate solution and 5 ml of 0.1 mol l^{-1} borate solution (pH 9.2) are added and mixed. A 10-ml volume of 0.02% dithizone–CCl_4 solution is added and shaken for 15 min. The two phases are separated by centrifugation (1500 *g*) for 10 min. After removing the aqueous phase, zinc(II) ion is back-extracted into the aqueous phase with 10 ml of 0.5 mol l^{-1} HCl solution.

By the combined use of this pretreatment method and the recommended procedure, Cu^{2}, Cr^{3+}, Co^{2+}, Fe^{2+}, Ni^{2+} and Sn^{2+} were tolerated in amounts up to 100 μg (see Table 1, method C).

Application to real samples

Zinc(II) in various tap water samples was determined by the recommended procedure without preliminary separation by the dithizone extraction method. The results (Table 2) show reasonable agreement with the results obtained by atomic absorption spectrometry.

In order to determine 1 ng Zn^{2+} ml^{-1}, generally, flame atomic absorption spectrometry (detection limit 1 μg l^{-1}) [22], inductively coupled plasma atomic emission spectrometry (ICP-AES) (1 μg l^{-1}) [22] and ICP–mass spectrometry (0.07 μg l^{-1}) [22] have been widely used. Compared with these methods, not only is the present spectrofluorimetric method nor inferior with respect to detection limit, but also the cost per determination ion is very low and the recommended procedure is rapid and simple. Hence it is expected that this method will be extensively applied to industrial and environmental samples.

REFERENCES

1 J. Itoh, T. Yotsuyanagi and K. Aomura, Anal. Chim. Acta, 74 (1975) 53.
2 S. Igarashi, J. Kobayashi, T. Yotsuyanagi and K. Aomura, Nippon Kagaku Kaishi (1979) 602.
3 H. Ishii, H. Koh and K. Satoh, Analyst, 107 (1982) 647.
4 K.L. Chang, K. Ueno and T. Imamura, Handbook of Organic Analytical Reagents, CRC, Boca Raton, FL, 1988, p. 355, and references cited therein.
5 H. Ishii and H. Koh, Mikrochim. Acta, I (1983) 279.
6 K. Kawamura, S. Igarashi and T. Yotsuyanagi, Anal. Sci., 4 (1988) 175.
7 H. Ishii, Y. Satoh and K. Satoh, Anal. Sci., 5 (1989) 713.
8 X. Xu, H. Zhang, C. Zhang and J. Cheng, Anal. Chem., 63 (1991) 2529.
9 M. Tabata and K. Kaneko, Analyst, 116 (1991) 1185.
10 J. Itoh and T. Komata, Mikrochim. Acta, 106 (1992) 109.
11 S. Igarashi, T. Yotsuyanagi and K. Aomura, Nippon Kagaku Kaishi, (1981) 60.
12 S. Igarashi, T. Yotsuyanagi and K. Aomura, Bunseki Kagaku, 28 (1979) 449.
13 Y. Onoue, K. Morishige, K. Hiraki and Y. Nishikawa, Bunseki Kagaku, 33 (1984) E23.
14 J.E. Falk, Porphyrins and Metalloporphyrins, Elsevier, Amsterdam, 1964, p. 30.
15 C. Grant. Jr. and P. Hambright, J. Am. Chem. Soc., 91 (1969) 4195.
16 H. Ishii, H. Koh and K. Satoh, Anal. Chim. Acta, 136 (1982) 347.
17 M. Tabata and M. Tanaka, Anal. Lett., 13 (1980) 427.
18 E.B. Fleisher, J.M. Palmer, T.S. Srivastava and A. Chatterjee, J. Am. Chem. Soc., 93 (1971) 3162.
19 A.D. Adler, F.R. Longo, F.D. Finarelli, J. Goldmacher, J. Assour and K. Korsakoff, J. Org. Chem., 32 (1968) 476.
20 M. Yasuda, K. Sone and K. Yamasaki, J. Phys. Chem., 60 (1956) 1667.
21 L.L. Merritt, Ind. Eng. Chem., Anal. Ed., 16 (1944) 758.
22 Analytical Chemical Society of Japan, Handbook of Analytical Chemistry, Maruzen, Tokyo, 1991, p. 216.

Analytica Chimica Acta, 281 (1993) 353–360
Elsevier Science Publishers B.V., Amsterdam

Effect of cationic micelles on the fluorescence of the zirconium–morin complex

Ying-Xin Fan [1] and Yong-Xi Zheng

Department of Chemistry, Tsinghua University, Beijing 100084 (China)

(Received 17th December 1992; revised manuscript received 23rd March 1993)

Abstract

The effect of cationic surfactants on the fluorescence of the zirconium–morin system is described. In sulphuric acid medium, the fluorescence intensity of this complex can be enhanced strongly by the cationic surfactant cetyltrimethylammonium bromide (CTAB). It was found that the decisive factor is the change in the composition of the analyte complex in the presence of CTAB. When the concentration of CTAB is near its critical micelle concentration, the absorptiometric measurement is favoured by the formation of a 1:3 [Zr(IV):morin] complex. On increasing the CTAB concentration, a mixed-ligand complex with the composition of Zr(IV):morin:SO_4^{2-} = 1:1:2 is formed, and the fluorescence intensity is enhanced dramatically. The role of CTAB in the formation of the mixed-ligand complex and the enhancement of the fluorescence is discussed.

Keywords: Fluorimetry; Cationic micelles; Morin complex; Surfactants; Zirconium

With the addition of certain surfactants, the sensitivity and selectivity of numerous analytical reactions are improved. The use of micelles in spectrophotometric methods of analysis is perhaps the most popular and oldest area of application of micelles in analytical chemistry [1–3]. In recent years, surfactants have been successfully applied in the fluorimetric determinations. Compared with the effect on molar absorptivity, the enhancement of fluorescence intensity by surfactants is much greater; in many instances a tenfold increase is observed. However, the mechanisms of the effects on absorption and fluorescence have hardly been investigated. An improved understanding would greatly facilitate the analytical exploitation of this effect and would be useful in explaining surfactant-solubilized interactions in other applications.

Although there is no general theory, some systematic studies have been done on the mechanism of micelle-modified spectrophotometry and several theories and hypotheses have been proposed [4]. Comparatively little has been done on the effect of surfactants on fluorescence. Sanz-Medel and co-workers [5] studied the effect of cationic surfactants on the fluorescence of complexes of niobium and tantalum with flavone derivatives (morin and quercetin) and the effects of non-ionic surfactants on niobium complexes in the presence of some "auxiliary ligands" [6]. Some trends existing in the fluorescence enhancement of metal chelates by micelles were elucidated. Zheng [7] has discussed absorbance and luminescence in micelle media.

Both absorption and fluorescence can be affected by surfactants and both are related to photophysical processes. The effects of surfac-

Correspondence to: Yong-Xi Zheng, Department of Chemistry, Tsinghua University, Beijing 100084 (China).
[1] Present address: Institute of Biophysics, Academia Sinica, Beijing 100101, China.

tants on these processes are similar in some respects, but not identical. The most obvious difference is that a higher surfactant concentration is required for fluorescence enhancement [5,8]. No comparisons have been made between the effects of micelles on absorption and fluorescence, which could provide significant evidence for explaining the sensitization mechanism.

Morin is one of the most widely used reagents for the fluorimetric determination of metals [9]. Surfactants have also been used to enhance the fluorescence of some metal–morin complexes [5,10–13]. It has been found that the fluorescence intensity of the zirconium–morin complex can be enhanced by cetyltrimethylammonium bromide (CTAB) and a method for the fluorimetric determination of zirconium with high sensitivity and excellent selectivity has been reported [14]. In order to study the mechanism of this enhancement, in this work a parallel study on the effect of CTAB on the absorption and fluorescence phenomena of the zirconium–morin complex was carried out. The fluorescence quenching by monomers of the surfactant and the influence of CTAB on the dissociation of morin were also studied.

EXPERIMENTAL

Apparatus

Fluorescence measurements were made on a Hitachi M-850 spectrofluorimeter with a 1-cm quartz cell. Both excitation and emission slits were set at 5 nm. A Shimadzu UV-2100s spectrophotometer with 1-cm matching quartz cells was employed for absorbance measurements. Surface tension measurements were made with a JzhY1-180 platinum ring tensiometer.

Reagents

Analytical-reagent grade chemicals and deionized water were used throughout. A 1.00 mg ml^{-1} zirconium stock standard solution was prepared by dissolving 0.8853 g of $ZrOCl_2 \cdot 8H_2O$ (Union Chimique) in 250.0 ml of 2 mol l^{-1} HCl. A 1.00 μg ml^{-1} working standard solution was prepared by appropriate dilution of the stock standard solution.

Cetyltrimethylammonium bromide was obtained from Merck and a 5×10^{-2} mol l^{-1} aqueous solution was prepared. Morin was obtained from Merck. A CTAB–morin mixed solution containing 8×10^{-4} mol l^{-1} morin and 5×10^{-2} mol l^{-1} CTAB was prepared; 2×10^{-3} mol l^{-1} morin–ethanol (1 + 1) solution without surfactant was prepared by dissolving morin in 125 ml of ethanol in a 250-ml volumetric flask and diluting to volume with deionized water.

Procedure

To a series of 10-ml spectrophotometric tubes containing a certain amount of standard zirconium solution, 0.4 ml of morin–ethanol (1 + 1) solution (or 1 ml of morin–CTAB mixed aqueous solution), 3.5 ml of 5×10^{-2} mol l^{-1} CTAB solution (2.5 ml of CTAB if morin–CTAB solution was employed) and 0.6 ml of 2 mol l^{-1} H_2SO_4 were added, then the contents were diluted to the mark with water and mixed thoroughly, heated for 5 min in a boiling water-bath and cooled to room temperature with tap water before measurement. With excitation at 424 nm, the fluorescence intensity at 508 nm was measured or the fluorescence spectra were scanned. All fluorescence spectra were uncorrected.

The above are the optimum conditions for the fluorimetric determination of zirconium [14]. Because of the lower sensitivity, absorbance measurements were made with higher zirconium concentrations, as indicated later.

pK_a values of morin in micelle media were obtained by a spectrophotometric approach [15].

RESULTS AND DISCUSSION

Effects of surfactants on the fluorescence intensity of the zirconium–morin complex and on the pK_a of morin

The effects of various surfactants were studied. It was found that another kind of cationic surfactant, cetylpyridinium bromide (CPB), also increases the fluorescence of the Zr(IV)–morin

TABLE 1

Effect of surfactants on the fluorescence of the Zr(IV)–morin complex [a]

Surfactant	Fluorescence intensity	Surfactant	Fluorescence intensity
None	7	Triton X-100	15
CTAB	218	SDS	4
CPB	48	SLS	6

[a] [Zr] = 1 μg in 10 ml; [morin] = 0.8×10^{-4} mol l^{-1}; [H_2SO_4] = 0.24 mol l^{-1}; concentration of each surfactant = 1.75×10^{-2} mol l^{-1}.

complex under the optimum conditions, but much less than CTAB (Table 1). The non-ionic surfactant Triton X-100 only enhanced the fluorescence slightly and the anionic surfactants sodium dodecyl sulphate (SDS) and sodium dodecyl sulphonate (SLS) had no obvious effect.

The dissociation constants of morin in the presence of CTAB and SDS and those in the absence of surfactant are given in Table 2. The pK_{a_1} value of morin decreased from 4.8 to 3.5 in CTAB media; however, it increased to 5.2 in the presence of SDS micelles. These results agree with "electrostatic potential models" [16].

Dependence of absorbance and fluorescence of the zirconium–morin complex on CTAB concentration

Figure 1 shows the fluorescence spectra of the complex under various conditions. The influence of CTAB concentration on the absorbance, fluorescence intensity and surface tension are shown in Fig. 2.

In absence of surfactants, the fluorescence intensity is very low (Fig. 1, curve 1) and unstable. At low CTAB concentrations, the surface tension

TABLE 2

Dissociation constants of morin

Medium	pK_{a_1}	pK_{a_2}	pK_{a_3}	pK_{a_4}
Aqueous solution (10% ethanol) [9]	4.8	7.0	9.0	13.0
CTAB solution (1.5×10^{-2} mol l^{-1})	3.5	4.7	9.6	13.0
SDS solution (1.5×10^{-2} mol l^{-1})	5.2	7.4	9.7	13.4

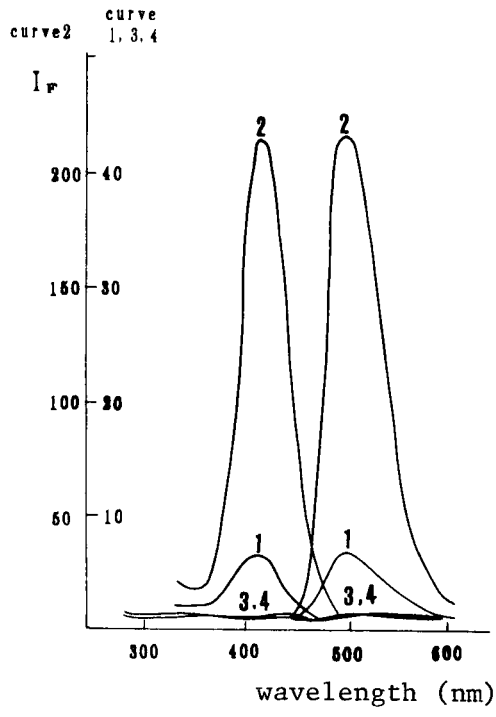

Fig. 1. Fluorescence spectra of the Zr(IV)–morin complex [Zr(IV)] = 1.00 μg in 10 ml; [morin] = 0.8×10^{-4} mol l^{-1}. 1 = Zr(IV)–morin–H_2SO_4 (0.25 mol l^{-1}); 2 = Zr(IV)–morin–CTAB (1.75×10^{-2} mol l^{-1})–H_2SO_4 (0.12 mol l^{-1}); 3 = Zr(IV)–morin–HCl (0.5 mol l^{-1}); 4 = Zr(IV)–morin–CTAB (1.75×10^{-2} mol l^{-1})–HCl (0.25 mol l^{-1}).

of the solution changes only slightly and CTAB exists mainly as monomers. In this instance, the decrease in fluorescence intensity is much more rapid than that in the absence of CTAB (Fig. 3), but the absorbance is increased slightly. On standing, the solution becomes turbid and a yellow precipitate settles out gradually. The decrease in the fluorescence intensity in the absence of CTAB is caused by polymerization of the complex owing to hydrophobic interactions. The long hydrophobic alkyl chain in the CTAB molecule interacts with the hydrophobic part of the complex and, as a result, the polymerization is accelerated. In addition, the cationic head of CTAB quenches the fluorescence [17]. The fluorescence intensity decreases nearly to zero at 4×10^{-6} mol l^{-1} CTAB.

The critical micelle concentration (CMC) of CTAB under the measurement conditions is 2 ×

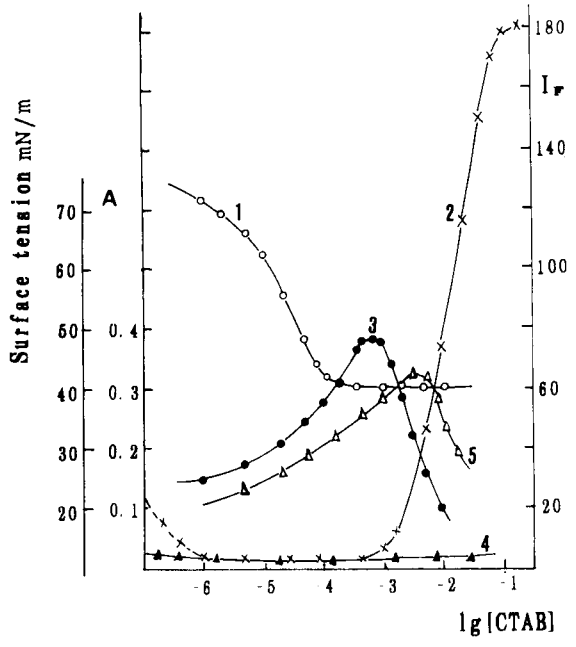

Fig. 2. Dependence of absorbance (A), fluorescence intensity (I_F) and surface tension of solutions of the Zr(IV)–morin complex on CTAB concentration. [Zr(IV)] = 1.00 μg in 10 ml; [morin] = 0.8×10^{-4} mol l^{-1}. 1 = Surface tension curve; 2 = I_F vs. log[CTAB] ([H_2SO_4] = 0.12 mol l^{-1}); 3 = A vs. log[CTAB] ([Zr] = 10 μg in 10 ml; [morin] = 1×10^{-4} mol l^{-1}; λ = 420 nm; [H_2SO_4] = 0.12 mol l^{-1}; reference = reagent blank); 4 = I_F vs. log[CTAB] ([HCl] = 0.24 mol l^{-1}); 5 = A vs. log[CTAB] ([Zr] = 10 μg in 10 ml; [morin] = 1×10^{-4} mol l^{-1}; λ = 420 nm; [HCl] = 0.24 mol l^{-1}; reference = reagent blank).

10^{-4} mol l^{-1} (Fig. 2, curve 1). When CTAB is dissolved in water at concentrations above the CMC, the cationic surfactant exists mainly as micelles. Because real micelle solubilization occurs, the solution becomes transparent and stable, and at the same time the absorbance increases to a maximum at 5×10^{-4} mol l^{-1} CTAB (Fig. 2, curve 3). On continuously increasing the CTAB concentration to 1×10^{-3} mol l^{-1}, the absorbance of the system remains constant, but the fluorescence intensity is still nearly zero.

When the CTAB concentration is higher than 1.0×10^{-3} mol l^{-1}, the absorbance diminishes with further increase in CTAB. The changes in absorbance with the surfactant concentration are in agreement with the "double-range-action" model [4]. However, the fluorescence intensity initially increases sharply at 1.0×10^{-3} mol l^{-1} CTAB (Fig. 2, curve 2), reaches a maximum at 1.7×10^{-2} mol l^{-1} CTAB and then remains constant. A strongly enhanced fluorimetric determination system is obtained (Fig. 1, curve 2).

Changes of composition of the zirconium–morin complex with CTAB concentration

The metal-to-dye ratio in the complex under various conditions was determined by Job's method with measurement of the absorbance of an isomolar series of solutions (Fig. 4). The stoichiometric ratio [Zr(IV) : morin] changes from 1 : 1 in the absence of CATB to 1 : 3 in the presence of CTAB at 5×10^{-4} mol l^{-1}, the concentration at which the absorbance reaches its maximum. However, at higher CTAB concentrations, up to 1.7×10^{-2} mol l^{-1}, the metal–dye stoichiometry changes to 1 : 1 again, although the fluorescence is strongly enhanced. The above changes were determined in 0.12 mol l^{-1} H_2SO_4. In HCl of the same acidity there was no obvious fluorescence at any CTAB concentration whereas the changes in absorbance were similar to those in H_2SO_4 (Fig. 2, curve 5). Sulphate ions must play an important role in the enhancement of the fluorescence. If the acidity is kept at 0.24 mol l^{-1} HCl and the concentration of SO_4^{2-} is adjusted by addition of sodium sulphate solution, the effect of SO_4^{2-} can

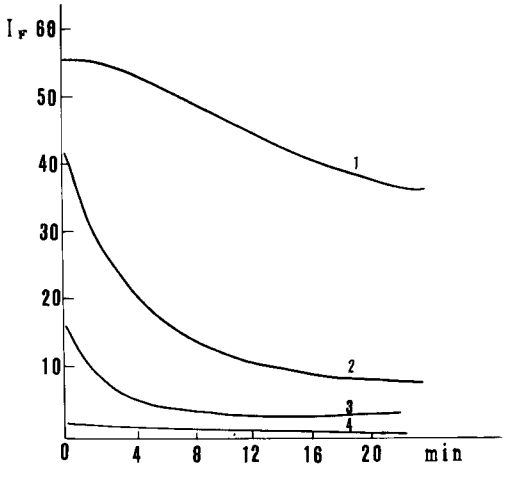

Fig. 3. Fluorescence decay of Zr(IV)–morin complex accelerated by CTAB monomer. [Zr(IV)] = 1.00 μg in 10 ml; [morin] = 0.8×10^{-4} mol l^{-1}; [H_2SO_4] = 0.2 mol l^{-1}. [CTAB]: 1 = 0; 2 = 1×10^{-6}; 3 = 2×10^{-6}; 4 = 4×10^{-6} mol l^{-1}.

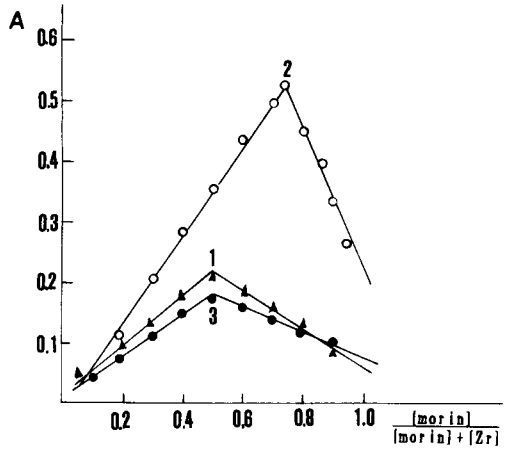

Fig. 4. Determination of Zr:morin ratio by Job's method with measurement of absorbance. [Zr]+[morin] = 5×10^{-5} mol l^{-1}; [H_2SO_4] = 0.12 mol l^{-1}; λ = 423 nm. [CTAB]: 1 = 0; 2 = 5×10^{-4}; 3 = 1.75×10^{-2} mol l^{-1}.

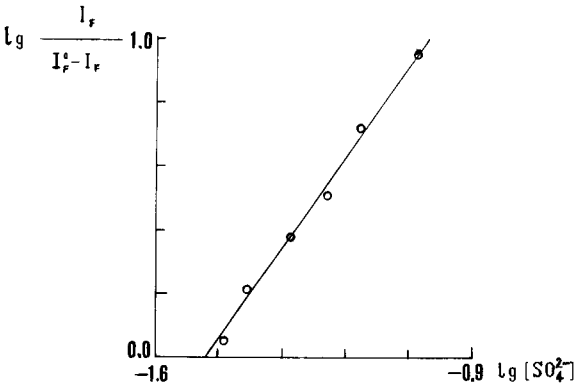

Fig. 6. Determination of Zr:SO_4^{2-} ratio by the equilibrium shift method with determination of fluorescence intensity. [Zr(IV)] = 1.00 μg in 10 ml; [CTAB] = 1.75×10^{-2} mol l^{-1}; [morin] = 0.8×10^{-4} mol l^{-1}; [HCl] = 0.24 mol l^{-1}; λ(ex) = 424 nm; λ(em) = 508 nm.

clearly be seen (Fig. 5). This indicates that alternative analyte species are formed under such experimental conditions, and SO_4^{2-} is one of the participants as an auxiliary ligand. The component ratio of zirconium and SO_4^{2-} was determined by a method based on the shift of the equilibrium by measurement of the fluorescence intensity of a series of solutions containing various amounts of SO_4^{2-}. The graph of $\log[I_F/(I_F^0 - I_F)]$ versus $\log[SO_4^{2-}]$, where I_F is the fluorescence intensity in the presence of a certain amount of SO_4^{2-} and I_F^0 is the maximum of I_F, is a straight line with a slope of 2 (Fig. 6). Hence it can be inferred that a mixed-ligand complex with the composition Zr(IV):morin:SO_4^{2-} = 1:1:2 is formed at high CTAB concentrations.

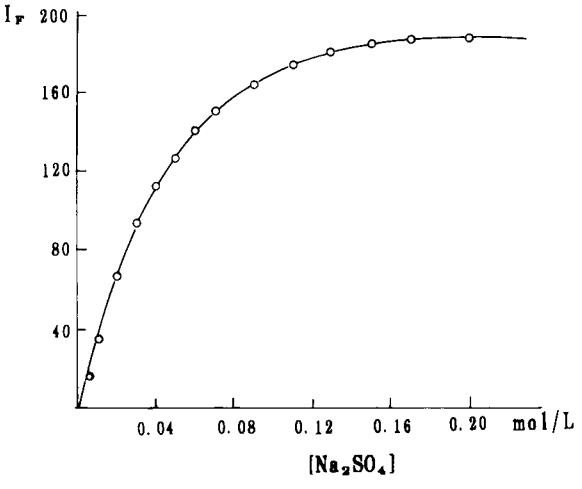

Fig. 5. Dependence of fluorescence intensity on sulphate ion concentration. [Zr(IV)] = 1.00 μg in 10 ml; [CTAB] = 1.75×10^{-2} mol l^{-1}; [morin] = 0.8×10^{-4} mol l^{-1}; [HCl] = 0.24 mol l^{-1}; λ(ex) = 424 nm; λ(em) = 508 nm.

Role of cationic micelle in changes in composition and enhancement of fluorescence

Zirconium can be precipitated from a sulphuric acid solution as a brick-red morin complex. The absence of characteristic absorption peaks of sulphate ion [18] in the IR spectrum of the dried precipitate indicates that sulphate ion does not participate in the complexation without the addition of CTAB. A stable higher order complex or mixed-ligand complex is formed at appropriate CTAB concentrations. This is due to the characteristics of the micelle.

Hydrophobic interactions between the solubilized complex and the micelle would be operative even in the interface [6,19]. The water and/or hydroxide ligands will be eliminated from the chelate. As a result, the coordination number is not saturated and other ligands, such as morin or SO_4^{2-}, could coordinate with zirconium more easily.

The positive charges on the cationic micelle surface neutralize the negative charges of the higher order complex or mixed-ligand complex, and favour the formation of these species. In turn, the negative charge of the mixed-ligand complex containing SO_4^{2-} facilitates a closer approach to the positively charged micellar surface with electrostatic interactions. Hence the exited singlet state would be protected more efficiently by the microenvironment of the micelle.

CPB acts in the same way as CTAB, but the pyridinium head of CPB facilitates the non-radiative relaxation of the excited singlet state and, as a result, the quantum yield is decreased [13]. Anionic surfactants, such as SDS and SLS, have also been applied to enhance spectrophotometric [19] and fluorimetric [20] determinations. Electrostatic and hydrophobic interactions between the anionic micelles and solubilized substrate are also operative. Hydrophobic interactions have an effect similar to that of cationic micelles, favouring the formation of higher order or mixed-ligand complexes, but the electrostatic interaction is unfavourable for the formation of the negative complexes. Whether these species form or not depends on the relative strength of the two interactions. For example, both the absorbance and fluorescence of the scandium–morin complex can be strongly enhanced by SDS at suitable concentrations, without any change in the composition of the chelate [20]. The enhancement mechanisms of the two kinds of surfactants are different.

Because the stability constant of the Zr(IV)–morin complex is higher than that of Zr(IV)–SO_4^{2-}, the absorbance is enhanced about threefold (Fig. 2, curve 3) with the formation of a 1:3 [Zr(IV):morin] complex at a CTAB concentration just above its CMC. However, the higher order complex shows no fluorescence; this is similar to fluorescence quenching by the association of dye molecules. The decrease in the pK_{a_1} value of morin also favours the formation of the higher order complex. At higher CTAB concentrations (1.0×10^{-3} mol l^{-1}), owing to "the compartmentalization effect" of the micelles [8], the solubilization of morin in an excess of micelles destroys the 1:3 complex, and the absorbance is diminished. It is at this CTAB concentration that the

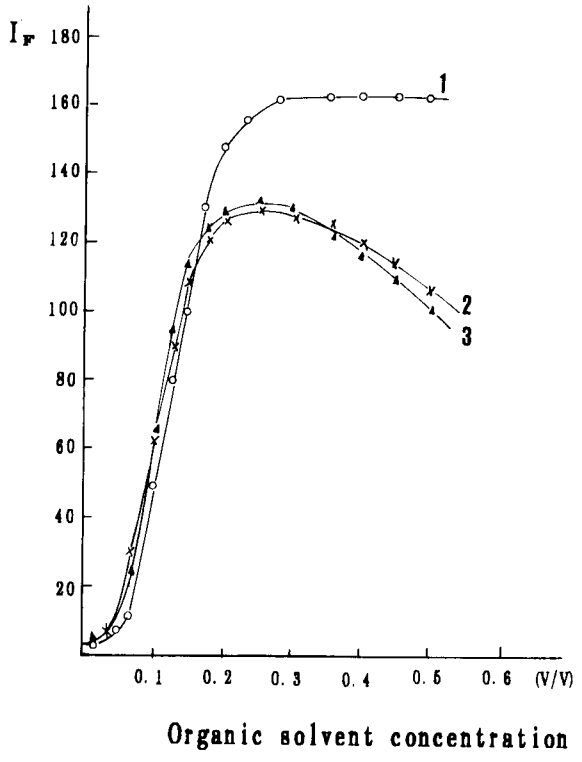

Fig. 7. Effect of organic solvent on the fluorescence of the Zr(IV)–morin complex. [Zr(IV)] = 1.00 μg in 10 ml; [morin] = 1×10^{-4} mol l^{-1}; [H_2SO_4] = 0.12 mol l^{-1}. 1 = Ethanol; 2 = dioxane; 3 = acetone.

Zr(IV)–morin–SO_4^{2-} mixed-ligand complex begins to form and the fluorescence intensity increases sharply. In other words, a higher CTAB concentration facilitates the formation of the mixed-ligand complex and enhancement of the fluorescence. In addition, the high-order structure of a micelle favours the formation of the mixed-ligand complex [5].

Once the Zr(IV)–morin complex is solubilized into a CTAB micelle, the microenvironment of the fluorescent particle is altered. The special microenvironment is similar to a mixed water–organic solvent, which often serves as a reference for exploring the nature of micelles [7,21]. Enhancement of the fluorescence of the zirconium–morin complex similar to that in cationic micelles was also observed in several two-component solvents in the presence of sulphuric acid (Fig. 7), but there was no obvious enhancement in hydro-

chloric acid of the same acidity. The formation of the zirconium–morin–SO_4^{2-} mixed-ligand complex and the enhancement of the fluorescence in those instances is due to a different environment compared with the bulk solution and some microscopic "ordering" and "rigidity" similar to that in a micelle [5,6] caused by the formation of hydrogen bonds.

Effect of other auxiliary ligands

Many significant analytical reactions are based on the formation of complexes with more than one ligand [22], i.e., mixed-ligand or ternary complexes. A lot of work has been done on fluorimetric determinations with extraction of the analyte species into a non-aqueous phase [23]. However, there are few reports concerning the formation of mixed-ligand complexes in the presence of micelles, which would lead to convenient determination methods without extraction. Sanz-Medel and Fernandez Perez [6] reported on the influence of auxiliary ligands on the niobium–lumogallion complex in the presence of non-ionic surfactants and a method for the fluorimetric determination of Nb(V) based on this reaction.

In addition to the sulphate ion, it was found that mixed-ligand complexes with special fluorescence characteristics can be formed with some other anions commonly used as complex agents of zirconium. Oxalate, tartrate, fluoride and chloride ions were tested. Of these, oxalate and fluoride act in the same way as the sulphate ion. The results are given in Table 3.

The formation of a mixed-ligand complex depends on several factors [23], such as the nature of the metal ions, electrostatic interactions, interactions between ligands, spatial effects and statistical factors. Competition between ligands is one of the most important factors. The complexation ability of each ligand can been evaluated on the basis of $\beta_{ML_i}[L]^i$, where β is the cumulative stability constant, L refers to ligands and i is the coordination number.

As can be seen in Table 3, the smaller the stability constant, the higher is the ligand concentration that is required. However, the stability constants would be changed when the ternary complex is formed, especially in the presence of surfactants. If the constants were determined under the measurement conditions, a qualitative result would be obtained.

Conclusions

This study clearly demonstrates that the composition of the complex changes with the concentration of CTAB. With the formation of different complexes i.e., Zr(IV)–morin (1:3) higher order complex and Zr(IV)–morin–SO_4^{2-} (1 : 1 : 2) mixed-ligand complex, both absorbance and fluorescence are enhanced. Electrostatic and hydrophobic interactions facilitate the changes in composition concurrently. Once the negatively charged complex is formed, the electrostatic interactions facilitate a closer approach of this complex to the positive micelles, and hydrophobic interactions do so also. Hence, the microenviron-

TABLE 3

Formation of mixed-ligand complexes and fluorescence characteristics in the presence of CTAB [a]

Auxiliary ligand	Maximum I_F	Emission wavelength (nm)	Optimum concentration (mol l^{-1})	Coordination constant [b]	Coordination ratio [c]
SO_4^{2-}	190	508	0.14	3.97, 6.64, 7.77	2
F^-	140	494	0.02	8.80, 16.12, 21.94	4
$(Oxalate)^{2-}$	150	513	1.4×10^{-5} mol l^{-1}	9.80, 17.14, 20.86, 21.15	2
$(Tartrate)^{2-}$	– [d]	–	–	– [e]	–
Cl^-	– [d]	–	–	– [e]	–

[a] [Zr] = 1 μg in 10 ml; [morin] = 0.8×10^{-4} mol l^{-1}, [HCl] = 0.24 mol l^{-1}, [CTAB] = 1.75×10^{-2} mol l^{-1}. [b] The values shown are cumulative stability constants in aqueous solution [24]. [c] The value was determined by the equilibrium shift method. [d] No fluorescence detected. [e] No value available.

ment experienced by the fluorescent probe changes, and such changes favour the fluorescence emission.

A similar enhancement was observed in mixed water–organic media. Because organic molecules, such as ethanol, acetone and dioxane, do not form micelles in aqueous solution, it could be inferred that the fluorescent complex should be located close to the micelle–bulk solution interface, rather than the hydrophobic core of the micelles [5]. Similar phenomena were reported by Sanz-Medel and Fernandez Perez [6] when they studied the effect of CTAB on the fluorescence of niobium and tantalum complexes with morin.

It was found that the mixed-ligand complexes of zirconium are formed with several anions in the presence of cationic surfactants and the fluorescence of the system is strongly enhanced. It is desirable to study such analytical reactions further in order to develop useful luminescence assays. In particular, the selectivity would be promoted by selecting favourable auxiliary ligands.

This project was supported by the Chinese National Sciences Foundation, Grant No. 29070237. The authors thank Miss B. Shi and Mr. M. Ju for assistance with the manuscript.

REFERENCES

1 G.L. McIntire, Crit. Rev. Anal. Chem., 21 (1990) 257.
2 X.W. He, W.L. Yang and H.M. Shi, Fenxi Shiyanshi, 6, No. 5 (1987) 1; G.Z. Zhang, W.L. Yang and H.M. Shi, Fenxi Shiyanshi, 8, No. 4 (1989) 86.
3 Y.X. Zheng, Fenxi Shiyanshi, 10, No. 4 (1991) 1.
4 Y.X. Zheng, Discussion of the Mechanism of Reaction in Micelle Solubilized Spectrophotometry, Geological Publishing House, Beijing, 1980; Y.X. Zheng, Yan Kuang Ceshi, 5 (1986) 169; 5 (1986) 253; 6 (1987) 1.
5 A. Sanz-Medel, J.I. Garcia Alonso and E.B. Gonzalez, Anal. Chem., 57 (1985) 1681.
6 A. Sanz-Medel and M.M. Fernandez Perez. Anal. Chem., 58 (1986) 2161.
7 Y.X. Zheng, Huaxue Tongbao, No. 5 (1991) 1.
8 Y.X. Zheng and L.D. Li, Fenxi Huaxue, 17 (1989) 760; 18 (1990) 292.
9 K.L. Cheng, K. Ueno and T. Imamura, CRC Handbook of Organic Analytical Reagents, CRC Press, Boca Raton, FL, 1982, p. 107.
10 J.M. Escriche, M. de la Guardia Cirugeda and F.H. Hernandez, Analyst, 108 (1983) 1386.
11 F.H. Hernandez, J.M. Escriche and M.T. Gasco Andreu, Talanta, 33 (1986) 537.
12 J. Medina, F.H. Hernandez, R. Marin and F.J. Lopez, Analyst, 111 (1986) 235.
13 H.M. Shi, W.C. Chun and R.J. Wang, Huaxue Xuebao, 41 (1983) 1029.
14 Y.X. Zheng and Y.X. Fan, in Proceedings of International Symposium of Overseas Chinese Scholars on Analytical Chemistry, B-12, October 20–24, 1992, Wuhan, China.
15 K.L. Cheng, in J.D. Winefordner (Ed.), Spectrochemical Methods of Analysis, Wiley, New York, 1971, p. 349.
16 E. Plizzati and E. Pramauro, Anal. Chim. Acta, 169 (1985) 1.
17 Y.B. Yang, J.G. Xu and G.Z. Chen, Sci. Sin. (Ser. B), (1991) 1028.
18 K. Makatmoto, Infrared and Rammam Spectra of Inorganic and Coordination Compounds, Wiley, New York, 4th edn., 1986, p. 260.
19 Y.X. Zheng and D.P. Chen, Huaxue Xuebao, 43 (1985) 868.
20 Y.X. Zheng and Y.X. Fan, Fenxi Shiyanshi, 12 (2) (1993) 8.
21 Y.X. Zheng and D.H. Lu, Mikrochim. Acta, 106 (1992) 3.
22 Y.X. Ci and T.Z. Zhou, Coordination Compounds in Analytical Chemistry, Beijing University Press, Beijing, 1986.
23 P.R. Haddad, Talanta, 24 (1977) 1.
24 Department of Chemistry, Hangzhou University, Handbook of Analytical Chemistry, Part I, Chemical Industry Press, Beijing, 1979, pp. 66–74.

Analytica Chimica Acta, 281 (1993) 361–372
Elsevier Science Publishers B.V., Amsterdam

Separation and preconcentration of actinides from acidic media by extraction chromatography

E. Philip Horwitz, Renato Chiarizia [1], Mark L. Dietz and Herbert Diamond

Argonne National Laboratory, Chemistry Division, Argonne, IL 60439 (USA)

Donald M. Nelson

Argonne National Laboratory, Environment, Safety, and Health Department, Argonne, IL 60439 (USA)

(Received 1st October 1992)

Abstract

A systematic examination of the effect of nitric and hydrochloric acid concentrations and of macro levels of selected elements on the sorption of actinide ions by a novel extraction chromatographic resin comprised of a solution of octyl(phenyl)-*N*,*N*-diisobutylcarbamoylmethylphosphine oxide in tri-*n*-butyl phosphate supported on an inert polymeric substrate is described. Actinide sorption is demonstrated to be most efficient at high (> 1 M) nitric acid concentrations, although tetra- and hexavalent actinides are strongly retained even from dilute (e.g., 0.05 M) nitric acid solutions. Macro concentrations of several common anions (e.g., PO_4^{3-} and SO_4^{2-}) or complexing agents (e.g., oxalic acid) are shown not to adversely affect the sorption of trivalent actinides, while reducing the sorption of tetravalents. Such effects, together with oxidation state adjustments, are shown to provide a basis for the sequential elution of individual actinides and for actinide isolation from environmental and biological matrices.

Keywords: Chromatography; Actinides; Extraction; Preconcentration

Increased public attention to radioactive waste disposal practices and the potential public health effects of releases of radioactive materials to the environment has made accurate and reliable methods for the determination of actinides in various environmental and biological samples increasingly important. Because of the low concentrations of these elements encountered in typical samples, some method of preconcentrating the actinides and of isolating them from both the large quantities of inactive substances present and potential interferents must usually precede the determination. Numerous methods have been described for effecting this separation and preconcentration, among them procedures based on ion exchange [1–3], liquid–liquid extraction [4], precipitation [5], adsorption [6], extraction chromatography [7], and combinations thereof [8].

In an earlier report in this journal [9], we described an extraction chromatographic resin comprised of a solution of a bifunctional organophosphorus extractant, octyl(phenyl)-*N*,*N*-diisobutylcarbamoylmethylphosphine oxide (abbreviated CMPO), in tri-*n*-butyl phosphate (TBP) supported on an inert, polymeric substrate (Amberlite XAD-7) and its application to the separation and preconcentration of actinides from urine. Although use of this material offered definite advantages over other techniques, yielding excel-

Correspondence to: E.P. Horwitz, Argonne National Laboratory, Chemistry Division, Argonne, IL 60439 (USA).

[1] On leave from ENEA, the Italian Agency for Nuclear and Alternative Energy, Rome, Italy.

lent actinide recoveries and permitting the preparation of essentially massless electrodeposits for high resolution alpha-spectrometry, the resin did suffer from a significant limitation. That is, the width of the elution bands observed and the occurrence of significant tailing precluded the sequential elution of individual actinides from the resin.

Recently, resins chemically indistinguishable from Amberlite XAD-7 but with smaller average particle diameters have become available. Because it is well known that a reduction in the particle size of a chromatographic material will lead to narrower elution bands [10,11], we have examined the chromatographic properties of a CMPO/TBP mixture sorbed on one of these small particle size supports. In this report, we present a systematic evaluation of the uptake of various actinide ions by the material from nitric and hydrochloric acid solutions and of the effect of various aqueous complexants and potential interferents on this uptake. In addition, we describe the elution behavior of a wide range of other cations, particularly those commonly encountered in biological or environmental matrices. Finally, we discuss the potential application of the results obtained to the separation and preconcentration of actinides, both as a group and individually, from soil, groundwater, bioassay samples, and radioactive waste samples.

EXPERIMENTAL

Reagents

Octyl(phenyl)-*N*,*N*-diisobutylcarbamoylmethylphosphine oxide (Atochem North America, Philadelphia, PA) was purified as previously described [12]. Tri-*n*-butyl phosphate was obtained from Eastman Chemicals and distilled (T = 143°C; pressure = 20 mm) before use. Nitric and hydrochloric acid solutions were prepared from the Ultrex reagents (Baker). All water was obtained from a Milli-Q2 water purification system. All other materials were ACS reagent grade and were used as received. Hydroquinone–hydrochloric acid solutions were prepared daily. Ascorbic acid solutions were prepared weekly. Radiochemical experiments were performed using ^{230}Th, ^{233}U, ^{237}Np, ^{239}Np·^{239}Pu, ^{241}Am, ^{45}Ca, ^{210}Bi, ^{210}Po, ^{59}Fe, and ^{85}Sr tracers. The ^{239}Np was "milked" from ^{243}Am in 9 M HCl using a BioRad™ AG-MP1 anion exchange column.

Procedures

Preparation of extraction chromatographic resin. The extraction chromatographic resin was prepared by impregnating Amberchrom CG-71ms with a 0.75 M solution of CMPO in TBP in the manner described previously for Amberlite XAD-7 [9]. Unlike XAD-7, however, the Amberchrom resin does not require water washing to remove preservatives prior to impregnation. This extraction chromatographic material, referred to hereafter as TRU · Spec™ (for *tr*ans*u*ranic *spec*ific), is now commercially available from EIChroM Industries (Darien, IL).

Determination of weight distribution ratios and column capacity factors. The sorption of actinide ions by the TRU · Spec resin from nitric and hydrochloric acid solutions was measured by contacting a known volume of a tracer-spiked acid solution of appropriate concentration with a known weight of resin [13]. Weight distribution ratios were converted to the number of free column volumes to peak maximum (i.e., the resin capacity factor), k', by dividing by 1.85. This factor takes into account the density of the extractant solution and the typical value of v_s/v_m (the ratio of the volumes of the stationary and mobile phase) for a column containing TRU · Spec. Details may be found in a previous report [13].

To ensure that any Np(V) present was reduced to Np(IV), neptunium load solutions were made ~ 0.01 M in Fe(II) and 0.11 M in hydroxylammonium nitrate. The ferrous nitrate stock solution (0.2 M) was prepared using ferric nitrate and a large excess of hydroxylammonium nitrate (2.2 M). Plutonium was maintained in the tetravalent oxidation state by making all acid solutions 0.05 M in sodium nitrite.

Column preparation and characterization. Columns were packed as previously described [14]. All column parameters (e.g., v_s, v_m, bed density) were measured as described in Ref. 13.

The resin capacity was determined as described earlier [13] except that a solution of 0.05 M neodymium nitrate in 2 M nitric acid was employed for all measurements.

Elution profiles for americium. The elution profile of americium with 2 M nitric acid as the eluent was measured with the same calibrated column employed for v_m and v_s measurements using procedures described previously [13].

Elution behavior of selected elements / matrix effects. The elution behavior of approximately thirty metal cations on a TRU · Spec column (bed volume = 1.0 ml; bed height = 5.0 cm) was evaluated using procedures described in a previous report [13]. 2 M nitric acid was employed for column rinsing and 0.05 M nitric acid for column stripping.

The effect of macro concentrations of various commonly encountered cations (e.g., Ca^{2+}, Fe^{3+}) and anions (e.g., SO_4^{2-}) or aqueous complexing agents (e.g., oxalic acid) upon americium and neptunium uptake by the resin was evaluated by measuring the sorption of ^{241}Am and ^{239}Np from 2 M nitric acid containing various concentrations of the test species.

The influence of Fe(II) on americium uptake was examined by reducing Fe(III) in 2 M nitric acid with a freshly prepared 0.8 M solution of ascorbic acid. [Upon addition of ascorbic acid to a solution of Fe(III), a blue color forms which disappears on mixing. When the blue color no longer forms, all Fe(III) has been reduced to Fe(II). Potassium thiocyanate may also be used to indicate the presence of Fe(III). When a red color no longer remains after addition of ascorbic acid, all the Fe(III) has been reduced to Fe(II).]

Sequential separation of actinides. The sequential separation of actinides was studied using a 2.84 mm i.d. column packed to a bed height of 9.8 cm (0.62 cm^3 bed volume, 0.422 cm^3 free column volume). A tracer stock solution containing ^{241}Am, ^{239}Pu, ^{237}Np, ^{233}U, and ^{230}Th in 2 M HNO_3 was utilized for the load. The solution was made 0.01 M in Fe by addition of ferric nitrate. The iron was reduced by addition of ascorbic acid as described above. The flow rate was maintained between 0.5 and 1.0 ml/cm^2/min throughout the column run except for the elution of thorium, during which it was necessary to elute at one-half this flow-rate. Alpha pulse-height analysis was used to analyze the individual fractions. For ^{237}Np, the characteristic L x-ray addition peak was also used.

Resin stability. The resistance of the TRU · Spec resin to extractant loss induced by the flow of aqueous phase was evaluated by determining the effect of extensive column rinsing upon the elution profile of ^{241}Am. Specifically, a small (1 μl) aliquot of an ^{241}Am stock solution was introduced atop the bed of a newly prepared TRU · Spec column and eluted with 0.3 M nitric acid. The effluent was sampled at intervals and gamma-counted. The column was then washed with ca. 250 FCV of deionized water and, after preconditioning with 0.3 M nitric acid (10 FCV), an aliquot of ^{241}Am was again eluted in the same manner. This process was repeated at ca. 250 FCV intervals until a total of 1000 FCV of rinsing had been carried out. Changes in peak position (k') and width were taken as indicators of a change in the condition of the resin arising from loss of stationary phase or a change in stationary phase configuration. v_m, the mobile phase or interstitial volume, was determined for the column by measuring the volume of effluent preceding ^{137}Cs breakthrough, both prior to any rinsing and after 1000 FCV.

Apparatus

Gamma counting was performed in either a Beckman Biogamma counter or a Packard Cobra Autogamma counter. Alpha- and beta-counting were performed via liquid scintillation on a Packard Model 2000CA counter. In sequential elution experiments, proportional counting with argon-methane 2π counters and alpha pulse analyses using surface-barrier silicon detectors were also carried out.

RESULTS AND DISCUSSION

Column characteristics

As already noted, our principal objective in this work was to prepare an extraction chromatographic resin capable of retaining tri-, tetra-, and

hexavalent actinides, which exhibits minimal band spreading and tailing, thereby providing an opportunity for sequential separation of the actinides. In addition, good overall actinide recoveries and satisfactory decontamination from inert constitutents and potential interferents were deemed essential. For convenience, the ability to operate under gravity flow and room temperature was also desired. To meet these specifications, we selected the same substrate and particle size utilized for our strontium-specific and uranium/tetravalent actinide-specific extraction chromatographic resins, described in previous reports [14,15]. Table 1 summarizes the characteristics of the bulk material and packed beds.

Nitric acid dependency of capacity factor, k'

The TRU · Spec chromatographic material was characterized by measuring k' (the number of free column volumes to peak maximum) as a function of nitric acid concentration for tri-, tetra-, penta- and hexavalent actinides and for selected non-actinide ions. Figure 1 depicts the nitric acid dependency of the resin capacity factor, k', for the various actinide ions. As can be seen, the sorption of most of the ions rises steadily with increasing acid concentration, as anticipated from results in the analogous liquid–liquid system [16,17]. (It is important to point out that attempts to compare the relative extractabilities of the actinides in the chromatographic and liquid–liquid systems must take into account the different CMPO concentrations in the two systems and the relationship between k' and D, the distribu-

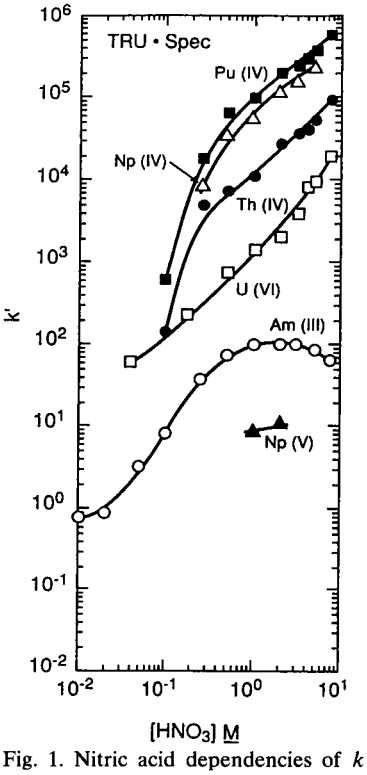

Fig. 1. Nitric acid dependencies of k' for selected actinide ions with TRU · Spec resin (T = 23–25°C; 50–100 μm particle size resin).

TABLE 1

Characteristics of the TRU · Spec extraction chromatographic material and packed columns

Bulk material	
Stationary phase	0.75 M CMPO in TBP (ρ = 0.971 g/ml)
Support	Amberchrom™ CG-71
Particle diameter	50–100 μm
Extractant loading	40%
Average density of extractant-loaded beads [a]	1.12 g/ml
Packed Columns	
v_s	0.152 ml/ml of bed
Bed density	0.370 g/ml
v_m (also FCV)	0.68 ml/ml of bed
v_s/v_m	0.223
Calculated capacity	5.49 mg Nd or 9.18 mg ^{241}Am/ml of bed
Experimentally measured capacity	4.1 mg Nd or 6.8 mg ^{241}Am/ml of bed

[a] Picnometric density and flotation density were 1.081 (in water) and 1.158 (in 4.9 M HNO_3) g/ml, respectively. The calculated density is 1.094 g/ml assuming 100% pore filling and no swelling.

tion ratio, $k' = Dv_s/v_m$.) It is interesting to note that the k' value for a given ion is typically 100–1000 times greater on TRU · Spec than on U/TEVA · Spec, a recently developed extraction chromatographic material containing the monofunctional extractant diamyl amylphosphonate [15]. This is significant because k'_{Am} on U/TEVA · Spec is too low to yield satisfactory retention. In contrast, TRU · Spec retains Am(III) (and other trivalent actinides) strongly over a wide range of nitric acid concentrations (0.5 to 8 M). Even Np(V) exhibits slight retention on TRU · Spec, although its k' (ca. 10) is not sufficiently high to be of any use in separating neptunium from common matrix constituents.

The extremely strong retention of U(VI), Np(IV), and Pu(IV), even at low acidities, means that the elution of these ions cannot be effected simply by lowering the aqueous nitric acid concentration. Rather, a different acid or a solution of an appropriate complexing agent (e.g., ammonium oxalate) must be employed. Americium can be eluted using only dilute (e.g., 0.025 M) nitric acid, but as is discussed in more detail below, its separation from plutonium is not complete.

Figure 2 shows the retention of selected non-actinides by TRU · Spec resin as a function of nitric acid concentration. The behavior of Fe(III) is of utmost importance because of its presence in significant concentrations in soil samples and its use as a coprecipitant for actinides. (The effect of Fe(III) on the sorption of Am(III) is discussed below in more detail below.) Calcium(II) is poorly retained at all acidities and therefore causes little interference with actinide sorption. Bismuth retention is important because of its occasional presence in fecal samples. The data in Fig. 2 show that Bi(III) retention is higher than that of Am(III) except at high (> 4 M) acidities. Polonium(IV) retention, although less than that of Am(III), is not negligible. This is important because ^{210}Po is present in urine and can interfere in alpha pulse-height analysis. Technetium is a constituent of high-level liquid waste (HLLW) and its separation from ^{241}Am is therefore important in the analysis of HLLW. Figure 2 shows that Tc(VII) retention is less than that of Am(III) at nitric acid concentrations greater than about 0.25 M. Therefore, its separation from americium can be effected simply by rinsing the TRU · Spec column with 1–10 M HNO_3.

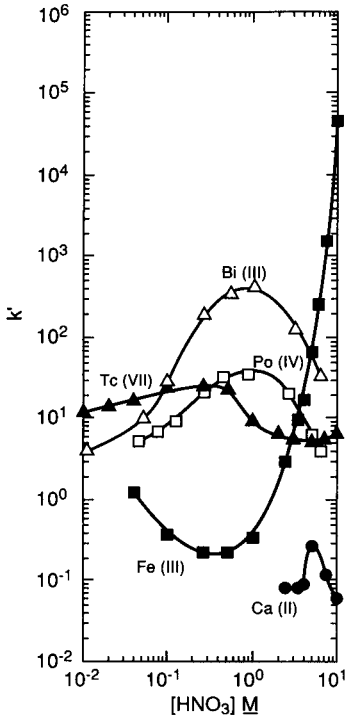

Fig. 2. Nitric acid dependencies of k' for selected non-actinide ions on TRU · Spec resin (T = 23–25°C; 50–100 μm particle size resin).

Elution behavior of Am and selected cations

Figure 3 shows the concentration profile for the elution of Am(III) from a TRU · Spec column

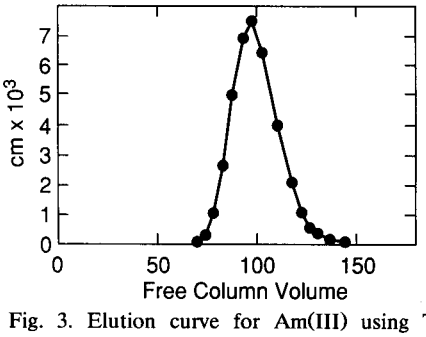

Fig. 3. Elution curve for Am(III) using TRU · Spec resin (eluent = 2.0 M HNO_3; T = 23°C; flow-rate = 1 to 2 ml/cm^2 min; 50–100 μm particle size resin; bed volume = 0.59 ml; bed length = 10.1 cm).

using 2 M HNO_3. The k'_{Am} obtained from the elution curve is 98, which is identical to that obtained in an uptake experiment. (See Fig. 1.) The height equivalent to a theoretical plate (HETP) is 0.11 cm, which is the same as that obtained in the elution of Sr(II) from a Sr · Spec column containing the same particle size substrate [13].

Table 2 shows the elution behavior of thirty different elements on a 1.0 cm^3 bed volume column packed with 50–100 μm TRU · Spec column material. (Essentially all of these elements are present in high-level radioactive waste solutions.) Two molar HNO_3 was used for column loading and for the first 30 free column volumes (FCV) of rinsing, while 0.05 M HNO_3 was used to strip sorbed Am(III) from the column (31–40 FCV). (A trivalent actinide was selected for this study because, as shown in Fig. 1, actinides in the tripositive oxidation state are generally the least strongly retained on TRU · Spec.) As can be seen, all constituents except zirconium and the lanthanides elute from the column in the first 10 FCV. The lower retention of La(III), Ce(III), and

TABLE 2

Elution behavior of selected elements on a TRU · Spec column [a]
(*Conditions*: T = 23°C, particle size = 50–100 μm diameter, 1 FCV = 0.60 ml)

Number of free column volumes							
Element	1–5 [b]	6–10 [b]	11–15 [b]	16–20 [b]	21–25 [b]	26–30 [b]	31–40 [c]
Li	98.4	< 19	–	–	–	–	–
Na	92.8	< 1.2	–	–	–	–	–
Mg	100	–	–	–	–	–	–
Al	99.8	< 2.9	–	–	–	–	–
K	81.8	40.9	–	–	–	–	–
Ca	100	–	–	–	–	–	–
Cr	100	–	–	–	–	–	–
Mn	100	–	–	–	–	–	–
Fe	102	< 12.3	–	–	–	–	–
Co	100	–	–	–	–	–	–
Ni	100	–	–	–	–	–	–
Cu	100	–	–	–	–	–	–
Zn	100	–	–	–	–	–	–
Sr	100	–	–	–	–	–	–
Y	23.4	76.8	3.5	–	–	–	–
Zr	–	–	–	–	–	–	75.0
Ru	82.6	< 19.2	–	–	–	–	–
Rh	100	–	–	–	–	–	–
Ag	100	–	–	–	–	–	–
Cd	100	–	–	–	–	–	–
Ba	100	–	–	–	–	–	–
La	–	–	–	–	–	30.0	72.0
Ce	–	–	–	–	–	< 25.0	75.0
Pr	–	–	–	–	–	–	100
Nd	–	–	–	–	–	–	96.0
Sm	–	–	–	–	–	–	100
Eu	–	–	–	–	–	–	> 99
Hg	(100)	(60)	(19)	–	–	–	–
Pb	100	–	–	–	–	–	–
Am [b]	–	–	–	–	–	–	> 99

[a] Because of uncertainties inherent in the ICP–AES method, the fractions shown for each element may not total 100%. Values in parentheses are subject to considerable uncertainty and are intended only as a rough guide. [b] 2 M HNO_3. [c] 0.05 M HNO_3. [d] radiometric.

Y(III) relative to Am(III) was anticipated based on comparison of light lanthanide and yttrium distribution ratios in liquid–liquid extraction systems involving solutions of CMPO-TBP [18]. (D_{Am}/D_Y, D_{Am}/D_{La} and D_{Am}/D_{Ce} are ~ 5, 2.5, and 1.5, respectively, with 0.25 M CMPO–0.75 M TBP in tetrachloroethylene [18]). The strong zirconium retention is also expected from prior liquid–liquid extraction studies [18], but it can be separated from actinides by making the feed solution 0.05 M in oxalic acid or by rinsing the column with 10 FCV of 2 M HNO_3–0.05 M oxalic acid.

Effect of matrix constituents

The nitric acid dependency data presented in Figs. 1 and 2 and the elution data in Table 2 are important not only because they show conditions that may be used to separate tri-, tetra-, and hexavalent actinides from various metal ions, but also because they indicate which elements may cause a significant diminution in actinide sorption if present at sufficiently high concentrations (i.e., those that represent more than 20% of the column capacity). Sodium, potassium, calcium, iron, and aluminum are major constituents of many environmental and geological samples (e.g., soils, minerals, and groundwaters). The effect of increasing concentrations of several of these matrix constituents on k'_{Am} was therefore measured. Figure 4 shows the effect of Ca(II), Al(III) and Fe(III) in 2 M HNO_3 on k'_{Am}. (The quantities of iron selected for the study were based on the application of $Fe(OH)_3$ to coprecipitate actinides from groundwater. Sodium and potassium were not included in the study because their retention on TRU · Spec is less than that of Ca.) The data show clearly that only Fe(III) has a significant negative impact on Am sorption, as expected from the acid dependency of its capacity factor (Fig. 2.). Al(III) actually enhances k'_{Am} through its salting-out effect. The effect of Fe(III) on k'_{Am}, even at low concentrations, is sufficiently pronounced that its presence must be considered in developing schemes involving TRU · Spec resin for the separation and preconcentration of actinides. Fortunately, when Fe(III) is reduced to Fe(II) with ascorbic acid, its effect on k'_{Am}, like

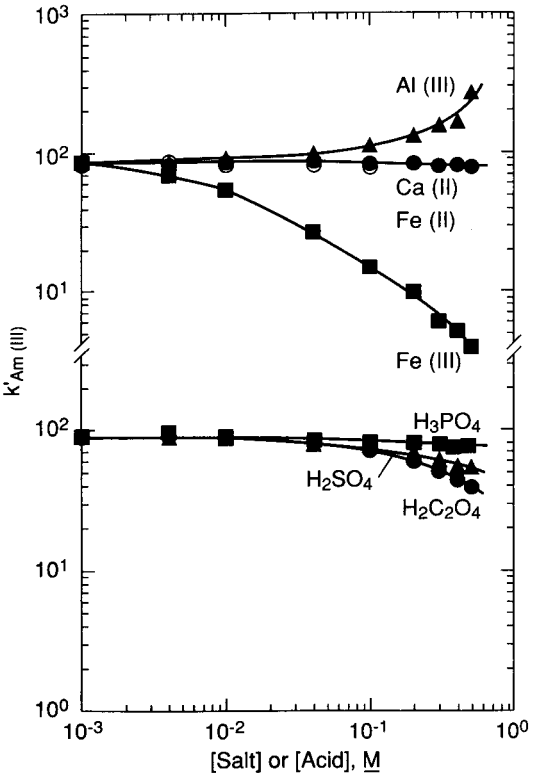

Fig. 4. Effect of matrix constituents and acidic complexing agents on Am retention. TRU · Spec resin/2 M HNO_3.

that of Ca(II), is practically negligible. The effect of Fe(III) and Fe(II) on the uptake of Am on TRU · Spec is also tabulated in Table 3.

The influence of phosphoric, sulfuric, and oxalic acids in 2 M HNO_3 on k'_{Am} is also shown in Fig. 4. None of the acids has a significant effect on k'_{Am} below 0.2 M. All three acids, as expected,

TABLE 3

Effect of Fe on Am uptake by TRU · Spec [a]

mg of Fe/10 ml	M of ascorbic acid	k'_{Am}
25	–	28
50	–	17
100	–	9.1
25	0.3	88
50	0.3	72
100	0.3	65

[a] Reference k'_{Am} at 2 M HNO_3 and 23°C = 98.

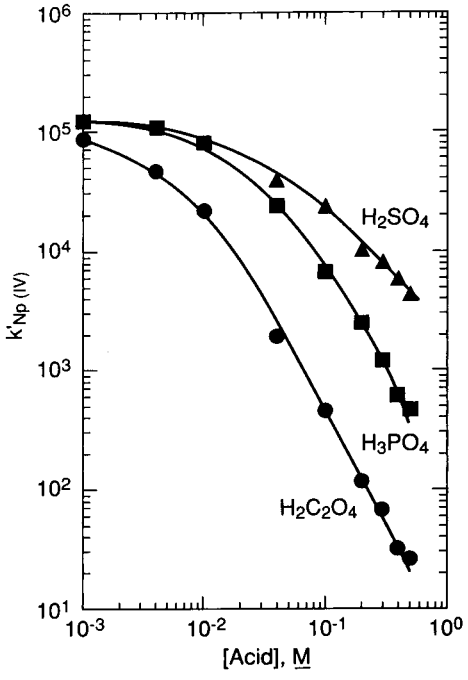

Fig. 5. Effect of acidic complexing agents on Np retention on TRU·Spec resin from 2 M HNO_3.

are much more influential on the sorption of tetravalent actinides, as represented by Np(IV) (Fig. 5). The influence of these acids (and presumably HF) on both Am(III) and Np(IV) sorption on TRU · Spec resin can be largely eliminated either by adding macroquantities of Al(III) or by increasing the nitric acid concentration to 4 M. Addition of aluminum ion effectively complexes the anions, reducing their concentrations, while raising the acidity effectively reduces the concentration of the complexing anion by protonation. Because k'_{Am} is only slightly influenced by nitric acid concentration above 0.5 M and because k'_{Np} is increased by high nitric acid concentrations, the latter approach is normally preferred. Note, however, that Fe(III) retention increases dramatically above 1 M HNO_3 (Fig. 2).

Sequential separations of actinides

Although the results presented in Figs. 1 and 2 and Tables 2 and 3 suggest that the separation of the actinides from a variety of matrices should be highly efficient, the sequential separation of individual actinides on the basis of the differences in their retention on TRU · Spec does not appear possible in nitric acid media, despite the improved chromatographic performance of the small particle size material. In fact, except for Am(III), none of the actinides can be readily eluted from a TRU · Spec column using only nitric acid. Moreover, when americium is eluted with dilute [(e.g., 0.025 M) nitric acid, 1 to 5% of the Pu is always found in the americium fraction. (Most likely, this is due to hydrolysis of Pu(IV).)]

Earlier studies on the liquid–liquid extraction of tri-, tetra-, and hexavalent actinides from chloride media [19] suggest that the situation may be improved through the use of hydrochloric acid as a stripping agent. In hydrochloric acid media, large separation factors between individual oxidation states can be achieved. In addition, the distribution ratios of tri- and tetravalent actinides are low in 1 to 2 M hydrochloric acid. Figure 6 shows the capacity factors, k', for tri-, tetra-, and hexavalent actinides as a function of hydrochloric acid concentration. Comparison of these results to those shown in Fig. 1 indicates that while the order of extractability of the various actinides from hydrochloric acid is essentially the same as that found in nitric acid, there are important differences between the two systems. Most notable is the extremely steep decline observed in k' for the tetravalent actinides as the hydrochloric acid concentration is lowered from 7–8 M. In the case of thorium(IV), for example, k' decreases from $> 10^4$ to ~ 1 as the hydrochloric acid concentration is reduced from ~ 8 M to 1 M. In nitric acid, however, a comparable reduction in acid concentration produces only a one order of magnitude drop in k'_{Th}, from 10^5 to 10^4. As a result, while it is not feasible to strip sorbed tetravalent actinides from a TRU · Spec column using dilute nitric acid, it is feasible with dilute hydrochloric acid. k'_U does not exhibit this same steep decline from its maximum at 4–5 M hydrochloric acid. In fact, k'_U exceeds 100 even at 0.7 M acid. Since k' values for neptunium, plutonium, and thorium are 10 or less at this acidity, the separation of uranium from tetravalents should pose little or no difficulty in an HCl

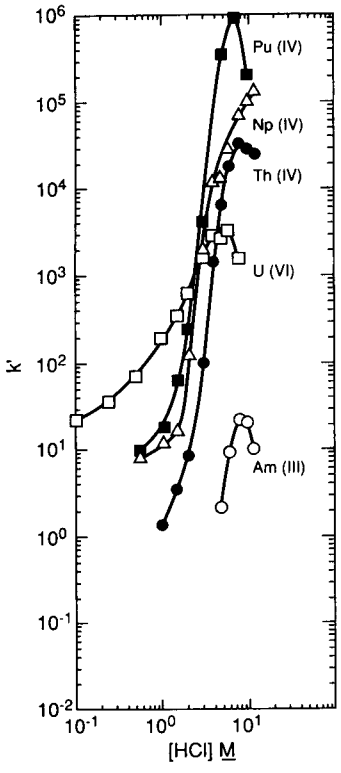

Fig. 6. Hydrochloric acid dependencies of k' for selected actinide ions on TRU · Spec (T = 23–25°C; 50–100 μm particle size resin.)

medium. The behavior of americium in this system also merits comment. As Fig. 6 shows, k'_{Am} never exceeds 30, even at high (e.g., 8 M) hydrochloric acid concentrations. Thus, a column rinse with, for example, 4 M hydrochloric acid will easily remove sorbed americium, while leaving U(VI) and tetravalents essentially untouched.

Taken together, these observations can serve as the basis of an elution scheme for the isolation of individual actinides using the TRU · Spec resin. Figure 7 summarizes one possible scheme which incorporates both nitric and hydrochloric acid rinse steps and various complex formation or oxidation state adjustment steps to effect the separation of actinides from both matrix constituents and one another. The sample load solution and column rinse are performed in nitric acid to take advantage of the high selectivity of the TRU · Spec for actinides over most matrix constituents in nitrate media (Table 2). Any iron present in the sample is reduced to Fe(II) to prevent interference with Am(III) retention (Table 3) and to ensure reduction of Np(V) to Np(IV). Two FCV of 9 M HCl are then used to convert the column to the chloride system. This reagent is used sparingly because Am is poorly retained in 9 M HCl. After the crossover to chloride, Am is eluted with 4 M HCl. The first 5 FCV contained > 99% of the Am and no detectable Pu. The third 5 FCV portion, however, contained 2.7% of the Pu activity. Next, plutonium is eluted with 4 M HCl–0.1 M hydroquinone. Approximately 91% of the Pu was found in the first 10 FCV. No detectable Am was found in the Pu fraction. Thorium and Np(IV) are eluted sequentially using 1.5 M HCl and 1.0 M HCl–0.03 M oxalic acid, respectively. Approximately 94% of the Th and 2% of the Pu was in the first 5 FCV of 1.5 M HCl. The third 5 FCV portion of 1.5 M HCl contained only 1% of the Th, 1.4% of the Pu, and 1.5% of the Np activities. Virtually all of the Np was eluted in the first 5 FCV of 1.0 M HCl–0.03 M oxalic acid and no other activity was discernible by alpha pulse-height analysis of

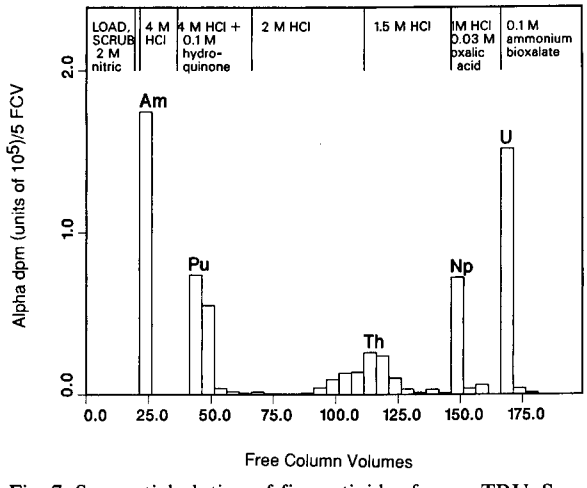

Fig. 7. Sequential elution of five actinides from a TRU · Spec column (column dimensions: bed diameter = 2.84 mm; bed length = 9.8 cm; flow-rate: 0.5–1.0 ml/ cm^2/min). 2 FCV of 9 M HCl follow the 2 M HNO_3 scrub.

this fraction. Finally, ~95% of the U is eluted with 5 FCV of 0.1 M ammonium bioxalate. No other activity was evident in the U fraction by alpha pulse-height analysis. The second 5 FCV portion contained only 2.4% of the U, but also contained ^{233}Pa (introduced from ^{237}Np).

Supplementary experiments have shown that Th must be eluted slowly when using hydrochloric acid to achieve good reproducibility. Tetravalent Np also shows slow kinetics when eluted with HCl alone, but not when elution is carried out with HCl and oxalic acid.

Alternative sequential separation schemes of actinides

Although the procedure depicted in Fig. 7 provides a reasonably good separation of the five actinides from each other, it is probably too tedious for routine analytical use. However, variations on this sequential elution scheme are possible in which TRU · Spec is used in conjunction with anion exchange columns to achieve an efficient separation with fewer manipulations. For example, tetravalent actinides (Th, Np, and Pu) may be selectively separated from trivalent and hexavalent actinides (Am, U) and all matrix constituents by using a strong-base anion exchange resin (preferably macroporous) loaded in and rinsed with 7 to 8 M HNO_3. [Separation of Th(IV) from Np(IV) and Pu(IV) or separation of all three elements from each other is carried out in the conventional manner.] The load and rinse solution from the anion exchange column may be treated in one of two ways. First, if the sample contains large quantities of matrix constituents (e.g., Fe and Ti), which is frequently the case with soils, a coprecipitation of the Am (and under certain conditions, U) on calcium oxalate gives a convenient feed material for dissolution and subsequent loading onto a TRU · Spec column. (The calcium oxalate is easily dissolved in 2 to 3 M HNO_3, but ascorbic acid should still be added before loading to ensure the absence of trivalent iron.) After loading and rinsing the TRU · Spec column with 2–3 M nitric acid, an abbreviated sequential separation is carried out in which Am is stripped with 4 M HCl, residual Pu (that was not retained by the anion exchange column) is stripped with 4 M HCl–0.1 M hydroquinone, residual Th and Np (also that was not retained by the anion exchange column) are stripped with 1.0 M HCl–0.05 M oxalic acid, and U is stripped with $NH_4HC_2O_4$. This procedure has several advantages. First, dissolved soil and ashed fecal or waste samples are much easier to keep in solution in strong nitric acid. Second, the anion exchange (coprecipitation) TRU · Spec scheme is robust and applicable to a wide range of sample types. Third, macroquantities of the Th and U are separated from the TRUs and thus do not interfere with alpha pulse-height analysis. Finally, the Am fraction is highly decontaminated from all other actinides. If the procedure is applied to soil samples, sufficient concentrations of lanthanides are usually present in the Am fraction to form a visible deposit that may interfere with alpha-pulse height analysis. In such cases, the Am is separated from the lanthanides.

A second method of treating the load and rinse solution from the anion exchange column involves eliminating the coprecipitation step and loading directly onto a TRU · Spec column. This procedure should only be used if macro quantities of Fe, Zr, and Bi are not present. A 2 M HNO_3–0.05 M oxalic acid rinse should be used prior to the HCl crossover step to remove traces of transition and post-transition elements. The balance of the procedure is as described above.

It is important to note that both of the alternate sequential separation schemes involve a Pu strip step using HCl–hydroquinone even though Pu(IV), like Th and Np(IV), can be eluted with HCl–oxalic acid. If this Pu strip step is eliminated, a significant fraction of the Np is found in the uranium fraction, presumably due to the presence of Np(VI). However, if one does not wish to recover U, then the TRU · Spec column can be stripped with 0.1 M $NH_4HC_2O_4$ following the stripping of Am with 4 M HCl.

Resin Stability

Column stability studies carried out with the TRU · Spec resin show that the americium elution band peaks at approximately 25 ml (~41 FCV) on a freshly prepared column when 0.3 M nitric acid is employed as the eluent. The first

and second column rinses (ca. 250 FCV and 500 FCV of rinse, respectively) produce a shift in this peak to higher volumes, ~ 32 ml and and 35 ml, respectively. Additional rinsing, however, produces a shift to smaller elution volumes until at 1000 FCV, the volume at peak maximum is only ~ 10% greater than that observed before any column rinsing. The initial increase in elution volume is consistent with the preferential dissolution of the more soluble TBP, the solvent for CMPO in TRU · Spec resin. The effect of such dissolution would be to increase the concentration of CMPO in the stationary phase and thus, the retention volume of sorbed ions. More extensive washing apparently removes CMPO as well, effectively stripping the stationary phase from the most readily accessible resin pores and leaving behind a material whose stationary phase composition more closely approximates that of the unwashed resin. Additional evidence of stationary phase loss is found in the fact that v_m, which was 0.60 ml initially, rises to 0.78 ml after 1000 FCV of washing, suggesting the presence of empty pores. Interestingly, estimates of theoretical plate numbers appear to indicate that in the early stages of column rinsing (500 FCV), column efficiency decreases, while additional rinsing yields a gradual improvement in efficiency. The reason for this behavior is unclear at present. What is clear is that the performance of TRU · Spec after ~ 1000 FCV of water washing does not differ substantially from that of pristine material. From the standpoint of analytical applications, this is significant for two reasons. First, it indicates that the resin could cope with a substantial load volume in a given run. Second, it indicates that a given column could be used more than one time, provided of course, that care is taken to ensure that all traces of sorbed ions are removed prior to reuse.

Conclusions

An extraction chromatographic resin comprised of a CMPO–TBP solution supported on an inert polymeric substrate provides an effective method for the separation and preconcentration of actinides from aqueous solution. The tri-, tetra-, and hexavalent actinides are efficiently sorbed by the resin from solutions containing a wide range of nitric acid concentrations. Under these same conditions, most other commonly encountered cations (e.g., Ca, Na) are only poorly retained, making the material potentially well-suited to the isolation of actinides from various environmental or biological samples. By exploiting differences in the retention of actinides in various oxidation states in hydrochloric acid in the presence and absence of oxalic acid, individual actinides can be separated from one another. This versatility too should make the resin applicable in a wide variety of analytical schemes for actinide separation and quantitation.

The authors wish to thank Dr. Claudia Felinto for assistance in the measurement of TRU · Spec resin stability. A portion of this work was performed under the auspices of the Office of Basic Energy Sciences, Division of Chemical Sciences, U.S. Department of Energy, under contract number W-31–109-ENG-38.

REFERENCES

1 Gmelin Handbook of Inorganic Chemistry, Uranium Supplement, D4, Cation-Exchange and Chromatograph, Springer-Verlag, Berlin, 1983.
2 J. Korkisch, Handbook of Ion-Exchange Resins: Their Application to Inorganic Analytical Chemistry, Vol. 2, CRC Press, Boca Raton, FL, 1989.
3 G.H. Coleman, The Radiochemistry of Plutonium, National Academy of Sciences, Springfield, VA, 1965.
4 T. Sekine and Y. Hasegawa, Solvent Extraction Chemistry: Fundamentals and Applications, Marcel Dekker, New York, 1977.
5 J.C. Veselsky, P.C. Kiel and N. Sezginer, J. Radioanal. Chem., 21 (1974) 97.
6 J.D. Eakins and P.J. Gomm, Health Phys., 14 (1968) 461.
7 T. Braun and G. Ghersini (Eds.), Extraction Chromatography, Elsevier, New York, 1975.
8 C.W. Sill, K.W. Puphal and F.D. Hindman, Anal. Chem., 46 (1974) 1725.
9 E.P. Horwitz, M.L. Dietz, D.M. Nelson, J.J. La Rosa, and W.D. Fairman, Anal. Chim. Acta, 238 (1990) 263.
10 A.M. Kistulovic and P.R. Brown, Reversed-Phase High Performance Liquid Chromatography: Theory, Practice, and Biomedical Applications, Wiley, New York, 1982.
11 D.A. Skoog and D.M. West, Fundamentals of Analytical Chemistry, Holt, Rinehart, and Winston, New York, 3rd edn., 1976.

12 R.C. Gatrone, L. Kaplan and E.P. Horwitz, Solvent Extr. Ion Exch., 5 (1987) 1075.
13 E.P. Horwitz, R. Chiarizia and M.L. Dietz, Solvent Extr. Ion Exch., 10 (1992) 313.
14 E.P. Horwitz, M.L. Dietz and D.E. Fisher, Anal. Chem., 63 (1991) 522.
15 E.P. Horwitz, M.L. Dietz, R. Chiarizia, H. Diamond, A.M. Essling, and D. Graczyk, Anal. Chim. Acta, 266 (1992) 25.
16 E.P. Horwitz, D.G. Kalina, H. Diamond, G.F. Vandergrift and W.W. Schulz, Solvent Extr. Ion Exch., 3 (1985) 75.
17 E.P. Horwitz and W.W. Schulz, The TRUEX Process: A Vital Tool for Disposal of U.S. Defense Nuclear Waste, in New Separation Chemistry Techniques for Radioactive Waste and Other Specific Applications, Rome, Italy, Elsevier Applied Science, London, 1991, p. 21.
18 E.P. Horwitz, K.A. Martin, H. Diamond and L. Kaplan, Solvent Extr. Ion Exch., 4 (1986) 449.
19 E.P. Horwitz, H. Diamond and K.A. Martin, Solvent Extr. Ion Exch., 5 (1987) 447.

Analytica Chimica Acta, 281 (1993) 373–383
Elsevier Science Publishers B.V., Amsterdam

Comparison of ultraviolet-laser induced and conventional fluorescence detection in conventional-size liquid chromatography of natively fluorescent analytes

R.J. van de Nesse, G.Ph. Hoornweg, C. Gooijer, U.A.Th. Brinkman and N.H. Velthorst

Department of General and Analytical Chemistry, Free University, De Boelelaan 1083, 1081 HV Amsterdam (Netherlands)

B. Law

Zeneca Pharmaceuticals, Drug Kinetics Group, Mereside, Alderley Park, Macclesfield, Cheshire SK10 4TG (UK)

(Received 20th January 1993; revised manuscript received 26th March 1993)

Abstract

The characteristics of laser-induced fluorescence (LIF) detection and state-of-the-art conventional fluorescence (CF) detection in the UV region below 300 nm in conventional-size column liquid chromatography are compared. An argon-ion laser system is used to provide four laser lines, i.e. 257 and 293 nm obtained by frequency-doubling of visible light and the UV lines at 334 and 352 nm. Light intensities inside the detector cell were measured by means of actinometry. Flicker noise, especially important for LIF detection was suppressed by simultaneously monitoring the laser light and ratioing sample and reference signals. On-line removal of fluorescent impurities in the eluent by means of a precolumn filled with carbon material resulted in a three-fold reduction of the background signal for LIF detection with 257-nm excitation. It is shown that LIF detection at 257 nm is more suitable than LIF at 293, 334 and 352 nm, not only for some pharmaceutical compounds that can only be excited below 300 nm, but also for polyaromatic hydrocarbons that absorb at wavelengths longer than 300 nm. Compared with CF detection at optimum excitation and emission settings, the detection limits obtained with the LIF system were improved typically by 5 to 10-fold.

Keywords: Fluorimetry; Liquid chromatography; UV-Visible spectrophotometry; Lasers; Polyaromatic hydrocarbons

In contrast to micro-column liquid chromatography (LC) and capillary electrophoresis, in conventional-size LC, lasers are not strictly required for sensitive fluorescence detection. Since the detector cell volumes usually are in the 5–10 μl range, focusing of radiation from a conventional light source is not a serious problem. Improvement of the detection limits by applying lasers is mainly due to the fact that the fluorescence signal intensity is proportional to the radiant power on the sample, which will be much higher for lasers than for conventional excitation sources (10^2–10^6-fold, depending on the system and the laser line considered) [1–4]. In the literature extremely low detection limits obtained in conventional-size LC with laser-induced fluorescence (LIF) have been reported for analytes exhibiting native fluorescence [6–8], or provided with a fluorescent tag [7,9,10], i.e. as low as 10^{-12} M. It should be realized, however, that these results were obtained for standard mixtures. In real-sample analysis, the detection limits are increased because of

Correspondence to: C. Gooijer, Department of General and Analytical Chemistry, Free University, De Boelelaan 1083, 1081 HV Amsterdam (Netherlands).

the high fluorescence background induced by interferences in the matrix. Under such conditions an increase in laser power does not improve the analyte detectability, since the noise on the background is dominated by fluctuations of the laser output (flicker noise); in other words, both the analyte fluorescence signal and the background noise are proportional to the radiant power [11]. For non-fluorescent analytes which require chemical derivatization, additional problems are encountered; in general derivatization of analytes at concentration levels as low as 10^{-8}–10^{-9} M in real samples gives rise to many interferences such as unwanted reaction products and reagent impurities which compromise the detection limits [12].

Nevertheless, for natively fluorescent analytes, the 10–100-fold improved analyte detectability obtained by applying LIF instead of CF in conventional-size LC is quite interesting. There are many analytes which possess native fluorescence, e.g., various drugs and their metabolites, steroids, vitamins and polynuclear aromatic hydrocarbons (PAHs) [13,14]. However, many of these have to be excited by UV radiation, a spectral region which is poorly covered by the lasers commonly used in LIF; these are the helium–cadmium laser (325 nm) and the argon-ion laser (only the large frame type provides UV lines at 334, 352 and 364 nm). It is our aim to investigate the potential of < 300 nm UV excitation in LIF by performing either direct or two-photon excitation [8,15]. In the present paper LIF at 257 and 293 nm, generated by frequency-doubling of visible light provided by an argon-ion laser, is compared with CF. Attention is focused on the determination of some pharmaceutical compounds, which can only be excited below 300 nm. In addition LIF experiments are performed for several PAHs which can also be excited by the argon-ion laser lines 334 and 352 nm. Short-wavelength excitation not only extends the range of (natively fluorescent) analytes that can be excited, it may also be advantageous for compounds absorbing at longer wavelengths because molar absorptivities are often highest for higher excited states and interference of Raman scattering from the eluent with the analyte fluorescence is more easily removed. A disadvantage of short-wavelength excitation is that fluorescent impurities in the eluent or flow cell walls are also efficiently excited, which produces higher backgrounds. Important parameters that have to be investigated therefore are the influ-

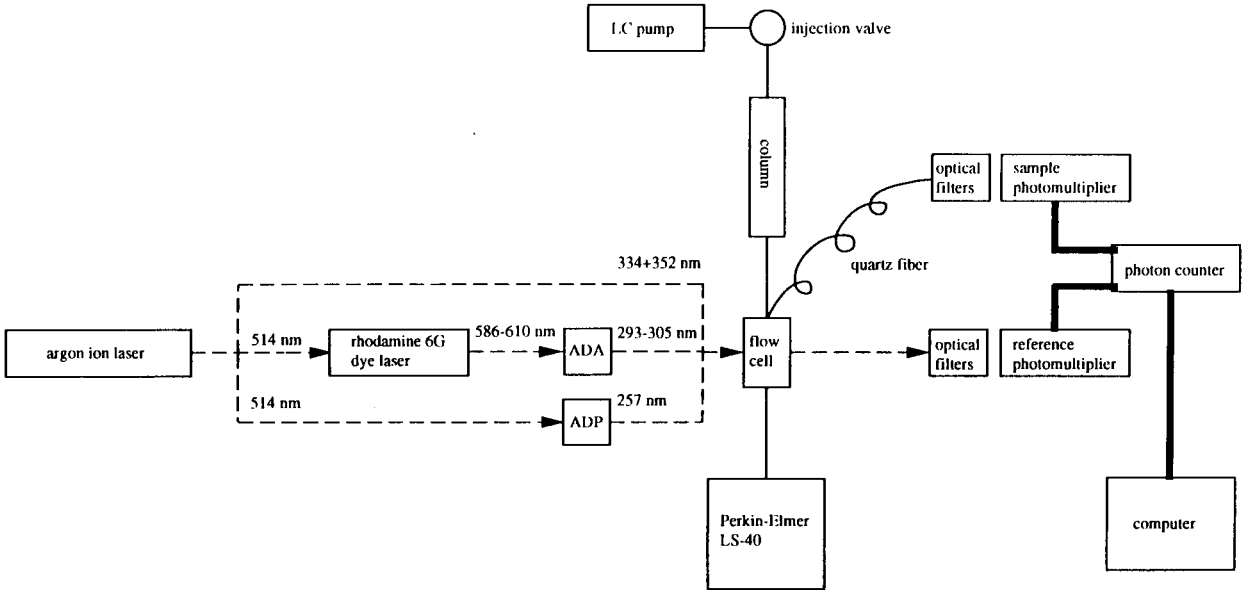

Fig. 1. Experimental set-up; for details, see Experimental.

ence of the laser wavelength and the LC eluent composition on the background fluorescence and also the stability of the laser lines.

EXPERIMENTAL

Chromatography

A Gynkotek (Germering, Germany) Model M300 pump and a laboratory-made injection valve with an external loop were used. PAHs were separated on a 200 × 3.0 mm i.d. column packed with 5-μm RoSil C_{18} (Research Separations Laboratories, Eke, Belgium) using methanol–water (90 : 10, v/v) at a flow-rate of 0.5 ml min^{-1} as the eluent; the injection volume was 10 μl. The pharmaceuticals were separated on a Zorbax Rx-C_8 150 × 4.6 mm i.d. column (Hichrom, Reading, UK) using methanol–0.2 M aqueous ammonium acetate (50 : 50, v/v) at a flow-rate of 1 ml min^{-1}; the injection volume was 25 μl. For the on-line removal of eluent impurities a 1 cm × 4 mm i.d. precolumn filled with either 40–70-μm CPP-50 graphitized carbon (Institute of Polymers, Slovak Academy of Sciences, Bratislava, Slovak Republic) or 40-μm C_{18} (Baker, Deventer, Netherlands) was used.

LIF measurements

The various excitation possibilities, provided by a Coherent (Palo Alto, CA) Innova 200-10 argon-ion laser, are schematically depicted in Fig. 1. The 334- and 352-nm laser lines were obtained directly as multi-line output; they were separated by a laser monochromator (Applied Photophysics, Leatherhead, UK) and attenuated by neutral density filters. Frequency-doubling of the mode-locked 514-nm laser line with a temperature-controlled ammonium dihydrogen-phosphate (ADP) crystal provided the 257-nm radiator. Excitation around 295 nm was achieved by frequency-doubling the output from a Coherent CR-590 rhodamine 6G dye laser via a temperature-controlled ammonium dihydrogenarsenate (ADA) crystal; the dye laser was synchronously pumped by the mode-locked 514-nm line. Laser light of the fundamental frequency and non-lasing plasma lines were rejected by quartz prisms and glass cut-off filters.

The laser light was focused on a laboratory-made quartz flow cell (Suprasil I quality) with external dimensions of 4 × 4 × 8 mm; the round internal bore was 1.1 mm diameter. The fluorescence light was collected by a 0.6 mm i.d. quartz fiber that was placed in the bore of the flow cell. Optical filters were used to select the emission light leaving the fiber. An XP2020Q photomultiplier tube (Philips, Eindhoven, Netherlands) was used for detection. After passing the flow cell, the excitation light was dispersed by a rugged quartz plate and detected with another XP2020Q photomultiplier that was used to monitor the fluctuations of the laser light. The signals from the sample and reference photomultiplier were simultaneously processed by a Stanford Research Systems (Sunnyvale, CA) SR400 photon counter; the integration time was 1 s. The chromatograms were recorded on an Apple Macintosh Plus computer (Cupertino, CA) together with the reference signal; corrections for the fluctuations of the excitation light were performed after the chromatographic run.

Conventional fluorescence detector

For conventional fluorescence detection, a Perkin-Elmer (Norwalk, CT) LS-40 fluorescence detector was used. The detector contained a 4 × 4 mm quartz flow cell with a length of 13 mm and a square internal bore of 1.0 × 1.5 mm. Excitation was provided by an 8-W pulsed xenon lamp. The time constant was 0.7 s; the excitation and emission slits were 10 nm. Chromatograms were recorded on a Kipp & Zonen (Delft, Netherlands) BD 8 strip-chart recorder.

Materials

Anthracene (Fluka, Buchs, Switzerland), fluoranthene (Aldrich, Milwaukee, WI), pyrene (E.G.A. Chemie, Steinheim, Germany), chrysene (Materials Limited, Englewood Cliffs, NJ), benzo[*b*]fluoranthene, benzo[*k*]fluoranthene and benzo[*a*]pyrene (all from Radiant Dyes, Wermelskirchen, Germany) were used as received.

Three pharmaceutical compounds were used in our study denoted at ICI 218356, IC 215001 and ICI 115338; they were obtained from the Zeneca Pharmaceuticals (Macclesfield, UK) compound collection. The former two are metabolites of compound Zeneca ZD7714 which is a β-3-agonist; ICI 115338 is an analogue of viloxazine. For convenience, the abbreviations X, Y, and Z are used for ICI 218356, ICI 215001 and ICI 115338, respectively.

Actinometry

The quantity of excitation radiation reaching the flow cell channel of the LS-40 and the LIF detector was determined using the potassium ferrioxalate actinometer, extensively described by Parker [16]. The actinometer is based on the light-induced conversion of iron(III) to iron(II). A solution of 0.006 M potassium ferrioxalate in 0.05 M sulphuric acid was flushed through the irradiated flow cell by a syringe pump and collected. An aliquot of 2 ml was buffered with 1 ml of 0.6 M sodium acetate in 0.18 M sulphuric acid; subsequently 2 ml of 0.1% 1,10-phenanthroline solution were added. The absorbance of the iron(II)–1,10-phenanthroline complex formed was measured at 510 nm. A calibration graph was made by carrying out the same procedure with standardized iron(II) sulphate solutions; blanks were measured under dark conditions. Despite the acid conditions and stainless-steel connections which might cause the presence of iron(II) impurities, the the blank absorption was never higher than 10% of the sample absorption. The radiant power was calculated from the flushed volume, the exposure time and a quantum efficiency of 1.25 for the photochemical reaction.

RESULTS AND DISCUSSION

In order to make a thorough and quantitative comparison between LIF and CF detection in conventional-size LC, four parameters were consecutively considered: (i) the radiances within the detector cell provided by the conventional and laser excitation sources; (ii) the fluorescence background observed at varying eluent compositions, studied at 257 nm, the shortest laser wavelength used; (iii) the optimum selection of the excitation wavelength depending on the absorption spectra of the analytes, the possible interference of Raman scattering (from the eluent) and analyte fluorescence as well as the laser-line source instabilities which are wavelength dependent because of the generation procedure; (iv) the selectivity aspects of LIF and CF detection, illustrated for real samples, e.g. a spiked dog plasma extract.

Radiance inside the detector cell

To make a quantitative comparison between LIF and CF below 300 nm, the radiant power provided by the Perkin-Elmer LS-40 in the tunable wavelength region below 300 nm was measured and compared with the two available discrete laser lines 257 and 293 nm. It was important to determine the intensity of the light reaching the inner part of the detector cell, which was responsible for the excitation of the eluting analytes. Measurement of this "effective radiant power" cannot be carried out in a straightforward manner for the LS-40 detector. First, the light intensity is very low; second, placing a power meter in the optical system disturbs the light paths and third, the light spot has larger dimensions than the flow cell channel. To overcome these problems a potassium ferrioxalate actinometer solution was used to measure the light intensity [16]. At 1 mm path length, a 0.006 M solution of this salt will absorb at least 95% of the excitation light at wavelengths shorter than 310 nm. With the actinometer, the excitation light that actually enters the flow cell channel is measured by flushing the solution through the flow cell during exposure to the light. The results of the actinometer measurements are shown in Table 1. The power of the attenuated laser lines at 334 and 352 nm measured with a conventional (instrumental) power meter are added for comparison; at these wavelengths the absorbance of the potassium ferrioxalate actinometer at 1 mm path length is not large enough for reliable measurements. For the 257-nm laser line, the actinometer measurements were also performed in a 1-cm light path absorption quartz cuvette to ex-

TABLE 1

Excitation power of LS-40 and LIF detection system [a]

Wavelength (nm)	Excitation power (mW)
LS-40	
260	0.020
285	0.023
310	0.027
LIF	
257 [b]	1.8
257 [c]	2.2
293 [b]	1.5
334	14
352	37

[a] Intensities of the laser at 334 and 352 nm were measured with a power meter; all other data were obtained with the potassium ferrioxalate actinometer ($n = 3$). [b] Measured in LIF flow cell. [c] Measured in 1-cm quartz cuvette.

amine the reflection/refraction losses at the round bore of the flow cell (the LS-40 flow cell has a square channel). The data show that such losses are about 20%. One should note that the radiant power of the LS-40 does not fall off sharply in going from 310 to 260 nm as is suggested by profiles of (non-pulsed) xenon lamps given in the literature [17]: the decrease is gradual and amounts to about 25%. The data in Table 1 also show that the intensities of the laser lines at 257 and 293 nm are almost 100 times higher than those of the LS-40 light source. Thus, assuming identical experimental parameters such as collection efficiency and photomultiplier response, the detection limits that can be achieved for these lines by applying LIF instead of CF detection will be about 10-fold lower if shot noise is dominant.

Fluorescence background at 257-nm excitation

In LIF detection in the UV region, background fluorescence is expected to play an important role since impurities in the eluent and flow cell material are more likely to be excited at shorter wavelengths. In order to acquire some insight into this effect, the fluorescence observed in LIF and CF when applying 257-nm excitation was studied as a function of LC eluent composition (methanol–0.1 M aqueous ammonium acetate). Besides, the on-line removal of fluorescent impurities present in the eluent was attempted by passing the eluent through a 1 cm × 4 mm i.d. precolumn filled with either C_{18}-bonded silica or carbon material at a flow-rate of 1.0 ml min^{-1}. The background signal was recorded as soon as a steady baseline was reached; an analytical column was not installed. Results obtained by LIF_{257} and

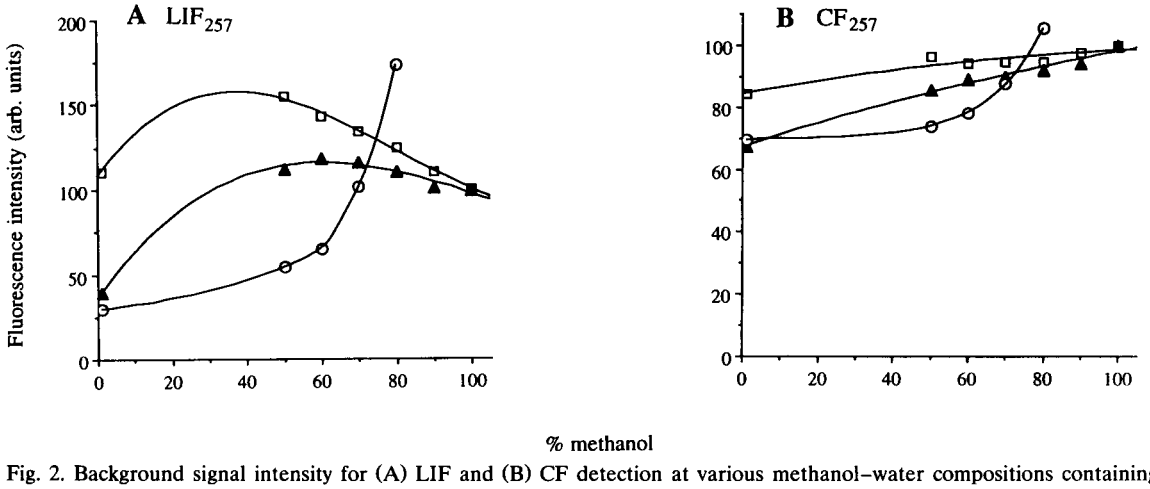

Fig. 2. Background signal intensity for (A) LIF and (B) CF detection at various methanol–water compositions containing 0.1 M ammonium acetate, performed at 257 nm excitation and 320 nm emission. The signal for pure methanol containing 0.1 M ammonium acetate is normalized to 100 (arbitrary units). The background signal is measured (□) without any purification of eluent, and after purification over a precolumn filled with (▲) C_{18} or (○) carbon material. No points were measured between 0 and 50% methanol; for convenience the data points are connected by solid lines.

the LS-40 detector utilizing the same excitation and emission settings are depicted in Fig. 2A and B. Since separations were only performed at high modifier concentrations, only data on methanol concentrations from 50 to 100% were considered. The data show that luminescent impurities in the eluent are removed, the reduction in background signal being dependent on eluent composition and precolumn packing material. Use of the C_{18}-bonded silica precolumn reduced the background signal at all eluent compositions; at lower methanol percentages eluent cleaning was more effective. The carbon column was only useful for methanol concentrations of less than 70%; under these conditions the impurities are more effectively removed than with the C_{18}-bonded silica column. At higher methanol contents impurities are probably released from the carbon material and the background is strongly increased.

Comparison of Fig. 2A and B reveals that the removal of impurities has much more effect on the background signal observed with LIF detection than with the LS-40. In other words, the background signal observed with the LS-40 is not only caused by impurities in the eluent but also by scattered light leaking through the monochromators or luminescence from the walls of the flow cell. For the eluent composition used in the LC separation of the pharmaceuticals, i.e. methanol–0.2 M aqueous ammonium acetate (50:50), the decrease in the background signal in LIF when using the carbon column is about 3-fold; for the LS-40 the improvement is only 30%. Minimizing the background signal has the largest effect if flicker noise is dominant; under these conditions the noise amplitude is linearly proportional to the background signal. For the LS-40 shot noise is dominant and the improvement is relatively small.

From a practical point of view, the time over which the cleaning activity of the precolumn can be maintained is essential. Using the C_{18}-silica bonded precolumn and 50% methanol, the background signal increased within an hour to a level which was only slightly smaller than that measured for non-purified eluent. The background signal of the carbon column, however, remained stable for at least 8 h while continuously pumping through eluent at 1.0 ml min^{-1}. The precolumn could be re-used after overnight flushing with methanol.

During the measurements on the pharmaceuticals, the carbon column was employed for on-line eluent purification. For the PAH measurements, the eluent consisted of methanol–water (90:10) and on-line removal of impurities could not successfully be applied.

Choice of excitation wavelength

The influence of the laser excitation wavelength on the analyte detectability was studied by recording chromatograms of three pharmaceutical compounds and a mixture of PAHs, utilizing LIF and CF detection.

The three pharmaceuticals, denoted as X, Y and Z (for abbreviations, see *Materials*), require

TABLE 2

Spectral characteristics (excitation and emission maxima and relative molar absorptivities $\epsilon_\lambda/\epsilon_{max}$) of the three pharmaceuticals and their limits of detection (LOD) using the LIF system and the Perkin-Elmer LS-40 fluorimeter

Compound	Spectral characteristics				LOD ($\mu g\ l^{-1}$) [a]			
					LIF		LS-40	
	$\lambda_{ex,max}$ (nm)	$\lambda_{em,max}$ (nm)	$\epsilon_{257}/\epsilon_{max}$	$\epsilon_{293}/\epsilon_{max}$	λ_{ex} = 257 nm [b]	λ_{ex} = 293 nm [c]	λ_{ex} = 257 nm [d]	Optimum $\lambda_{ex,em}$ [e]
X	286	327	0.10	0.65	1.5	1.7	25	3.1
Y	276	321	0.40	0.80	0.90	4.9	13	7.5
Z	251	308	0.85	n.a. [f]	0.25	n.a. [f]	2.3	2.0

[a] $S/N = 3$, $n = 5$. [b] λ_{em} = 334 nm, maximum transmittance 37%, full width at half maximum (FWHM) 54 nm. [c] λ_{em} = 349 nm, maximum transmittance 25%, FWHM 32 nm. [d] λ_{em} = 320 nm. [e] Maximum wavelength settings except for compound X: λ_{em} = 335 nm. [f] Not applicable.

excitation below 300 nm (see Table 2) so that in our LIF system only two laser lines can be used, i.e. 257 and 293 nm. Excitation with the shortest wavelength is favourable for rejection of Raman scattering, whereas at the longer wavelength X and Y exhibit higher molar absorptivities.

In Fig. 3 liquid chromatograms obtained by LIF and CF detection at 257-nm excitation are shown. It is difficult to compare the absolute signal intensities of both systems since in the LS-40 analog signal processing is performed and intensities are expressed in arbitrary units; nevertheless, an estimate will be made. Using the characteristic dependence of the shot noise (root-mean-square) on the square root of the signal and the fact that in photon counting processing the shot noise is equal to the square root of the number of counts, the LS-40 units can be converted into counts s^{-1} [11]. From a plot of signal versus noise it was calculated that in Fig. 3B one arbitrary readout unit corresponds to about 300 counts s^{-1}. This means that the LS-40 signals of the compounds X, Y and Z can be expressed as 1400, 2700 and 1500 counts s^{-1}, respectively. Compared with the LIF chromatogram in Fig. 3A these signal intensities are 100–200-fold lower. Since the radiant power provided by the LS-40 light source is 100-fold lower, this estimate indicates that the resultant of collection efficiency, emission filter function and photomultiplier response for the two systems is of the same order of magnitude.

In Table 2 the limits of detection (LODs) are listed using a minimum detectable signal-to-noise ratio (peak-to-peak) of 3. The LODs in LIF are 10–20 times better than in CF. The improvement is of course largely due to the 100-fold higher radiant power of the laser (see Table 1). A small part can be attributed to the difference in background observed: with CF the signal-to-background is about 4-fold lower than in Fig. 3A, due to contributions of scattered excitation light and luminescence from the flow cell walls to the background signal of the LS-40.

It is obvious, especially for compounds X and Y, that excitation at 257 nm is relatively far from the optimum excitation wavelengths, which are 286 and 276 nm, respectively. Utilizing optimum wavelength settings, in CF detection the LODs are improved by a factor of 8 and 1.7, respectively. Unfortunately, these wavelengths are not provided by our laser system. Since the shortest

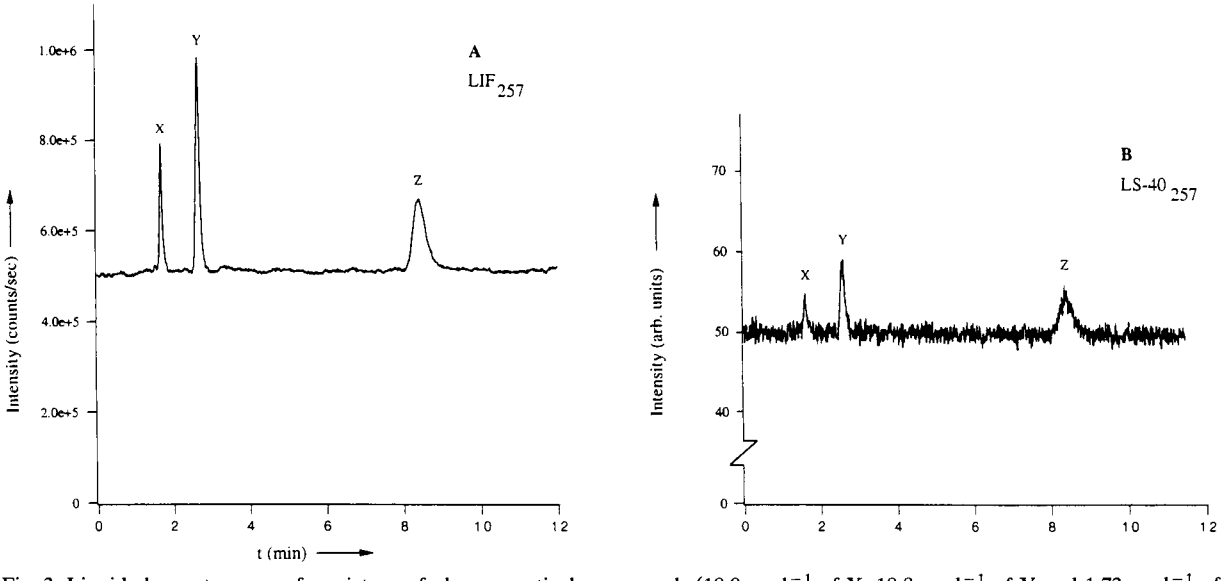

Fig. 3. Liquid chromatograms of a mixture of pharmaceutical compounds (18.9 $\mu g\ l^{-1}$ of X, 18.8 $\mu g\ l^{-1}$ of Y and 1.73 $\mu g\ l^{-1}$ of Z), recorded with (A) LIF_{257} and (B) CF at the same excitation wavelength. The fluorescence detection window in (A) was maximum at 334 nm (37%, FWHM 54 nm); in (B) the fluorimeter was set at 320 nm. For LC conditions, see Experimental.

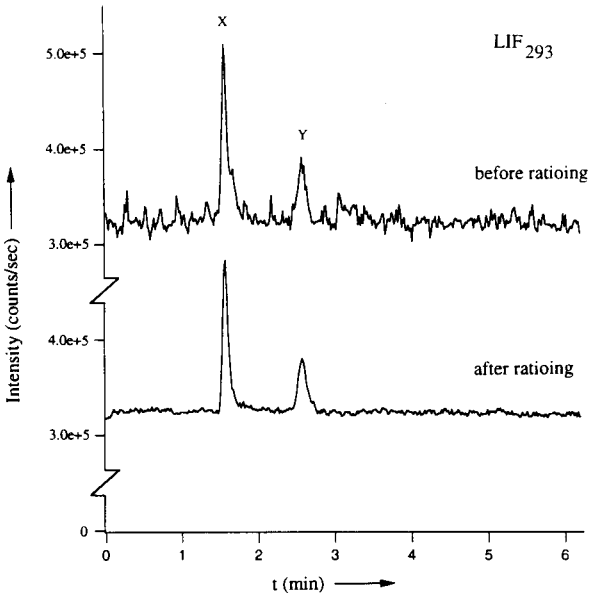

Fig. 4. Liquid chromatogram of standard solution containing 18.9 $\mu g\ l^{-1}$ of X and 18.8 $\mu g\ l^{-1}$ of Y, recorded with LIF_{293} before and after ratioing the signal with a reference photomultiplier that monitors the laser fluctuations. The emission was detected in a window with maximum transmittance at 349 nm (25%, FWHM 32 nm). For LC conditions, see Experimental.

wavelength generated by frequency-doubling the output of a rhodamine-6G dye laser (synchronously pumped by the 514-nm argon-ion line) is 293 nm, this laser line was used in an attempt to obtain better detection of compounds X and Y. Unfortunately, as is obvious from Fig. 4, its output is rather unstable; the peak-to-peak fluctuation is as large as 5–10%, so that flicker noise is very important. Even after reduction of the flicker noise by applying the ratioing procedure outlined in the experimental section, the LODs for X and Y are higher than those obtained after excitation at 257 nm (see Table 2). The small power difference within the flow cell (1.8 mW at 257 nm and 1.5 mW at 293 nm, see Table 1) cannot account for this fact. The main reason is that for 257-nm excitation, a more favourable emission window can be used. When applying 293-nm excitation, the Raman spectrum of methanol–water extends to about 330 nm, so that the fluorescence has to be measured at longer wavelengths and cannot be efficiently detected.

The above results suggest that LIF_{257} is an appropriate detection mode at wavelengths < 300 nm: it is generally applicable and despite the high background caused by fluorescence impurities, it provides favourable LODs because Raman scattering can be largerly eliminated.

It is interesting to examine whether 257 nm is also the LIF excitation wavelength of choice for analytes that can be excited in the near UV, using the laser lines at 334 and 352 nm which are directly provided by the argon-ion laser (without frequency-doubling). For this reason seven PAHs were studied with LIF detection at 257 and 293 nm and also at 334 and 352 nm; the latter two

TABLE 3

Detection limits (LOD; $\times 10^{-10}$ M) [a] of seven PAHs using the LIF system and the Perkin Elmer LS-40 fluorimeter with molar absorptivities (10^{-4} ϵ, l mol^{-1} cm^{-1}) in parentheses

Compound	LIF				LS-40 fluorimeter	
	λ_{ex} (nm)				λ_{ex} (nm)	Optimum $\lambda_{ex,em}$ (nm)
	257 [b]	293 [b]	334 [c]	352 [d]	257	
Anthracene	2.5 (1.1)	75 (0.0064)	3.0 (0.37)	3.0 (0.59)	30	3.0 (ex 250, em 399)
Fluoranthene	30 (1.2)	250 (0.21)	10 (0.60)	9.0 (0.69)	400	55 (ex 286, em 462)
Pyrene	10 (1.3)	40 (0.43)	1.5 (4.3)	260 (0.045)	230	60 (ex 273, em 383)
Chrysene	2.5 (7.8)	20 (1.2)	220 (0.076)	900 (0.049)	110	15 (ex 268, em 381)
Benzo[*b*]fluoranthene	5.5 (4.7)	12 (2.3)	4.5 (1.1)	4.0 (1.1)	70	30 (ex 297, em 430)
Benzo[*k*]fluoranthene	2.0 (2.1)	1.0 (4.0)	1.5 (0.53)	3.0 (0.36)	20	5.0 (ex 308, em 428)
Benzo[*a*]pyrene	2.5 (4.4)	2.0 (6.2)	4.5 (0.56)	3.0 (1.2)	30	10 (ex 292, em 403)

[a] $S/N = 3$, $n = 4$. [b] $\lambda_{em} = 400$ nm, maximum transmittance 54%, full width at half maximum (FWHM) 52 nm. [c] $\lambda_{em} = 410$ nm, maximum transmittance 36%, FWHM 29 nm. [d] $\lambda_{em} = 423$ nm, maximum transmittance 17%, FWHM 21 nm.

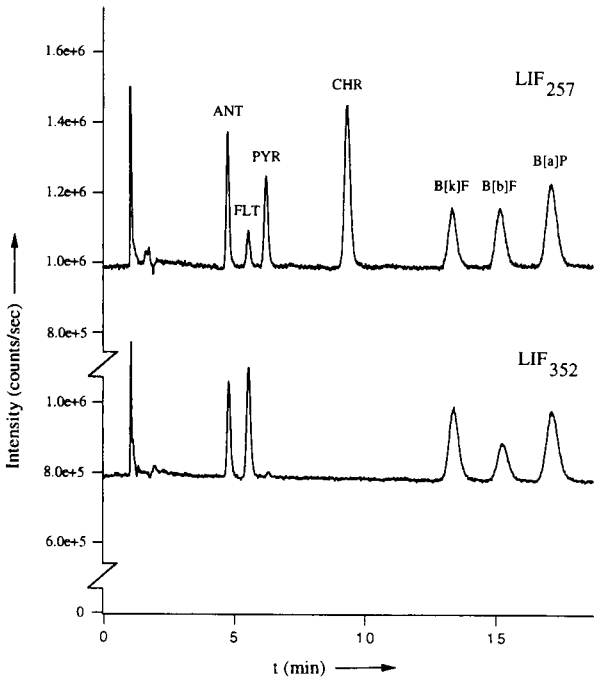

Fig. 5. Liquid chromatograms of a mixture of 3.0×10^{-9} M anthracene (ANT), 1.0×10^{-8} M fluoranthene (FLT), 1.0×10^{-8} M pyrene (PYR), 4.0×10^{-9} M chrysene (CHR), 3.0×10^{-9} M benzo[*b*]fluoranthene (B[*b*]F), 1.2×10^{-9} M benzo[*k*]fluoranthene (B[*k*]F) and 2×10^{-9} M benzo[*a*]pyrene (B[*a*]P) measured with LIF_{257} and LIF_{352}. The fluorescence with LIF_{257} was measured in a window with a maximum transmittance at 400 nm (54%, FWHM 52 nm); with LIF_{352} the maximum transmittance was at 423 nm (17%, FWHM 21 nm). For LC conditions, see Experimental.

laser lines were used with excitation powers of 14 and 37 mW, respectively (see Table 1). In Table 3 the chromatographic detection limits are reported and in Fig. 5 the chromatograms recorded at 257- and 352-nm excitation are shown. As expected on the basis of the molar absorptivities, LIF_{257} is generally applicable whereas with LIF_{334} and LIF_{352} chrysene is poorly detected. Additionally pyrene and fluoranthene are not clearly detected with LIF_{352} and LIF_{293}, respectively. A more interesting point from Table 3 is that for the analytes that can be excited at all the wavelengths considered, LIF_{257} provides detection limits which are comparable to those obtained for LIF_{334} and LIF_{352}. The data for LIF_{293} are relatively unfavourable except for benzo[*k*]fluoranthene and benzo[*a*]pyrene; in fact the lowest LOD is obtained for benzo[*k*]fluoranthene with LIF_{293}, i.e. 1.0×10^{-10} M corresponding to an injected amount of 250 fg.

Confining our attention to a comparison of LIF_{257} with LIF_{352} detection, three parameters play a role here which apparently largely compensate each other: on the negative side for 352-nm excitation, the emission window has to be shifted to longer wavelengths to prevent detection of Raman scattering, which means a loss of fluorescence intensity; secondly, at 352 nm the molar absorptivities are lower. On the positive side for 352-nm excitation the background signal is about 3-fold lower than at 257 nm. This ratio can be estimated from Fig. 5, which shows a 20% lower background at 352 nm while the excitation power is 17-fold higher and the throughout of the emission filter 7-fold lower.

Finally, it should be mentioned that for all laser lines the background signal contains about 1% flicker noise (peak-to-peak), even after applying ratioing; in other words, the LODs cannot be improved by applying higher excitation powers.

When the LS-40 detector and the LIF system are used at the same excitation wavelength, i.e. 257 nm, the LODs obtained with LIF are considerably lower, viz. from 10-fold for benzo[*k*]fluoranthene to 40-fold for chrysene. Comparison of the two detection systems when they are both operated at optimum settings indicates a less distinct preference for LIF detection. However, even under these conditions the gain in analyte detectability generally is at least 5–10-fold. For pyrene the 40-fold improvement (cf. 1.5×10^{-10} M for LIF_{334} and 60×10^{-10} M for CF) is due to the narrow absorption bands of this compound which is not efficient for CF excitation in view of the 10-nm spectral bandwidth of the LS-40. In contrast, with anthracene no gain is observed; this compound exhibits much lower molar absorptivities at wavelengths longer than 250 nm and cannot efficiently be excited with our LIF system. Finally it is noted that the LIF_{257} data in this study, measured with a Yeung-type fiber-optics flow cell [18], are about twice as high as those reported earlier for an LIF_{257} system in

which the fluorescence was collected with a flow cell box mounted on a photomultiplier [8]. These slight differences in LODs should mainly be ascribed to the differences in experimental parameters such as emission window and column performance.

Selectivity aspects

An important difference between LIF and CF detection is the monochromaticity of the excitation light. However, the extreme narrow bandwidth of laser lines cannot be exploited in liquid solutions since absorption spectra of organic fluorophores are generally broad and featureless. Figure 6 shows the LIF and CF chromatograms of a dog plasma extract spiked with the pharmaceuticals X, Y and Z. The strong resemblance of the LIF_{293} and CF_{285} chromatograms demonstrates that the monochromaticity of the laser light does not provide enhanced selectivity. The determination of the analytes in the biological sample is obviously hindered by interfering components which strongly show up at short excitation and emission wavelengths. In Fig. 6 only component Z elutes at 8.5 min almost free from interferences and, in line with Table 2, LIF_{257} provides an 8-fold gain in detectability compared to optimum CF detection (excitation at 251 nm). In contrast, detection of X and Y with LIF suffers strongly from interferences. Applying longer-wavelength excitation, i.e. LIF_{293}, the signal intensities of the interferences decrease considerably, and X can now be observed more clearly (for Y LIF_{293} is much less efficient than LIF_{257} detection, see Table 2). Nevertheless there is no significant increase in detectability when using LIF_{293} instead of CF_{285}. Or, in other words, in order to fully profit from the gain in analyte detectability proper optimization of the sample treatment and/or LC separation procedure must be carried out.

Conclusions

Natively fluorescent analytes can be sensitively detected by applying LIF in the < 300 nm UV region. The decrease in flicker noise, which is important for laser lines generated by frequency-doubling, is essential; this can successfully be

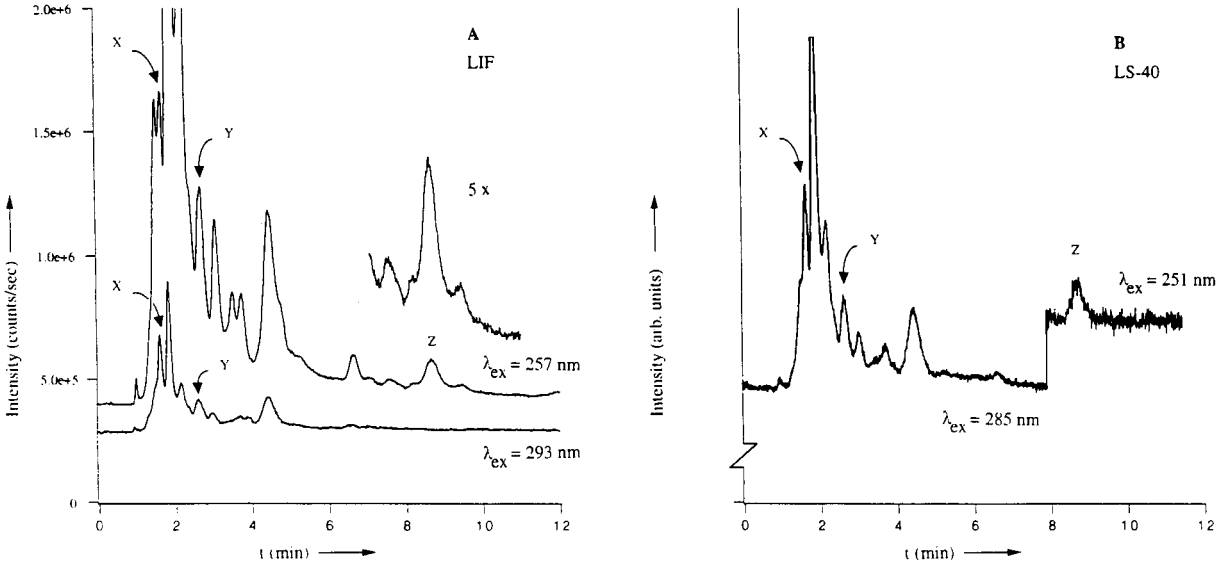

Fig. 6. Liquid chromatograms of a dog plasma sample spiked with 18.9 $\mu g\ l^{-1}$ of X, 18.8 $\mu g\ l^{-1}$ of Y and 1.73 $\mu g\ l^{-1}$ of Z, measured with (A) LIF_{257} (upper curve) and LIF_{293} (lower curve) and (B) conventional fluorimetry with 285/335 nm and 251/308 nm excitation/emission, respectively. The fluorescence detection windows for LIF were the same as in Figs. 3 and 4. For LC conditions, see Experimental.

realized by monitoring the laser light and applying a ratioing procedure. For the analytes that can be excited in the near UV (i.e. at wavelengths higher than 300 nm), LIF_{257} detection is also useful: it is generally applicable and Raman scattering generated by the cluent can be largely eliminated without the loss of fluorescence intensity.

In comparison with conventional fluorescence detection, representing the state-of-the-art in fluorescence instrumentation, the gain in analyte detectability provided by LIF_{257} typically is about one order of magnitude. This difference in performance between LIF and CF detection is in line with the data reported in Ref. 6 in which a 6-fold gain was achieved using a helium–cadmium laser based LIF system. It is emphasized that these results apply to conventional-size liquid chromatography; of course in miniaturized systems the differences in performance that can be obtained with LIF and CF detection will be far more pronounced, since CF is much less compatible with small-volume flow cells.

Recent developments in laser technology have broadened the excitation potential of the argon-ion laser in the UV region below 300 nm. Modification of the plasma tube and mirrors have made 275.4-nm output feasible, while intra-cavity frequency doubling provides high power at 257 and 244 nm. The first papers on these new LIF systems have recently been published [19,20] and it is to be expected that these excitation possibilities will be explored in the near future for LIF detection in LC.

The investigation was supported by the Netherlands Foundation for Chemical Research (SON) with financial aid from the Netherlands Organization for the Advancement of Scientific Research (NWO), grant no. 700-344-006.

REFERENCES

1 A. Berthod, Spectrochim. Acta, 13 (1990) 11.
2 T. Imasaka and N. Ishibashi, Prog. Quantum Electr., 14 (1990) 131.
3 E.S. Yeung, Anal. Chem., 52 (1980) 1465A.
4 E.S. Yeung in E.H. Piepmeier (Ed.), Analytical Applications of Lasers, Wiley, New York, 1986, p. 557.
5 S. Folestad, L. Johnson and B. Josefsson, Anal. Chem., 54 (1982) 925.
6 J.M. Bostick, J.W. Strojek, T. Metcalf and T. Kuwana, Appl. Spectrosc., 46 (1992) 1532.
7 C.M.B. van den Beld and H. Lingeman, in W.G.R. Baeyens, D. de Keukeleire and K. Korkidis (Eds.), Luminescence Techniques in Chemical and Biochemical Analysis, Marcel Dekker, New York, 1991, pp. 287–288.
8 R.J. van de Nesse, G.Ph. Hoornweg, C. Gooijer, U.A.Th. Brinkman and N.H. Velthorst, Anal. Chim. Acta, 227 (1989) 173.
9 M.C. Roach and M.D. Harmony, Anal. Chem., 59 (1987) 411.
10 C.M.B. van den Beld, H. Lingeman, G.J. van Ringen, U.R. Tjaden and J. van der Greef, Anal. Chim. Acta, 205 (1988) 15.
11 J.D. Ingle, Jr. and S.R. Crouch, Spectrochemical Analysis, Prentice Hall, Englewood Cliffs, NJ, 1988, Chap. 5.3.
12 D.S. Stegehuis, U.R. Tjaden, C.M.B. van den Beld and J. van der Greef, J. Control. Rel., 13 (1990) 129.
13 N. Ichinose, G. Schwedt, F.M. Schnepel and K. Adachi, in J.D. Winefordner (Ed.), Fluorimetric Analysis in Biomedical Chemistry, Wiley, New York, 1991, Chaps. 4 and 5.
14 W. Karcher, R.J. Fordham, J.J. Dubois, P.G.M. Glaude and J.A.M. Ligthart, Spectral Atlas of Polycyclic Aromatic Compounds, Reidel, Dordrecht, 1983.
15 R.J. van de Nesse, A.J.G. Mank, G.Ph. Hoornweg, C. Gooijer, U.A.Th. Brinkman and N.H. Velthorst, Anal. Chem., 63 (1991) 2685.
16 C.A. Parker, Photoluminescence of Solutions, Elsevier, Amsterdam, 1968, p. 208.
17 J.D. Winefordner, S.G. Schulman and T.C. O'Haver, in P.J. Elving and I.M. Kolthoff (Eds.), Luminescence Spectrometry in Analytical Chemistry, Wiley, New York, 1972, p. 148.
18 M.J. Sepaniak and E.S. Yeung, J. Chromatogr., 190 (1980) 377.
19 D.F. Swaile and M.J. Sepaniak, J. Liq. Chromatogr., 14 (1991) 869.
20 T.T. Lee and E.S. Yeung, J. Chromatogr., 595 (1992) 319.

Analytica Chimica Acta, 281 (1993) 385–389
Elsevier Science Publishers B.V., Amsterdam

Determination of acetylacetone and alcohols in titanium chelates

Erik Kissa

Research and Development Division, Jackson Laboratory – Chemicals Department, E.I. Du Pont de Nemours and Company, Deepwater, NJ 08023 (USA)

(Received 3rd March 1993; revised manuscript received 12th April 1993)

Abstract

Acetylacetone (2,4-pentanedione) and alcohols in titanium chelates have been determined by gas chromatography of the solvolyzed chelate. For the determination of acetylacetone, the titanium chelate is cleaved with acetic acid at 140–150°C for 2–4 h in a closed system. The acetylacetone liberated is determined by capillary gas chromatography as the trimethylsilyl derivative. Normal alcohols elute as acetates, isopropyl alcohol elutes as a mixture of the corresponding acetate and trimethylsilyl derivative. The cleavage of a titanium chelate with acetic anhydride by heating at 130°C for 2 h converts alcohols, including isopropyl alcohol, quantitatively to their acetates which elute as a single peak for each alcohol. Acetylacetone decomposes partially under these conditions and the acetic anhydride method is useful only for the determination of alcohols.

Keywords: Gas chromatography; Acetylacetone; Alcohols; Solvolysis; Titanium chelates

A titanium diketochelate of acetylacetone [bis(2,4-pentanedionate-*O*,*O'*)bis(2-propanolato)-titanium] is represented by the formula I [1]

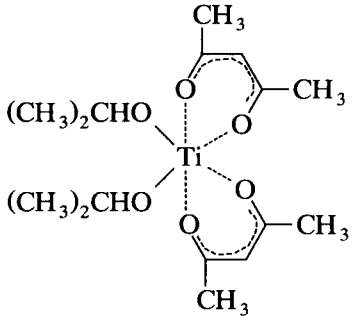

(I)

The chelate is synthesized by reacting tetraisopropyl titanate with 2 mol of acetylacetone. The isopropyl alcohol liberated in the process remains in the product as a diluent, is stripped or replaced with *n*-butanol and methanol.

The determination of acetylacetone in an organic titanate poses several problems:

(1) Acetylacetone exists in two tautomeric forms [2–5]:

$$CH_3COCH_2COCH_3 \longleftrightarrow CH_3\overset{\overset{H}{|}}{\underset{|}{C}}{=}CHCOCH_3$$

In most organic solvents the enol form predominates, in water the keto form is predominant.

(2) Acetylacetone, reacting as an enol, forms with titanium a stable chelate that is more resistant to hydrolysis than the titanates derived from alcohols [6]. Hence liberation of acetylacetone from the chelate requires conditions which are drastic but do not degrade the acetylacetone liberated.

(3) If alkali is used to hydrolyze the chelate, the acetylacetone liberated may undergo hydroly-

Correspondence to: E. Kissa, Research and Development Division, Jackson Laboratory – Chemicals Department, E.I. Du Pont de Nemours and Company, Deepwater, NJ 08023 (USA).

sis in the alkaline medium [2]:

$$CH_3COCH_2COCH_3 + NaOH \longrightarrow CH_3COONa + CH_3COCH_3$$

(4) If strong acids are used for hydrolysis of the chelate, acetylacetone may react with the alcohols liberated from the chelate:

$$ROH + CH_3COCH_2COCH_3 \xrightarrow{H^+} CH_3COCH_3 + CH_3COOR$$

In view of these complications the determination of acetylacetone and alcohols in organic titanium compounds presented an interesting challenge. The main difficulty of the problem was to cleave the titanium chelate quantitatively under conditions amenable for gas chromatography.

To suppress solvolysis of acetylacetone we decided to use acetic acid as the reagent for cleaving the titanium chelate.

EXPERIMENTAL

A weighed sample (300–400 mg) of the acetylacetone titanium diketochelate and 2 ml of acetic acid are heated in a closed 10-ml septum vial for 4 h at 140°C. The vial is cooled in water and its contents are transferred to a 100-ml volumetric flask and diluted to volume with acetonitrile containing *n*-decane as the internal standard. A portion (about 2 ml) of the solution is withdrawn with a syringe and filtered through a PTFE membrane (Acrodisc CR) filter of a 0.45 μm pore size. 1 ml of the clarified solution is transferred to a septum vial and reacted with 0.25 ml of *N,O*-bis(trimethylsilyl)trifluoroacetamide (BSTFA). 0.5 μl of the silylated analate is injected (using an autosampler) into a gas chromatograph equipped with a flame ionization detector (FID). A 60 m long, 0.75 mm i.d. wide bore SPB-5 capillary

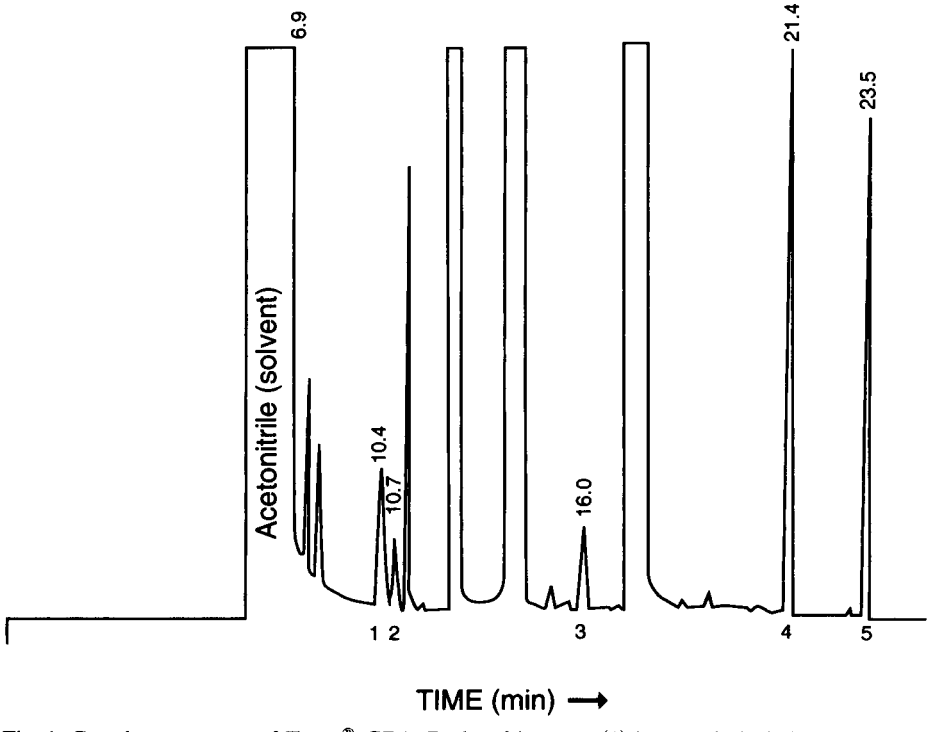

Fig. 1. Gas chromatogram of Tyzor® GBA. Peaks of interest: (1) isopropyl alcohol, as the trimethylsilyl derivative; (2) isopropyl acetate; (3) *n*-butyl acetate; (4) *n*-decane (internal standard); (5) acetylacetone, as the trimethylsilyl derivative.

column, film thickness 1.0 μm, or a 30 m long, 0.25 mm–0.32 mm i.d., SPB-5 or DB-5 capillary column is used.

The operating conditions for the Varian 6000 equipped with the megabore (0.75 mm i.d.) column in a splitless mode are as follows: carrier gas (helium) 5 ml/min, make up gas (helium) 30 ml/min, injector temperature 220°C, detector temperature 300°C, initial column temperature 40°C, pre-program hold 6 min, temperature rise 6°C/min, temperature limit 200°C, and post-program hold 0 min. The conditions for operating the HP 5890 chromatograph equipped with the 0.25 mm i.d. capillary column were similar, except for a 1:50 split ratio, a carrier gas flow of 0.8 ml/min, and a 8-min pre-program hold.

The response factors are determined by analyzing a reference sample (a titanium chelate of acetylacetone and the alcohol of interest).

A gas chromatogram is shown in Fig. 1.

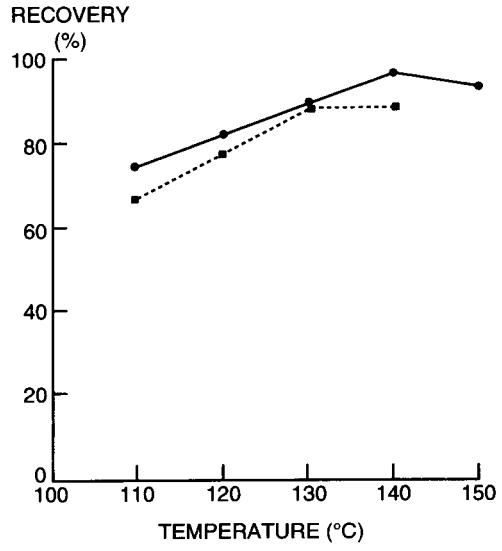

Fig. 2. Acetylacetone recovery from the acetylacetone–isopropyl alcohol titanium chelate as a function of solvolysis temperature (solid line: 2 h solvolysis time, dotted line: 1 h solvolysis time).

RESULTS AND DISCUSSION

Determination of acetylacetone

Acetic acid reacts with the titanium chelate and liberates acetylacetone and the alcohol(s):

$$Ti(OR)_2(CH_3COCHCOCH_3)_2 + 4CH_3COOH \rightarrow Ti(OOCCH_3)_4 + 2ROH + 2CH_3COCH_2COCH_3$$

The reaction mixture is silylated to convert the excess acetic acid into a non-acidic form, $CH_3COOSi(CH_3)_3$, more suitable for gas chromatography. Silylation of the reaction mixture with BSTFA [*N*,*O*-bis(trimethylsilyl)trifluoroacetamide] is sufficiently rapid at the ambient temperature.

BSTFA converts the liberated acetylacetone to the trimethylsilyl derivative of the enol form [7]:

$$CH_3C(OSi(CH_3)_3)=CHCOCH_3$$

The quantitative separation of acetylacetone from its titanium chelate by solvolysis with acetic acid requires drastic conditions. The yield of acetylacetone increases with increasing temperature to about 140–150°C (Fig. 2) and time to 4–5 h (Fig. 3). However, acetylacetone is stable under these reaction conditions, as indicated by recovery experiments (Table 1).

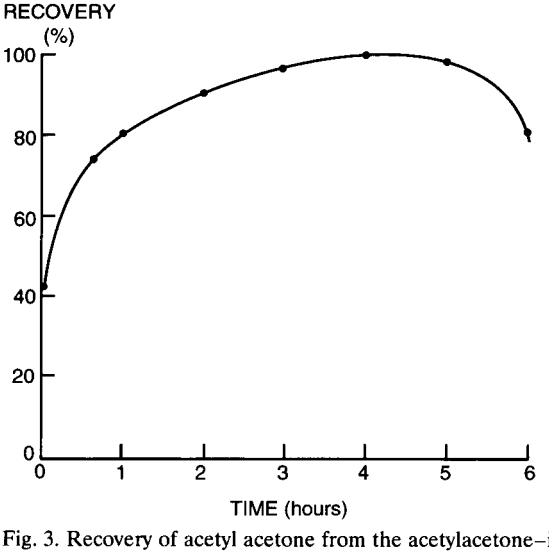

Fig. 3. Recovery of acetyl acetone from the acetylacetone–isopropyl alcohol titanium chelate as a function of solvolysis time at 140°C.

TABLE 1

Recovery of acetylacetone

Reaction mixture [a]	Recovery (%)		
	Heated for 1 h at 140°C	Heated for 2 h at 140°C	Heated for 4 h at 150°C
ACAC + acetic acid	96	97	100
ACAC + isopropyl alcohol + *n*-butyl alcohol	96	97	
ACAC + acetic acid + tetraisopropyl titanate	84	90	

[a] ACAC = acetylacetone. The reagents were used in concentrations usually present in the solvolysis medium.

TABLE 2

Precision of the acetic acid method [b]

	$\bar{x}$ (%)	σ (%)	CL (%)
Ti diacetylacetonate diisopropylate [a]			
Acetylacetone	41.3	±0.32	±0.82
Isopropyl alcohol	49.6	±0.21	±0.54
"Tyzor"® GBA			
Acetylacetone	45.3	±0.23	±0.59
Isopropyl alcohol	27.4	±0.33	±0.85
n-Butyl alcohol	9.3	±0.07	±0.17

[a] The calculated value for acetylacetone is 41.3% and for isopropyl alcohol 49.6%, based on the titanium content of 9.9%. $\bar{x}$ = Average value; σ = standard deviation; CL = 95% confidence limits.

For practical purposes the optimum solvolysis time of 4 h can be shortened to 2 h at 140°C, if a reference sample is analyzed simultaneously as a calibration standard.

Determination of alcohol

The liberated alcohol(s) are converted by acetic acid to the corresponding acetates but, depending on the alcohol structure and the reaction time, the esterification reaction may not go to completion:

$$2ROH + 2CH_3COOH \rightarrow 2CH_3COOR + 2H_2O$$

The esterification of the "free" alcohol is initially rapid because the esterification reaction is catalyzed by the titanium chelate initially present. As the solvolysis proceeds the rate of esterification decreases because solvolysis eliminates the catalytic effect of the titanium chelate. A complete esterification of isopropyl alcohol, as a secondary alcohol, requires therefore an excessively long reaction time. The relative amount of residual isopropyl alcohol decreases with the increasing solvolysis time and becomes insignificant when the solvolysis time is extended to 6 h at 140°C. *n*-Butyl alcohol, being a primary alcohol, is esterified at faster rate and 2 h heating at 140°C is sufficient for complete esterification.

The fraction of isopropyl alcohol not esterified by acetic acid is silylated with BSTFA to the trimethylsilyl ether $ROSi(CH_3)_3$. A complete esterification of isopropyl alcohol requires a longer reaction time than required to liberate acetylacetone. Hence isopropyl alcohol elutes as two peaks: as isopropyl acetate and the trimethylsilyl derivative of isopropyl alcohol. Both peak areas have to be taken in account for a quantitative result.

A complete esterification of isopropyl alcohol in already 2 h at 140°C can be achieved by using acetic anhydride for the solvolysis of the titanium chelate. Presumably acetic anhydride displaces alkoxide groups bonded to titanium and forms hexaacetoxydititanoxane and the corresponding acetate:

$$2Ti(OR)_4 + 7(CH_3CO)_2 \rightarrow (CH_3COO)_3Ti - O - Ti(OOCCH_3)_3 + 8CH_3COOR$$

However, acetylacetone is partially degraded by hot acetic anhydride and cannot be quantita-

TABLE 3

Accuracy and precision of the acetic anhydride method

Isopropyl alcohol			*n*-Butyl alcohol found (%)
Added (%)	Found (%)	Deviation abs. (%)	
0	8.05	–	80.7
0.77	8.75	−0.07	
1.53	9.78	+0.20	81.6
1.56	9.41	−0.20	
3.09	11.27	+0.13	80.6
			Avg. 81.0 [a]

[a] The calculated value for 100% purity is 87.1% *n*-butyl alcohol. The value found is 93% of the calculated value, in agreement with 8% isopropyl alcohol found in the sample of tetra-*n*-butyl titanate.

tively determined. Hence the acetic anhydride method is useful only for the determination of alcohols in titanium chelates or in titanates.

Accuracy and precision

The accuracy of the method was determined adding known amounts of acetylacetone to tetraisopropyl titanate, which reacts rapidly with acetylacetone and forms the chelate. The recovery of acetylacetone after heating for 1 or 2 h at 140°C in acetic acid was essentially quantitative in the absence of tetraisopropyl titanate but incomplete in the presence of tetraisopropyl titanate. This indicates that the complete cleavage of the chelate formed and not the degradation of acetylacetone is limiting the accuracy of the method. Increasing the solvolysis time increases the acetylacetone recovery until an essentially complete recovery is achieved at 140°C in 4–5 h after which the recovery decreases.

The precision of the method using acetic acid as the reagent for solvolysis is shown in Table 2 for titanium diacetylacetonate diisopropylate (I) and for "Tyzor" GBA, both analyzed six times.

The accuracy and precision of the acetic anhydride method was determined by analyzing tetra-*n*-butyl titanate spiked with known amounts of isopropyl alcohol (Table 3).

The author acknowledges the assistance of Ward R. Gibson with gas chromatography.

REFERENCES

1 C.S. Rondestvedt, Jr., in Kirk-Othmer Encyclopedia of Chemical Technology, Vol. 23, Wiley, New York, 3rd edn., 1983, p. 176.
2 S. Coffey (Ed.), Rodds's Chemistry of Carbon Compounds, Vol. I, Part D, Elsevier, Amsterdam, 1965, p. 71.
3 L. Knorr, Ber. Dtsch. Chem. Ges., 44 (1911) 2771.
4 M.L. Eidinoff, J. Am. Chem. Soc., 67 (1945) 2072.
5 G. Schwarzenbach and K. Lutz, Helv. Chim. Acta, 23 (1940) 1147.
6 Polyfunctional Tyzor® Organic Titanates, Du Pont Co., 1983.
7 R. West, J. Am. Chem. Soc., 80 (1958) 3246.

Analytica Chimica Acta, 281 (1993) 391–396
Elsevier Science Publishers B.V., Amsterdam

Investigation of liquid chromatographic systems for the separation of sulphonium salts

Valérie Massardier

Laboratoire des Matériaux Organiques, Centre National de la Recherche Scientifique, B.P. 24, F-69390 Vernaison (France)

Jean Vialle

Service Central d'Analyse, Centre National de la Recherche Scientifique, B.P. 22, F-69390 Vernaison (France)

(Received 16th November 1992)

Abstract

The liquid chromatographic separation of basic compounds encounters often many problems related to interactions between these analytes and the usual silica-based stationary phases. In this study, the difficulty of separating sulphonium salts used in the synthesis of poly(*p*-phenylenevinylene) is discussed. A chromatographic system using a polymer-based column for the separation of these compounds was developed that also demonstrated the high reactivity and instability of some tetrahydrothiophenium salts.

Keywords: Liquid chromatography; Poly(*p*-phenylenevinylene); Sulphonium salts

Disulphonium salts are now widely used for the preparation of the promising electrically conducting poly(*p*-phenylenevinylene) (PPV). The commonly used method for obtaining PPV is through its soluble precursor by the Wessling route [1], as shown by the reaction

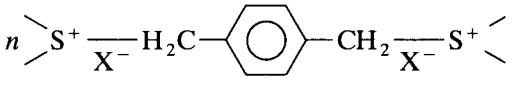

II

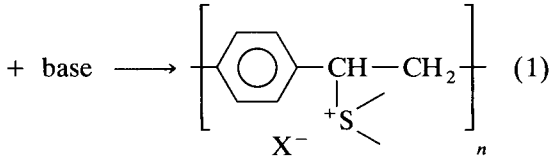

IIIa (1)

where $S^+\!\!<$ = cyclic or aliphatic sulphonium and X^- = halide anion. This method leads to high molecular weight products and it could be of interest to limit and control it by adding a monosulphonium molecule according to

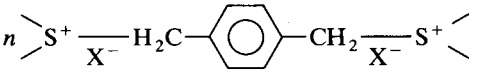

II

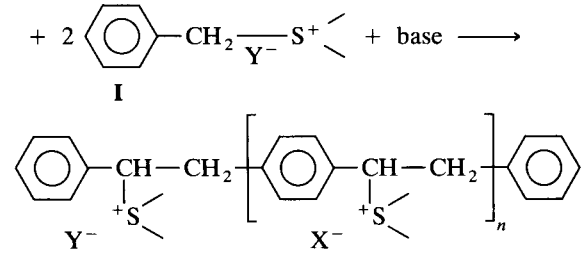

IIIb (2)

where Y^- = halide anion.

Correspondence to: J. Vialle, Service Central d'Analyse, Centre National de la Recherche Scientifique, B.P. 22, F-69390 Vernaison (France).

An analytical procedure can be derived for the kinetic study of both reactions 1 and 2 through the determination of disulphonium compounds, benzyl tetrahydrothiophenium bromide (**I**) and *p*-xylylene tetrahydrothiophenium chloride (**II**) in the above case. The residual amounts of these two molecules can be determined in the reaction medium by chromatographic analysis after precipitation of polymer **III** by counter ion exchange [2].

As **I** and **II** have both ionic and lipophilic character, several routes could be considered to achieve their separation by liquid chromatography (LC). As described by Vialle et al. [3] for ammonium salts, separation by an ion-exchange mechanism was first investigated. Ion pairing on a bonded silica stationary phase and on a more efficient polymer-based reversed-phase packing was also tried.

EXPERIMENTAL

Ion-exchange chromatography was performed on a computerized LIREC Automatic C.917 system with a LIREC 907 S UV detector at 254 nm. The column was Nucleosil SA (sulphonated bonded silica) with 5-μm particles (25 cm $\times$ 4.6 mm i.d.). Injections were made using a Rheodyne valve with a 20-μl loop. The mobile phases were hydrochloric acid–potassium chloride buffer solutions (pH 2) with added potassium nitrate concentrations between 0.01 and 0.04 M.

Reversed-phase LC was performed using a Waters pump and a Waters Model 455 spectrophotometer at 254 nm. The columns used were Nucleosil C_{18} (5 μm) (15 cm $\times$ 4.6 mm i.d.) and Hamilton PRP-1 (5 μm) (15 cm $\times$ 4.1 mm i.d.). Injections were made using a Valco N60 valve equipped with a 10-μl loop.

With the Nucleosil C_{18} column the mobile phases were methanol–water or acetonitrile–water solutions with sodium pentanesulphonate added to obtain 1.0×10^{-3}–1.0×10^{-2} M concentrations and with 2.0×10^{-2}–7.4×10^{-2} g l^{-1} potassium nitrate as a masking agent of silanols [4].

With the Hamilton PRP-1 column the mobile phases were methanol–water or acetonitrile–water, with or without added 3.0×10^{-3}–1.0×10^{-2} M sodium pentanesulphonate, as indicated in Table 1.

In all the instances, the compounds were dissolved in deionized water, mobile phases were degassed ultrasonically and the mobile phase flow-rate was 1 ml min^{-1}.

RESULTS AND DISCUSSION

Ion-exchange chromatography

The various systems investigated did not give successful results and none of the mobile phases permitted the elution of both monomers, contrary to what was obtained for ammonium compounds in similar conditions [3]. This difficulty seems to be due to strong interactions between sulphonic acid salts and sulphonium groups, as discussed below.

Ion-pair chromatography on C_{18} packings

When separations of sulphonium salts were carried out, the mobile phase was acetonitrile–water. Addition of potassium nitrate was necessary to avoid excessive tailing of the peaks obtained for **I** and **II**, probably due to the strong interaction of these basic compounds with residual silanols. However, it was not possible to eliminate peak tailing totally, as shown in Fig. 1. Moreover, as will be shown later, the presence of pentanesulphonate as an ion-pairing agent adversely affects the use of this system as a general separation method for such ionic compounds because some sulphonium salts react with sodium pentanesulphonate.

Reversed-phase chromatography on polymer packings

These packings were used to remove the influence of residual silanols of the C_{18} column. In Table 1 are displayed the retention volumes obtained on injecting compounds **I** and **II** on to a PRP-1 column, with different mobile phase compositions. Chromatograms are shown in Figs. 2–4. The first experiments were done with mobile phases containing acetonitrile as organic solvent and pentanesulphonate as ion-pairing agent. As

expected, the peak tailing was reduced and for organic solvent contents below 25% the differences in retention for **I** and **II** led to a satisfactory separation. However, in the presence of pentanesulphonate in the mobile phase, injection of **II** always gave two peaks, as shown in Fig. 2a. Without pentanesulphonate, a single peak was observed for this compound and the retentions were only slightly decreased for both **I** and **II**, as shown by comparing experiments (d) and (e) in Table 1. The elution was performed without peak tailing as shown in Fig. 3. Increasing the water content of the mobile phase improved the separation, as displayed by experiments (e) to (i) in Table 1, whichever organic solvent, acetonitrile or methanol, was used. With pure water as eluent, the peaks were slightly broadened but with no tailing and the resolution was excellent, as shown in Figs. 3b and 4.

These results clearly show that, even when an ion-pairing salt is added to the mobile phase, the retention of sulphonium compounds is caused to a large extent by a lipophilic rather than an ion-pairing mechanism. It shows also that **II** has a lower lipophilic character than **I** owing to the presence of two ionic sites instead of one and despite the larger hydrocarbon framework of molecule **I**.

Behaviour of p-xylylene sulphonium in the presence of sodium pentanesulphonate

As mentioned above, experiments carried out in the presence of sodium pentanesulphonate gave two distinct peaks, IIa and IIb, for **II**,

TABLE 1

Evolution of the retention for sulphonium compounds with various mobile phases on a PRP-1 column.

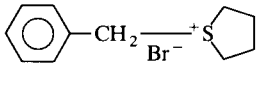

I

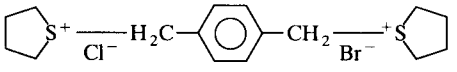

II

Mobile phase composition [a]	Injected sample [a]	Retention volume, V_r (ml)	Corresponding Fig.
(a) ACN–H_2O (12.5 : 87.5), 3.0×10^{-3} M PS	**I**	4.3	
	II	1.4–2.6	
(b) ACN–H_2O (16.7 : 83.3), 3.0×10^{-3} M PS	**I**	3.0	
	II	1.4–2.4	
(c) ACN–H_2O (25.0 : 75.0), 3.0×10^{-3} M PS	**I**	2.2	
	II	1.4–2.0	
(d) ACN–H_2O (25.0 : 75.0), 1.0×10^{-2} M PS	**I**	2.3	
	II	1.4–2.0	2a
	II + PS	2.0	2b
(e) ACN–H_2O (25.0 : 75.0)	**I**	2.0	
	II	1.4	3a
(f) MeOH–H_2O (25.0 : 75.0)	**I**	2.5	
	II	1.4	
(g) MeOH–H_2O (15.0 : 85.0)	**I**	2.8	
	II	1.4	
(h) MeOH–H_2O (5.0 : 95.0)	**I**	4.1	
	II	1.4	
(i) H_2O	**I**, freshly prepared	6.3	4a
	II	1.9	3b
	I after 1 h	2.1–4.5–6.1	4b
	I after 6 months	2.1–5.3	4c

[a] ACN = acetonitrile; PS = pentanesulphonate.

whereas a single peak was always obtained for benzyl tetrahydrothiophenium [experiments (a) to (d) in Table 1]. Moreover, on adding this sulphonate salt to an aqueous sample of **II**, only peak IIb remained, as shown in Fig. 2, corresponding to a compound eluted at a higher retention time, and therefore possessing a more lipophilic character. On the basis of these results and of reaction 1, it can be considered that the basic character of pentanesulphonate can bring about the formation of oligomers with **II** but it is not strong enough to react with the more ionic **I**. Similar compounds to **II** such as *p*-xylylene diethyl sulphonium could show the same behaviour.

NMR analyses are consistent with these results. The ^1H NMR spectrum of an equimolar mixture of monomer **II** and sodium pentanesulphonate, after reaction for 24 h, is shown in Fig. 5. It may correspond to a mixture of monomeric and oligomeric structures. Whereas there is only one type of aromatic protons in pure **II**, a second peak appears at a higher chemical shift, characteristic of oligomers, for **II** in the presence of pentanesulphonate. Under the same conditions, freshly prepared monomer **I** does not seem to react with pentanesulphonate, as it gives no change in the NMR spectrum.

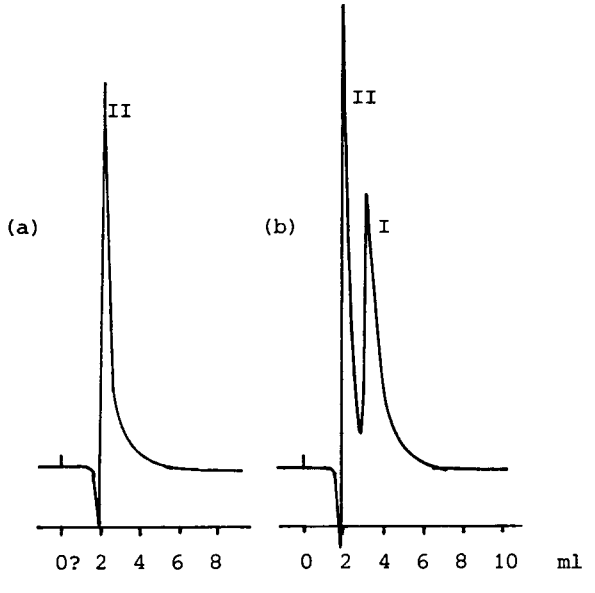

Fig. 1. Chromatograms of (a) compound **I** and (b) a mixture of **I** and **II** with a Nucleosil C_{18} column. Mobile phase, acetonitrile–water (25:75, v/v) containing 0.037 M potassium nitrate.

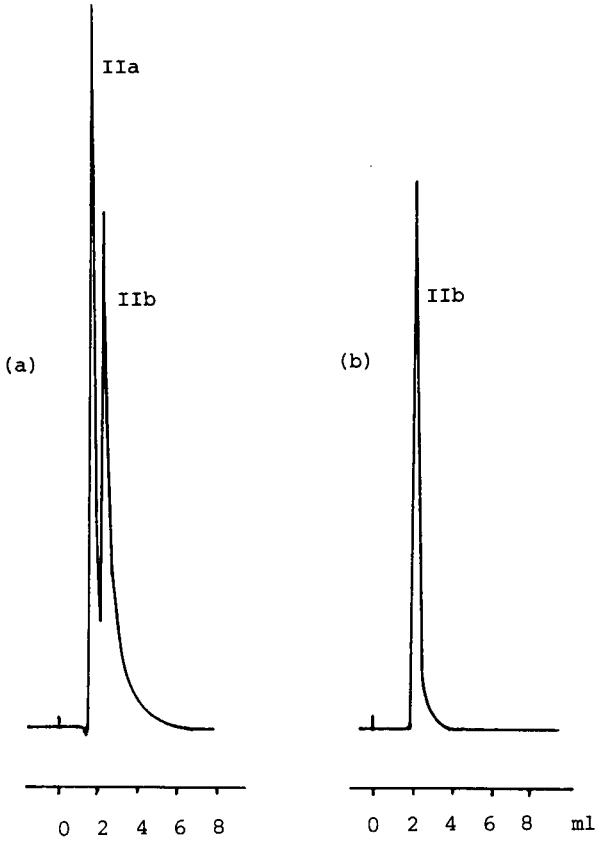

Fig. 2. Chromatograms of compound **II** on a Hamilton PRP-1 column. (a) Injection of an aqueous sample; (b) injection of an aqueous sample with pentanesulphonate added. Mobile phase, acetonitrile–water (25:75, v/v) containing 0.01 M pentanesulphonate.

In conclusion, as both the chromatographic and ^1H NMR results are in good agreement, it can be stated that sodium pentanesulphonate is probably a strong enough base for generating a rapid oligomerization of monomer **II**. This clearly shows why the two previously described chromatographic systems (with Nucleosil SA and Nucleosil C_{18} columns) must be used carefully, because sulphonate salts are present in them as ionic sites or as ion-pairing compounds. Among the three columns tested, the Hamilton PRP-1 column is the only one that works successfully, whichever sulphonium compound is present. Monosulphonium molecules seem less reactive,

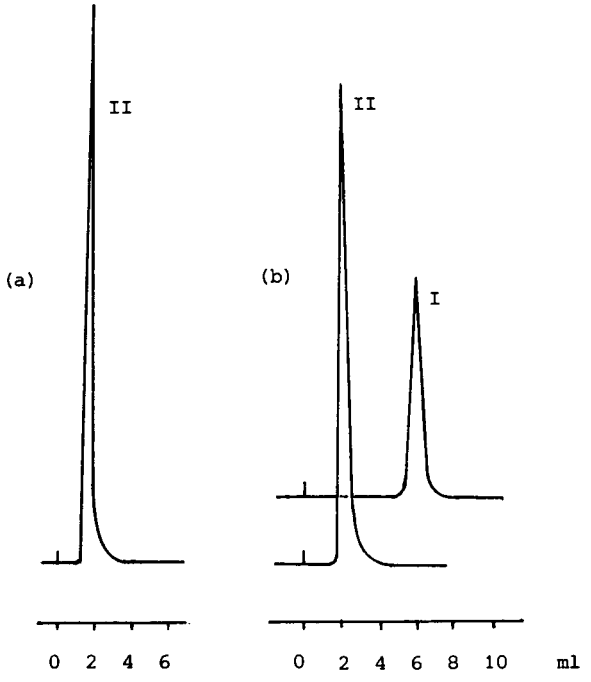

Fig. 3. Chromatograms of **I** and **II** on a Hamilton PRP-1 column with different mobile phases; (a) acetonitrile–water (25:75, v/v); (b) water.

but as they are highly unstable, as shown below, in particular in water, it is more difficult draw conclusions with certainty.

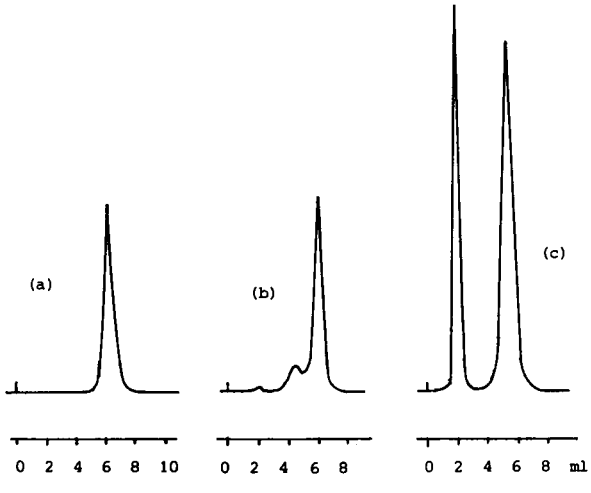

Fig. 4. Study of the stability of **I**. (a) Freshly prepared sample; (b) after storage for 1 h; (c) after storage for 6 months. Column, PRP-1; mobile phase, water.

Reagent stability

Stability tests were performed after storage for 6 months in the dark at −20°C. After this time, monomer **II** gave only one peak with a water eluent whereas the chromatography of monomer **I** led to several peaks, as shown in Fig. 4. Before the elution of molecule **I**, two other compounds are eluted at lower retention volumes. In aqueous medium, this monosulphonium compound is highly unstable as it was observed that in less than 1 h after its preparation, it led to two additional peaks, the height of which increased with ageing. After storage for 6 months, a single degradation peak was left. Under similar conditions, an aqueous solution of monomer **II** remained stable for several days [(i) in Table 1 and Fig. 3a)].

Chromatographic analysis of some sulphonium salts

The validity of the chromatographic system based on the Hamilton PRP-1 column was studied with several other sulphonium salts: *p*-xylylene tetrahydrothiophenium bromide (**IV**), *p*-xylylene diethylsulphonium bromide (**III**), tetra-

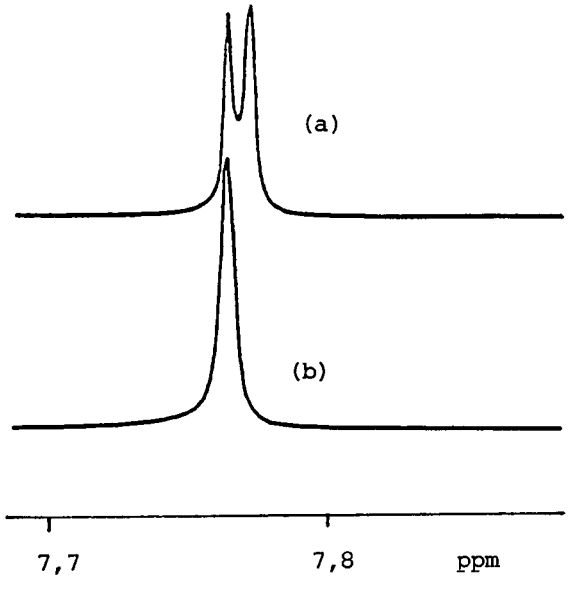

Fig. 5. ^{1}H NMR spectra of monomer **II** (a) with and (b) without added pentanesulphonate, 0.10 M in a 0.10 M deuterated water solution. Spectrometer, Bruker AC 250.

TABLE 2

Retention volumes of sulphonium salts

Formula	Injected sample	Retention volume, V_r (ml)
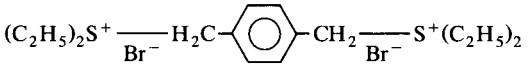	III	2.4
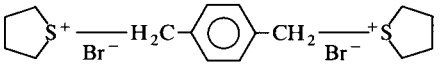	IV	2.1
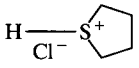	V	1.5
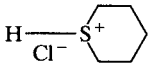	VI	1.4
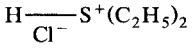	VII	1.3

hydrothiophenium chloride (**V**), hexamethylene sulphonium chloride (**VI**) and diethylsulphonium chloride (**VII**). They can be eluted without or with weak peak tailing but their retention volumes are generally very low, as shown in Table 2, because most of them (**V**, **VI** and **VII**) have a very weak lipophilic character.

Conclusion

This work provided consistent results that show the interactions that can occur between some sulphonium and sulphonate salts. On the basis of these observations, chromatographic systems based on ion-pairing interactions between these two kinds of compounds must be used carefully. Even if a Nucleosil C_{18} column can be used for some sulphonium salts, it is much more judicious to use a Hamilton PRP-1 column, which creates stronger lipophilic interactions with sulphonium compounds. Moreover, it does not require addition of sodium sulphonate to the mobile phase while maintaining good efficiency compared with a bonded silica-based column. This polymer packing with water as eluent seems to be of general use for the separation of sulphonium salts. However, the stability of some of these salts is questionable, as shown for molecule **I**.

REFERENCES

1 R.A. Wessling and R.G. Zimmerman, US Pat., 3 401 152 (1968).
2 J.M. Machado, F.R. Denton, J.B. Schlenoff, F.E. Karasz and P.M. Lahti, J. Polym. Sci., Part B, 27 (1989) 199.
3 J. Vialle, P. Navarro, T.T. Nguyet, P. Lanteri and R. Longeray, J. Chromatogr., 549 (1991) 159.
4 M. Khalil, Thesis, University of Lyon, Lyon, 1986.

Analytica Chimica Acta, 281 (1993) 397–400
Elsevier Science Publishers B.V., Amsterdam

β-Cyclodextrin in the capillary isotachophoretic separation of chlorophenols

Petr Praus

Chemical Laboratory, Povodí Odry, Varenská 49, 701 26 Ostrava (Czech Republic)

Václav Dombek

Institute of Industrial Landscape Ecology, Czech Academy of Sciences, Hladnovská 9, 710 00 Ostrava (Czech Republic)

(Received 5th January 1993)

Abstract

The separation of pentachlorophenol, 2,4,6-trichlorophenol, 2,4,5-trichlorophenol and 2,4-dichlorophenol by capillary isotachophoresis was studied. Complete resolution of these compounds was achieved by adding β-cyclodextrin to the leading electrolyte.

Keywords: Electrophoresis; Chlorophenols; Cyclodextrin; Isotachophoresis

The ability of cyclodextrins (CDs) to separate structurally different compounds has been used in analytical applications for several years. These cyclic oligosaccharides, mostly consisting of 6–8 linked glucose units (α-, β-, γ-CD), are modelled as conical cavities with a hydrophobic interior surface and a hydrophilic rim (primary and secondary hydroxyl groups) [1,2]. The separation mechanism based on the formation of cyclodextrin inclusion complexes with separands has been described theoretically [3] and investigated by a variety of instrumental methods [4,5].

The applications of CDs in some chromatographic [1,6–8] and electromigration methods [9,10] have been reviewed. A substantial proportion of the latter applications is represented by isotachophoretic (ITP) separations [11–21]. CDs, added to leading electrolytes, do not undergo ionization over a wide pH range and do not migrate electrophoretically. The separation effects of CDs are not restricted to separands and an influence on counter ions has also been observed [13].

The ITP separation conditions of chlorophenols were studied recently [22]. The four widespread chlorophenols pentachlorophenol (PCP), 2,4,6-trichlorophenol (2,4,6-TCP), 2,4,5-trichlorophenol (2,5,6-TCP) and 2,4-dichlorophenol (2,4-DCP) were separated isotachophoretically in two-electrolyte systems. The aim of this work was to test the use of β-CD for the separation of chlorophenols in a model solution.

EXPERIMENTAL

Instrumentation

A CS Isotachophoretic Analyser (VVZ PJT, Spišská Nová Ves) in a one-column configuration (150 × 0.3 mm i.d.) provided with a conductivity detector was used for all measurements. The

Correspondence to: P. Praus, Chemical Laboratory, Povodí, Varenská 49, 701 26 Ostrava (Czech Republic).

current was kept constant at 75 μA and after about 600 s was switched to 25 μA. Isotachopherograms were recorded on a TZ 4200 two-channel recorder (Laboratorní přístroje, Prague) at a chart drive speed of 1 mm s^{-1}. The pH values of the operational systems were measured with a digital pH meter from Radelkis (Budapest). Sampling was performed with Hamilton microsyringes (maximum volume 10 μl).

Chemicals

All chemicals were of analytical-reagent grade. Hydrochloric acid, methanol, sodium hydroxide and barium hydroxide were obtained from Lachema (Brno), L-asparagine monohydrate from Merck (Darmstadt), tris(hydroxymethyl)aminomethane (Tris) from Serva (Heidelberg), poly(vinyl alcohol) (PVA) from Riedel-de Haën (Seelze, Germany) and chlorophenols from Supelco (Bellefonte, PA). β-Cyclodextrin was obtained as a gift from Professor E. Smolková-Keulemansová (Department of Analytical Chemistry, Charles University, Prague).

Tris was purified by recrystallization from methanol. PVA was purified on a mixed-bed ion exchanger. Standard solution of chlorophenols (100 mg l^{-1}) was prepared by dissolution of PCP, 2,4,5-TCP, 2,4,6-TCP and 2,4-DCP in 0.1 M sodium hydroxide solution and dilution to volume with demineralized water (specific conductivity up to 2 μS cm^{-1}).

RESULTS AND DISCUSSION

Isotachophoretic separation

As reported previously, chlorophenols can be sufficiently separated according to their pK values [22]. In this work, the possibility of breaking down a mixture of these compounds by adding β-CD to the leading electrolyte was tested. For this purpose operational systems at pH_L (pH of leading electrolyte) 6.25 (Table 1) and 7.80 [22] were used. The former system is not sufficiently buffered. More mobile OH^- ions penetrate into zones of chlorophenols and make them alkaline. Under these conditions, the migration of 2,4-DCP is possible. PCP and 2,4,6-TCP migrate in a stable mixted zone and 2,4,5-TCP and 2,4-DCP are separated according to their pK values similarly to that at $pH_L = 7.80$. The main advantage of this system is the stability over a wide pH_L range (tested from 6.10 to 7.30).

TABLE 1

Operational system used in the separation of chlorophenols

Parameter	Leading electrolyte	Terminating electrolyte
Anion	Cl^-	Asparagine
Concentration (mM)	10	5
Counter ion	Tris	Ba^{2+}
pH	6.25	9.5–10.0
Complex-forming agent	β-CD	–
Concentration range (mM)	0–8.0	–
Additive	PVA	–
Concentration (%, w/v)	0.05	–
Solvent	Water	Water

To demonstrate the effect of β-CD on the effective mobilities of chlorophenols, the relative step heights (rsh) obtained from the response of the conductivity detector were plotted against the molar concentration of β-CD in the leading electrolyte (Fig. 1). The rsh values were calculated using the equation

$$\text{rsh} = (h_i - h_L)/(h_T - h_L) \quad (1)$$

where h_i, h_L and h_T are the step heights of the analyte, leading and terminating ions, respectively.

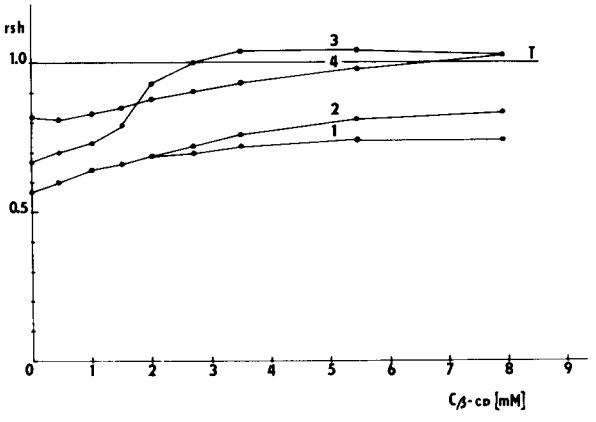

Fig. 1. Effect of the amount of β-CD added to the leading electrolyte on the rsh values of (1) PCP, (2) 2,4,6-TCP, (3) 2,4,5-TCP and (4) 2,4-DCP. T = Asparagine.

It is known that the inclusion mechanism of CDs is based not only on the penetration of a separand inside the cavity but also on Van der Waals interactions, which are regarded as the dominant binding forces [1]. From NMR and circular dichroism studies [4,5], the existence of strong hydrogen bonding between host and guest molecules was also demonstrated.

Figure 1 illustrates the migration behaviour of chlorophenols on adding β-CD to the leading electrolyte. With increasing amount of complex-forming agent, improvement of the ITP resolution of PCP and 2,4,6-TCP is achieved. In this instance, the molecular dimensions of 2,4,6-TCP make it more suitable than the bulky PCP insertion into the β-CD cavity. The 2,4,5-isomer is much more strongly retarded so that at higher concentrations of β-CD it migrates in an inverse zone. This stable complex with β-CD can be explained by the formation of hydrogen bonds. The migration of 2,4-DCP also indicates a significant influence of β-CD. The effective mobility of 2,4-DCP gradually decreases until its zone forms an inverse mixed zone with 2,4,5-TCP. This finding is consistent with the relatively small size of this compound, which facilitates its penetration into the β-CD cavity. Similar results were obtained from measurements of rsh values at $pH_L = 7.80$.

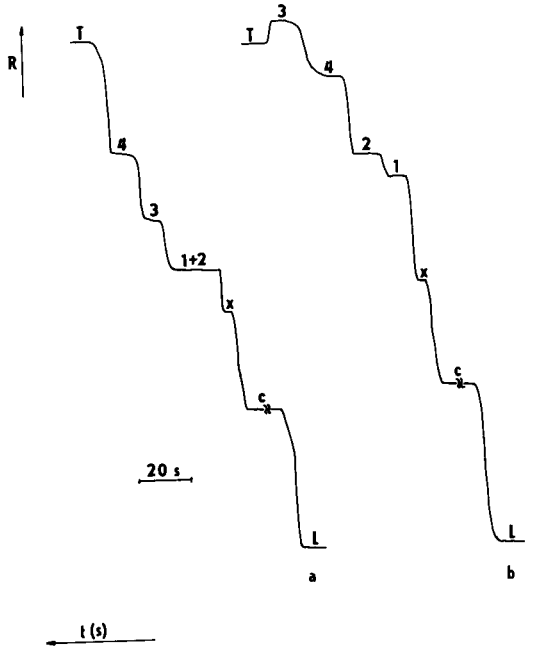

Fig. 2. Isotachopherograms for the separation of chlorophenols. Injection volume, 2 μl of standard mixture; detection current, 25 μA. (a) Without β-CD; (b) with 4 mM β-CD. 1 = PCP; 2 = 2,4,6-TCP; 3 = 2,4,5-TCP; 4 = 2,4-DCP; c = HCO_3^-; x = impurity; L = CL^-; T = asparagine. t = Time; R = resistance.

TABLE 2

Parameters of the regression equation of the calibration lines ($y = a + bx$) [a] in the concentration range 50–500 ng μl^{-1}

Compounds	a	b	Correlation coefficient	No. of data points
PCP	2.21	4.78	0.9977	10
2,4,6-TCP	−0.48	6.27	0.9986	9
2,4,5-TCP	1.15	6.75	0.9974	10
2,4-DCP	1.84	7.03	0.9987	10

[a] x = Volume in μl; y = zone length in mm.

From Fig. 1, the optimum concentration of β-CD in the leading electrolyte was calculated to be 4 mM in order to determine all chlorophenols in one ITP run with sufficient resolution (Fig. 2). The stability of the separated zones was verified by construction of calibration lines (Table 2). The zone lengths were evaluated from the differential conductivity signal.

Conclusion

The ITP separation of chlorophenols is possible not only according to their pK values in several systems but also in one operational system by adding β-CD to the leading electrolyte. A successful separation of PCP, 2,4,6-TCP, 2,4,5-TCP and 2,4-DCP using β-CD was achieved.

Note: The authors apologize for the wrong description of the concentration axes in Fig. 3a and b of Ref. 22. The concentrations of chlorophenols should be given in ng/μl.

REFERENCES

1 E. Smolková, in J. Zýka (Ed.), Nové Směry v Analytické Chemii, Svazek II, SNTL Prague, 1984, p. 58.
2 S. Krýsl and E. Smolková-Keulemansová, Chem. Listy, 79 (1985) 912.

3 R.E. Boehm and D.E. Martire, Anal. Chem., 60 (1988) 522.
4 S. Li and W.C. Purdy, Anal. Chem., 64 (1992) 1405.
5 M. Hoshino, M. Imamura, K. Ikehara and Y. Hama, J. Phys. Chem., 85 (1981) 1820.
6 M. Příhoda, V. Miller, V. Pacáková and K. Štulík, Chem. Listy, 85 (1991) 583.
7 M. Petro and D. Berek, Chem. Listy, 86 (1992) 816.
8 W.L. Hinze, D.Y. Pharr, Z.S. Fu and W.G. Burkert, Anal. Chem., 61 (1989) 422.
9 J.D. Olechno, J.M.T. Tso, J. Thayer and A. Wainright, Int. Lab., May (1991) 42.
10 J. Snopek, I. Jelínek and E. Smolková-Keulemansová, J. Chromatogr., 452 (1988) 571.
11 S. Fanali, J. Chromatogr., 470 (1989) 123.
12 J. Snopek, I. Jelínek and E. Smolková-Keulemansová, J. Chromatogr., 411 (1987) 153.
13 I. Jelínek, J. Snopek and E. Smolková-Keulemansová, J. Chromatogr., 557 (1991) 215.
14 I. Jelínek, J. Snopek and E. Smolková-Keulemansová, J. Chromatogr., 405 (1987) 379.
15 I. Jelínek, J. Dohnal, J. Snopek and E. Smolková-Keulemansová, J. Chromatogr., 435 (1988) 496.
16 J. Snopek, I. Jelínek and E. Smolková-Keulemansová, J. Chromatogr., 438 (1988) 211.
17 I. Jelínek, J. Snopek and E. Smolková-Keulemansová, J. Chromatogr., 439 (1988) 386.
18 J. Snopek, E. Smolková-Keulemansová, I. Jelínek, J. Dohnal, J. Klinot and E. Klinotová, J. Chromatogr., 450 (1988) 373.
19 I. Jelínek, J. Dohnal, J. Snopek and E. Smolková-Keulemansová, J. Chromatogr., 464 (1989) 139.
20 J. Snopek, I. Jelínek and E. Smolková-Keulemansová, J. Chromatogr., 472 (1989) 308.
21 I. Jelínek, J. Snopek, J. Dian and E. Smolková-Keulemansová, J. Chromatogr., 470 (1989) 113.
22 P. Praus and V. Dombek, Anal. Chim. Acta, 277 (1993) 97.

Analytica Chimica Acta, 281 (1993) 401–411
Elsevier Science Publishers B.V., Amsterdam

Determination of boron in human serum by inductively coupled plasma mass spectrometry after a simple dilution of the sample

Hans Vanhoe and Richard Dams

Laboratory of Analytical Chemistry, University of Ghent, Institute of Nuclear Sciences, Proeftuinstraat 86, B-9000 Ghent (Belgium)

Carlo Vandecasteele

Department of Chemical Engineering, University of Louvain, de Croylaan 46, B-3001 Heverlee (Belgium)

Jacques Versieck

Department of Internal Medicine, Division of Gastroenterology, University Hospital, De Pintelaan 185, B-9000 Ghent (Belgium)

(Received 27th January 1993; revised manuscript received 21st April 1993)

Abstract

A method for the determination of boron in human serum is described. Serum samples were only treated with 0.14 M HNO_3 (a five-fold dilution). After addition of beryllium as internal standard to correct for matrix effects, samples were introduced with a concentric nebulizer to an inductively coupled plasma mass spectrometer. The magnitude of the boron ion signal was optimized by adjusting the lens voltages and the nebulizer gas flow rate and memory effects, which can be experienced with the conventional methodology for sample introduction, were reduced to an acceptable level by the use of a short (2 min) cleanout procedure. To avoid the overlap from the intense $^{12}C^+$-peak with the $^{11}B^+$-peak, the $^{10}B^+$-peak was used for the boron determinations. This procedure gave a boron blank level of about 1.7 $\mu g\ l^{-1}$ and a detection limit of 0.5 $\mu g\ l^{-1}$ for human serum. External calibration was applied for the quantitation of boron. The proposed method was tested by analysing a "second-generation" biological reference material Freeze-Dried Human Serum (University of Ghent). Results are also given for three other biological reference materials, namely Wheat Flour SRM 1567a, Bovine Liver SRM 1577a and Total Diet SRM 1548 (National Institute of Standards and Technology). Analyses of serum samples from twelve healthy individuals yielded boron concentrations ranging from 4.1 to 25.8 $\mu g\ l^{-1}$.

Keywords: Mass spectrometry; Sample preparation; Boron; Plasmas; Serum

Boron is known to be essential for higher plants [1]. Although there are no indications that it is also essential for animal or human life, a determination of the element in biological materials is desirable because of the increasing evidence of the nutritional importance of boron, more particularly as an agent for optimum calcium and, thus, bone metabolism [2]. Another field where boron determinations are necessary is the study of the potential usefulness of various tumor-localizing boron-containing compounds for boron neutron capture therapy of cancer [3]. The extensive use of boron in the nuclear industry, in agriculture, in metal production and in electron-

Correspondence to: H. Vanhoe, Laboratory of Analytical Chemistry, University of Ghent, Institute of Nuclear Sciences, Proeftuinstraat 86, B-9000 Ghent (Belgium).

ics makes this element also a possible monitor for environmental pollution.

The determination of boron in biological samples is a difficult analytical task, because of the very low concentrations found in several tissues and fluids (e.g. blood serum). In addition, samples can be readily contaminated with boron during the sample preparation, especially if mineral acids are used in combination with borosilicate glassware. Published analytical methods for boron include neutron-capture prompt γ-ray activation analysis (PGAA) [4–6], neutron activation mass spectrometry (NA-MS) [7,8], thermal ionization mass spectrometry (TIMS) [9], inductively coupled plasma (ICP)- [10,11] and direct current plasma (DCP)- [12] atomic emission spectroscopy (AES). Disadvantages of some of these methods (PGAA, NA-MS and TIMS) are an extensive sample preparation, a long analysis time and a low sample throughput; the others (ICP-AES and DCP-AES) offer rather high detection limits (40 $\mu g\ l^{-1}$ [10]) and are not suitable for ultra-trace analyses. ICP-MS has the advantage of a faster analysis time, a less complicated sample preparation and a high sensitivity. ICP-MS has been used for the determination of boron concentrations and isotope ratios in geological [13], environmental [14], industrial [15] and biological [16,17] materials.

In the course of a systematic study of the determination of trace and ultra-trace elements in human serum by ICP-MS [18–21], we noticed that low detection limits for boron in serum can be obtained. Therefore, we decided to study the determination of the element in human serum in detail. Abou-Shakra et al. [16] described the boron determination in several biological tissues (including blood serum), after digestion with nitric acid, resulting in a blank level of 13.8 $\mu g\ l^{-1}$ and a detection limit of 3.3 $\mu g\ l^{-1}$. Smith et al. [17] reported the determination of boron in a variety of biological samples (including blood plasma) by the isotope dilution technique, after a sodium carbonate fusion and a separation of the matrix components using a boron selective ion-exchange resin. This sample preparation was necessary in order to determine accurately the $^{10}B/^{11}B$ ratio. Contrary to the boron determinations in serum by ICP-MS described above, we kept the pretreatment of the serum samples to a minimum. No other pretreatment than a five-fold dilution with 0.14 M nitric acid and an addition of an internal standard (beryllium) was carried out. An advantage of this method is that no acids, employed for the digestion step, increases the boron blank levels. Much attention was paid to the optimization of the magnitude of the boron ion signal by adjusting the lens voltages and the nebulizer gas flow rate and to the reduction of memory effects which may be observed with the conventional methodology for sample introduction. As mentioned by Smith et al. [17] the intense peak from $^{12}C^+$ in biological samples can complicate the measurement of $^{11}B^+$. In the present work, this problem was studied in detail and it was shown that for human serum ^{10}B instead of ^{11}B must be used when boron is not separated from the matrix and is determined by external calibration.

To check the accuracy and precision of the proposed method a serum reference material was employed, namely a "second-generation" biological reference material Freeze-Dried Human Serum prepared by Versieck et al. [22] under rigorously controlled conditions to avoid extraneous additions so that the element concentrations are comparable to those in normal human serum. Because no certified value for boron is available, other biological reference materials were also analysed, namely Wheat Flour SRM 1567a, Bovine Liver SRM 1577a and Total Diet SRM 1548 from the National Institute of Standards and Technology (NIST). As an application, serum samples from twelve healthy individuals were analysed in order to establish the boron concentration in normal human serum.

EXPERIMENTAL

Instrumentation

A VG PlasmaQuad (VG Elemental Ltd., a daughter of Fisons Instruments, Winsford, UK) was used, equipped with a Gilson Minipuls-2 peristaltic pump operating at an uptake rate of 0.9 ml min^{-1} using polyvinylchloride (PVC) tubing (internal diameter of 0.76 mm), a Meinhard

concentric glass nebulizer (type TR-30-A3), a Scott-type double pass spray chamber with surrounding liquid jacket made of borosilicate glass, a connecting elbow made of glass and a quartz Fassel-type torch. Details of the operating conditions are summarized in Table 1.

Reagents and standards

High-purity water was obtained with a Millipore Milli-Q water purification system (resistivity of 18 MΩ cm). Concentrated nitric acid (14 M) was prepared by sub-boiling distillation in a quartz still using analytical reagent grade nitric acid (Pleuger) as feedstock.

External calibration, with boron standards between 1 and 50 $\mu g\ l^{-1}$, was employed to calculate the corresponding concentration. A boron stock solution (1 $g\ l^{-1}$) was prepared by dissolving an amount of boric acid [Isotopic Reference Material-011 from the Central Bureau for Nuclear Measurements (CBNM, Geel, Belgium)] in 0.14 M nitric acid. This material has a certified natural isotopic abundance for boron (^{10}B: 19.824%; ^{11}B: 80.176%). The standard solutions mentioned above were freshly prepared before each analysis sequence with 0.14 M nitric acid as diluent. In the final solutions beryllium [commercial AAS-standard solution (Janssen Chimica)] was also present as internal standard in a concentration of 10 $\mu g\ l^{-1}$ identical to the one in the serum solutions.

Sample preparation

Collection and preparation of serum samples. Blood samples were collected in the University Hospital and processed according to the sampling protocol developed at our laboratory and described in detail by Versieck and Cornelis [23]. Briefly, blood was taken with a polypropylene intravenous catheter, mounted on a trocar [Intranule® 110 16 (Vygon)] and collected in thoroughly cleaned, high-purity quartz tubes with

TABLE 1

ICP-MS operating conditions

Stage	Parameter	Conditions
Plasma	rf-Power:	
	Forward	1.35 kW
	Reflected	< 10 W
	Gas flows:	
	Plasma	13 l min^{-1}
	Auxiliary	1 l min^{-1}
	Nebulizer	0.780 l min^{-1}
	Peristaltic pump	Minipuls 2 (Gilson) pumped at 0.9 ml min^{-1}
	Nebulizer	Meinhard Tr-30-A3 concentric glass nebulizer
	Spray Chamber	Double-pass Scott type, water cooled (10°C)
Ion sampling	Sampling cone	Nickel; 1.0-mm orifice
	Skimmer cone	Nickel; 0.75-mm orifice
	Sampling depth	10 mm (from load coil)
Vacuum	Expansion stage	2.4 mbar
	Intermediate stage	$1.0.10^{-4}$ mbar
	Analyser stage	$4.0.10^{-6}$ mbar
Scanning conditions	Mass range	4–11 u
	Number of channels	512
	Number of sweeps	400
	Dwell time	320 μs
	Measuring time	ca. 1 min

PTFE stoppers. This procedure avoids significant sample contamination. After clotting – no anticoagulant was added – serum was separated by centrifugation [3500 rpm for ca. 30 min (g = 2264)] and decanted into thoroughly cleaned, polyethylene screw-cap containers. Serum samples were stored at −25°C in a commercial deep freezer. With the exception of its collection all sample manipulation was done in a clean laboratory in the Institute of Nuclear Sciences. During transport, samples were kept in a carefully cleaned, air-tight plastic transport container.

After defrosting and homogenization, 5 ml of liquid serum, taken with a polyethylene pipette (Kartell®), was transferred to a 25-ml polyethylene volumetric flask. After addition of 2.5 ml of a 100 μg l^{-1} beryllium solution, the volume was adjusted with 0.14 M nitric acid, prepared by sub-boiling distillation, to obtain 25 ml of the serum solution with a beryllium concentration of 10 μg l^{-1}. A blank solution was prepared in the same way as the serum solutions but without sample. For lyophilized serum, the form in which the "second-generation" biological reference material Freeze-Dried Human Serum is available, first a reconstitution with Millipore Milli-Q water was carried out in a PTFE beaker (6 ml water for 500 mg sample) before quantitative transfer to a volumetric flask. All these manipulations were carried out on a clean-bench.

Sample preparation for Wheat Flour, Bovine Liver and Total Diet. Wheat Flour SRM 1567a, Bovine Liver SRM 1577a and Total Diet SRM 1548 were digested with concentrated nitric acid using a domestic microwave oven (Amana Radarange microwave oven, Model R.S. 560A). The microwave oven destruction technique has the advantage that only a limited amount of acid is necessary for the digestion so that the boron blank level is kept to a minimum. In addition, as the digestion takes place in a closed system, no loss of volatile boron compounds is expected. Therefore, about 400 mg sample was weighed directly into a 60-ml digestion vessel made of perfluoroalkoxy teflon or PFA-PTFE (Savillex Corporation, USA) and 1 ml of concentrated nitric acid was added. The dissolution programme consisted of a three-step heating cycle: 8 min at 20%, 8 min at 40% and 4 min at 60% power (maximum power: 700 W). Subsequently, after the sample was cooled in an ice/water-bath, a further 1.5 ml of concentrated nitric acid was added and a second three step-heating cycle was applied: 6 min at 20%, 6 min at 40% and 8 min at 60% power. The three-step programme with increasing power settings was necessary to avoid leakage and deformation of the vessels as described by Vermeir et al. [24]. After cooling, the digest was transferred quantitatively into a 25-ml polyethylene volumetric flask and 2.5 ml of a 100

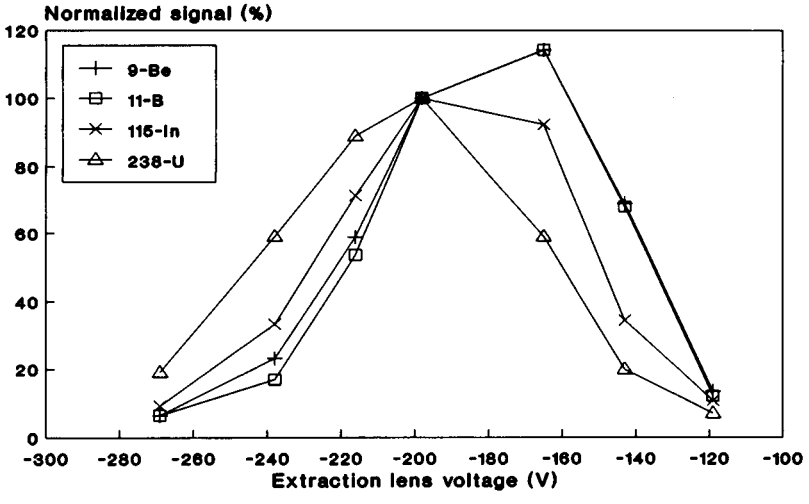

Fig. 1. Influence of the extraction lens voltage on the ion signal for ^{9}Be, ^{11}B, ^{115}In and ^{238}U.

$\mu g\ l^{-1}$ beryllium solution was added as internal standard to obtain a final concentration of 10 $\mu g\ l^{-1}$. The volume was further adjusted with Millipore Milli-Q water. Blank solutions were prepared in the same way but without sample.

Analysis procedure

Optimization of the magnitude of the boron ion signal. Since boron is present at low concentrations in human serum – and more generally in biological materials – several instrumental parameters must be optimized to obtain a maximum signal. One of these is the adjustment of the voltages on the focusing lenses. In our optimization study, we observed a different behaviour for various nuclides, as illustrated in Fig. 1 which shows the relation between the normalized ion signals for ^{9}Be, ^{11}B, ^{115}In and ^{238}U and the varying voltages on the extraction lens directly behind the skimmer cone. These results were obtained as follows: firstly, the voltages on all lenses were optimized to obtain a maximum signal for ^{115}In (reference settings), afterwards, the voltage on the extraction lens was varied while the other voltages were kept constant. The normalized signals for each nuclide were calculated by dividing every signal by that obtained in the first experiment (reference settings). From this figure it is clear that the ion signals for the four nuclides do not behave in the same way. ^{9}Be and ^{11}B, however, do not behave in a different way. The mass dependency of the trajectories that the ions describe through the electrostatic lens system is in agreement with the conclusions of Schmit and Chtaib [25] and Vaughan and Horlick [26]. Therefore, before each analysis sequence, these voltages were optimized for the ion signal of beryllium in order to get a maximum response. Instead of beryllium boron could not be used because large memory effects were experienced when measuring solutions of high boron concentration. In this way, count rates of 2×10^{6} to 3×10^{6} counts per second could be obtained for 1 $mg\ l^{-1}$ Be.

Besides the lens voltages the nebulizer gas flow rate can also significantly influence the sensitivity. As described by Vanhaecke et al. [27] the optimum nebulizer gas flow rate [the nebulizer flow rate at which a maximum signal for a positive ion (M^{+}) is obtained] is also mass dependent with the low mass elements having a higher nebulizer flow rate than high mass elements. For this reason, the nebulizer gas flow rate was optimized at 0.780 l min^{-1} as given in Table 1.

Measuring conditions. Several experiments showed that, as expected, when the measuring time is increased detection limits improve proportionally to the square root of the measuring time.

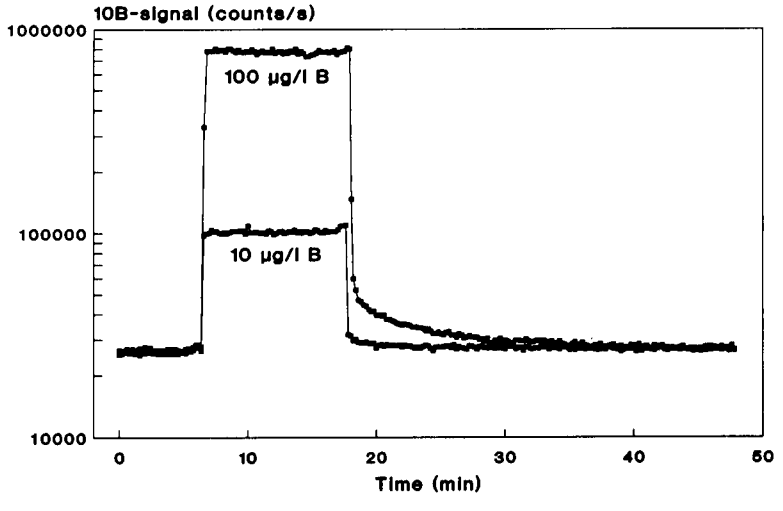

Fig. 2. Signal for boron (^{10}B) as a function of time. Measurement of, successively, a blank solution (5 min), a B standard solution (10 or 100 $\mu g\ l^{-1}$, 10 min) and a blank solution (ca. 30 min).

Since the boron levels in human serum are low, it is necessary to obtain the optimum detection limit. For this reason, only a very small part of the mass range is scanned, using scanning conditions summarized in Table 1. The mass range between 4 and 11 u is scanned 400 times (number of sweeps). 512 channels are used for stockage of the data and each channel is measured for 320 μs (dwell time) so that short term fluctuations on the ion signal are largely eliminated. In this way one measurement lasted about one minute. In cases where also ^{11}B was measured, the mass range was extended to 12 u (a skipped region between 12 and 23 u is present).

Memory effects. Experimentally, it was observed that a substantial memory effect occurs for boron with the conventional sample introduction system. This means that after measurement of a solution containing boron a remaining boron signal can be observed, which may lead to a systematic error for the next sample. Therefore, the memory effect for boron was studied in more detail. An example is given in Fig. 2 where the behaviour of the ^{10}B-signal is plotted as a function of time for two solutions. First a blank solution (0.14 M nitric acid) was measured for 5 min, then a boron solution (10 and 100 μg l^{-1} respectively) for 10 min and subsequently the same blank solution for about 30 min. It is clear that the blank signal decreases almost immediately to a normal blank level after measurement of a 10 μg l^{-1} boron solution; for the 100 μg l^{-1} boron solution, however, the blank signal remains relatively high. It takes at least 15 min before an acceptable level is obtained. It can be concluded that the measurement of low boron concentrations necessitates the use of boron standard solutions with a concentration between 10 and 50 μg l^{-1}. As an additional precaution, the sample introduction system was rinsed for several minutes after measurement of each solution and the blank level controlled. A rinsing time of 2 min sufficed to reduce the memory effects to an acceptable level. It can be noticed that no significant differences between water, 0.14 M nitric acid and 1.4 M nitric acid as rinsing solutions were observed. Because 0.14 M nitric acid was used as diluent for the serum samples it was also employed as rinsing solution.

Analysis sequence and calculations. In order to reduce memory effects, the following analysis sequence was applied: first a blank for the samples was measured, then several biological samples, next a blank for the standard, and only at the end of the sequence several boron standard solutions were measured. Five replicate measurements were made on each solution. After the measurement of each solution the sample introduction system was rinsed for two minutes with 0.14 M nitric acid as mentioned above.

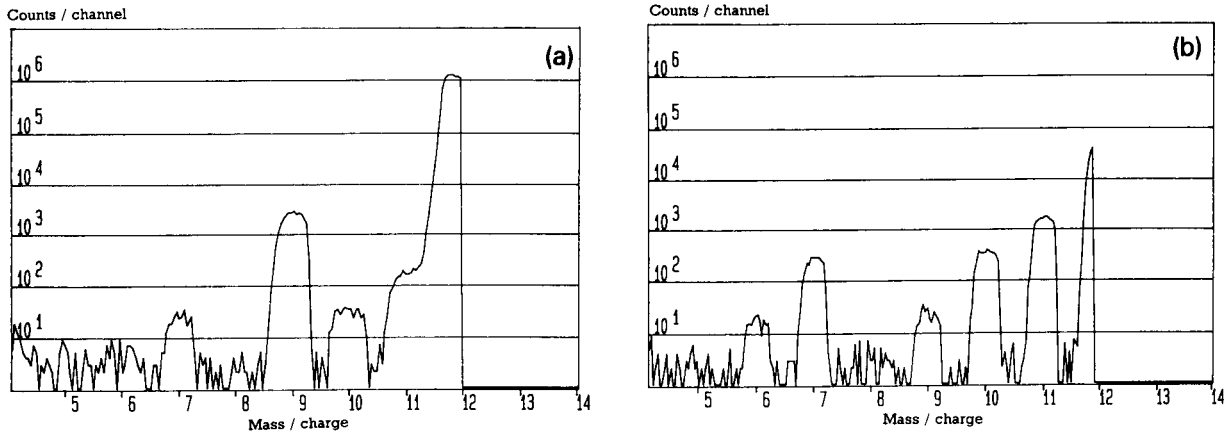

Fig. 3. (a) Mass spectrum between 4 and 14 u for a five-fold diluted serum solution (addition of 10 μg l^{-1} Be as internal standard) (normal resolution setting). (b) Mass spectrum between 4 and 14 u for a 100 μg l^{-1} B solution with 0.14 M nitric acid as diluent (normal resolution setting).

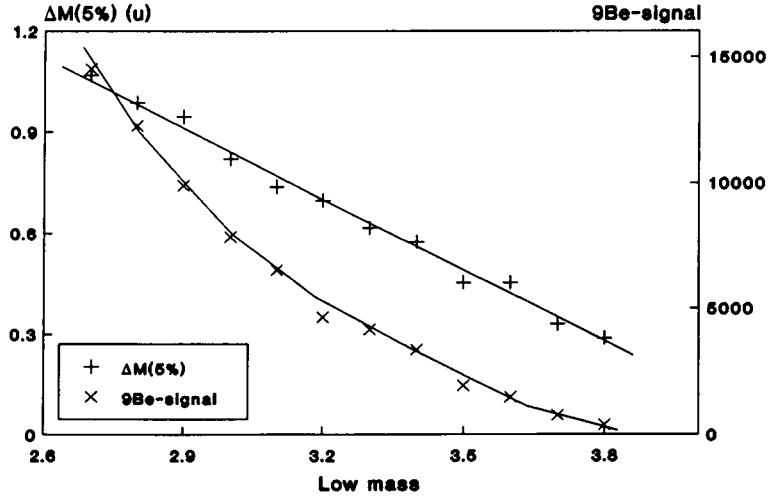

Fig. 4. Influence of the "low mass" setting on the peak width at 5% of the peak maximum [ΔM(5%)] and on the ion signal for beryllium (^{9}Be).

For each solution (blank, sample, standard), the signal (peak area integrated over 0.8 u around the peak maximum) of boron (^{10}B) was divided (or normalized) by the signal of the internal standard (^{9}Be). The mean and standard deviation of the five resulting normalized signals of each solution were calculated. The average normalized signal of the blank was subtracted from that of the serum solutions. External calibration was employed to calculate the corresponding concentrations.

Choice of the nuclide. As already mentioned in the introduction the intense peak from $^{12}C^{+}$ can complicate the measurement of boron using ^{11}B

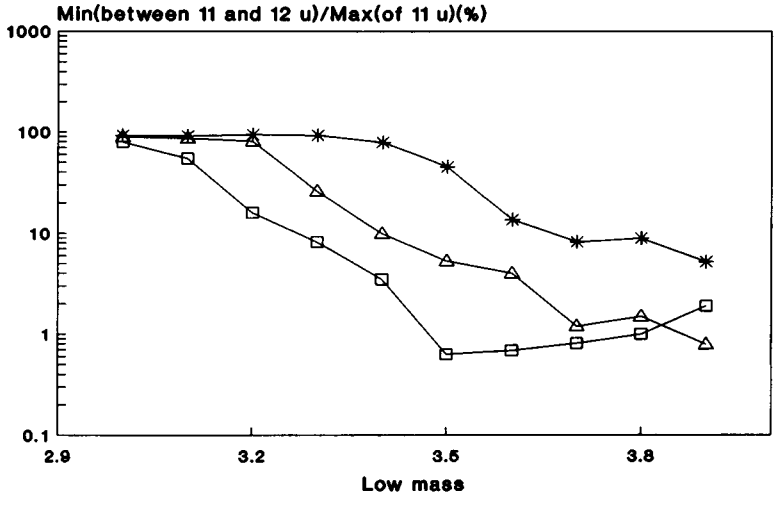

Fig. 5. Influence of the "low mass" setting on the separation of the ^{11}B- and ^{12}C-peaks for a five-fold diluted serum solution: * without destruction; △ after destruction with HNO_3; □ after destruction with $HNO_3/HClO_4$. The ratio of the minimum value between the two peaks at mass 11 and 12 u to the maximum value of the peak at mass 11 u is given as a function of the "low mass" setting.

(80%). This is illustrated in Fig. 3a that gives a mass spectrum between 4 and 14 u for a five-fold diluted serum solution. The very high amount of carbon in a diluted serum solution – The International Commission on Radiological Protection [28] reports a value of 40.7 g l^{-1} for human blood plasma – prevents resolution of the ^{11}B- and ^{12}C-peaks. The mass spectrum of a 100 μg l^{-1} B solution with 0.14 M HNO_3 as diluent in Fig. 3b shows that in the absence of high amounts of carbon a perfect separation of the two peaks can be observed. The resolution used in these experiments was about 16 ($R = M/\Delta M$ with $\Delta M = 0.7$ u for a peak width at 5% of the peak maximum). In an attempt to solve this problem the resolution was optimized. Since the considered ion peaks are at the low mass side of the spectrum, the only usable parameter of the VG PlasmaQuad is the "low mass" parameter (the "coarse" and the "fine" parameters only influence the peaks with a relatively high mass (above 40 u)). The influence of the "low mass" settings on peak width and peak signal is illustrated in Fig. 4 whereas that on the separation of the ^{11}B- and ^{12}C-peaks for human serum is shown in Fig. 5, which gives the relation between the "low mass" setting and the ratio of the minimum between the peaks at mass 11 and 12 u (lowest number of counts in a valley channel) to the maximum at mass 11 u (maximum number of counts in a peak channel). This ratio never reaches a value below 5% indicating that the peaks at mass 11 and 12 u are not separated completely. In addition, this situation corresponds to a relatively low sensitivity since the transmission through the quadrupole mass spectrometer decreases with increasing resolution (Fig. 4). In additional experiments, the influence of a destruction of the organic matrix on the separation of the two peaks was examined. Figure 5 also summarizes the results, obtained after an open destruction of the serum sample respectively with concentrated nitric acid and with a mixture of nitric and perchloric acid. Under standard conditions ("low mass": 3.3) the contribution of the ^{12}C-peak to the peak at mass 11 u is respectively 25 and 8%. From these experiments we can conclude that after destruction of a serum sample the carbon is not totally volatilised as carbon dioxide even when perchloric acid is used. An increase of the resolution results in a decrease of this contribution (to about 1% in both cases) corresponding, however, to a lower sensitivity. In addition, the use of perchloric acid (Merck, suprapur) introduces a relatively high blank signal. Therefore, because of the lower sensitivity and the blank problem it is not optimal to use ^{11}B for the determination of the low boron concentrations in human serum even after a destruction procedure. Therefore ^{10}B, with a lower isotopic abundance (20%), has been used for all boron determinations in human serum.

RESULTS AND DISCUSSION

Non-spectral interferences

In previous work [18–21] we reported that the ion signal in diluted human serum is influenced by the serum matrix. In addition, we noticed that the high mass elements are suppressed to a greater extent than the low mass elements. Therefore, a boron recovery study was carried out and in order to correct for signal suppression the choice of a suitable internal standard was examined. Five-fold diluted serum solutions were spiked with 100 μg l^{-1} B and compared with a blank solution containing 0.14 M nitric acid and 100 μg l^{-1} B. The relative signal intensity was $85.6 \pm 5.2\%$ using ^{10}B as nuclide indicating significant signal suppression. Because the influence is mass dependent the internal standard should have a comparable mass to that of the analyte. Application of beryllium (^{9}Be) as internal standard yielded a relative signal intensity of $99.6 \pm 2.5\%$ which demonstrates that beryllium corrects effectively for the signal suppression. As demonstrated before, beryllium can also be applied as internal standard for lithium determinations in human serum [21]. Moreover, the internal standard corrects for instability of the ion signal so that a relative standard deviation on the results of 4% or better can be expected in cases with sufficient counting statistics.

Boron blank and detection limit

Besides by memory effects, the boron blank

level can be elevated by other factors. The reagents used for the sample preparation are the major sources of boron blanks, as illustrated in Table 2. The analysed waters, namely Millipore Milli-Q water, deionized water and distilled water, contain different degrees of boron impurity with Millipore Milli-Q water having the lowest value. Moreover, it appears that the sub-boiled nitric acid does not elevate the boron blank signal as the boron concentration (1.51 $\mu g\ l^{-1}$) is not significantly different from that of the Millipore Milli-Q water which was used as diluent. In additional experiments, the origin of the boron blank was studied in more detail. Because the conventional sample introduction system consists merely of borosilicate glass, boron blank signals were compared with those of an inert sample introduction system (VG Elemental) consisting of a De Galan-type nebulizer made of an organic polymer, a water cooled spray chamber and a connecting elbow both made of PTFE, and a torch with a central tube made of alumina. With this system, the aspirated solution never comes in contact with glass so that the blank value for boron can expected to be low. However, results showed that the observed boron blank signal does not originate from the conventional sample introduction system: for the glass sample introduction system boron concentrations of 2.28 (0.08) and 1.92 $\mu g\ l^{-1}$ (0.06) were found for water and 0.14 M nitric acid respectively, whereas for the inert sample introduction system the concentrations are respectively 1.91 (0.12) and 2.08 $\mu g\ l^{-1}$ (0.07). The values between brackets are standard deviations. Most likely, the observed boron blank signal is originating from the Millipore Milli-Q water. These conclusions are confirmed by preconcentration experiments carried out with Millipore Milli-Q water.

TABLE 2

Boron concentrations ($\mu g\ l^{-1}$) in four types of water and in 0.14 M sub-boiled nitric acid

Reagent	B concentration
Millipore Milli-Q water	1.71 ± 0.04 [a]
Deionized water	5.00 ± 0.15
Distilled water	2.20 ± 0.17
Tap water	18.9 ± 0.5
0.14 M sub-boiled nitric acid	1.51 ± 0.05

[a] Standard deviation of the mean.

TABLE 3

Boron results (ng g^{-1}) for three biological reference materials

Material	Present work (ICP-MS)	Literature values
Wheat Flour SRM 1567a	610 (30) [a]	580 ± 20 (NA-MS) [8]
	530 (40)	
Bovine Liver SRM 1577a	860 (60) [a]	590 ± 80 (NA-MS) [8]
	950 (30)	1040 ± 130 (PGAA) [6]
Total Diet SRM 1548	2668 (21) [a]	2500 [b]
	2700 (17)	2410 ± 50 (NA-MS) [8]
	2688 (5)	2610 ± 120 (PGAA) [6]

[a] Standard deviation of the measurements ($n = 5$). [b] Indicative value.

In optimum conditions, a boron detection limit ($3s$-definition, with s the standard deviation obtained after ten measurements of a blank solution) of 0.5 $\mu g\ l^{-1}$ for serum could be achieved taking into account a five-fold dilution of the serum sample.

Wheat Flour, Bovine Liver and Total Diet SRMs

In order to check the accuracy of the calibration and internal standardization method three other biological reference materials were analysed, namely Wheat Flour SRM 1567a, Bovine Liver SRM 1577a and Total Diet SRM 1548. A summary of the results is given in Table 3. The boron concentrations found in these materials are comparable or only a few times higher than those of lyophilized human serum. The two results obtained for Wheat Flour are in good agreement with the value reported by Iyengar et al. [8] using neutron activation mass spectrometry (NA-MS). For Bovine Liver, our result is not significantly different from that of Anderson et al. [6] who used neutron-capture prompt γ-ray activation analysis (PGAA). The value of Iyengar et al. [8] is

about a factor of two lower. For Total Diet, finally, our result is comparable with that of Anderson et al. [6] and somewhat higher (about 10%) than the indicative value and the value of NA-MS. From these results, it can be concluded that the proposed procedure for boron determinations is quite accurate.

"Second-generation" biological reference material Freeze-Dried Human Serum

Table 4 summarizes the results obtained after measurement of the "second-generation" biological reference material Freeze-Dried Human Serum. Boron was determined both in the lyophilized form, as it is available to the scientific community, and directly in the liquid material. For each form, four samples were each analysed five times. A mean boron value of 227 ng g^{-1} with a 95% confidence limit of 18 ng g^{-1} was found for the lyophilized form, whereas for the liquid material the values are respectively 20.3 and 1.2 $\mu g\ l^{-1}$ (corresponding to 224 and 13 ng g^{-1} lyophilized material). As can be deduced from the individual results the relative standard deviations for one sample varied from 1.6 to 5.2%. The contribution of the blank signal to the boron signal in a five-fold diluted serum sample varies between 20 and 40%. This contribution is relatively high but as it probably originates from impurities present in the reagents it is rather stable. The present value can only be compared with that reported by Abou-Shakra [29]: 222 ng g^{-1} dry weight with a standard deviation of 6 ng g^{-1}. This result was also obtained with ICP-MS after digestion of the serum sample with nitric acid. The agreement is excellent.

TABLE 4

Boron results (ng g^{-1} dry weight) for the "second-generation" biological reference material Freeze-Dried Human Serum

	Lyophilized form	Liquid form
Individual results	217.7 (6.8) [a]	212 (11) [a]
	241 (10)	226.7 (7.1)
	218.5 (3.6)	225.0 (8.9)
	230.0 (7.7)	231.0 (6.2)
Means	227 ± 18 [b]	224 ± 13 [b]

[a] Standard deviation of the measurements ($n = 5$). [b] 95% confidence limits.

TABLE 5

Literature values for boron in normal human serum

Authors	Method	Concentration ($\mu g\ l^{-1}$)	Number of persons
This work	ICP-MS	13.9 ± 6.9 (4.1–25.8)	12
Abou-Shakra et al. [16]	ICP-MS	22.3 (8.3–48.1)	50
Smith et al. [17]	ICP-MS	24 ± 4	1
Iyengar et al. [8]	NA-MS	30 ± 2	1

Normal human serum

Boron determinations were also made on serum samples taken from twelve staff members working in this laboratory (8 females and 4 males with ages ranging from 23 to 51 years). A mean boron concentration of 13.9 $\mu g\ l^{-1}$ with a standard deviation of 6.9 $\mu g\ l^{-1}$ was found. The lowest and highest values were respectively 4.1 and 25.8 $\mu g\ l^{-1}$, whereas the geometric mean was 12.1 $\mu g\ l^{-1}$. It can be deduced from these results that the boron concentration in the "second-generation" biological reference material Freeze-Dried Human Serum agrees with that expected for normal human serum. The boron concentration in human serum is not extensively described in the literature, owing to the low concentration, which can only be determined with a few sensitive techniques. Some literature values are given in Table 5. They range from 8.3 to 48.1 $\mu g\ l^{-1}$ with a mean value of 25.4 $\mu g\ l^{-1}$ and are in good agreement with the range found in this work.

Grateful acknowledgement is made to L. Vanballenberghe for her contribution to the preparation of the serum samples. The PlasmaQuad was acquired by a grant from the Fund for Medical Scientific Research (FGWO).

REFERENCES

1 A. Kabata-Pendias and H. Pendias, Trace Elements in Soils and Plants, CRC Press, Boca Raton, FL, 1984, p. 127.

2 F.H. Nielsen, in R. Zeisler and V.P. Guinn (Eds.), Nuclear Analytical Methods in the Life Sciences, Humana Press, Clifton, NJ, 1990, p. 599.
3 R.F. Barth, A.H. Soloway and R.G. Fairchild, Cancer Res., 50 (1990) 1061.
4 M.P Failey, D.L. Anderson, W.H. Zoller, G.E. Gordon and R.M. Lindstrom, Anal. Chem., 51 (1979) 2209.
5 N.I. Ward, J. Radioanal. Nucl. Chem., Articles, 110 (1987) 633.
6 D.L. Anderson, W.C. Cunningham and E.A. Mackey, Fresenius' Z. Anal. Chem., 338 (1990) 554.
7 W.B. Clarke, M. Koekebakker, R.D. Barr, R.G. Downing and R.F. Fleming, Appl. Radiat. Isot., 38 (1987) 735.
8 G.V. Iyengar, W.B. Clarke and R.G. Downing, Fresenius' Z. Anal. Chem., 338 (1990) 562.
9 N.L. Duchateau, A. Verbruggen, F. Hendrickx and P. De Bièvre, Anal. Chim. Acta, 196 (1987) 41.
10 T. Kumamaru, H. Matsuo, Y. Okamoto, M. Yamamoto and Y. Yamamoto, Anal. Chim. Acta, 186 (1986) 267.
11 S.R. Tamat, D.E. Moore and B.J. Allen, Anal. Chem., 59 (1987) 2161.
12 R.F. Barth, D.M. Adams, A.H. Soloway, E.B. Mechetner, F. Alam and A.K.M. Anisuzzaman, Anal. Chem., 63 (1991) 890.
13 D.C. Gregoire, Anal. Chem., 59 (1987) 2479.
14 D.C. Gregoire, J. Anal. At. Spectrom., 5 (1990) 623.
15 F. Vanhaecke, H. Vanhoe, C. Vandecasteele and R. Dams, Anal. Chim. Acta, 244 (1991) 115.
16 F.R. Abou-Shakra, J.M. Havercroft and N.I. Ward, Trace Elements Med., 6 (1989) 142.
17 F.G. Smith, D.R. Wiederin, R.S. Houk, C.B. Egan and R.E. Serfass, Anal. Chim. Acta, 248 (1991) 229.
18 H. Vanhoe, C. Vandecasteele, J. Versieck and R. Dams, Anal. Chem., 61 (1989) 1851.
19 C. Vandecasteele, H. Vanhoe, L. Vanballenberghe, A. Wittoek, J. Versieck and R. Dams, Talanta, 37 (1990) 819.
20 C. Vandecasteele, H. Vanhoe, R. Dams and J. Versieck, Anal. Lett., 23 (1990) 1827.
21 H. Vanhoe, C. Vandecasteele, J. Versieck and R. Dams, Anal. Chim. Acta, 244 (1991) 259.
22 J. Versieck, L. Vanballenberghe, A. De Kesel, J. Hoste, B. Wallaeys, J. Vandenhaute, N. Baeck, H. Steyaert, A.R. Byrne and F.W. Sunderman, Jr., Anal. Chim. Acta, 204 (1989) 63.
23 J. Versieck and R. Cornelis, Trace Elements in Human Plasma or Serum, CRC Press, Boca Raton, FL, 1988, p. 48.
24 G. Vermeir, C. Vandecasteele and R. Dams, Anal. Chim. Acta, 220 (1989) 257.
25 J.P. Schmit, M. Chtaib, Can. J. Spectrosc., 32 (1987) 56.
26 M.A. Vaughan and G. Horlick, Spectrochim. Acta, 45B (1990) 1301.
27 F. Vanhaecke, C. Vandecasteele, H. Vanhoe and R. Dams, Mikrochim. Acta, 108 (1992) 41.
28 International Commission on Radiological Protection. Report of the Task Group on Reference Man, ICRP Publication 23, Pergamon Press, Oxford, 1975.
29 F.R. Abou-Shakra, personal communication.

Analytica Chimica Acta, 281 (1993) 413–419
Elsevier Science Publishers B.V., Amsterdam

State analysis and relationship between lattice constants and compositions including minor elements of synthetic magnetite and maghemite

Tsutomu Fukasawa, Masaaki Iwatsuki and Masahito Furukawa

Department of Applied Chemistry and Biotechnology, Faculty of Engineering, Yamanashi University, 4-3-11 Takeda, Kofu 400 (Japan)

(Received 8th February 1993)

Abstract

Chemical formulae were constructed after the determination of the compositions including the minor elements in commercially available synthetic magnetite and maghemite, which gave similar x-ray diffraction patterns with close diffraction lines. The contents of FeO in reagent grade magnetite and high-purity magnetite powders were about 8 mol% less and that in a needle-shaped magnetite powder was about 24 mol% less than the 50 mol% in the expected composition ($FeO \cdot Fe_2O_3$) of magnetite. They were solid solutions of magnetite–maghemite (γ-Fe_2O_3) including minor elements in the lattice. A linear relationship was found between the total mole percentage of divalent iron, manganese and zinc oxides and their lattice constants a_c corrected by increments of the lattice constant based on the replacement of divalent iron with manganese and zinc atoms. The possibility of a non-destructive total analysis of the same iron oxide samples by an x-ray method is discussed. It was found that magnetite was considerably oxidized in air even at 110°C to form a solid solution, but not to form any separated compound.

Keywords: X-ray diffraction; Iron oxides; Lattice constants; Maghemite; Magnetite

Naturally produced magnetite (Fe_3O_4 or $FeO \cdot Fe_2O_3$) has been used as a black pigment since ancient times. Nowadays synthetic magnetites prepared by various chemical methods are also used in different industries and as magnetic materials and catalysts. Recently, magnetic hybrids such as magnetic enzyme, which consists of magnetite and an enzyme, have been applied in medical science and biotechnology [1]. However, magnetite powder may tend to be partially oxidized, and some doubts about the nominal purities of commercially available reagent grade magnetite have been expressed in a study of the x-ray diffractometric determination of iron oxides in airborne particulates [2]. Hence it was decided to carry out this study on magnetite and maghemite.

From the viewpoint of state analysis or speciation analysis, studies have been carried out as follows. The relationship between the oxidation number of iron and the chemical shift of the Fe $K\beta_{1,3}$ line from synthetic magnetite and various ferrites has been studied using a two-crystal type x-ray spectrometer [3]. The depth dependence of the chemical states of iron oxides, which was produced on the surface of a pure iron rod by heating in air at 1000°C, has been studied from the chemical shifts of O $K\alpha$, Fe $L\alpha$ and Fe $L\beta$ lines, their intensity ratio and spectral patterns by use of an x-ray microanalyser [4]. These studies, however, were not quantitative but qualitative. Basta [5] discussed the relationship between the lattice constants and the main composition of

Correspondence to: T. Fukasawa, Department of Applied Chemistry and Biotechnology, Faculty of Engineering, Yamanashi University, 4-3-11 Takeda, Kofu 400 (Japan).

natural minerals of magnetite–maghemite (γ-Fe_2O_3) solid solutions. However, he noted that a precise correlation between them was hardly to be expected as the exact manner of the distribution of minor ions in the lattice could not be established and the calculated mineral compositions were somewhat arbitrary.

This paper describes the results of chemical analysis of iron oxides including minor constituents such as manganese and zinc, and discusses the relationship between their compositions and the results of powder x-ray diffraction (XRD) for the measurement of the lattice constants. The results revealed that even commercially available reagent grade magnetite and high-purity magnetite had compositions with about 8 mol% less iron(II) oxide (FeO) and needle-shaped magnetite had a composition with about 24 mol% less FeO than the 50 mol% expected from the chemical formula ($FeO \cdot Fe_2O_3$) of magnetite. A plot of mol% of Fe_2O_3 or (Fe, Mn, Zn)O against their lattice constants corrected for the contents of the minor constituents, was found to be linear, i.e., they were not magnetite but solid solutions of magnetite and maghemite in which divalent iron atoms were partially replaced with the minor elements. In addition to the above finding, the relationship may be applicable to new rapid and non-destructive total analysis of the samples as described here with the help of non-destructive x-ray fluorescence (XRF) determination of the minor constituents. It was found that iron(II) atoms in magnetite powder were partially oxidized to form magnetite–maghemite solid solutions in air even at 110°C, but not to form any separated compound.

EXPERIMENTAL

X-ray fluorescence analysis

A Philips PW1410 semi-automatic XRF spectrometer was used for the detection of minor constituents in the samples in advance. The sample powder was placed in a small bag made of 6-μm Mylar film, fitted into a standard sample holder and analysed under conventional experimental conditions using tungsten and chromium target x-ray tubes for heavy and light elements, respectively.

TABLE 1

Conditions for XRD

Target	Fe	Divergence and anti-scatter slit	1°
Voltage	35 kV	Receiving slit	0.3 mm
Current	10 mA	Time constant	4 [a] or 1 [b] s
Filter	Mn	Scanning speed	1/4 [a] or 2° min^{-1} [b]
		Chart speed	20 mm min^{-1}

[a] For measurements of lattice constant. [b] For identification.

X-ray diffraction analysis and measurements of lattice constants

A Rigaku x-ray diffractometer equipped with a proportional counter was used for XRD analysis under the conditions given in Table 1. A powder sample packed in a standard sample holder was placed in the goniometer for analysis. For measurements of lattice constants, the sample was previously mixed with silicon powder in a ratio of 2 + 1, packed in a standard sample holder and analysed. The diffraction lines of silicon and magnetite or maghemite which appear at over 70° (2θ), as shown in Table 2, were recorded twice on a chart at a slow scanning rate, and each line profile was approximated to a triangle. Each diffraction angle was estimated as the centre of gravity of the triangle and corrected using the diffraction angles of the silicon. Another specimen was prepared from the sample and analysed in the same way, and finally the lattice constant (a_0) was obtained from the average of the duplicate measurements.

Samples and reagents

Table 3 shows the samples used, which were subjected to XRF analysis to find previously mi-

TABLE 2

XRD lines used for measurements of lattice constants

Sample		Silicon standard	
hkl	2θ (°)	*hkl*	2θ (°)
511	73.7– 74.2	311	72.539
440	81.5– 82.1	422	121.675 [a]
533	98.4– 99.2		
731	125.1–126.2		

[a] For Fe Kα_1. Others for Fe Kα.

nor constituents. Silicon powder of nominal 99.9% purity and 100 mesh (Wako) was used as an internal standard for the correction of the diffraction angle.

Chemical analysis

Determination of Fe(II) and Fe(III) [6]. A sample of 0.1–0.4 g was placed in a platinum dish (60 mm in diameter, 50 ml), moistened with a few drops of hot water and decomposed with 20–30 ml of H_2SO_4 (1 + 1) and 1.0–1.2 ml of HF (46%) under a carbon dioxide atmosphere on a hotplate. The resulting solution was transferred under a carbon dioxide gas flow into a 200-ml beaker which contained 35-ml of a saturated solution of boric acid previously boiled to remove dissolved oxygen. It was titrated with a 0.01 M $KMnO_4$ standard solution to determine Fe(II). The titrated solution was transferred into a zinc amalgam reductor of the Kobayashi type and shaken in a carbon dioxide atmosphere to reduce Fe(III) to Fe(II). Then the solution was titrated with the same $KMnO_4$ solution to determine the amount of total iron. The amount of Fe(III) was calculated by subtracting the amount of Fe(II) from the total iron. The determinations of Fe(II) and Fe(III) were carried out after careful training using ammonium iron(II) and iron(III) sulphates.

Determination of Mn [7]. A sample of 0.5 or 0.15 g was decomposed in 30 ml of mixed acid [nitric acid–sulphuric acid–phosphoric acid–water (10 + 6 + 7 + 37)] in a 200-ml beaker. After dilution, a small amount of silver nitrate solution was added. Manganese in the solution was oxidized to permanganate with ammonium peroxydisulphate and determined by spectrophotometry.

Determination of Zn [8]. A sample of 0.2 g was decomposed in hydrochloric and nitric acids and zinc was determined by atomic absorption spectrometry.

RESULTS AND DISCUSSION

Chemical composition

It was found that all the samples except A contained manganese and zinc as minor constituents and chromium as a trace element, as shown in Table 3. Chromium is not discussed in this paper because of its trace concentrations.

Table 4 gives the mole percentages found for each constituent in the samples. High-purity magnetite A and reagents grade magnetites B and C had 7.0–7.7 mol% higher contents of Fe_2O_3 than the 50 mol% expected content in magnetite, i.e., the magnetite contents in these samples were estimated to be ca. 85% on the basis of the mol% of FeO or MO (total divalent metal oxides). This means that these magnetites were not pure.

On heating in air at 110°C, the FeO content in sample D decreased from 25.5 to 20.1 mol% owing to the formation of Fe_2O_3. This shows that magnetite powder tends to be oxidized in air.

Maghemite sample F included small amounts of divalent iron, i.e., FeO, different from its expected composition of Fe_2O_3.

XRD patterns and lattice constants

The XRD patterns of magnetite and maghemite samples were very similar, with close diffraction lines, as shown in Table 5, because both minerals have the same structure of the inverse spinel type constructed with the same main elements, except that magnetite includes

TABLE 3

Samples

Sample [a]	Description [b]	Particle size (μm)	Minor elements detected by XRF [c]		
			Mn	Zn	Cr
A	High-purity Fe_3O_4, 99.9%	1–2	–	–	–
B	Reagent grade Fe_3O_4	ca. 1	+ + + +	+ + +	+
C	Reagent grade Fe_3O_4	< 1	+ + +	+	+
D	Needle-shaped magnetite	< 1	+ + +	+ + + +	+
D′	Sample D kept at 110°C for 3 h	< 1	+ + +	+ + + +	+
E	Needle-shaped maghemite	< 1	+ + +	+ + + +	+
F	Needle-shaped maghemite	< 1	+ + +	+ +	+

[a] B, from W company; C, from K company. [b] Expected chemical formula of magnetite: Fe_3O_4. Maghemite: γ-Fe_2O_3. [c] + = trace; + + = weak; + + + = medium; + + + + = strong; – = not detected.

divalent and trivalent iron. The XRD patterns of samples E and F, which were close to the expected composition of maghemite, Fe_2O_3, were characterized by additional weak lines due to a super-lattice of maghemite [9]. No lines due to other substances were observed in the diffraction patterns. All samples gave broad XRD lines without $K\alpha_1$–$K\alpha_2$ splitting, which shifted out to the higher angle side with decrease in FeO content. Their lattice constants were calculated from the measurement of the four diffraction angles shown in Table 2. Table 6 gives the averages and standard deviations of the observed lattice constants together with data from the literature. All the lattice constants observed were different from each other and also from those of magnetite [10] and maghemite [9,11] in the JCPDS files. In addition to the analytical results, those described above indicate that the samples used here should not be considered to be mixtures but rather solid solutions.

Relationship between lattice constant and composition

Divalent ions of manganese and zinc are liable to replace iron ions of the same valency in the crystal structure because of their similar ionic radii. The chemical formulae were constructed from the mole percentages in Table 4 for each sample and are given in Table 7.

The values of the lattice constants were plotted against the total mole percentages of the divalent metal oxides, i.e., FeO, MnO and ZnO, in Table 4. The lattice constants of samples 1, A and 3 lay approximately on a straight line, but those of the other samples, including D′, deviated from the straight line depending on contents of the minor elements and their ionic radii (Mn^{2+} > Zn^{2+} > Fe^{2+}).

The lattice constants were then corrected for the contents of the minor constituents, assuming that a complete series of solid solutions are formed among magnetite ($Fe^{II}Fe_2^{III}O_4$), jacobsite ($Mn^{II}Fe_2^{III}O_4$) and franklinite ($Zn^{II}Fe^{III}O_4$) by isomorphous replacement of Fe(II) in magnetite by Mn(II) and/or Zn(II), as follows: increment based on replacement of Fe(II) in magnetite by Mn(II),

$$\Delta a_{Mn} = (a_{Mn} - a_{Fe}) f_{Mn}$$

and increment based on replacement of Fe(II) by Zn(II),

$$\Delta a_{Zn} = (a_{Zn} - a_{Fe}) f_{Zn}$$

where a_{Fe} is the lattice constant of magnetite, which is 8.3967 Å [10], a_{Mn} is that of jacobsite, which is 8.499 Å [12], and a_{Zn} is that of franklinite, which is 8.4411 Å [13]; f_{Mn} and f_{Zn} are mole ratios in the chemical formula constructed for each sample. The corrected lattice constant is

$$a_c = a_o - \Delta a_{Mn} - \Delta a_{Zn}$$

where a_o is the lattice constant observed.

The corrected lattice constants of all the samples except maghemite 2 gave linear plots with a

TABLE 4

Results of chemical analyses

Sample	Concentration (%, w/w)					Concentration (mol%)			
	Fe_2O_3	FeO	MnO	ZnO	Total	Fe_2O_3	FeO	MnO	ZnO
Fe_3O_4 [a]	69.0	31.0	–	–	100.0	50.0	50.0	–	–
A	75.1	24.8	0.00	0.00	99.9	57.7	42.3	0.00	0.00
B	74.7	24.3	0.81	0.25	100.1	57.0	41.2	1.39	0.37
C	75.6	24.8	0.28	0.01	100.7	57.5	42.0	0.48	0.01
D	84.2	13.3	0.27	0.87	98.6	72.5	25.5	0.52	1.47
D′	87.8	10.2	0.27	0.87	99.1	77.9	20.1	0.54	1.51
E	96.6	0.0	0.26	0.88	97.7	97.6	0.0	0.59	1.75
F	97.2	0.2	0.26	0.04	97.7	98.9	0.4	0.60	0.08
Fe_2O_3 [a]	100.0	–	–	–	100.0	100.0	–	–	–

[a] Expected formula.

TABLE 5

XRD data from various samples of magnetite and maghemite

hkl cubic	JCPDS19-629 magnetite		Sample A		B		C		D		E		F		JCPDS24-81 maghemite		JCPDS25-1402 maghemite		*hkl* tetragonal
	d (Å)	I/I_1	*d* (Å)	I/I_1	*d* (Å)	I/I_1	*d* (Å)	I/I_1	*d* (Å)	I/I_1	*d* (Å)	I/I_1	*d* (Å)	I/I_1	*d* (Å)	I/I_1	*d* (Å)	I/I_1	
													7.95	1			7.91	1	101
											6.94	1	6.94	1			6.94	2	102
110											5.92	4	5.92	5	5.90	2	5.90	6	103
																	5.33	1	112
111	4.852	8	4.86	9	4.86	9	4.86	10	4.85	7	4.83	5	4.84	4	4.82	5	4.82	6	113
											4.29	1	4.29	1			4.29	2	105
200															4.18	1			
210											3.735	4	3.739	6	3.73	5	3.730	6	203
211											3.410	4	3.413	5	3.41	2	3.400	7	116
											3.221	1	3.221	1			3.200	3	205
220	2.967	30	2.969	30	2.971	29	2.972	30	2.966	33	2.954	35	2.953	38	2.95	34	2.950	30	206
221											2.780	3	2.776	3	2.78	19	2.780	3	216
310											2.639	1	2.639	2	2.64	–	2.638	4	109
311	2.532	100	2.531	100	2.534	100	2.532	100	2.528	100	2.519	100	2.519	100	2.52	100	2.514	100	119
222	2.4243	8	2.422	4	2.424	5	2.425	5	2.423	3	2.410	1	2.411	2	2.41	1	2.408	2	226
320											2.312	1	2.313	2	2.32	6	2.315	2	209
321															2.23	< 1	2.230	2	316
400	2.0993	20	2.098	23	2.100	23	2.100	24	2.095	22	2.088	21	2.087	20	2.08	24	2.086	15	$00\underline{12}$
420															1.87	< 1	1.865	1	406
													1.821	1			1.820	3	$2\underline{112}$
422	1.7146	10	1.713	7	1.714	8	1.714	8	1.710	9	1.704	10	1.704	10	1.70	12	1.701	9	$2\underline{212}$
																	1.670	2	500
511	1.6158	30	1.614	23	1.616	24	1.615	24	1.612	21	1.607	25	1.607	24	1.61	33	1.604	20	$11\underline{15}$
333																			

TABLE 6

Lattice constants observed

Sample	a_0 (Å)		c_0 ($=3a_0$) (Å)
	Av. [b]	σ [b]	
Magnetite [10] [a]	8.3967		
A	8.387	±0.001	
B	8.396	±0.001	
C	8.392	±0.001	
D	8.377	±0.001	
D′	8.369	±0.001	
E	8.346	±0.001	
F	8.344	±0.001	
Maghemite [11]	8.350		
Maghemite [9] [c]	8.34		25.02

[a] Co, 0.01–0.1%; Ag, Al, Mg, Mn, Mo, Ni, Si, Ti, Zn, 0.001–0.01%. [b] $n = 4$. [c] Shown as tetragonal.

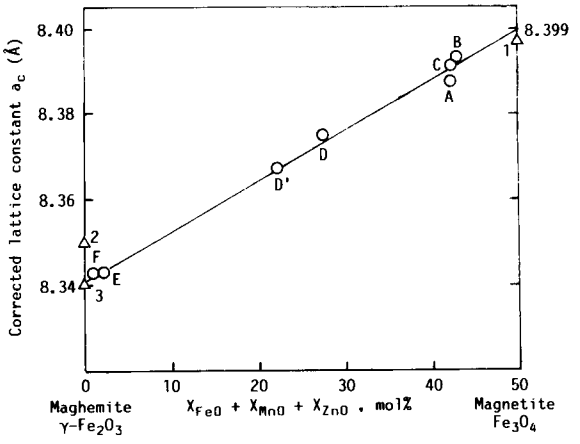

Fig. 1. Relationship between corrected lattice constant (a_c) and sum of mole percentages of FeO, MnO and ZnO ($X_{FeO} + X_{MnO} + X_{ZnO}$). $a_c = 8.342 + 0.001135(X_{FeO} + X_{MnO} + X_{ZnO})$; $\sigma(x) = 1.6$ mol%. 1 = Fe_3O_4, JCPDS 19-629, 8.3967 Å; 2 = γ-Fe_2O_3, JCPDS 24-81, 8.350 Å; 3 = γ-Fe_2O_3, JCPDS 25-1502, 8.34 Å.

standard deviation of 1.6 mol%, as shown in Fig. 1. This linear relationship means that the samples B, C and D were not magnetite or mixtures of iron oxides, but solid solutions between magnetite and maghemite, where Fe(II) atoms in the structure were partially replaced with Mn(II) and/or Zn(II). It also reveals that sample D′ was a solid solution of the same system and magnetite was oxidized in air to form the solid solutions without depositing any other type of iron oxide separately.

The relationship shown in Fig. 1 also may be used for the non-destructive total analysis of the samples as described here, with the help of the non-destructive XRF analysis of the minor constituents. The non-destructive total analysis of the same samples will be reported in another paper.

Conclusion

Commercially available magnetite and maghemite powders (even reagent grade magnetite or high-purity magnetite) appear to be magnetite–maghemite solid solutions, instead of pure powders. Even at 110°C iron(II) atoms in magnetite powder were oxidized partially in air. A linear relationship was found between the total mole percentage of divalent iron and minor metal ox-

TABLE 7

Chemical formulae and corrected lattice constants

Sample	Formula	a_c (Å)
Fe_3O_4	$FeO \cdot Fe_2O_3$	8.3967 [10]
A	$(FeO)_{0.846}(Fe_2O_3)_{1.154}$	8.387
B	$(Fe_{0.824}Mn_{0.0278}Zn_{0.0074})O_{0.859}(Fe_2O_3)_{1.141}$	8.393
C	$(Fe_{0.840}Mn_{0.0096}Zn_{0.0002})O_{0.850}(Fe_2O_3)_{1.150}$	8.391
D	$(Fe_{0.510}Mn_{0.0104}Zn_{0.0294})O_{0.550}(Fe_2O_3)_{1.450}$	8.375
D′	$(Fe_{0.402}Mn_{0.0108}Zn_{0.0302})O_{0.443}(Fe_2O_3)_{1.557}$	8.367
E	$(Mn_{0.0118}Zn_{0.0350})O_{0.047}(Fe_2O_3)_{1.953}$	8.344
F	$(Fe_{0.008}Mn_{0.0120}Zn_{0.0016})O_{0.022}(Fe_2O_3)_{1.978}$	8.343
γ-Fe_2O_3	Fe_2O_3	8.341 [9] [a]

[a] Calculated from original diffraction data of high angles by the present authors.

ides and the lattice constants corrected for the replacements of the iron with minor metal atoms.

REFERENCES

1 Y. Kodera and Y. Inada, Kagaku to Kogyo, 41 (1988) 40.
2 M. Iwatsuki and T. Fukasawa, Taiki Osen Gakkaishi, 27 (1992) 218.
3 J. Kanazawa, H. Maekawa and T. Yokogawa, X-sen Bunseki no Shimpo, 13 (1982) 9.
4 K. Honma, T. Kimura, Y. Kawasaki and H. Soezima, Bunseki Kagaku, 23 (1974) 591.
5 E.Z. Basta, Econ. Geol., 54 (1959) 698.
6 I. Iwasaki, T. Katsura, M. Yoshida, and T. Tarutani, Bunseki Kagaku, 6 (1957) 211.
7 Nippon Gakujutsu Shinkoukai, Tekkou Kagaku Bunseki Zensho, Vol. 9, Nikkan Kogyo Shimbunsha, Tokyo, new edn., 1963, p. 38.
8 JIS M8124, Methods for Determination of Zinc in Ores, Japanese Industrial Standards Committee, Tokyo, 1979.
9 JCPDS, Powder Diffraction File, Int. Centre for Diffraction Data, Swarthmore, PA, No. 25-1402 (1975).
10 JCPDS, Powder Diffraction File, No. 19-629 (1969).
11 JCPDS, Powder Diffraction File, No. 24-81 (1974).
12 JCPDS, Powder Diffraction File, No. 10-319 (1960).
13 JCPDS, Powder Diffraction File, No. 22-1012 (1972).

Analytica Chimica Acta, 281 (1993) 421–428
Elsevier Science Publishers B.V., Amsterdam

Applicability of photon correlation spectroscopy for measurement of concentration and size distribution of colloids in natural waters

Anna Ledin, Stefan Karlsson, Anders Düker and Bert Allard

Department of Water and Environmental Studies, Linköping University, S-581 83 Linköping (Sweden)

(Received 16th November 1992; revised manuscript received 5th April 1993)

Abstract

The suitability of photon correlation spectroscopy (PCS) for the determination of concentration and size distribution of colloidal matter was tested in a surface water and in a deep groundwater. Well-defined colloids (sizes predominately in the range 50–500 nm) of α-Fe_2O_3, γ-$Al(OH)_3$, SiO_2, kaolinite, illite and a humic acid in aqueous solutions were used as references for calibration of the PCS-instrument (signal vs. concentration). The intensity of the scattered light was dependent on the composition of the colloid. The concentration ranges, where a quantitative determination of the colloid could be achieved, were 0.03–2 mg/l, 0.1–2 mg/l, 0.1–7 mg/l, 0.5–10 mg/l, 0.5–50 mg/l and 0.5–75 mg/l for α-Fe_2O_3, γ-$Al(OH)_3$, SiO_2, kaolinite, illite and humic acid, respectively (in homogeneous systems). The colloidal populations in the surface waters (inlet and outlet of a lake) had a size distribution in the range 100–500 nm. The measured count rates were around 330 kcps and 30 kcps at the inlet and outlet, respectively, which correspond to totally 2.8 mg/l and 0.9 mg/l of colloidal matter according to gravimetric determinations (collected on clogged 0.015 μm filters). Comparisons of concentrations estimated from measurements of reference colloids with PCS and gravimetric determinations of the colloidal matter showed that a combination of the two methods would be needed. The measurements of a deep groundwater were performed on-line and in situ with a PCS technique. The content of colloidal matter in the groundwater was below the detection limit for the PCS-equipment, which corresponds to a concentration not above 0.5 mg/l and probably below 0.1 mg/l in the present system. The feasibility and advantages of using PCS for non-disturbing size characterisation and concentration measurements of colloids in aquatic systems have been demonstrated, as well as some limitations of the method.

Keywords: Colloids; Photon correlation spectroscopy; Waters; Size distribution

It is well known that many trace elements in natural waters tend to be associated with colloidal matter, that serves as a mobile carrier phase in transport and redistribution processes (cf. [1,2]). The colloidal fraction in natural waters is usually defined as particulate matter with a diameter less than 1 μm. Dominating discrete inorganic components and/or surface films are usually oxides and hydroxides of Al, Fe, Mn and Si, clay minerals as well as Ca and Ca–Mg carbonates. Coatings of humic matter are common [3,4]. There is, however, only limited information about the size distribution and concentration of the suspended matter of colloidal size in natural aquatic systems, particularly in groundwaters.

The use of various methods for the characterisation of colloidal matter, as well as the limitations of the methods applied in field systems,

Correspondence to: A. Ledin, Department of Water and Environmental Studies, Linköping University, S-581 83 Linköping (Sweden).

have recently been summarised within an international inter comparison exercise [5].

Measurements of mass and size distribution of the particulate phase have often been made by gravimetric determination of the fraction retained by filters of different nominal pore sizes. Filtration is usually considered as a simple straightforward procedure, but precautions are required to maintain the original distribution of both dissolved and solid constituents, e.g. in waters of low redox potential (Eh) when an oxidation and gradual precipitation of Fe(III) will take place after exposure to air. Loss of solid matter and dissolved trace elements by adsorption to the filters must be considered when filters with large surface areas, e.g. ultra and cellulose derivative filters as well as hollow fibres, are used [6,7]. Screen filters (e.g. thin films of polycarbonate) are non-sorbing but suffer from clogging. This disadvantage may be increased due to their tendency to adsorb particles at the pore edges reflecting the electrical charge distribution [6]. Size distributions from scanning or transmission electron microscopy (SEM and TEM) suffer from changes induced during the sample preparation, since the original samples (often wet filters and grids) have to be dried. Dehydration of amorphous precipitates can lead to a consolidation, and agglomeration of organic macromolecules as well as inorganic colloids may take place when the ionic strength increases during drying. Additional alterations can be caused by changes in pH, also as a result of the drying procedure. Instrumental limitations in counting particles below 100 nm by SEM limits the use of this technique even further [8]. It is therefore important that results obtained with various batch-type techniques can be validated with complementary studies, if possible by using procedures suitable for field work on original water samples.

Photon correlation spectroscopy (PCS) is a non-destructive technique which requires a minimum of sample treatment. It is suitable for measurements of size distributions and concentrations of particles of homogeneous composition and fairly uniform size distribution (diameter less than 500 nm) in aqueous systems [9]. Delgado and Matijevic [10] stated, that PCS would be preferable compared to electron microscopy, particularly for monodisperse samples, since sample treatment and exposure to the electron beam can alter the composition and size distribution of the colloidal matter. PCS has previously been used for determination of size distributions, in studies of the stability of inorganic colloids [11–16], as well as for measurements of the particle character of natural organic macromolecules [17–19] and studies of natural colloidal matter [20–23] under laboratory conditions. The technique has not been applied for studies of natural water colloids in situ, largely because the instrument requires high voltage and efficient cooling of the laser light source. Also, the possibilities to characterise natural heterogeneous samples (with respect to size distribution, particle geometry and elementary composition) are limited [24].

The aim of this study was, besides size distribution measurements, to test the application of the PCS-technique for concentration measurements of natural colloids in waters by designing a suitable calibration procedure with well-defined homogeneous reference substances (laboratory) as well as by using a flow-through cell for direct continuous measurements (in situ).

MATERIALS AND METHODS

PCS equipment

Size distribution and concentrations of the colloidal fractions (in laboratory and field systems) were measured with a Brookhaven BI-90 instrument, equipped with a 2 W argon-laser (Lexel). Light scattering was recorded at 488 nm and with laser effects of 700 mW or 900 mW. The general theory of PCS has previously been presented elsewhere [25,26,9]. The solution of the auto-correlation function that is needed for evaluation of the scattered light from the various size populations was in the present studies achieved by inverse Laplace transform routines with the original software [27].

Measurements were performed in closed polystyrene cuvettes, rinsed 4 times with Milli-Q water prior to the measurements. All sample preparations were performed in a Laminar flow

bench in order to prevent contamination with particles from the air. A flow-through cuvette was constructed for continuous on-line measurements (for more details see [28]).

Calibration with reference colloids

The colloids of α-Fe_2O_3 and γ-$Al(OH)_3$ were precipitated according to Penners and Koopal [29] and Hiemstra et al. [30], respectively. A vibration mill was used to produce colloidal size suspensions of SiO_2 from natural crystalline quartz, kaolinite (from Washington County, GA, USA) and illite (from Harwell Borehole, USA) [16]. The colloids were allowed to equilibrate with Milli-Q water and settle (in the dark at 8°C) in a sedimentation funnel for a minimum of 4 weeks. This procedure produced relatively monodisperse colloid populations with fairly narrow size distributions (see below). Solutions with the suspended colloids were sequentially diluted with Milli-Q water (at constant pH), equilibrated for 10 min, whereafter the count rate (photon counts per time unit) were recorded. The mass of the colloids was determined gravimetrically after collection on 0.015 μm polycarbonate membrane filters. Humic acid (HA) from Aldrich (Na-salt, Cat NoH1, 675-2) was diluted in 0.005 mol/l $NaClO_4$ at pH 10, ultrasonicated for 10 min, followed by acidification to pH 6.0. The stock solution was sequentially diluted with the ionic medium and analysed with the same procedure as the inorganic colloids.

Field sampling and PCS measurements in situ

Water was sampled in two field systems (surface waters and groundwater) with different colloid composition, redox potential, gas pressures and temperature.

The colloidal fraction was generally collected on 0.015 μm polycarbonate membrane filters for gravimetric determination as well as analysis of major cationic elements. The solid phase was digested in a mixture of concentrated sulphuric and nitric acids, followed by dissolution in condensed phosphoric acid. All chemicals were of analytical quality or better. The concentrations of Al, Ca, Fe, Mg, Mn and Si in the solids were determined by atomic absorption spectrophotometry. Mineral composition and possible surface coatings of macromolecular organic matter were studied by Fourier transform infrared spectroscopy (FT-IR) on replicate samples. The groundwater samples were equilibrated with the atmosphere for 72 h prior to the filtration.

Surface water samples. These were collected in Lake Risten, Åtvidaberg, Sweden, in May 1992. Information about the area has previously been summarised by Allard et al. [31]. The samples were collected in polypropylene bottles at the inlet and outlet of the lake at 0.3 m below the water surface. The bottles were capped under water and transported in the dark at the original temperature to the laboratory for immediate PCS measurements. The samples were prefiltered through 1.2 μm membrane filters of polycarbonate in order to reduce disturbances in the instrument readings from any large particles. Sampling and analysis were completed within 6 h.

Groundwater samples. These were collected in the crystalline granitic rock at the Äspö Hard Rock Laboratory, about 20 km NNE of Oskarshamn, Sweden, at a depth of 75 m in the bedrock. Information about the building and operation of the underground rock laboratory is given in [28] and [32]. The geology and hydrological conditions are described in [32], and the chemical composition of the water at the present sampling place is given in [28] and [33]. The PCS instrument was installed in the underground tunnel in a caravan modified to a chemical field laboratory and equipped with filters to remove dust from the ambient air. A PTFE tubing connected to a hosing in the bedrock (sampling hole KR0013B) provided groundwater flowing from a fracture zone (at 400 ml/min), thus allowing a continuous water sampling and subsequent analysis in the caravan. During the measurements the water was allowed to flow through the cuvette, placed in measuring position in the PCS-instrument, at 10 ml/min for at least 5 min (equivalent to more than 12 cuvette volumes) before the flow was stopped and the PCS measurement began. Samples were also prepared traditionally for comparative purposes by filling the sample cuvettes under nitrogen (Alfax, N60 atmosphere) in a glove bag. The cuvettes were sealed, removed from the

glove bag and measured by PCS, with repeated measurements after 6 h.

RESULTS AND DISCUSSION

Instrument performance and calibration

The count rate (expressed as counts per seconds, kcps) is in principal determined by the number of particles in the scattering volume. A minimum of 100 particles is required [24], which corresponds to a count rate above 10 kcps for the PCS-equipment used in this study. Other parameters influencing the intensity of the scattered light are e.g. the refractive index of the particles as well as their geometric shapes.

The count rate was proportional to the colloid concentration, however in concentration ranges that were individual for the materials (Fig. 1 and Table 1). Assessed initial size distributions (Fig. 2 and Table 1) were confirmed from SEM micrographs from which the geometric shapes of the colloids could be studied. The α-Fe_2O_3 and SiO_2 were largely spherical while α-Fe_2O_3, γ-$Al(OH)_3$, kaolinite and illite were disc like. Examination of HA with SEM indicated a structure similar to amorphous hydroxides where no typical geometric shape is evident. Neither the number of particles in the scattering volume (estimated from size distributions, geometry and densities) nor in the refractive indices can alone explain the large differences between the colloids, as given by the observed signal to mass relationship. Effects of absorption (particularly HA) and shape (e.g. number of edges and corners) are difficult to estimate.

Field studies

The colloidal populations in the *surface waters* had size distributions in the range 100–500 nm and 100–300 nm at the inlet and outlet, respectively (Fig. 3). FT-IR spectra indicated the presence of a predominantly illitic clay with minor contributions of organics. The presence of Al and Fe in the solid fraction was indicated from chemical analysis of the solids [35]. Saturation indices, calculated with the geochemical code PHREEQE [36] indicated an oversaturation with respect to

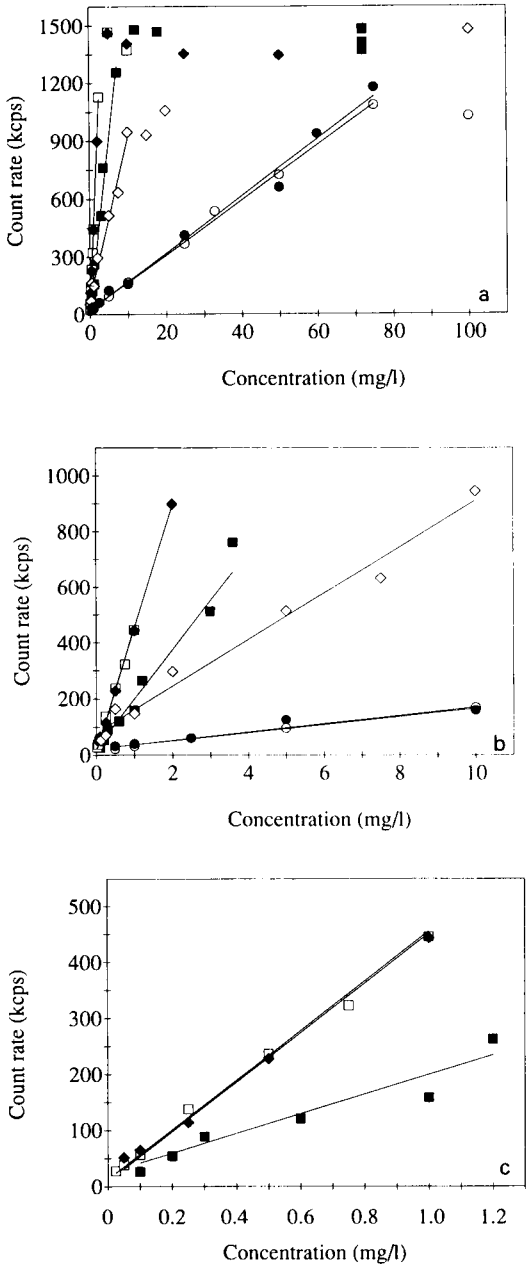

Fig. 1. Relationship between the PCS count rate and the concentration of the reference colloids. □ Fe_2O_3; ♦ $Al(OH)_3$; ■ SiO_2; ◇ kaolinite; ○ illite; ● humic acid. (a) Concentration range 0–110 mg/l. (b) Concentration range 0–11 mg/l. (c) Concentration range 0–1.3 mg/l.

Al and Fe hydrous oxides in the inlet sample (c.f. analysis of the colloidal fractions in Table 2). The concentrations were below saturation at the out-

TABLE 1

Characteristics of the reference colloids according to the PCS measurements

Colloidal phase	Concentration range (mg/l) [a]	Initial distribution (nm)	Refractive index [34]
α-Fe_2O_3	0.03– 2	10– 75	2.94; 3.22
γ-$A(OH)_3$	0.1 – 2	100–325	1.56–1.60
SiO_2	0.1 – 7	50–300	1.55
Kaolinite	0.5 –10	115–350	1.55–1.57
Illite	0.5 –50	50–400	1.54–1.61
Humic acid [b]	0.5 –75	70–250	

[a] Range where the concentration is proportional to the count rate. [b] From Aldrich; soil origin.

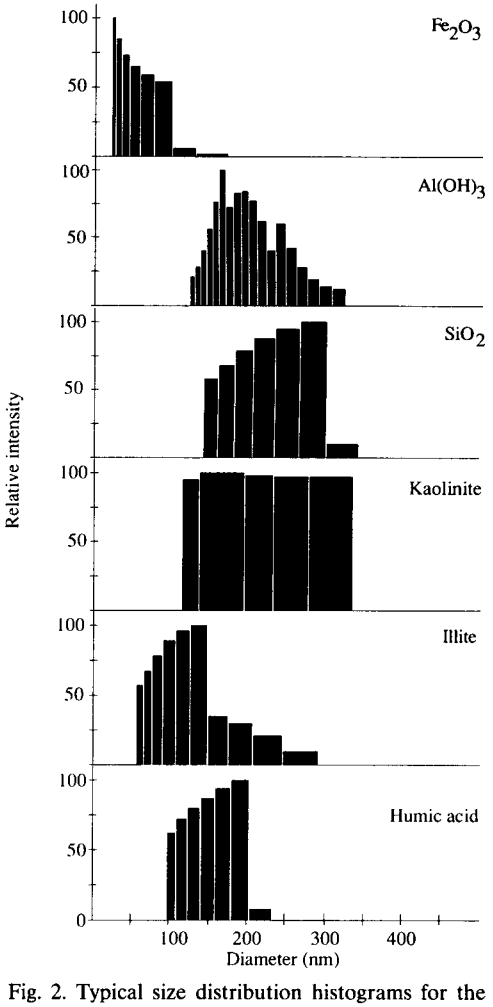

Fig. 2. Typical size distribution histograms for the reference colloids (pH 6.0 ± 0.5).

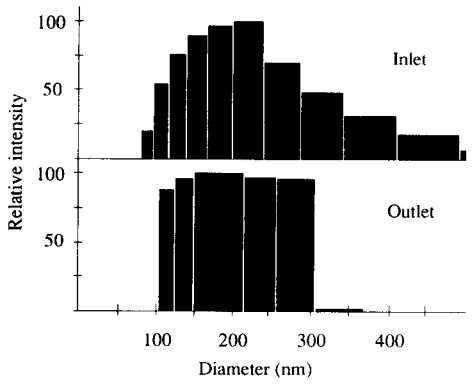

Fig. 3. Typical size distribution histograms for the colloidal matter in the surface water samples.

let, where the presence of Al in the colloids would originate from the illite, while Fe could be present in association with humic substances on the surfaces [35].

The measured count rates were around 330 kcps and 30 kcps at the inlet and outlet, respectively, corresponding to 2.8 and 0.9 mg/l, according to the gravimetric determinations. A count rate of 30 kcps (outlet) corresponds to less than 0.1 mg/l of Fe_2O_3, $Al(OH)_3$ or SiO_2 (below detection limit), considering the count rate vs. concentration for homogeneous systems (Fig. 1). This count rate would also be close to the detection limit of 0.5 mg/l for illite as well as humic matter. The observed colloid concentration of 0.9 mg/l (from gravimetry) reflects a composition of predominantly illite-humics, which is in qualitative agreement with FT-IR data for the filter residues.

TABLE 2

Concentrations of metals (acid soluble) in the surface water samples

Metal.	Concentration (μg/l)	
	Inlet	Outlet
Al	1535	121
Ca	19.0	13.9
Fe	333	35.3
Mn	58.3	4.5
Si	4990	309

A count rate of 330 kcps would correspond to 20–25 mg/l of illite or illite-humics. However, the results from the gravimetric determination (2.8 mg/l) at the inlet seem reasonable when considering the heterogeneous surface coatings consisting of organic matter and precipitates of Al and Fe (also indicated from the analyses and calculations of saturation indices).

Storing at room temperature for 24 h did not significantly alter the count rates and size distributions of the present samples. This indicates that the samples were largely at equilibrium with atmospheric oxygen prior to analysis.

The results illustrate that PCS readings must be calibrated against gravimetrically quantified colloidal matter from each individual field site, or with several reference systems chosen according to the results from a detailed chemical or mineralogical analysis of the composition of the colloidal phase, particularly concerning surface coatings. A combination between the two techniques (gravimetry and PCS) is required.

Groundwater samples, prepared in the glovebag or measured on-line, had *initial* count rates below the detection limit of the instrumental set-up. Thus, the PCS-equipment was not sensitive enough to measure the low colloid concentrations found in the present saline groundwater. According to the reference colloids the observed count rates would correspond to colloid concentrations less than 0.5 mg/l, assuming inorganic colloids consisting of kaolinite and illite or organic colloids with HA as the main component. If a dominating original colloidal fraction of SiO_2, $Al(OH)_3$ or Fe_2O_3 are assumed, the corresponding upper limits would be 0.1 mg/l and 0.03 mg/l, respectively. Thus, a colloid concentration lower than 0.03–0.5 mg/l can be assumed. These results can be compared to studies performed in various groundwaters using other methods for determination of the colloid concentrations. Degueldre et al. [8] estimated the colloid concentration (size range of 100–1000 nm) to 0.2 mg/l inorganic colloids or 0.1 mg/l organic colloids in samples from a subsurface fracture in granitic rock at the Grimsel Test Site, Switzerland. Miekeley et al. [37] reported an inorganic colloid concentration (< 450 nm) of less than 1 mg/l in waters from the Osamu Utsumi mine and Morro do Ferro analogue study sites, Pocos de Caldas, Brazil. These estimations were largely based on SEM analyses of particles collected on filters, assuming that the colloids were either organic (density of 1 g/cm^3) or inorganic (density of about 2 g/cm^3). The concentration of colloids in deep Swedish granitic groundwater has previously been assessed to be below 0.4 mg/l, according to Laaksoharju [38]. This concentration level was estimated from analysis of groundwater particles collected on filters, combined with calculated saturation indices as indications of probable particle compositions.

The formation of colloidal particles in the groundwater samples was observed in a matter of minutes after exposure to air, and was in fact evident within 6 h even in the closed cuvette, due to diffusion of air into the system [28]. This particle fraction had an average diameter of 210 nm, a size distribution in the range 125–385 nm and a count rate of 80 kcps. The latter would correspond to a particle concentration in the range 0.1–4 mg/l, depending on the composition (cf. Fig. 1).

Due to the low particle content in the groundwater and the fact that a new colloidal phase was formed immediately after exposure to air it was not possible to determine the composition of the original colloidal matter. The particulate material was filtrated after equilibration with air and analysed. It contained hydrous oxides of Fe (40% dry weight) as major part but also Ca and Ca–Mg carbonates (26%), hydrous oxides of Al and Si (12%) and associated organic matter (22%) [28]. The colloidal fraction precipitating after exposure to air represented the precipitation of hydrous oxides of Fe, but possibly also with a contribution of a mixed carbonate phase precipitating by the exposure to CO_2 [38] and by the temperature increase. The original colloidal fraction would then largely consist of hydrous SiO_2, possibly with a minor fraction of clay minerals. The organic matter is predominantly fulvic acid of low molecular weight (see [28]) which would not exhibit a particle character at this concentration level. Thus, total colloidal concentration of 0.1 mg/l or below seems reasonable.

Conclusions

The following general conclusions may be drawn.

The measured count rate was proportional to the colloid concentration in the concentration ranges 0.03–2 mg/l, 0.1–2 mg/l, 0.1–7 mg/l, 0.5–10 mg/l, 0.5–50 mg/l and 0.5–75 mg/l for α-Fe_2O_3, γ-$Al(OH)_3$, SiO_2, kaolinite, illite and a high molecular weight humic acid, respectively. Thus, it is in principle feasible to perform non-disturbing direct measurements of size distribution as well as concentrations down to at least 0.5 mg/l or even lower (down to 0.1 mg/l for Al and Si systems; down to 0.03 mg/l in homogeneous Fe systems), providing that the phase composition is known.

Great precaution is, however, needed when the PCS-technique is used for measurements of colloid concentrations in heterogeneous systems, like most natural waters. The results can be totally erroneous if the calibration is performed with improper reference materials. Consequently, accurate determinations of the colloid concentrations with PCS-technique require in principle a detailed knowledge of the mineralogic composition of the colloids or possibly even a calibration of the instrument with natural colloidal matter from the specific field area.

The PCS-technique can be adapted for direct measurements in situ and on-line with a minimum of disturbing sample treatment or storage. The upper colloid concentration can be assessed in waters with extremely low colloidal content, e.g. deep groundwaters.

The detection limit of 0.5 mg/l or below is at least as good as what is achievable with other techniques but with the advantage of a minimum of undesired side-reactions. There is probably no other technique that could be used for quantitative non-interacting characterisation of colloids (concentration as well as size distribution) at these concentration levels (below 0.5 mg/l down to 0.03 mg/l), in field systems.

Technical assistance by Mr. P. Bengtsson, Brookhaven Instrument AB, and by Mr. G. Thörnell, Labora Co. is gratefully acknowledged. We thank Dr. C. Degueldre for fruitful discussion and advise concerning the technical limitations and possible errors in the interpretation of data when using the PCS-technique as well as Mr. M. Laaksoharju for comments concerning the possible role of changing CO_2 pressure. This project has partly been financed by the Swedish Nuclear Fuel and Waste Handling Co. (SKB), the Swedish Environmental Protection Agency (SNV) and the Swedish Natural Science Research Council (NFR).

REFERENCES

1 W. Stumm and J.J. Morgan, Aquatic Chemistry, Wiley, New York, 1981.
2 W. Salomons and U. Förstner, Metals in the Hydrocycle, Springer-Verlag, Berlin, 1984.
3 E. Tipping and D. Cooke, Geochim. Cosmochim. Acta, 46 (1982) 75.
4 R. Beckett and N.P. Le, Coll. Surf., 44 (1990) 35.
5 C. Degueldre, Grimsel colloid exercise, CEC Report EUR No. 12660 EN, Brussels, 1990.
6 K.C. Fan and J.W. Gentry, Environ. Sci. Technol., 12 (1978) 1289.
7 B. Salbu, H.E. Björnstad, N.S. Lindström, E. Lydersen, E.M. Brevik, J.P. Rambaek and E.P. Paks, Talanta, 32 (1985) 907.
8 C. Degueldre, B. Baeyens, W. Goerlich, J. Riga, J. Verbist and P. Stadelmann, Geochim. Cosmochim. Acta, 53 (1989) 603.
9 T.F. Rees, J. Cont. Hydrol., 1 (1987) 425.
10 A. Delgado and E. Matijevic, Part. Part. Syst. Charact., 8 (1991) 128.
11 B.E. Novich and T.A. Ring, Clays Clay Miner., 32 (1984) 400.
12 B.E. Novich and T.A. Ring, J. Chem. Soc. Faraday Trans., 81 (1985) 1455.
13 J.D.F. Ramsay, R.G. Avery and P.J. Russel, Radiochim. Acta, 44/45 (1988) 119.
14 R. Amal, J.R. Coury, J.A. Raper, W.P. Walsh and T.D. Waite, Coll. Surf., 46 (1990) 1.
15 U. von Gunten and W. Schneider, J. Coll. Interf. Sci., 145 (1991) 127.
16 A. Ledin, S. Karlsson and B. Allard, Appl. Geochem., (1993) in press.
17 M.S. Caceci and A. Billon, Org. Geochem., 15 (1990) 335.
18 M.S. Caceci and V. Moulin, in B. Allard, H. Borén and A. Grimvall (Eds), Humic Substances in the Aquatic and Terrestrial Environment, Springer-Verlag, Berlin, 1991, p. 97.
19 P.M. Reid, A.E. Wilkinson, E. Tipping and M.N. Jones, J. Soil Sci., 42 (1991) 259.

20 A. Billon, M. Caceci, G. Della Mea, T. Dellis, J.C. Dran, V. Moulin, S. Nicholson, J.C. Petit, J.D.F. Ramsay, P.J. Russell and M. Theyssier, The role of colloids in the transport of radionuclides in geological formations, CEC Report EUR No. 13506, Brussels, 1986.
21 P.M. Gschwend and M.D. Reynolds, J. Cont. Hydrol., 1 (1987) 309.
22 S. Nicholson and J.D.F. Ramsay, in C. Degueldre, G. Longworth, V. Moulin and P.Vilks (Eds), Grimsel colloid exercise, PSI Report No. 19, Willigen, (1990) p. 33.
23 T.F. Rees and J.F. Ranville, J. Cont. Hydrol., 6 (1990) 241.
24 B. Weiner, in Proc. 25th Anniversary Conf. of the Particle Characterisation Group of the Analytical Division of the Royal Society of Chemistry, Univ. of Technology in Loughborough, 1991.
25 B. Chu, Laser Light Scattering, Academic Press, New York, 1974.
26 B. Berne and R. Pecora, Dynamic Light Scattering with Applications to Chemistry, Biology and Physics, Wiley-Interscience, New York, 1976.
27 Brookhaven Instruments Corporation, Instruction Manual for Model BI-90 Particle Sizer, Holtsville, 1986.
28 A. Ledin, S., Karlsson, A. Düker and B. Allard, Water Res., submitted for publication.
29 N.H.G. Penners and L.K. Koopal, Coll. Surf., 19 (1986) 337.
30 T. Hiemstra, W.H. van Riemsdijk and M.G.M. Bruggenwert, Neth. J. Agric. Sci., 35 (1987) 281.
31 B. Allard, S. Bergström, M. Brandt, S. Karlsson, U. Lohm and P. Sandén, Nord. Hydrol., 18 (1987) 279.
32 J. Smellie and M. Laaksoharju, Hydrochemical investigations in relation to existing geologic and hydrologic conditions, SKB SHRL Progress Report 25–91–05, Stockholm, 1991.
33 Geotab, Ground water chemistry in the database Geotab, Swedish Nuclear Fuel and Waste Handling Co. (SKB), Stockholm, 1992.
34 Handbook of Chemistry and Physics, CRC Press, Boca Raton, FL, 1983–84.
35 A. Ledin, S. Karlsson and K. Håkansson, Nord. Hydrol., to be published.
36 D.L. Parkhurst, D.C. Thorstenson and L.N. Plummer, U.S.G.S. Water-Res. Investig., 80–96 (1984) 210.
37 N. Miekeley, H. Countinho de Jesus, C.L. Porto da Silveira and C. Degueldre, Chemical and physical characterisation of suspended particles and colloids in waters from the Osamu Utsumi mine and Morro de Ferro analogue study sites, Pocos de Caldas, Brazil, SKB Technical Report 90–18, Stockholm, 1991.
38 M. Laaksoharju, Colloidal particles in deep Swedish granitic groundwater, SKB Arbetsrapport 90–37, Stockholm, 1990.

Analytica Chimica Acta, 281 (1993) 429–433
Elsevier Science Publishers B.V., Amsterdam

Preconcentration of nickel-63 in sea water for liquid scintillation counting

Jem-Mau Lo, Bor-Jen Cheng, Chia-Lian Tseng and Jun-Der Lee

Institute of Nuclear Science, National Tsing Hua University, Hsinchu 30043 (Taiwan)

(Received 9th March 1993)

Abstract

A preconcentration procedure for enriching ^{63}Ni from sea water for measurement by liquid scintillation counting (LSC) was established. ^{63}Ni was first enriched by adsorption on hydrous magnesium oxide. The precipitate was collected and dissolved in concentrated HCl. ^{63}Ni was separated from the HCl solution by extraction with diethyldithiocarbamate in chloroform followed by back-extraction into Au^{3+} solution. Finally, ^{63}Ni in the Au^{3+} solution was extracted with dimethyl glyoxime in xylene and the organic phase containing ^{63}Ni was withdrawn for LSC. The optimum conditions of the above preconcentration procedure were investigated by means of an *r*-emitter, ^{65}Ni, instead of ^{63}Ni, which is a weak β-emitter, as a radioactive tracer. The preconcentration procedure was applied in conjunction with LSC to the analysis of a ^{63}Ni-containing simulated sea-water sample and was found to be feasible and practical.

Keywords: Radiochemical methods; Liquid scintillation counting; Nickel; Preconcentration; Sea water; Waters

Nickel-63 is one of the major radioactive corrosion products existing in the water coolant of nuclear power reactors. It arises from neutron capture of the nickel released from the steel pipings due to corrosion. Nickel-63 is a long-lived radionuclide ($t_{1/2} = 9.2$ years) and emits weak β-radiation ($E_{max} = 0.067$ MeV). This radionuclide is included in the list of low-level, long-lived radioactive wastes from nuclear power reactors specified in the NRC Regulation 10 CFR Part 61 published by the Nuclear Regulatory Commission in 1982. Nickel-63 may be released from nuclear power reactors and have a radiological impact on the natural environment; one of the possible ways is from the water coolant via a leaking condenser into the cooling sea water.

Correspondence to: Jem-Mau Lo, Institute of Nuclear Science, National Tsing Hua University, Hsinchu 30043 (Taiwan).

The determination of ^{63}Ni in solid samples such as sludge and resins was reported in NUREG/CR-4101/Part 1 [1]. The sludge or resin was dissolved in mixed strong acids. Fe^{3+} ion was added together with ammonia solution to the solution in order to effect $Fe(OH)_3$ precipitation. ^{63}Ni remained in the supernatant solution as an ammonia complex. To the supernatant solution, dimethyl glyoxime (DMG) was added and ^{63}Ni settled out as an Ni–DMG complex. The complex was separated and dissolved in HNO_3–$HClO_4$ (1 + 1) and then the solution was heated nearly to dryness. The salt was dissolved in water and used to measure the ^{63}Ni activity by liquid scintillation counting (LSC). Determination of ^{63}Ni in steel has been reported by Radwan et al. [2]. Steel shavings were dissolved in a mixture of HNO_3 and HCl and ^{63}Ni was separated from the solution, after the appropriate pH adjustment, by extraction with DMG in toluene. The organic

phase was withdrawn and liquid scintillator solution was added for ^{63}Ni activity measurement.

As illustrated in the examples mentioned above, the separation and purification of ^{63}Ni from the original sample matrices is essential for its measurement by LSC owing to its weak β-radiation and the possible interference from coexisting radionuclides. In this study, it was attempted to establish a method for determining low-level activity of ^{63}Ni in sea water. Enrichment of ^{63}Ni from sea water by the proposed preconcentration procedure, including adsorption by MgO and extraction with dithiocarbamate, was undertaken prior to the common process of DMG extraction followed by LSC activity measurement.

EXPERIMENTAL

Reagents

Magnesium oxide was purchased from Hanawa (Osaka, Japan) in a "light" form and of chemically pure reagent grade. Sodium diethyldithiocarbamate (NaDDC), xylene, ammonia solution, hydrochloric acid, ammonium citrate, dimethyl glyoxime (DMG), 2,5-diphenyloxazole (PPO) and 1,4-bis-2-(4-methyl-5-phenyloxazolyl)benzene (DMPOPOP) were all of analytical-reagent grade from Merck (Darmstadt). Goldmetal ($\geqslant$ 98% purity) was purchased from a local jewellery store. Pure water was produced in a Taiwan Water Purification Industrial apparatus through serial purification steps including cation- and anion-exchange resin beds, a mixed bed of ion-exchange resins and reverse osmosis. Sea water was collected from the coast of Taiwan Strait near Hsinchu, Taiwan, and filtered through a Toyo 100 filter-paper.

A 1% DMG solution was freshly prepared by dissolving 1 g of the compound in 100 ml of ethanol. The solution used for LSC was prepared by dissolving 1 g of PPO and 0.6 g of DMPOPOP in 100 ml of xylene. A 30% ammonium citrate solution was prepared by dissolving 3 g of the compound in 10 ml of water. Gold was dissolved in aqua regia, evaporated to dryness and the residue dissolved in water to make a 500 mg l^{-1} Au^{3+} solution.

Radiotracers

Nickel-63 ($t_{1/2}$ = 92 years, 0.067 MeV β-radiation) was purchased in the form of $NiCl_2$ solution with specific activity ca. 50 μCi μg^{-1} from NEN (Boston, MA). Nickel-65 [$t_{1/2}$ = 2.564 h, 0.65 MeV (30%), 1.02 MeV (11%) and 2.14 MeV (58%) β-radiation; 0.365 MeV (45%), 1.115 MeV (16%) and 1.418 MeV (25%) r-radiation] was produced via the $^{64}Ni(n,r)^{65}Ni$ reaction by irradiating nickel metal in the Tsing Hua open-pool reactor. Iron-59 [$t_{1/2}$ = 45.6 days, 0.273 MeV (48%), 0.475 MeV (51%) and 1.573 MeV (0.30%) β-radiation; 0.143 MeV (0.8%), 0.192 MeV (2.8%), 1.095 MeV (56%) and 1.292 MeV (44%) r-radiation] was produced via the $^{58}Fe(n,r)^{59}Fe$ reaction by irradiating iron metal in the reactor. Both of the irradiated metals were dissolved in concentrated HCl, evaporated to dryness and the residue was dissolved in water to an appropriate concentration.

Preconcentration procedure

To establish the optimum procedure for preconcentration of ^{63}Ni from sea water to the final LSC activity measurement, ^{65}Ni was used in place of ^{63}Ni as a radiotracer in all of the following experiments. This is due to the convenience of the presence of r-rays from ^{65}Ni, which can be counted with an NaI(Tl) crystal without taking into account the effect of self-absorption of the sample matrix. A 4-l volume filtered sea water was taken and radioactive nickel was added to give a simulated sea-water sample. A 4-g amount of MgO was weighed and added to the sea-water sample to adsorb radioactive nickel. The solution was stirred for 30 min to ensure that all of the radioactive nickel was adsorbed on MgO. After waiting for 1 h, the supernatant was decanted and the MgO solid was collected. Thereafter concentrated HCl was added in a the minimum amount to dissolve the MgO solid. The solution was evaporated to dryness and the residue was dissolved in water. After adjusting the pH to ca. 1, 60 mg of NaDDC were added to chelate the radioactive nickel. A 10-ml volume of chloroform was then

added and the Ni–DDC chelate was extracted into the organic phase by shaking mechanically for 10 min. After standing for 10 min, the organic solution was separated. Then 10 ml of the aqueous 500 mgl^{-1} Au^{3+} solution were added. After shaking for 5 min, the radioactive nickel in the Ni–DDC chelate was replaced with Au^{3+} and stripped into the aqueous solution. Finally, radioactive nickel in the aqueous solution was separated and extracted with 1% DMG with xylene as the organic solvent; previously, 2 ml of 1% ammonium citrate were added as the masking agent for shielding Au^{3+}. The radioactive Ni–DMG complex in the xylene obtained was withdrawn and mixed with the cocktail solution for LSC activity measurement.

Radioactivity measurements

An NaI(Tl) crystal connected to a single-channel analyser was used for measuring both ^{65}Ni and ^{59}Fe activities. A Packard Model 4530 liquid scintillation counter was used for measuring the ^{63}Ni activity. The liquid scintillator solutions for LSC measurement were added to the final enriched ^{63}Ni in the DMG complex in xylene. The external standard calibration method was used for quenching correction.

RESULTS AND DISCUSSION

It is difficult to detect ^{63}Ni directly in environmental or biological matrices owing to a serious self-absorption effect. The separation and purification of ^{63}Ni from the sample matrices are essential prior to the final activity measurement by LSC. A preconcentration procedure has been developed for the determination of ^{63}Ni in sea water, including serial steps, mainly adsorption by MgO, extraction with DDC, back-extraction with Au^{3+} and extraction with DMG. The preconcentration procedure serves the dual purposes of removing the major matrix material together with other radioactive nuclides and of increasing the concentration of ^{63}Ni for the final LSC counting. ^{65}Ni was employed in place of ^{63}Ni as the tracer to investigate the optimum conditions of the proposed preconcentration procedure.

TABLE 1

Influence of amount of magnesium oxide on the adsorption efficiency of ^{65}Ni from 4 l of sea water [a]

MgO added (g)	Adsorption efficiency (%)	MgO added (g)	Adsorption efficiency (%)
1.5	82	5.0	99%
3.0	91	10.0	99
4.0	97		

[a] The original amount of ^{65}Ni added was 10 μg with an activity of 2 μCi.

The radioactive nickel in the sea water was first concentrated by the MgO adsorption technique as reported previously [3]. A 4-l volume of the sea water was taken and ^{65}Ni tracer was added to give the simulated sample for analysis. It was estimated from the tracer technique that at least 4 g of MgO were required for 4 l of sea water to adsorb completely the radioactive nickel (see Table 1). Part of the amount of the MgO added will be consumed owing to considerable dissolution in such a large volume of sea water. The surface of the MgO solid will be hydrated in the form of $Mg(OH)_2$ in equilibrium with MgO_2^{2-}. Hence the hydrous MgO can function as a cation exchanger to adsorb the radioactive nickel in the form of Ni^{2+}. In addition, the hydrous MgO will simultaneously adsorb most of the other divalent or multivalent cations in sea water, if present, based on a similar rationale [3]. The rate of adsorption by MgO of the radioactive nickel is very rapid; stirring for 20 min was sufficient. The hydrous MgO solid was found to settle rapidly in the a form of a dense precipitate. Subsequently, the MgO solid was collected and then dissolved in the minimum volume of concentrated HCl. The solution was adjusted to pH 1 by adding 6 M NaOH. An appropriate amount of NaDDC (ca. 60 mg) was added and mixed with the solution (see Table 2).

At this stage, the final pH of the solution should be adjusted to the range 1–2 for the following extraction. The pH should not be lower than 1 to avoid the decomposition of DDC, and should not be higher than 2 to avoid the hydrolysis of Mg^{2+} to form colloidal $Mg(OH)_2$. The amount of Mg^{2+} was found not to influence the

TABLE 2

Effect of amount of sodium diethylthiocarbamate on the extraction efficiency of ^{65}Ni from a solution of 5 g of MgO in HCl [a]

NaDDC (mg)	Extraction efficiency (%)	NaDDC (mg)	Extraction efficiency (%)
10	47	100	> 99
30	96	200	> 99
50	> 99		

[a] The original amount of ^{65}Ni added was 10 μg with an activity of 2 μCi; the pH of the aqueous solution was adjusted to ca. 1 before extraction.

extraction of Ni^{2+} by DDC into chloroform (see Table 3). The extraction of Ni^{2+} with DDC was readily achieved with high efficiency as reported [4]. The organic phase was separated and back-extraction of the radioactive nickel in the organic solution with 500 mgl^{-1} Au^{3+} was subsequently applied. The Au^{3+} ion was selected as the stripping agent because the extraction constant of the Au–DDC complex is higher than that of Ni–DDC [5]. It should be noted that Au^{3+} may be the only metallic ion capable of stripping the nickel by the metal-to-metal replacement reaction from the organic phase. Most other metal ions are unsuitable as their extraction constants with DDC are lower than of Ni–DDC. The Au^{3+} back-extraction method is reported here for the first time. The kinetics of the back-extraction were investigated and found to be slow. As shown in Fig. 1, the shaking time should be longer than 25 min to obtain the maximum back-extraction efficiency.

The last step in the proposed preconcentration procedure is extraction with DMG. The radioactive nickel in the Au^{3+}-stripped aqueous solution

TABLE 3

Influence of mass of magnesium ion on the extraction efficiency of ^{65}Ni by NaDDC–chloroform from 100 ml water (pH 1.0–2.0) [a]

Mg^{2+} (g)	Recovery (%)
2	99
5	99
10	98

[a] The original amount of ^{65}Ni added was 10 μg with an activity of 2 μCi.

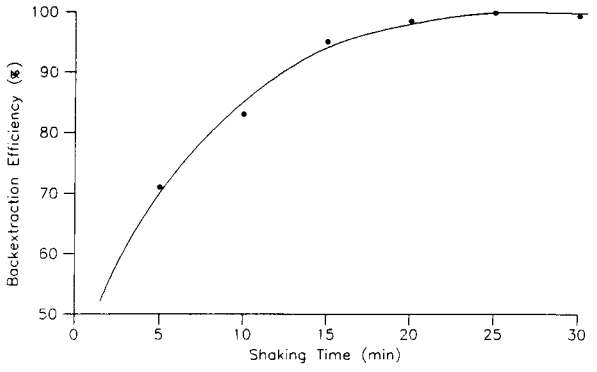

Fig. 1. Relationship between shaking time and back-extraction efficiency of ^{65}Ni in Ni–DDC in chloroform solution with an aqueous Au^{3+} solution.

was extracted with 1% DMG in xylene. Ammonium citrate was added beforehand to the solution. The role played by ammonium citrate was found to be twofold: as the buffer for pH control at 9.5 and as the agent for masking Au^{3+} and Fe^{3+}. Without adding ammonium citrate, Au^{3+} remaining from the proceding step would cause the formation of colloidal $Au(OH)_3$ in the pH 9.5 medium and Fe^{3+}, possibly emanating from the original sea water, and the reagents, e.g., MgO and NaDDC, would form a complex with DMG [2]. Either of the two cases would be a serious obstacle for the Ni extraction. In a separate study using ^{59}Fe as a tracer, iron ions were found not to be extracted from the ammonium citrate medium by the DMG–xylene system. The extraction effi-

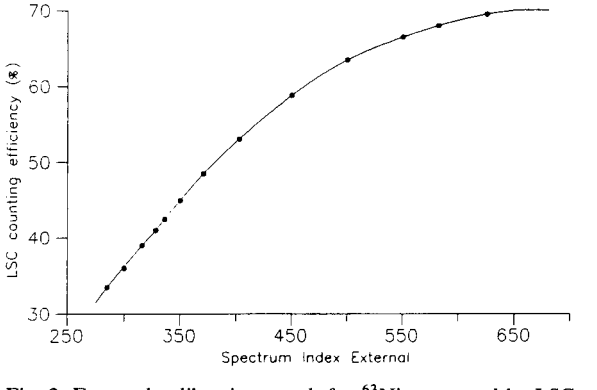

Fig. 2. External calibration graph for ^{63}Ni measured by LSC.

TABLE 4

Analytical results for a simulated sea-water sample spiked with ^{63}Ni [a]

Run No.	^{63}Ni activity added (cpm)	^{63}Ni activity found (cpm)
1	22200	21353
2	22200	21705
3	22200	20355

[a] All the ^{63}Ni activities were measured by LSC; the ^{63}Ni activity found was corrected for the chemical recovery of the preconcentration procedure, i.e., ca. 90%, obtained by ^{65}Ni tracer work.

ciency of radioactive nickel by the DMG–xylene system was found to be ca. 95%.

The Ni–DMG–xylene solution was the final radioactive nickel counting sample given by the preconcentration procedure. The overall yield of radioactive nickel from the original sea water to the final LSC counting sample was calculated to be ca. 90%. The enrichment factor of radioactive nickel is ca. 400 in accord with the preconcentration procedure mentioned above. The factor can be further enhanced, e.g., by increasing the volume of the sea water and/or by decreasing the volume of the final Ni–DMG–xylene solution.

The proposed preconcentration procedure was applied to the analysis of sea water for ^{63}Ni. A simulated sea water sample was produced by spiking filtered sea water with ^{63}Ni. A 4-l volume of the ^{63}Ni-spiked sea water were taken and subjected to the complete procedures described above. All the ^{63}Ni activities were measured by LSC; the counting sample was the DMG extract in xylene. The external standard correction method was used to obtain the LSC counting efficiency (Fig. 2). The LSC counting efficiency of the ^{63}Ni–DMG extract in xylene was ca. 67%. The analytical results for the simulated sea water sample are given in Table 4. The results show that the proposed preconcentration procedure is applicable in conjunction with LSC for determining ^{63}Ni in sea water.

REFERENCES

1 Assay of Long-Lived Radionuclides in Low-Level Wastes from Power Reactors, NUREG/CR-4101, Nuclear Regulatory Commission, Washington, DC, 1985.
2 M. Radwan, A. Przybylska, E. Mykowska and K. Gibas, Int. J. Appl. Radiat. Isot. 32 (1981) 91.
3 C.L. Tseng, J.M. Lo and S.J. Yeh, Anal. Sci., 3 (1987) 437.
4 J.M. Lo, J.C. Yu, F.I. Hutchison and C.M. Wai, Anal. Chem., 54 (1982) 2536.
5 J.M. Lo, C.L. Tseng and S.J. Yeh, Anal. Chim. Acta, 126 (1981) 191.

Analytica Chimica Acta, 281 (1993) 435–442
Elsevier Science Publishers B.V., Amsterdam

Factors affecting maximum relative concentrations of binary and ternary complexes in solutions

Marina Zelić

Center for Marine Research Zagreb, Rudjer Bošković Institute, P.O.B. 1016, 41001 Zagreb (Croatia)

(Received 24th December 1992; revised manuscript received 19th March 1993)

Abstract

Factors affecting maximum possible relative concentrations of simple (MA_a) and/or mixed-ligand (MA_aB_b) complexes in solutions are given for three cases: formation of simple species MA_a only; parallel formation of MA_a and MB_b complexes; and parallel formation of binary and ternary species. Equations that give the concentrations of A (in the absence of B or in the presence of a constant level of B), at which the highest percentage of the total dissolved metal is bound in the species of interest, are derived, assuming different values of the maximum coordination number. The application of such results in experimental work is discussed.

Keywords: Complexation; Metal complexes

In a system that consists of a metal ion (M) and a ligand (A), different coordination species can usually be formed [1], depending on the concentration of the complex-forming agent. Taking into account that each individual species is characterized by some specific properties such as charge, colour, surface activity or electroactivity, it can be useful or even necessary, for analytical or some other purposes, to convert the highest possible fraction of the total dissolved metal (M_t) into a chosen binary complex (MA_p). The percentage of the latter (P_p) in such a mixture is given by the expression

$$P_p = 100\beta_{p0}[A]^p / \left(1 + \sum_{a=1}^{N} \beta_{a0}[A]^a\right) \qquad (1)$$

where β denotes the corresponding overall formation constant and N is the highest possible coordination number. In a distribution diagram that gives the dependence of P_p on log [A], each curve, except the last one which reflects the presence of MA_N, is bell-shaped. The maximum of such a function, i.e., the ligand concentration at which the complex of interest constitutes the highest possible percentage of the total metal and the value of this percentage, can be found without difficulty. However, in textbooks on complex equilibria [2–5], this problem is only briefly discussed, if at all.

The situation is more complicated if an additional ligand is also present in the solution either as a consequence of the sample pretreatment (masking or precipitation of interfering metal ions) or because of the original sample composition. Such examples, which occur more often in experimental work than single-ligand systems, can be classified into two different groups according to whether mixed-ligand species are formed or not. For both of them the optimum measuring conditions can be predicted.

In this paper, the equations that give ligand concentrations at which the individual complexes reach their maxima are derived for the three mentioned situations and for a range of N val-

Correspondence to: M. Zelić, Center for Marine Research Zagreb, Rudjer Bošković Institute, P.O.B. 1016, 41001 Zagreb (Croatia).

ues. Possible applications of such results in experimental work are discussed. Attention is mainly focused on simple, i.e., binary, complexes because mixed-ligand species have already been treated in previous papers [6,7].

EQUILIBRIA

In a single-ligand system only reactions of the type:

$$M + aA \rightleftharpoons MA_a \quad (2)$$

are important, each of them being characterized by the value of the corresponding cumulative formation constant:

$$\beta_{a0} = [MA_a]/[M][A]^a \quad (3)$$

If another ligand (B) is also present in the solution, an additional series of complexes (MB_b) is also formed:

$$M + bB \rightleftharpoons MB_b \quad (4)$$

$$\beta_{0b} = [MB_b]/[M][B]^b \quad (5)$$

Under such conditions ternary species (MA_aB_b) should also be taken into account:

$$M + aA + bB \rightleftharpoons MA_aB_b \quad (6)$$

$$\beta_{ab} = [MA_aB_b]/[M][A]^a[B]^b \quad (7)$$

In the three cases mentioned (formation of one, two or three series of complexes), the following mass balance equations for the total metal concentration ($[M]_t$) are valid:

$$[M]_t = [M]\left(1 + \sum_{a=1}^{N} \beta_{a0}[A]^a\right) \quad (8)$$

$$[M]_t = [M]\left(1 + \sum_{a=1}^{N} \beta_{a0}[A]^a + \sum_{b=1}^{N} \beta_{0b}[B]^b\right) \quad (9)$$

$$[M]_t = [M]\left(1 + \sum_{a=1}^{N} \beta_{a0}[A]^a + \sum_{b=1}^{N} \beta_{0b}[B]^b + \sum_{a=1}^{N-1} \sum_{b=1}^{N-a} \beta_{ab}[A]^a[B]^b\right) \quad (10)$$

(Equation 10 is better than the corresponding expression given in [7].)

The concentrations of both ligands should greatly exceed the total metal level. Under such conditions, their free concentrations can be taken as being equal to the total, i.e., $[A] = [A]_t$ and $[B] = [B]_t$, assuming that protonation is not important. This is true for halides and other anions, formed by dissociation of strong acids. If not, free concentrations are primarily governed by the acidity of the solution and should be calculated from $[A]_t$ (or $[B]_t$), pH and the corresponding protonation constants [1].

In the two-ligand systems [B] is kept constant while [A] is gradually increased at constant values of the ionic strength (I) and total metal concentration. This is the way in which the two-ligand systems are usually studied [8] and is also a model for many real situations.

The mathematical procedure consists in searching for the maximum of the corresponding function (P as a function of [A] at constant [B]). For such a purpose the concentration of A should be found at which the first derivative of this function is equal to zero.

RESULTS AND DISCUSSION

Single-ligand solutions

For $N = 2$ the concentration of A ($[A]_m$) at which the MA complex reaches its maximum possible relative concentration is given by

$$[A]_m = \beta_{20}^{-1/2} \quad (11)$$

By introducing this relationship into Eqn. 1, the expression for the maximum possible percentage (P_m) of $[M]_t$ in the form of MA is obtained:

$$P_m = 100\beta_{10}/\beta_{20}^{1/2}/\left(2 + \beta_{10}/\beta_{20}^{1/2}\right) \quad (12)$$

which can be further reduced taking into account that $\beta_{10} = K_1$ and $\beta_{20} = K_1K_2$ (where each K denotes the corresponding stepwise stability constant):

$$P_m = 100(K_1/K_2)^{1/2}/\left[2 + (K_1/K_2)^{1/2}\right] \quad (13)$$

Equations 11–13 can be found in the literature [4], but the corresponding expressions for higher values of N are lacking.

To find the optimum ligand level for the maximum percentage of MA at $N = 3$, the equation

$$2\beta_{30}[A]^3 + \beta_{20}[A]^2 - 1 = 0 \quad (14)$$

should be solved. The value of [A] calculated in this way, when introduced into the equation for P_1:

$$P_1 = 100\beta_{10}[A]/\left(1 + \beta_{10}[A] + \beta_{20}[A]^2 + \beta_{30}[A]^3\right) \quad (15)$$

gives the maximum percentage of MA in a given system.

If $N = 4$, the above approach results in the following equation:

$$3\beta_{40}[A]^4 + 2\beta_{30}[A]^3 + \beta_{20}[A]^2 - 1 = 0 \quad (16)$$

for the optimum ligand concentration.

It is obvious that Eqns. 11, 14 and 16, together with those which correspond to higher N values, can all be presented in the same general form:

$$\sum_{a=1}^{N} (a-1)\beta_{a0}[A]^a = 1 \quad (17)$$

The whole procedure, repeated for MA_2 complex species and a range of maximum coordination numbers, gives the general equation

$$\sum_{a=1}^{N} (a-2)\beta_{a0}[A]^a = 2 \quad (18)$$

and for MA_3 species the final result is

$$\sum_{a=1}^{N} (a-3)\beta_{a0}[A]^a = 3 \quad (19)$$

The last three equations together with those which correspond to higher complexes (MA_4, MA_5, etc.) are all involved in the expression

$$\sum_{a=1}^{N} (a-p)\beta_{a0}[A]^a = p \quad (20)$$

which indicates that the ligand concentration necessary to reach the maximum percentage of the total metal in the form of a given MA_p species depends on the formation constants of all other complexes in the solution but not on the β_{p0} value (obviously, p can be any integer from 1 to $N-1$).

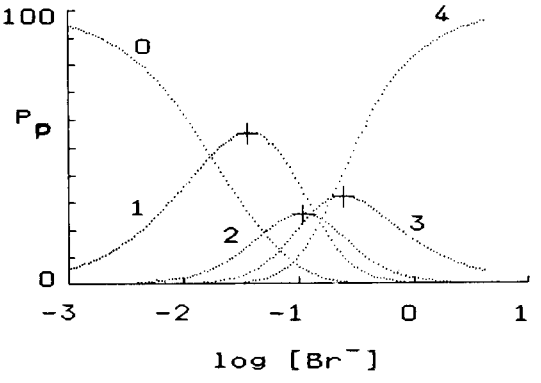

Fig. 1. Distribution of dissolved cadmium among different bromide complexes at $I = 4$ mol l^{-1} ($\log \beta_{10} = 1.76$, $\log \beta_{20} = 2.6$, $\log \beta_{30} = 3.5$, $\log \beta_{40} = 4.22$ [10]). Numbers on the curves denote p values of the corresponding $CdBr_p$ species. Crosses indicate the coordinates of the maxima calculated by means of Eqns. 20 and 1.

If the highest possible coordination number is 2, the calculations of $[A]_m$ and P_m values for MA species are simple. They can be of help in comparing the complexation of a given metal ion with different ligands and in presenting the results in the form of illustrative diagrams (see later).

At higher maximum coordination numbers the situation is more complicated and numerical methods [9] need to be applied in the calculations of the optimum ligand concentrations. Graphical presentations in two dimensions cannot be produced because the values of interest ($[A]_m$ and P_m) are functions of several variables, i.e., stability constants.

Although the given approach works (Fig. 1) and can be useful in recognizing some complex concentration–ligand concentration–stability constant relationships, routine application of the above equations is not to be expected. The reason is that complete distribution diagrams of the type given in Fig. 1 can be obtained rapidly by means of a relatively simple mathematical procedure. Hence the single-ligand systems and all equations derived for their description should mainly be taken as the starting point in the study of more complex situations.

Mixtures of binary complexes

In a two-ligand system, not complicated by the presence of mixed species, a simple distribution diagram cannot be constructed because the fraction of the total dissolved metal bound in each MA_a complex depends on the concentrations of both complexants. Hence the complete presentation can only be made in three dimensions. Usually, however, mixtures of ligands are studied under conditions that include a constant level of B and a gradually increasing concentration of A. In such a situation the distribution diagram can be calculated again. It is, however, different for each individual level of [B]. In Fig. 2 this type of graphical presentation is given for the Cd^{2+}–Br^- system at two different chloride levels assuming (not in accordance with reality [11]) that ternary complexes are not important. In comparison with Fig. 1, it can be observed that only complexes of the $CdCl_b$ type are present at lower concentrations of Br^- whereas $CdBr_a$ species become important at significantly higher bromide levels than in the absence of another complexant.

In a mixture of binary complexes if $N = 2$ and under the condition

$$[A]^2\beta_{20} = 1 + \beta_{01}[B] + \beta_{02}[B]^2 \qquad (21)$$

the complex MA will reach its maximum percentage according to the equation

$$P_m = 100\beta_{10}/\beta_{20}^{1/2}/(2G^{1/2} + \beta_{10}/\beta_{20}^{1/2}) \qquad (22)$$

where $G = 1 + \beta_{01}[B] + \beta_{02}[B]^2$; G will be used throughout the paper to denote the sum $1 + \beta_{01}[B] + \beta_{02}[B]^2 + \ldots + \beta_{0N}[B]^N$ at any N.

If $N = 3$, the equation analogous to Eqn. 21 is

$$2\beta_{30}[A]^3 + \beta_{20}[A]^2 = 1 + \beta_{01}[B] + \beta_{02}[B]^2 + \beta_{03}[B]^3 \qquad (23)$$

indicating that the maximum percentage of MA species is generally defined by the expression

$$\sum_{a=1}^{N} (a-1)\beta_{a0}[A]^a = G \qquad (24)$$

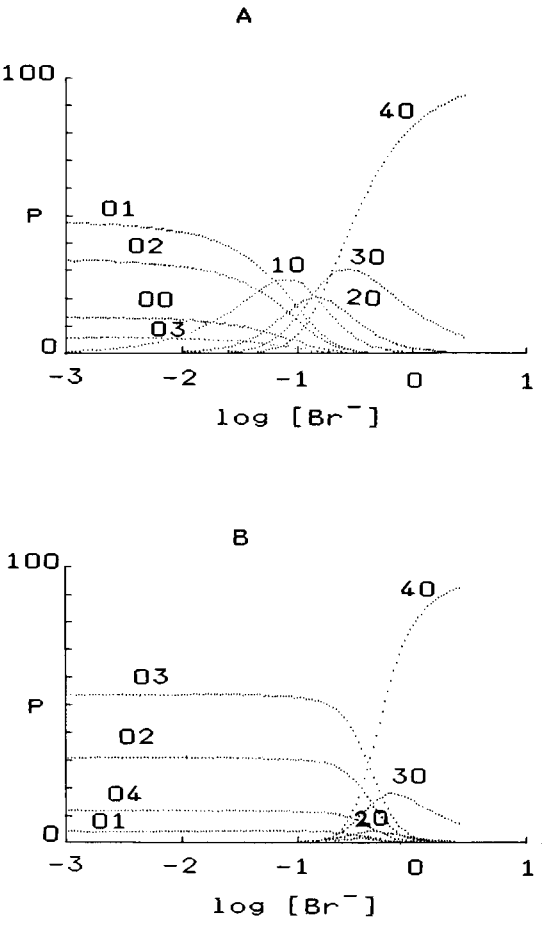

Fig. 2. Distribution of dissolved cadmium in chloride–bromide mixtures calculated under the assumption that mixed species are not present. $[Cl^-]$ = (A) 0.1 and (B) 1 mol/l. $\log \beta_{01} = 1.57$, $\log \beta_{02} = 2.42$, $\log \beta_{03} = 2.66$, $\log \beta_{04} = 2.0$ [12]. Pairs of numbers on the curves denote a and b values of the corresponding $CdBr_aCl_b$ complexes.

Corresponding expressions for MA_2 and MA_3 maxima are of the type

$$\sum_{a=1}^{N} (a-2)\beta_{a0}[A]^a = 2G \qquad (25)$$

and

$$\sum_{a=1}^{N} (a-3)\beta_{a0}[A]^a = 3G \qquad (26)$$

By comparison of the above equations with the results obtained for single-ligand systems, it fol-

lows that in order to include another series of simple species the constant term in the previously derived expressions should be multiplied by G. In other words, the optimum concentration of A (at a given [B]) for reaching the maximum of any MA_p species in a system of interest is given by

$$\sum_{a=1}^{N} (a-p)\beta_{a0}[A]^a = pG \qquad (27)$$

In the light of the above equation, the role of the constant ligand becomes obvious. If B is present at a high level and/or its complexes are much stronger than the corresponding MA_a species, the latter will not be important within the concentration range of A that can be used in real experiments. Additionally, even if all species of the MA_a type are formed in the presence of another ligand, their maximum relative concentrations will be lower than in the corresponding single-ligand solutions. For MA complexes and $N = 2$ this follows from the comparison of Eqns. 12 and 22. At higher N values a similar effect occurs but all complexes are not influenced in the same. MA is more affected than MA_2, MA_3, etc., because it appears under conditions characterized by the presence of a significant fraction of $[M]_t$ in the form of MB_b species, which decreases at higher concentrations of A (Fig. 2).

It follows that in a given system for each [B] the corresponding concentration of A can be calculated at which the complex of interest reaches its maximum percentage with respect to the total metal concentration. Additionally, this percentage can be found for each [B] and the optimum [A]. Such a presentation (calculated for an unrealistically wide chloride concentration range to show the trend) is given in Fig. 3A and B for the system from Fig. 2. It clearly demonstrates the already mentioned fact that $[A]_m$ increases whereas P_m decreases with increasing concentration of the ligand B.

Mixtures of binary and ternary species

When binary and ternary complexes are simultaneously formed, the problems with distribution diagrams are the same as described for mixtures of simple species. They are even more pronounced here because of the increased number of possible complexes, especially at higher maximum coordination numbers, which makes the corresponding plots more complicated and not easy to survey. In such a situation one should consider a partial diagram from which all the complexes, not important for the current discussion, are eliminated. An example is given in Fig. 4 for copper(II) complexation in oxalate–ethylene-

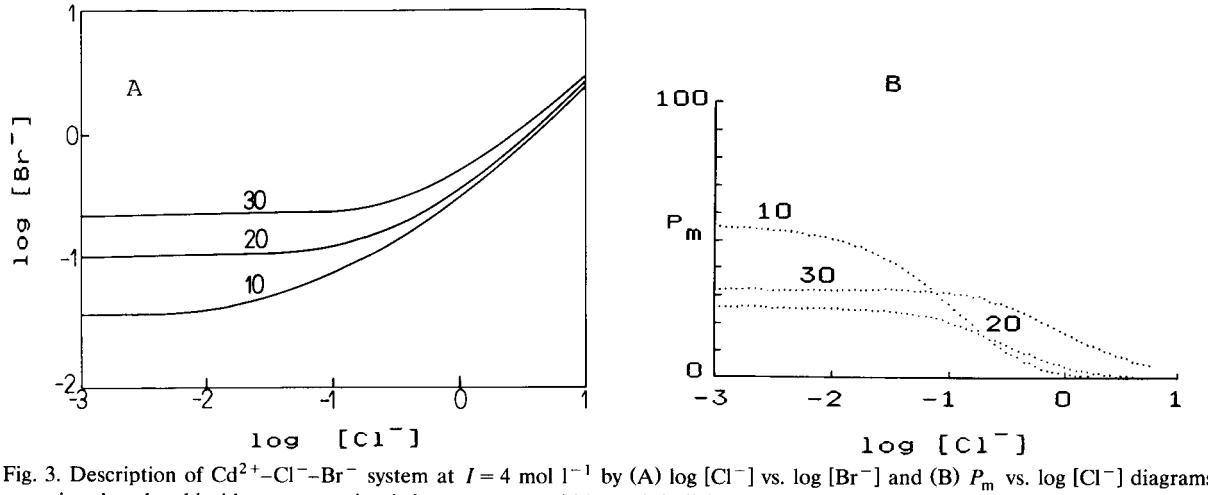

Fig. 3. Description of Cd^{2+}–Cl^-–Br^- system at $I = 4$ mol l^{-1} by (A) log $[Cl^-]$ vs. log $[Br^-]$ and (B) P_m vs. log $[Cl^-]$ diagrams, assuming that the chloride concentration is kept constant within each individual series of measurements. Pairs of numbers on the curves denote a and b values of the corresponding $CdBr_aCl_b$ species.

diamine mixtures [8]. Partial three-dimensional diagrams for Cu(en)ox (Fig. 4A) and Cu(en) Fig. 4B and C) species show the role of the ligand concentrations in the formation of "interesting" complexes. It seems that this type of presentation is mainly useful for the illustration of some principles, i.e., for drawing qualitative or semi-quantitative conclusions. In the design of experiments, interpretation of experimental results or for reading exact concentrations and percentages, the "old-fashioned", two-dimensional log [B] vs. log [A] and log [B] vs. P_m plots can give information of better quality.

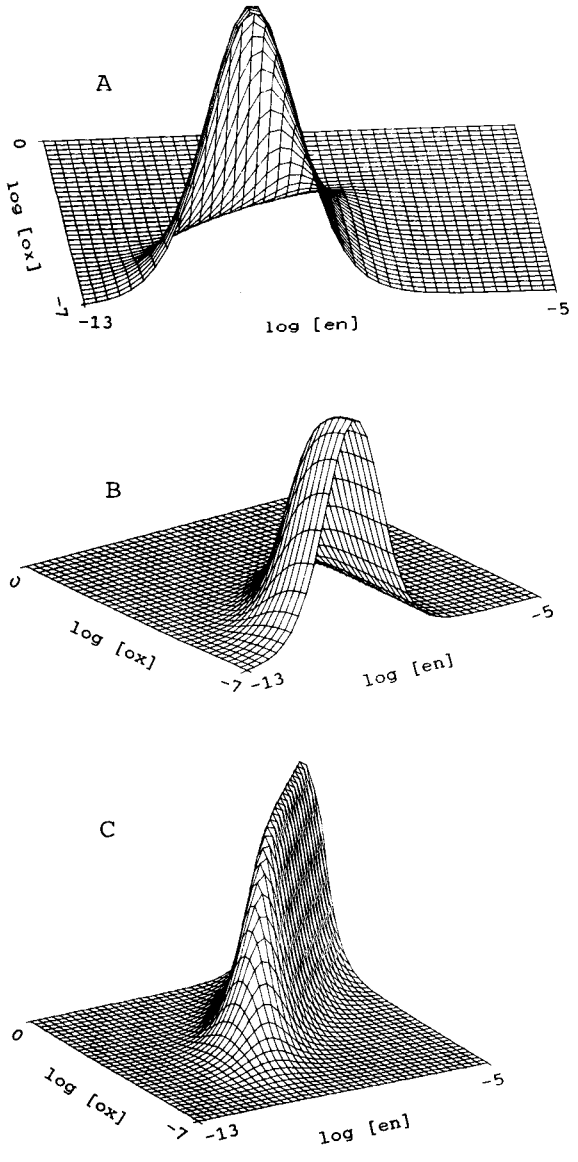

Fig. 4. Formation of (A) Cu(en)ox and (B and C) Cu(en) as a function of both ligand concentrations at $I = 1$ mol l^{-1} assuming the statistically expected β_{11} constant. Log $\beta_{10} = 10.8$, log $\beta_{20} = 20.3$, log $\beta_{01} = 5.7$, log $\beta_{02} = 9.2$ [8], log $\beta_{11} = 15.05$.

As pointed out previously [6], with the present design of experiments all the complexes, simple and mixed, that contain the same number of A units will reach their maxima at the same concentration of the variable ligand. For $N = 2$, the MAB species constitutes the highest fraction of $[M]_t$ if

$$[A] = \left(\left(1 + \beta_{01}[B] + \beta_{02}[B]^2\right)/\beta_{20}\right)^{1/2} \quad (28)$$

and the same holds for the MA complex. Of course, their P_m values will be different but both depend strongly on the level of [B]. The maximum percentage of the ternary species is given by

$$P_m = \left(100\beta_{10}/\beta_{20}^{1/2}\right) / \left(2G^{1/2} + \beta_{10}/\beta_{20}^{1/2} + \beta_{11}[B]/\beta_{20}^{1/2}\right) \quad (29)$$

whereas for the MA complex

$$P_m = \left(100\beta_{10}/\beta_{20}^{1/2}\right) / \left(2G^{1/2} + \beta_{10}/\beta_{20}^{1/2} + 2\beta_{02}^{1/2}[B]\right) \quad (30)$$

The concentration ratio (R) between MA and MAB is given by

$$R = \beta_{10}/\beta_{11}[B] \quad (31)$$

which indicates that the binary species dominates over the ternary species only if [B] is low because β_{11} is usually significantly higher than β_{10}. In other words, if a ternary complex is formed, the maximum percentage of MA species will always be lower, not only with respect to the situation in single-ligand solutions but also to the corresponding mixtures of binary species. The $[A]_m$ value is, however, the same in both types of solutions with two ligands, i.e., Eqns. 21 and 28 are identical. Unfortunately, this is true only for $N = 2$.

At higher coordinations the importance of individual MA_a complexes is even smaller because of the increased number of competing ternary species. This results in domination of mixed over

simple complexes, especially at higher concentrations of B. At the same time, $[A]_m$ is shifted towards higher concentrations in comparison with the values calculated for the corresponding mixtures of binary species.

If $N = 3$, the concentration of A at which MAB and MAB_2 reach their maximum percentages with respect to the total dissolved metal is given by the equation [7]

$$2\beta_{30}[A]^3 + \beta_{20}[A]^2 + \beta_{21}[A]^2[B] - G = 0 \quad (32)$$

which also holds for MA species. Complexes that contain two A ligands bound to the central metal ion, i.e., MA_2 and MA_2B, will consitute the highest fraction of $[M]_t$ if the following equation [7] is satisfied:

$$\beta_{30}[A]^3 - \beta_{10}[A] - \beta_{11}[A][B] - \beta_{12}[A][B]^2 - 2G = 0 \quad (33)$$

From the given expressions, together with those for $N = 4$ which are not presented here, it can be concluded that in a given system at a chosen level of B, the concentration of A at which the complex of interest reaches its maximum depends on the stability constants of all the species except those which contain the same number of A molecules (or ions) as the studied complex. This type of relationship for any maximum coordination number and any complex, binary or ternary, which contains ligand A (except MA_N) is given by the general equation

$$\sum_{a=1}^{N} \sum_{b=0}^{N-a} (a-p)\beta_{ab}[A]^a[B]^b = pG \quad (34)$$

in which $p \leq N - 1$.

Possible applications

Equations 11–13, and graphical presentations based on them, can be useful in designing experiments. Complexation of a given metal with a series of ligands or interaction of a chosen complexant with different metal ions can be compared with respect to the ligand concentrations at which MA complexes constitute the highest percentage of the total dissolved metal and to the value of this percentage. Such a presentation is given in Fig. 5 for 2,2-dimethyl-1,3-diaminopropane at $I = 1$ mol l^{-1} ([1], Vol. 2). It clearly shows that more than 80% of the total Co^{2+}, Ni^{2+} or Cu^{2+} but only 33% of the total Zn^{2+} can be transformed into coordination species of the MA type.

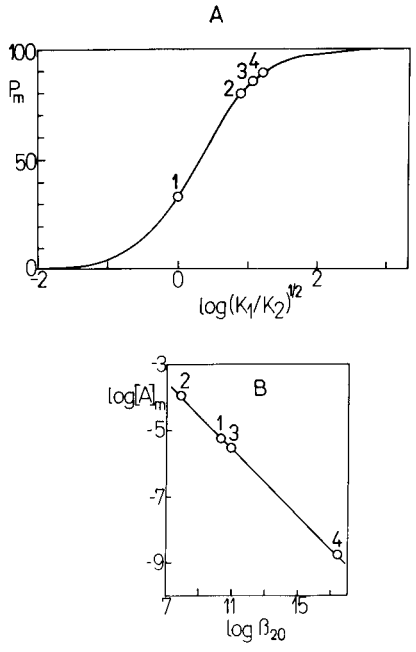

Fig. 5. Complexation of (1) Zn^{2+}, (2) Co^{2+}, (3) Ni^{2+} and (4) Cu^{2+} with 2,2-dimethyl-1,3-diaminopropane at $I = 1$ mol l^{-1} represented by (A) highest possible percentages of the total metal in the form of MA species and (B) ligand concentrations at which individual complexes reach their maxima, both as a function of the values of the stability constants of the corresponding MA_2 species.

From the equations that describe the situation in two-ligand systems, the following recommendations for experimental work can be given. If a simple complex MA_p is the species of interest (where $p \leq N$-1) and if the presence of the ligand B cannot be avoided, but its character and/or concentration can be chosen (within some limits) then: the level of B should be as low as possible; MB_b complexes should be weaker than the corresponding MA_a species; and a combination of ligands that does not give ternary species MA_aB_b should be chosen. Additionally, the log [A] vs. log [B] diagram can be constructed for any complex of interest (binary or ternary) that gives optimum pairs of ligand concentrations at which such a species will reach its own maximum in solutions containing two ligands.

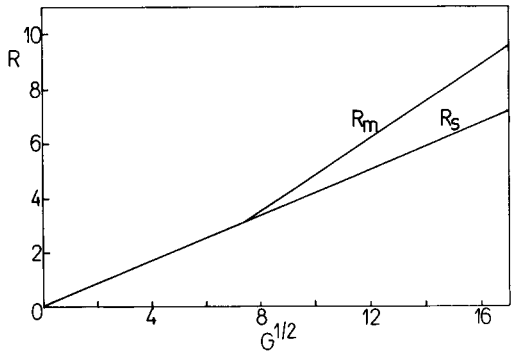

Fig. 6. The ratio (R) between maximum possible concentrations of Cu(en) in solutions of ethylenediamine and their mixtures with oxalate assuming the absence (R_s) and presence (R_m) of Cd(en)ox mixed-ligand complex with the statistically expected formation constant.

From Eqns. 12, 22 and 30, it follows that, assuming $N = 2$, the ratio (R) between the maximum possible relative concentrations of MA in single- and two-ligand systems characterized by the presence (R_m) and absence (R_s) of mixed species is given by

$$R = (P_m)_{\text{single-ligand}}/(P_m)_{\text{two-ligand}} \quad (35)$$

$$R_m = \{2G^{1/2} + (\beta_{10} + \beta_{11}[B])/\beta_{20}^{1/2})\} / (2 + \beta_{10}/\beta_{20}^{1/2}) \quad (36)$$

$$R_s = (2G^{1/2} + \beta_{10}/\beta_{20}^{1/2})/(2 + \beta_{10}/\beta_{20}^{1/2}) \quad (37)$$

This means that the plot of R_s vs. $G^{1/2}$ will be a straight line (Fig. 6) with slope $2/(2 + \beta_{10}/\beta_{20}^{1/2})$ and intercept $\beta_{10}/\beta_{20}^{1/2}/(2 + \beta_{10}/\beta_{20}^{1/2})$. If the MAB species is also formed, the linearity can be maintained only at low concentrations of the constant ligand. At higher values of [B] R_m will increase faster than R_s. Assuming that there is a method by which only the concentration of MA species can be followed, the difference between calculated (R_s) and experimentally obtained (R_m) R values at a given G can be used for the detection of the mixed species and the calculation of its formation constant. In order to obtain the whole diagram of the type given in Fig. 6, several series of measurements at different levels of B should be performed and the corresponding maximum (relative) concentrations of MA complex determined. The constant β_{11}, however, can be calculated from only one series assuming that the obtained R value is significantly higher than expected for a mixture of binary species because

$$R_m - R_s = \beta_{11}[B]/(2\beta_{20}^{1/2} + \beta_{10}) \quad (38)$$

Finally, many of the given equations can be applied in the construction of three-dimensional graphs, by means of which very illustrative presentations of important relationships can be obtained.

It should be pointed out that all equations were derived assuming the absence of solubility problems. In other words, the total metal concentration was not treated as a factor important for the present discussion. However, this assumption is not always fulfilled. Some neutral species, binary (PbI_2) or ternary (PbFBr) [13], are poorely soluble. This means that the mentioned equations can sometimes be applied only in a limited metal concentration range inside which formation of the solid phase does not take place.

This work was supported by the Ministry of Science, Technology and Informatics of the Republic of Croatia.

REFERENCES

1 R.M. Smith and A.E. Martell, Critical Stability Constants, Vols. 1–6, Plenum, New York, 1974–89.
2 H. Freiser and Q. Fernando, Ionic Equilibria in Analytical Chemistry, Wiley, New York, 1960.
3 D. Dyrsen, D. Jagner and F. Vengelin, Computer Calculation of Ionic Equilibria and Titration Procedures, Almqvist and Wiksell, Stockholm, 1968.
4 H. Rosotti, The Study of Ionic Equilibria, Longman, New York, 1978.
5 M.T. Beck and I. Nagypal, Chemistry of Complex Equilibria, Horwood, Chichester, 1990.
6 M. Zelić and M. Branica, Anal. Chim. Acta, 238 (1990) 393.
7 M. Zelić, Anal. Chim. Acta, 271 (1993) 275.
8 W.B. Schaap and D.L. McMasters, J. Am. Chem. Soc., 83 (1961) 4699.
9 B. Carnahan, H.A. Luther and J.O. Wilkes, Applied Numerical Methods, Wiley, New York, 1969.
10 M. Zelić and M. Branica, Anal. Chim. Acta, 262 (1992) 129.
11 M. Zelić and M. Branica, Electroanalysis, 4 (1992) 701.
12 M. Branica, I. Pižeta, G. Branica-Jurković and M. Zelić, Mar. Chem., 28 (1989) 227.
13 A.M. Bond and G. Hefter, J. Electroanal. Chem., 42 (1973) 1.

Analytica Chimica Acta, 281 (1993) 443–449
Elsevier Science Publishers B.V., Amsterdam

Tensammetric studies of separation of surfactants

Part 2. Investigation of adsorption and preconcentration of non-ionic surfactants in PTFE tubes [1]

Andrzej Szymanski and Zenon Lukaszewski

Institute of Chemistry, Technical University of Poznan, 60-965 Poznan (Poland)

(Received 23rd November 1992; revised manuscript received 16th March 1993)

Abstract

Separation of non-ionic surfactants from aqueous solution (concentration of the order of 10 $\mu g\ l^{-1}$) with the aid of commercially available PTFE tubes of small diameter was investigated. Passing the sample through the PTFE tube and subsequently washing it with methanol enables surfactants to be separated from water, with the aim both of preconcentration and of cleaning of the solution. Such preconcentration enables one to detect signals of surfactants of the order of 1 $\mu g\ l^{-1}$, i.e., below the detection limit of adsorptive stripping tensammetry. A broader range of ethoxylates can be separated from water in this way than with the methods currently used. Non-ionic surfactants differ in their adsorptive ability on PTFE. These differences are dependent on the length of the oxyethylene chain in the molecule of surfactant and create the possibility of separation of non-ionic surfactants.

Keywords: Polarography; Preconcentration; Surfactants; Tensammetry; Waters

Further progress in surfactant analysis in the environment requires the development of effective separation methods, because surfactants in the environment are present in multi-component mixtures that may contain more than 100 individual substances. Even partial success in this area would be important, e.g., determination of narrower fractions of surfactants. Improved methods for the separation of non-ionic surfactants from water matrices with the aim of further determination are also required.

Separation of surfactants from aqueous solutions is also important in voltammetric analysis. Surfactants cause inhibition of electrode processes, which changes considerably the conditions for the determination of different metals. Among voltammetric methods, stripping methods are very sensitive to such impurities. Therefore, methods for purifying solutions from traces of surfactants have been developed [1–4]. Inhibition effects appear starting from concentrations of the order of $\mu g\ l^{-1}$ or tens of $\mu g\ l^{-1}$, depending on the preconcentration time used [5,6].

Adsorptive stripping tensammetry (AST) is an excellent tool for the investigation of different processes for the separation of surfactants [7], although AST itself is not so useful for quantitative determinations because of the complex behaviour of surfactant mixtures [8,9]. AST uses a very effective preconcentration procedure and therefore it permits the determination of surfac-

Correspondence to: Z. Lukaszewski, Institute of Chemistry, Technical University of Poznan, 60-965 Poznan (Poland).

[1] Dedicated to Professor Zenon Kublik on the occasion of his 70th birthday.

tant concentration of the order of 10 $\mu g\ l^{-1}$ (10^{-6}%). The analytical signal in AST is selective to a certain extent.

Adsorption of surfactants on different polymeric materials, both synthetic and natural, has been investigated using both classical tensammetry [10,11] and UV spectrophotometry [12–15] for control. Measurements performed by classical tensammetry concerned adsorption of the cationic-type surfactant hexadecylpyridinium chloride on different textile fibres [10,11]. UV spectrophotometric measurements were limited to surfactants having a benzene ring. Therefore, the adsorption of oxyethylated alkylphenols as representatives of non-ionic surfactants on polyacrylic and polymethacrylic acids [12,14], cation-exchange resins of the Amberlyte type [13] and adsorbents of Amberlyte XAD type [15] has been investigated. However, these investigations concerned a comparatively high concentration range (10 mg l^{-1}–10 g l^{-1}). Within this range the adsorptive ability is different from that in the $\mu g\ l^{-1}$ region owing to the presence of surfactants in associated form in more concentrated solutions. Except for AST and polarographic maxima suppression, the methods for the concentration range below 1 mg l^{-1} are in the initial stages of development. This seems to be the main reason for the lack of reports in this area.

An investigation of the adsorption of several representative non-ionic surfactants on the surface of measuring cells used in AST at concentrations of the order of 10 $\mu g\ l^{-1}$ has been reported [16]. Different materials were used for construction of the cell, e.g., PTFE, polyethylene, polypropylene and polystyrene. All these cells indicated strong adsorption of non-ionic surfactants, although a certain specificity was observed in this respect. A PTFE cell showed stronger adsorption of oxyethylated alkylphenols than oxyethylated alcohols.

The investigation of the adsorption of non-ionic surfactants in a PTFE tube seems to be important because of its possible use for trapping and separation of non-ionic surfactants. The future combination of such a separation with AST or the indirect tensammetric method seems to be promising. Such an investigation could also indicate "memory" effects of PTFE tube with respect to surfactants (added either deliberately or accidentally), which can be important in flow-injection analysis.

The aim of this work was the investigation of the adsorption of representative non-ionic surfactants at concentrations of the order of 10 $\mu g\ l^{-1}$ on a commercially available PTFE tube of small diameter, and evaluation of the possibility of removing surfactants from aqueous solutions both with the aim of cleaning the solution and for trapping surfactants. AST was used as a semi-quantitative technique for control of the separation.

EXPERIMENTAL

Apparatus and reagents

A Radelkis OH-105 polarograph was used with a voltage scan rate of 400 mV min^{-1}. The applied amplitude of the alternating voltage was 2 mV. Controlled-temperature hanging mercury drop electrode (HMDE) equipment (Radiometer), having an additional platinum wire auxiliary electrode, was used. All potentials cited are measured against the saturated calomel electrode. The glass beaker of the measuring cell was replaced with a quartz beaker. The ceramic frit at the end of the salt bridge was protected by the fitting of a polyethylene tube. This ceramic frit exhibits a very high adsorptive ability [16], and this fitting of a tube very effectively reduces the adsorptive losses of surfactants.

Commercially available PTFE tubes (Millipore) of diameter 1.5 mm and length 1 or 7 m were used.

The following surfactants were used without additional purification (the average number of oxyethylene subunits is given in parentheses): oxyethylated isooctylphenol, Triton X-100 (9.5) (Rohm and Haas; supplied by Serva); oxyethylated alcohols having a C_{10-13} hydrophobic part of the molecule, Oxetal D104(4), Oxetal T105(5) and Oxetal C114(14) (all from Zschimmer und Schwarz); oxyethylated alcohols having a C_{16-18} hydrophobic part of the molecule, Marlipal 1618/18(18), Marlipal 1618/25(25) and Marlipal

1618/40(40) (all from Hüls); oxyethylene–oxypropylene block copolymer, Pluronic F108 (300) (Wyandotte), having an average number of oxypropylene subunits of 55; poly(propylene glycol) with a molecular weight of 1025 (PPG 1025) (Schuchardt); and poly(ethylene glycol) with a molecular weight of 9000 (PEG 9000) (Fluka).

Methanol of analytical-reagent grade was used. Purified sodium sulphate was used for the preparation of the aqueous 0.5 M base electrolyte [17]. All solutions were prepared in water triply distilled from quartz. Only freshly distilled water was used.

Preconcentration was done for 300 s in a stirred solution at −1.20 V vs. SCE with a new mercury drop [17]. The preconcentration time was measured from the moment of drop formation. The tensammetric curve was recorded in the negative direction after a 30 s rest period.

Typical experiment

A 500-ml volume of surfactant solution (most frequently 40 μg l^{-1}) was placed in a separation funnel and passed through a PTFE tube of 1.5 mm diameter; 1- and 7-m long PTFE tubes were used. Fractions of 25 ml of the solution passing through the tube were collected. Each fraction was diluted 1 + 1 with 1 M sodium sulphate solution (supporting electrolyte). Tensammetric curves of each fraction were recorded; the peak heights reflect the changes in surfactant concentration. Under the conditions used, the height is roughly linearly dependent on concentration within the concentration range studied [17–19]. An example of a sequence of tensammetric curves corresponding to consecutive fractions of Triton X-100 solution (50 μg l^{-1}) passing through a 7-m PTFE tube is shown in Fig. 1 (curves b–i). The peak of Triton X-100 in the original fractions is much smaller than that expected, assuming lack of adsorption (curve m). The strongly reduced peak heights indicate strong adsorption of Triton X-100 in the tested tube.

RESULTS AND DISCUSSION

The influence of flow-rate on the adsorption on a PTFE tube was examined for a solution of

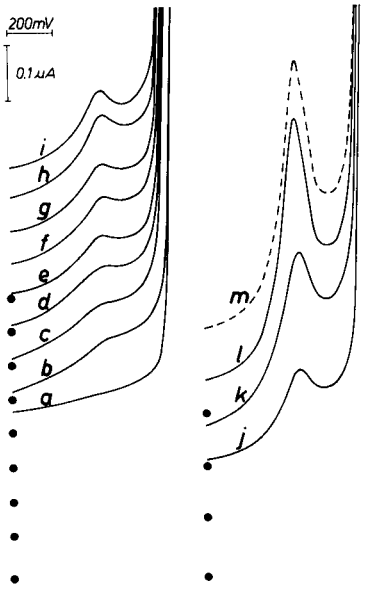

Fig. 1. Tensammetric curves for Triton X-100 belonging to one series of successive 25-ml samples obtained on passage of the initial solution through a PTFE tube (curves b–i). Curves j, k and l correspond to passage of 300, 400 and 500 ml of the initial solution, respectively. The dashed curve m refers to the initial solution of Triton X-100. Curve a is for the base electrolyte. Initial concentration of surfactant, 50 μg l^{-1}; length of tube, 7 m; flow-rate, 8 ml min^{-1}; preconcentration potential, −1.20 V vs. SCE; preconcentration time, 300 s. • represents zero of current for respective tensammetric curves.

Triton X-100 (50 μg l^{-1}). Two flow-rates (2 and 36 ml min^{-1}) were tested. The results in normalized form referred to the peak height of the initial solution of Triton X-100 are shown in Fig. 2. The slight non-linearity of the calibration graph for Triton X-100 was neglected. As could be expected, the "saturation curves" show much higher adsorption at slower flow-rates than in the opposite case. A substantial shift of the "saturation curve" can be achieved by changing this parameter. The length of the tube should also have an influence on the "saturation curves".

Series of non-ionic surfactants were investigated for adsorption in a 7-m long PTFE tube. The concentration of surfactants was 40 μg l^{-1} and the flow-rate was 8 ml min^{-1} in all instances. Six of the investigated surfactants were oxyethylated alcohols having different hydrophobic parts of the molecule and different lengths of the oxyethylene chain. This group of surfactants is

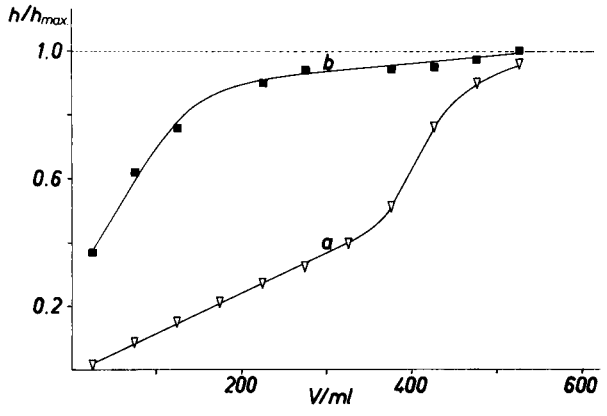

Fig. 2. "Saturation curve" of 1-m PTFE tube with Triton X-100 at flow-rates of (a) 2 and (b) 36 ml min^{-1}. Initial concentration of surfactant, 50 $\mu g\ l^{-1}$.

the major component of non-ionic surfactants. "Saturation curves" for these surfactants together with that for Triton X-100 (standard surfactant) are shown in Fig. 3. The results are given in normalized form referred to the peak height of the corresponding surfactant before adsorption. PEG 9000, PPG 1025, Triton X-100 and Pluronic F108 were added to this series. Triton X-100 represented the group of oxyethylated alkylphenols and Pluronic F108 the group of oxyethylene–oxypropylene block copolymers. The results

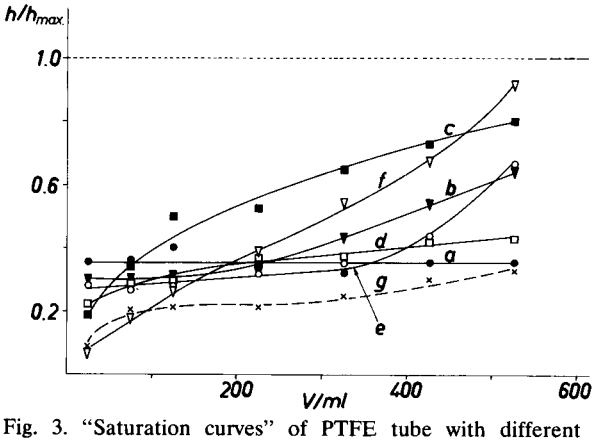

Fig. 3. "Saturation curves" of PTFE tube with different oxyethylated alcohols: (a) Marlipal 1618/40; (b) Marlipal 1618/25; (c) Marlipal 1618/18; (d) Oxetal C114; (e) Oxetal T105; (f) Oxetal D104. The dashed curve g corresponds to Triton X-100 (reference surfactant). Initial concentration of surfactant, 40 $\mu g\ l^{-1}$; other conditions as in Fig. 1.

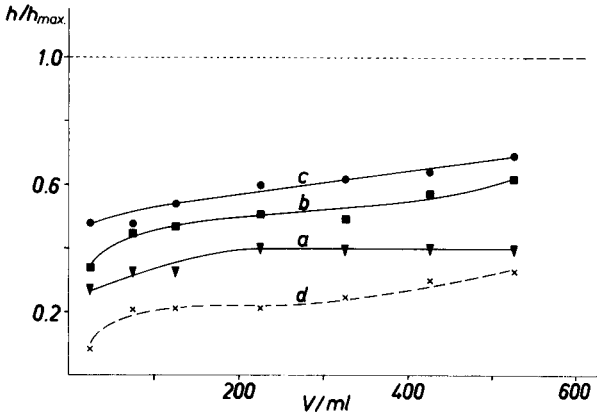

Fig. 4. "Saturation curves" of PTFE tube with (a) PPG 1025, (b) Pluronic F108 and (c) PEG 9000. The dashed curve d corresponds to Triton X-100 (reference surfactant). Conditions as in Fig. 3.

are shown in Fig. 4, also in normalized form.

Substantial differences in the "saturation curves" of the different surfactants are apparent. The adsorption is stronger for surfactants having longer oxyethylene chains. This is visible in the series Marlipal 1618/40, 1618/25 and 1618/18, having the same hydrophobic part of the molecule and 40, 25 and 18 oxyethylene subunits, respectively (curves a, b and c in Fig. 3). The same tendency can be seen for the series Oxetal C114, T105 and D104, having 14, 5 and 4 oxyethylene subunits, respectively, although the hydrophobic parts of their molecules differ slightly (see curves d, e and f in Fig. 4). Triton X-100, representing oxyethylated alkylphenols, exhibits the strongest adsorption of the investigated oxyethylated alcohols. This supports expectations based on previous investigations [16]. PEG 9000 and PPG 1025 exhibit comparatively strong adsorption, although that of the latter is the stronger and both are adsorbed more weakly than Triton X-100 (see curves a, c and dashed curve d in Fig. 4). Pluronic F108 (curve b in Fig. 4), being composed of blocks of PEGs and PPGs, forms a "saturation curve" intermediate between those of PEG 9000 and PPG 1025.

The possible use of the separation of surfactants in a PTFE tube would be characterized by the following differences in comparison with the method currently used for the separation of non-

ionic surfactants from surface water samples [20,21]: PEGs are adsorbed by the PTFE tube whereas in the methods currently used PEGs remain in the aqueous phase; surfactants having long oxyethylene chains (Marlipal 1618/40, Pluronic F108) and those having very short oxyethylene chains (Oxetal D104 and T105) are adsorbed by the PTFE tube whereas in the methods currently used these surfactants are lost. Methods currently used as a standard [20,21] permit the determination of ethoxylates having more than 5–7 and less than 30–40 oxyethylene subunits. These differences would allow the separation of a broader range of non-ionic surfactants from surface water samples than in the methods currently used. It is clear from Figs. 2–4 that several cycles of separation are necessary in order to achieve complete separation of surfactants from the aqueous phase at concentrations of the order of 10 μg l^{-1}. Additionally, the observed differences in the adsorptive abilities of the different surfactants on the PTFE tube create a possibility for their partial separation.

An attempt at the complete isolation of Triton X-100 as a representative surfactant from aqueous solutions using a PTFE tube was undertaken. A 500-ml sample of water solution containing 20 μg of Triton X-100 was passed three times through the 7-m tube with control by means of AST. It is obvious from the "saturation curves" shown in Figs. 2 and 3 that at this concentration a single passage of sample through the tube would result in only partial separation. The tube was cleaned with methanol between the subsequent passages of the solution through the tube. Figure 5 illustrates this experiment. Curves a and b show the base electrolyte curve and the curve of non-separated Triton X-100, respectively. The first 25 ml of the first passage of test solution through the tube show a lack of Triton X-100 (curve c). However, the whole 500-ml sample shows the signal of Triton X-100 (curve d), although much smaller than the signal of the original sample (curve b). Hence a partial separation of Triton X-100 has occurred.

The whole 500-ml sample obtained after the second passage of the solution through the tube (cleaned in between with methanol) shows only a trace of a peak of Triton X-100 (curve e), whereas the whole sample obtained after the third passage of the solution through the tube shows the lack of a peak of Triton X-100 (curve f). Hence 20 μg of Triton X-100 was removed from the aqueous phase. It is clear that the main part of Triton X-100 was separated during the first cycle of separation (compare the heights of peaks b and d).

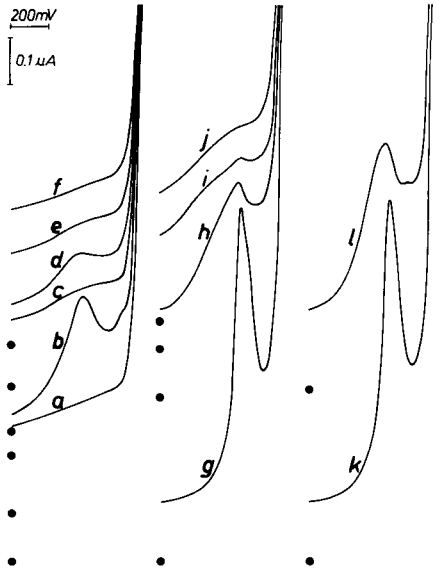

Fig. 5. Tensammetric curves illustrating trapping of 20 μg of Triton X-100 in a PTFE tube (curves c–f) and removal of adsorbed Triton X-100 from the tube with methanol (curves g–l), performed in three cycles. Curves d, e and f show the signals after the first, second and third cycles of trapping, respectively, and curve c shows the signal of the first 25-ml portion of the first cycle of trapping. Curves g–j show the signals of successive washings of Triton X-100 adsorbed during the first cycle of trapping. Curves k and l show the signals of washing of the tube after the second and the third cycles of separation, respectively. Curve a for the base electrolyte and curve b for initial solution of Triton X-100. Other conditions as in Fig. 1.

The cleaning of the tube with methanol was semi-quantitatively controlled with AST. In order to simplify the measurements, methanol was added to the base electrolyte (0.5 M sodium sulphate) without evaporation. The presence of such amounts of methanol in the sample only slightly modifies the analytical signal of surfactants in AST [22].

The first washing with 5 ml of methanol of the tube saturated with Triton X-100 leads to a signal that is much enhanced in comparison with that of the original Triton X-100 solution (compare curves g and b). Three consecutive washings of the tube with 5-ml portions of methanol lead to removal of the residual amount of Triton X-100 from the tube (see curves h, i and j).

The PTFE tube perfectly cleaned after the first cycle of separation was used for the second cycle of separation of the water sample originally containing 20 μg, as described above. After passage of the separated solution the tube was again washed with four 5-ml portions of methanol. The signal corresponding to the first washing is shown in curve k. It is roughly the same as the corresponding signal obtained after the first cycle of separation. The tube cleaned (four washings with methanol) after the second cycle of separation was used for the third separation cycle and then it was also washed with four 5-ml portions of methanol. The analytical signal corresponding to the first portion of this washing is shown in curve l. It is much smaller than the corresponding signals obtained after the previous two cycles and corresponds to about 1 μg of Triton X-100 in the sample. These results show that the main part of 20 μg of Triton X-100 originally introduced into the separation process is separated during the first two cycles of separation and the third cycle operates with the residual amount of surfactant.

The described separation process consisting of three cycles of adsorption and washing the tube allowed the transfer of 20 μg of Triton X-100 from a large volume of aqueous solution to a small volume of methanol. It must be stressed that this amount of surfactant is too small to perform a determination with the other methods currently used for determination of non-ionic surfactants. Tensammetric methods, i.e. both AST [16–19] and the indirect tensammetric method [23], can work within this concentration range.

A separation process similar to that described above was performed with a very small amount of Triton X-100 to demonstrate the possibility of enriching the sample and of determining the concentration of surfactant when it is below the detection limit of AST. A 0.5-μg amount of Triton X-100 was trapped from 500 ml of solution on the 7-m PTFE tube (one cycle). The tube was then washed with 5 ml of methanol, diluted with the base electrolyte and water to 25 ml. AST measurement was performed. The tensammetric curves corresponding to this separation are shown in Fig. 6. Curve b, free of signal, represents the original solution of concentration 1 μg l^{-1}, far below the detection limit. Such a concentration is also below the inhibition effects [5,6]. Curve c shows the signal of Triton X-100 separated on the tube and washed with methanol, and curve e gives the expected signal assuming complete separation. Both signals have similar heights. The small difference can be explained by the presence of methanol in the real sample in contrast to the model sample. Curve d in Fig. 6 represents the signal obtained after the second washing of the tube with methanol and shows completeness of the first washing. The described experiments show the possibility of the effective preconcentration of surfactants by a PTFE tube and, in this way, an improved detection limit of AST.

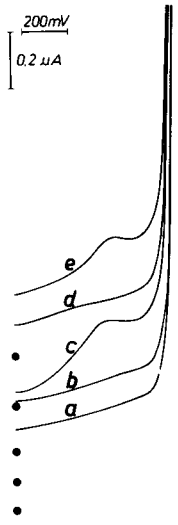

Fig. 6. Tensammetric curves illustrating trapping of 0.5 μg of Triton X-100 in a PTFE tube performed in one cycle. Curve c represents Triton X-100 trapped in the tube and washed with methanol, curve d the solution obtained after second washing of the tube and curve e the signal expected assuming ideal preconcentration. Curve a is for the base electrolyte and curve b for the initial solution of Triton X-100. Other conditions as in Fig. 1.

Conclusions

Passing an aqueous solution of surfactants through a PTFE tube and subsequent washing of the tube with methanol permits the separation of surfactants from water, with the aim of both preconcentration and cleaning of the solution. Such preconcentration enables surfactant concentrations below the detection limit of AST to be detected. A broader range of ethoxylates can be separated from water in comparison with the methods currently used.

Non-ionic surfactants have different adsorptive abilities on PTFE. These differences are dependent on the length of the oxyethylene chain in the molecule of the surfactant and create the possibility of separating particular non-ionic surfactants or, at least, subdividing them into fractions.

Strong adsorption of non-ionic surfactants on a PTFE tube should be taken into account in flow-injection analysis if surfactants participate in measurement (as reagents or analytes); memory effects of the tube and remobilization of the surfactant shifted in time should be expected.

This work was supported by the Committee of Scientific Research (Institutional Grant for Institute of Chemistry of Technical University of Poznan, No. DB/649/92/31–3).

REFERENCES

1 E. Bednarkiewicz and Z. Kublik, J. Electroanal. Chem., 165 (1984) 195.
2 W.W. Kubiak and J. Wang, J. Electroanal. Chem., 258 (1989) 41.
3 W.W. Kubiak and J. Wang, Talanta, 36 (1989) 821.
4 R. Kalvoda, Abh. Dtsch. Akad. Wiss. Berlin, Kl. Chem. Geol. Biol., (1962) 286.
5 Z. Lukaszewski and M.K. Pawlak, Chem. Anal. (Warsaw), 24 (1979) 221.
6 A. Ciszewski and Z. Lukaszewski, Talanta, 32 (1985) 1101.
7 B. Wyrwas, A. Szymanski and Z. Lukaszewski, Anal. Chim. Acta, 278 (1993) 197.
8 H. Batycka and Z. Lukaszewski, Anal. Chim. Acta, 162 (1984) 215.
9 M.K. Pawlak and Z. Lukaszewski, Anal. Chim. Acta, 202 (1987) 97.
10 H.-J. Jacobasch, I. Grosse and U. Schumann, Faserforsch. Textiltech., 22 (1971) 571.
11 H.-J. Jacobasch, H. Jehring and U. Schumann, Faserforsch. Textiltech., 23 (1972) 42.
12 S. Saito and T. Taniguchi, J. Am. Oil Chem. Soc., 50 (1973) 276.
13 S. Saito, T. Taniguchi and M. Yukawa, Tenside Deterg., 12 (1975) 100.
14 S. Saito, Tenside Deterg., 14 (1977) 113.
15 P. Anielak and K. Janio, Tenside Surfact. Deterg., 27 (1990) 113.
16 A. Szymanski and Z. Lukaszewski, Anal. Chim. Acta, 231 (1990) 77.
17 H. Batycka and Z. Lukaszewski, Anal. Chim. Acta, 162 (1984) 207.
18 A. Szymanski and Z. Lukaszewski, Electroanalysis, 3 (1991) 17.
19 A. Szymanski and Z. Lukaszewski, Electroanalysis, 3 (1991) 963.
20 D. Brown, H. De Henau, J.T. Garigan, P. Gerike, M. Holt, E. Keck, E. Kunkel, E. Matthijs, J. Waters and J. Watkinson, Tenside Deterg., 23 (1986) 190.
21 T.M. Schmitt, M.C. Allen, D.K. Brain, K.F. Guin, D.E. Lemmel and Q.W. Osburn, J. Am. Oil Chem. Soc., 67 (1990) 103.
22 A. Szymanski and Z. Lukaszewski, unpublished data.
23 A. Szymanski and Z. Lukaszewski, Anal. Chim. Acta, 260 (1992) 25.

PUBLICATION SCHEDULE FOR 1994

	S'93	O'93	N'93	D'93	J	F						
Analytica Chimica Acta	281/1 281/2 281/3	282/1 282/2 282/3	283/1 283/2	283/3 284/1 284/2	284/3 285/1 285/2	285/3 286/1 286/2						
Vibrational Spectroscopy		6/1			6/2							

INFORMATION FOR AUTHORS

Detailed "Instructions to Authors" for *Analytica Chimica Acta* was published in Volume 256, No. 2, pp. 373–376. Free reprints of the "Instructions to Authors" of *Analytica Chimica Acta* and *Vibrational Spectroscopy* are available from the Editors or from: Elsevier Science Publishers B.V., P.O. Box 330, 1000 AH Amsterdam, The Netherlands. Telefax: (+31-20) 5862845.

Manuscripts. The language of the journal is English. English linguistic improvement is provided as part of the normal editorial processing. Authors should submit three copies of the manuscript in clear double-spaced typing on one side of the paper only. *Vibrational Spectroscopy* also accepts papers in English only.

Abstract. All papers and reviews begin with an Abstract (50–250 words) which should comprise a factual account of the contents of the paper, with emphasis on new information.

Figures. Figures should be prepared in black waterproof drawing ink on drawing or tracing paper of the same size as that on which the manuscript is typed. One original (or sharp glossy print) and two photostat (or other) copies are required. Attention should be given to line thickness, lettering (which should be kept to a minimum) and spacing on axes of graphs, to ensure suitability for reduction in size on printing. Axes of a graph should be clearly labelled, along the axes, outside the graph itself. All figures should be numbered with Arabic numerals, and require descriptive legends which should be typed on a separate sheet of paper. Simple straight-line graphs are not acceptable, because they can readily be described in the text by means of an equation or a sentence. Claims of linearity should be supported by regression data that include slope, intercept, standard deviations of the slope and intercept, standard error and the number of data points; correlation coefficients are optional.

Photographs should be glossy prints and be as rich in contrast as possible; colour photographs cannot be accepted. Line diagrams are generally preferred to photographs of equipment.

Computer outputs for reproduction as figures must be good quality on blank paper, and should preferably be submitted as glossy prints.

Nomenclature, abbreviations and symbols. In general, the recommendations of the International Union of Pure and Applied Chemistry (IUPAC) should be followed, and attention should be given to the recommendations of the Analytical Chemistry Division in the journal *Pure and Applied Chemistry* (see also *IUPAC Compendium of Analytical Nomenclature, Definitive Rules*, 1987).

References. The references should be collected at the end of the paper, numbered in the order of their appearance in the text (*not* alphabetically) and typed on a separate sheet.

Reprints. Fifty reprints will be supplied free of charge. Additional reprints (minimum 100) can be ordered. An order form containing price quotations will be sent to the authors together with the proofs of their article.

Papers dealing with vibrational spectroscopy should be sent to: Dr J.G. Grasselli, 150 Greentree Road, Chagrin Falls, OH 44022, U.S.A. Telefax: (+1-216) 2473360 (Americas, Canada, Australia and New Zealand) or Dr J.H. van der Maas, Department of Analytical Molecule Spectrometry, Faculty of Chemistry, University of Utrecht, P.O. Box 80083, 3508 TB Utrecht, The Netherlands. Telefax: (+31-30) 518219 (all other countries).

0003-2670/93/$06.00

This issue is printed on acid-free paper.

PRINTED IN THE NETHERLANDS

BIOAFFINITY CHROMATOGRAPHY

By **J. Turková,** Czechoslovak Academy of Sciences, Institute of Organic Chemistry and Biochemistry, Prague, Czech Republic

Journal of Chromatography Library Volume 55

Bioaffinity chromatography is now the preferred choice for the purification, determination or removal of many biologically active substances. The book includes information on biologically active substances with their affinants, solid supports and methods of coupling, summarized in tables covering classical, high-performance liquid and large-scale bioaffinity chromatography.

Optimization of the preparation and the use of highly active and stable biospecific adsorbents is discussed in several chapters. Following a chapter dealing with the choice of affinity ligands, affinity-sorbent bonding is described in detail. Other chapters give information on solid supports, the most common coupling procedures and a general discussion of sorption and elution. Several applications of bioaffinity chromatography are described, e.g. quantitative evaluation of biospecific complexes and many applications in medicine and in the biotechnology industry.

Contents:

© 1993 819 pages Hardbound
Price: Dfl. 495.00 / US $ 282.75
ISBN 0-444-89030-0

ORDER INFORMATION
For USA and Canada
ELSEVIER SCIENCE PUBLISHERS
Judy Weislogel, P.O. Box 945
Madison Square Station
New York, NY 10160-0757
Fax: (212) 633 3880
In all other countries
ELSEVIER SCIENCE PUBLISHERS
P.O. Box 330
1000 AH Amsterdam
The Netherlands
Fax: (+31-20) 5862 845
US$ prices are valid only for the USA & Canada and are subject to exchange rate fluctuations; in all other countries the Dutch guilder price (Dfl.) is definitive. Customers in the European Community should add the appropriate VAT rate applicable in their country to the price(s). Books are sent postfree if prepaid.

ELSEVIER
SCIENCE PUBLISHERS

0003-2670(19930910)281:2;1-D